

CLIMATE EXTREMES AND THEIR IMPLICATIONS FOR RISK AND RESILIENCE IN INDIA

Ph.D. Thesis

By
SRINIDHI JHA



**DISCIPLINE OF CIVIL ENGINEERING
INDIAN INSTITUTE OF TECHNOLOGY INDORE
AUGUST 2020**

CLIMATE EXTREMES AND THEIR IMPLICATIONS FOR RISK AND RESILIENCE IN INDIA

A THESIS

*Submitted in partial fulfillment of the
requirements for the award of the degree
of*
DOCTOR OF PHILOSOPHY

by
SRINIDHI JHA



**DISCIPLINE OF CIVIL ENGINEERING
INDIAN INSTITUTE OF TECHNOLOGY INDORE
AUGUST 2020**



INDIAN INSTITUTE OF TECHNOLOGY INDORE

CANDIDATE'S DECLARATION

I hereby certify that the work which is being presented in the thesis entitled **CLIMATE EXTREMES AND THEIR IMPLICATIONS FOR RISK AND RESILIENCE IN INDIA** in the partial fulfillment of the requirements for the award of the degree of **DOCTOR OF PHILOSOPHY** and submitted in the **DISCIPLINE OF CIVIL ENGINEERING, Indian Institute of Technology Indore**, is an authentic record of my own work carried out during the time period from December, 2017 to August, 2020 under the supervision of Dr. Manish Kumar Goyal, Associate Professor, Discipline of Civil Engineering, Indian Institute of Technology Indore.

The matter presented in this thesis has not been submitted by me for the award of any other degree of this or any other institute.

Signature of the student with date
SRINIDHI JHA

This is to certify that the above statement made by the candidate is correct to the best of my knowledge.

Signature of Thesis Supervisor

Dr. Manish Kumar Goyal

SRINIDHI JHA has successfully given his Ph.D. Oral Examination held on **January 8, 2021**.

Signature of Chairperson (OEB)
Date: January 8, 2021

Signature of External Examiner
Date: 08 January 2021

Signature(s) of Thesis Supervisor(s)
Date:

Signature of PSPC Member #1
Date:

Signature of PSPC Member #2
Date:

Signature of PSPC Member #3
Date:

Signature of Convener, DPGC
Date: 14/01/2021

Signature of Head of Discipline
Date: 08/01/2021

ACKNOWLEDGEMENTS

I would like to place on record my deep sense of gratitude and sincere thanks to my thesis supervisor Dr. Manish Kumar Goyal, Associate Professor, Discipline of Civil Engineering, Indian Institute of Technology Indore for his invaluable guidance and full hand cooperation throughout all aspects of this research work. I also admire his patient explanation of the concepts and basic principles.

I am grateful to Dr. Lalit Borana, Dr. Abhishek Rajput and Dr. Sumanta Samal for their valuable suggestions and kind support during the completion of the research work. Their technical inputs and valuable suggestions have greatly helped me in shaping this thesis.

My sincere acknowledgement and respect to Prof. Neelesh Kumar Jain, Director, Indian Institute of Technology Indore for providing me the opportunity to explore my research capabilities at Indian Institute of Technology Indore. Also, I express my gratitude to Dr. Sandeep Chaudhary and Dr. Neelima Satyam for their valuable time and support at the institute for the administrative purposes.

I am thankful to my parents Shri Jitendra Kumar and Smt. Sushma Jha, and sister Wricha Jha for their blessings and unconditional support for bringing me to such level. Without their faith in me, I would not have been able to carry out this study.

Special thanks to Dr. Jew Das, Dr. Shivam, Dr. Uttam Puri Goswami, Dr. Ashutosh Sharma, Bhargava and Dr. Gilbert Hinge for providing crucial inputs during my research work. I am thankful to my lab-mates Vikas, Saket, Nikhil and Shivam Singh for their cooperation and support. I am grateful to the entire scientific staff of the Discipline of Civil Engineering who have always been helpful to me.

Finally, I am thankful to all who directly or indirectly contributed, helped and supported me.

Dedicated to my parents.

ABSTRACT

Novel approaches to assess the occurrence, distribution and dependence of climate extremes are required to understand their implications for risk and resilience. The complexity of climate systems, intricate ecosystem-climatic interactions, inter-dependence of the climate extremes and prevailing nonstationarity make the risk and resilience assessment a challenging task. Moreover, the risk due to extreme climatic events does not only depend on the magnitude of extremes themselves but also different components of risk, such as exposure and vulnerability. The risk reduction and adaptation to climate change are significantly dependent upon the accurate estimation of hazardous physical event and its interaction with exposure and vulnerability parameters such as population, infrastructure, environmental services and economic assets. Therefore, in context of climate change, a better understanding of the climate extremes in terms of their occurrence, dependence on different factors, dynamics and predictability is necessary to evaluate the implications for risk and resilience further. This thesis presents the study carried out to deliver a comprehensive assessment of extreme climatic conditions over India and their implications for risk and resilience.

The initial part of the thesis is devoted to explain the evolution of nonlinearity and determinism in the precipitation and temperature profiles in India during the past century. The investigation is carried out using Delay Vector Variance (DVV) approach, which allows the quantification of the nonlinear component in a time series based on the comparison of variance measures. The results show that both precipitation and temperature exhibit a high degree of nonlinearity and decreasing predictability, particularly in the extreme climate zones of the country.

In the second part, the evolution of climate extremes under the influence of global scales modes is analysed. To account for external forcings, the influence of El Nino Southern Oscillation (ENSO), Indian Ocean Dipole (IOD) and North Atlantic Oscillation (NAO) on extreme precipitation over

24 major river basins of India is estimated using the nonstationary extreme value analysis in Bayesian setting. It is found that extreme precipitation events in the country are dominated by these oscillations, most significantly in central India. Further, the stationary return levels are not reliable for the purpose of risk analysis as compared to their nonstationary counterparts.

The assessment of the occurrence of climate extremes is approached from a joint dependence perspective in the next part. A Copula based bivariate probabilistic study of the impacts of extreme climatic conditions on terrestrial ecosystem functioning is carried out. It is observed that the Croplands are most likely to be affected by drought-like conditions, which is of paramount concern for the country's food security. Further, possible lowering in soil moisture content could significantly alter the terrestrial ecosystem functioning in most parts of the country.

The final portion of the study is aimed at discussing a comprehensive framework for estimating the risk and resilience to extreme climatic conditions. Nonstationary return levels of annual maximum one-day rainfall and extremely long wet spells are estimated. These return levels, along with their uncertainty, are used to derive the hazard measures. These measures are combined with the exposure and capacity indicators to calculate the district-wise risk due to extreme rainfall. It is observed that one-third of India's districts are under high risk due to extreme rainfall. Further, the resilience of terrestrial ecosystems to withstand precipitation deficit is also estimated. It is observed that at least one-third area of 18 out of 24 major river basins are non-resilient to such extreme conditions.

LIST OF PUBLICATIONS

Journal papers published

- **Jha, Srinidhi**, Das, J., Sharma, A., Hazra, B., Goyal, M. K. (2019). “Probabilistic evaluation of vegetation drought likelihood and its implications to resilience across India.” *Global and Planetary Change*. (176), 23-35 (*Impact Factor: 4.448*)
- **Jha, Srinidhi**, Das, J., Goyal, M. K. (2019). Assessment of risk and resilience of terrestrial ecosystem productivity under the influence of extreme climatic conditions over India. *Scientific Reports*, 9(1), 1-12. (*Impact Factor: 3.998*)
- **Jha, Srinidhi**, Goyal, M. K., Das, J, (2020). Low-frequency global-scale modes and its influence on rainfall extremes over India: nonstationary and uncertainty analysis, *International Journal of Climatology* (*Accepted*)
- Das, J., **Jha, Srinidhi**, Goyal, M. K. (2019). Nonstationary and copula-based approach to assess the drought characteristics encompassing climate indices over the Himalayan states in India. *Journal of Hydrology*, 580,124356. (*Impact Factor: 4.500*)
- Sinha, J., **Jha, Srinidhi**, Goyal, M. K. (2019). Influences of watershed characteristics on long-term annual and intra-annual water balances over India. *Journal of Hydrology*, 577, 123970. (*Impact Factor: 4.500*)
- Das, J., **Jha, Srinidhi.**, Goyal, M. K. (2020). On the relationship of climatic and monsoon teleconnections with monthly precipitation over meteorologically homogenous regions in India: Wavelet & global coherence approaches. *Atmospheric Research*, 238, 104889. (*Impact Factor: 4.676*)

Journal papers under review

- **Jha, Srinidhi**, Das, J., Hazra B., Goyal, M. K. (2020). Assessment of nonlinearity and determinism in Indian climate using Delay Vector Variance approach. *Journal of Environmental Informatics (Under review)* (**Impact Factor: 4.604**)
- **Jha, Srinidhi**, Goyal, M. K., Gilleland E., Das, J. (2020). Extreme precipitation risk in India and the role of global climatic oscillations and local socio-economic factors under nonstationary setting *Journal of Hydrology (Under review)* (**Impact Factor: 4.500**)

Book chapters published

- Goyal, M.K., **Jha, Srinidhi**, Rao, Y. S. (2020), “Sustainable systems for groundwater resource management”, Chapter 25 in *Sustainability: Fundamentals and Applications*, Publisher: John Wiley and Sons Ltd., ISBN: 9781119433965
- Das, J., **Jha, Srinidhi**, Goyal, M.K., Rao, Y. S. (2020), “Challenges of sustainability in agricultural management”, Chapter 16 in *Sustainability: Fundamentals and Applications*, Publisher: John Wiley and Sons Ltd., ISBN: 9781119433965

TABLE OF CONTENTS

ABSTRACT	i
LIST OF PUBLICATIONS	iii
LIST OF FIGURES	ix
LIST OF TABLES	xv
NOMENCLATURE	xvi
ACRONYMS	xviii
GLOSSARY	xxiii
Chapter 1	1
Introduction	1
1.1 Climate change and variability	1
1.2 Climate extremes and their impacts	2
1.2.1 Climate extremes and their impacts in India.....	4
1.3 Assessment of extreme climate risk and resilience.....	4
1.4 Limitations and gaps in approaches for risk and resilience assessment	6
1.5 Objectives of the study	7
1.6 Organization of the thesis	8
Chapter 2	9
Literature review	9
2.1 Introduction.....	9
2.2 The predictability of Indian climate.....	9
2.3 Climate extremes: past and future.....	10
2.3.1 Rainfall extremes in India and its association with oscillations	14
2.3.2 Climate extremes and their influence on terrestrial ecosystems	17
2.4 Probabilistic and multivariate assessment of extremes.....	20
2.5 Nonstationary analysis of extremes.....	23
2.6 Extreme climate risk and resilience.....	26
2.7 Conclusions	29
Chapter 3	31
Predictability of temperature and precipitation in the past century	31
3.1 Introduction.....	31
3.2 Data and methodology	32

3.2.1	Precipitation and temperature data.....	32
3.2.2	Scaling properties and memory persistence	34
3.2.2.1	Generalised Hurst method.....	35
3.2.2.2	Detrended fluctuation analysis	36
3.2.2.3	Rescaled Range analysis	37
3.2.3	Analysis of nonlinearity and determinism	38
3.2.3.1	Delay Vector Variance method.....	38
3.2.3.2	Selection of embedding parameters	39
3.3	Results.....	40
3.3.1	Optimum embedding dimensions and time lag.....	40
3.3.2	Assessment of nonlinearity	46
3.3.3	Scale dependence and nonlinearity	56
3.3.4	Assessment of determinism	61
3.4	Discussions	67
3.5	Conclusions.....	69
Chapter 4	71
Low-frequency global-scale modes and their influence on rainfall extremes	71
4.1	Introduction.....	71
4.2	Data and methodology	72
4.2.1	Study area and data	72
4.2.2	Methods.....	75
4.2.2.1	Trend analysis of the extreme precipitation indices.....	75
4.2.2.2	Nonstationary modelling of extreme precipitation indices	77
4.2.2.3	Bayesian framework for parameter uncertainty	82
4.3	Results.....	84
4.3.1	Temporal variability of extreme precipitation	84
4.3.2	Parameters and their uncertainty	87
4.3.3	Return levels, magnitude and variability of extreme precipitation	89

4.4 Discussion.....	106
4.5 Conclusions.....	107
Chapter 5	109
Dependence of terrestrial ecosystem functioning on extreme climatic conditions	109
5.1 Introduction.....	109
5.2 Data and methodology	110
5.2.1 River basins of India and land cover types	110
5.2.2 Climate data	112
5.2.3 NDVI and NPP data.....	112
5.2.4 Copula based bivariate probabilistic model	113
5.3 Results.....	116
5.3.1 Selection of suitable thresholds.....	116
5.3.2 Risk to terrestrial ecosystem functioning	117
5.3.2.1 Impact on vegetation condition.....	117
5.3.2.2 Impact on net primary productivity	128
5.4 Discussions	135
5.5 Conclusions.....	137
Chapter 6	138
Risk and resilience to climate extremes: inferences from the analysis	138
6.1 Introduction.....	138
6.2 Data and Methodology.....	140
6.2.2 Methodology for extreme rainfall risk estimation	140
6.2.3 Methodology for terrestrial ecosystem resilience estimation.....	142
6.3 Results.....	144
6.3.1 Risk due to heavy downpour and extremely long wet spells	144
6.3.2 Resilience of terrestrial ecosystems to dry conditions	148
6.4 Discussions	151
6.5 Conclusions.....	153
Chapter 7	154
Conclusions and scope for future work	154

7.1 Summary	154
7.2 Future scope of work	157
REFERENCES	159

LIST OF FIGURES

Figure 3.1 Flowchart of the methodology	33
Figure 3.2 Location and details of demonstrating stations (blue triangles) and the coverage of districts used in this study (green dots). The boundaries of six different climatic zones have been given in red	34
Figure 3.3a Distribution of optimal time lag and embedding dimensions for precipitation in different time periods	41
Figure 3.3b Distribution of optimal time lag and embedding dimensions for temperature in different time periods	42
Figure 3.4ab District-wise spatial distribution of (a) embedding dimension and (b) time lag for temperature	43
Figure 3.4cd District-wise spatial distribution of (c) normalised RMSE and (d) normalised minimum target variance for temperature	44
Figure 3.5ab District-wise spatial distribution of (a) embedding dimension, (b) for precipitation	47
Figure 3.5cd District-wise spatial distribution of (c) normalised RMSE and (d) normalised minimum target variance for precipitation	48
Figure 3.6a DVV scatter plots for six districts in different time periods for precipitation	49
Figure 3.6b DVV scatter plots for six districts in different time periods for temperature	50
Figure 3.7a Distribution of normalised RMSE and normalised minimum variance values for precipitation in different time periods	52

Figure 3.7b Distribution of normalised RMSE and normalised minimum variance values for temperature in different time periods	53
Figure 3.8 Absolute percentage change in nonlinearity and determinism for (a,c) precipitation and (b,d) temperature	55
Figure 3.9ab Hurst exponents values for (a) precipitation and (b) temperature using generalised Hurst, rescaled range and detrended fluctuation analysis methods	57
Figure 3.9cd (c) and (d) represent the change in Hurst exponent ($H(q)$) with changing orders of moment (q) for precipitation and temperature, respectively	58
Figure 3.10a DVV plots for six districts in different time periods for temperature. Red and black lines denote target variance values for original and surrogate data sets	62
Figure 3.10b DVV plots for six districts in different time periods for precipitation. Red and black lines denote target variance values for original and surrogate data sets	63
Figure 3.11a DVV plots for two representative stations during (1901-1934), (1935-1968) and (1969-2002) for temperature. Red and black lines denote target variance values for original and surrogate data sets	64
Figure 3.11b DVV plots for two representative stations during (1901-1934), (1935-1968) and (1969-2002) for precipitation. Red and black lines denote target variance values for original and surrogate data sets	65
Figure 4.1 River basins and their IDs used in the study	73

Figure 4.2 Methodological flowchart	76
Figure 4.3a The spatial map of annual mean of extreme precipitation indices over 1951-2013	85
Figure 4.3b The spatial map of standard deviation of extreme precipitation indices over 1951-2013	86
Figure 4.3c The spatial map of trend significance (Z statistics) of extreme precipitation indices over 1951-2013	88
Figure 4.4a-i Spatial distribution of the mean parameter samples from the posterior distribution for Rx1day and SDII. Here, P1, P2 and P3 represent the location, scale and shape parameters respectively	90
Figure 4.4a-ii Spatial distribution of the mean parameter samples from the posterior distribution for R10 and CWD. Here, P1, P2 and P3 represent the location, scale and shape parameters respectively	91
Figure 4.4b-i Spatial distribution of the standard deviation of parameter samples from the posterior distribution for Rx1day and SDII. Here, P1, P2 and P3 represent the location, scale and shape parameters, respectively	92
Figure 4.4b-ii Spatial distribution of the standard deviation of parameter samples from the posterior distribution for Rx1day and SDII. Here, P1, P2 and P3 represent the location, scale and shape parameters, respectively	93
Figure 4.5a-i Spatial distribution of return levels both for the nonstationary and stationary cases for R10 at different return periods	96

Figure 4.5a-ii Spatial distribution of return levels both for the nonstationary and stationary cases for CWD at different return periods	97
Figure 4.5b-i Spatial distribution of return levels both for the nonstationary and stationary cases for Rx1day at different return periods	98
Figure 4.5b-ii Spatial distribution of return levels both for the nonstationary and stationary cases for SDII at different return periods	99
Figure 4.6a The nonstationary and stationary return levels of Rx1 Day for different return periods	100
Figure 4.6b The nonstationary and stationary return levels of SDII for different return periods	101
Figure 4.6c The nonstationary and stationary return levels of R10 for different return periods	102
Figure 4.6d The nonstationary and stationary return levels of CWD for different return periods	103
Figure 4.7a Spatial variability in the return levels for Rx1day and SDII. The variability is defined in terms of standard deviation over 1951-2013	104
Figure 4.7b Spatial variability in the return levels for R10 and CWD. The variability is defined in terms of standard deviation over 1951-2013	105
Figure 5.1. River basins IDs and details of Land Cover types considered for analysis	111
Figure 5.2 Methodological flowchart	114
Figure 5.3 Conditional likelihood of $n_{NPP} \leq 10^{th}$ percentile in different scenarios of S/P/T in nonmonsoon season to understand the best possible threshold of NPP and climatic data	118

Figure 5.4 Conditional likelihood of $n_{NPP} \leq 20^{th}$ percentile in different scenarios of S/P/T in nonmonsoon season to understand the best possible threshold of NPP and climatic data	119
Figure 5.5 Conditional likelihood of $n_{NPP} \leq 20^{th}$ percentile in different scenarios of S/P/T in monsoon season to understand the best possible threshold of NPP and climatic data	120
Figure 5.6 Conditional likelihood of $n_{NPP} \leq 20\%$ in different scenarios of S/P/T in monsoon season to understand the best possible threshold of NPP and climatic data	121
Figure 5.7 Conditional probabilities of $n_{NDVI} \leq 30^{th}$ percentile at (a) annual (b) nonmonsoon and (c) monsoon season scale	122
Figure 5.8 Percent areas of land cover types showing high likelihood risk for (a) NDVI-Soil Moisture Content, (b) NDVI-Temperature and (c) NDVI-Precipitation	125
Figure 5.9 Conditional probabilities of $n_{NPP} \leq 30^{th}$ percentile at (a) annual (b) nonmonsoon and (c) monsoon season scale	129
Figure 6.1 Overall methodology for estimating the risk due to extreme precipitation	143
Figure 6.2 Distribution of optimal covariate combination for location and scale parameters of NS-GEV models for (a,b) Rx1 day and (c,d) CWD indices. The x-axis labels represent the linear combination of individual, double and all three covariates	145

Figure 6.3 Distribution of districts under different classes of risk due under (a,b) nonstationary and (a,b) stationary scenarios	146
Figure 6.4 District-wise distribution of risk in (a,b) nonstationary and (c,d) stationary scenarios of extreme downpour (Rx1 day) and extremely long wet days (CWD)	147
Figure 6.5 Percentage of districts in different states at high risk due to heavy downpour and extremely long wet spells	148
Figure 6.6 Spatial distribution of resilience (R_i) values	149
Figure 6.7 Non-resilient area at (a) river basins and (b) vegetation types scales	150

LIST OF TABLES

Table 3.1 Number of districts in different ranges of m and τ	45
Table 3.2 Number of districts in different ranges of RMSE and minimum target variance	54
Table 3.3 Optimal embedding dimension, time lag, RMSE, minimum target variance and Hurst exponent measures of sample stations in different time periods for temperature data	59
Table 3.4 Optimal embedding dimension, time lag, RMSE, minimum target variance and Hurst exponent measures of sample stations in different time periods for precipitation data	60
Table 4.1 Description of the models used in the present study	79
Table 5.1 Area under high risk at annual scale in stressed climate at river basin level	124
Table 5.2 Vegetation area under high risk in nonmonsoon season in stressed climate at river basin level	126
Table 5.3 Vegetation area under high risk in monsoon season in stressed climate at river basin level.	127
Table 5.4 NPP area under high risk at annual scale in stressed climate at river basin level	130
Table 5.5 NPP area under high risk in monsoon season in stressed climate at river basin level	132
Table 5.6 NPP area under high risk in nonmonsoon season in stressed climate at river basin level.	133
Table 5.7 NPP area under high risk in different seasons and annual scale in stressed climate at LULC level.	134

NOMENCLATURE

$H(q)$	Hurst exponent
q	Order of moment
R_n	Range
τ	Time lag
m	Embedding dimensions
μ_d	Mean over Euclidian distances
σ_d	Standard deviation
σ_k^2	Target variance
μ	Location parameter
σ	Scale parameter
ξ	Shape parameter
θ	Parameter vector
$L(\theta)$	Likelihood function
p	Probability of occurrence
$\hat{\theta}$	Estimated parameter vector
F	Cumulative distribution function
C	Copula function
$Risk_D$	District-wise Risk index value

P_{DTR}	The hazard measure
P_{DCN}	The exposure measure (children population)
P_{DON}	The exposure measure (old population)
P_{DRA}	The vulnerability measure (road infrastructure)
P_{DEA}	The vulnerability measure (economic activity)
R_i	Resilience index
$NDVI_m$	Mean NDVI
$NDVI_d$	NDVI In the driest year

ACRONYMS

ACF	Autocorrelation Function
AR5	5 th Assessment Report
CASA	Carnegie–Ames–Stanford Approach
CL	Croplands
CNV	Cropland/Natural Vegetation Mosaic
CRU	Climate Research Unit
CWD	Consecutive Wet Days
DBF	Deciduous Broadleaf Forest
DFA	Detrended Fluctuation Analysis
DMI	Dipole Mode Index
DNB	Day/Night Bands
DNF	Deciduous Needleleaf Forest
DV	Delay Vector
DVV	Delay Vector Variance
EBF	Evergreen Broadleaf Forest
EFRGKB	East flowing rivers between Godavari and Krishna basins
EFRKPB	East flowing rivers between Krishna and Pennar basins

EFRMGB	East flowing rivers between Mahanadi and Godavari basins
EFRPCB	East flowing rivers between Pennar and Cauvery basins
EFRSCB	East flowing rivers between Subernrekha and Cauvery basins
ENF	Evergreen Needleleaf Forest
ENSO	El Nino Southern Oscillation
EOS	Earth Observation System
ESRL-NOAA	Earth System Research Laboratory of National Oceanic Atmospheric Administration
ETCCDI	Expert Team on Climate Change Detection and Indices
EVT	Extreme Value Theory
fBm	Fractional Brownian Motion
GDP	Gross Domestic Product
GEV	Generalized Extreme Value
GIMMS	Global Inventory Modeling and Mapping Studies
GL	Grasslands
GP	Generalized Pareto

iAAFT	Inverse Iterated Amplitude Adjusted Fourier Transform
IDW	Inverse Distance Weightage
IMD	India Meteorological Department
IOD	Indian Ocean Dipole
IPCC	Intergovernmental Panel on Climate Change
JAMSTEC	Japan Agency for Marine-Earth Science and Technology
LCI	Land Cover Institute
LR	Likelihood Ratio
LRD	Long Range Dependence
MCMC	Markov Chain Monte Carlo
MF	Mixed Forest
MK	Mann Kendall
MLE	Maximum Likelihood Estimation
MODIS	Moderate Resolution Imaging Spectroradiometer
MRFB	Minor rivers flowing into Bangladesh
MRFM	Minor rivers flowing into Myanmar
NAO	North Atlantic Oscillation

NDVI	Normalized Difference Vegetation Index
nllh	Negative Log Likelihood
NOAA	National Oceanic and Atmospheric Administration
NPP	Net Primary Productivity
NS-GEV	Nonstationary Generalized Extreme Value
R/S	Rescaled Range
R10	Number of days when rainfall is above 10 mm
RMSE	Root Mean Squared Error
Rx1 day	monthly maximum one day precipitation
SDII	Simple Daily Precipitation Intensity Index
S-GEV	Stationary Generalized Extreme Value
SPI	Standardised Precipitation Index
SRD	Sort Range Dependence
SST	Sea Surface Temperature
SVI	Standardised Vegetation Index
UN-OCHA	United Nations Office for the Coordination of Humanitarian Affairs
VCI	Vegetation Condition Index
VegDRI	Vegetation Drought Response Index

VIIRS	Visible Infrared Imaging Radiometer Suite
WG	Western Ghats
WS	Woody Savannas

GLOSSARY

Climate	Average weather conditions over a certain period, 30 years in general.
Climate change	According to the Intergovernmental Panel on Climate Change (IPCC), climate change can be defined as the alteration in the mean and/ or the variability in its properties for a long period of time, generally considered in decades.
Climate extremes	The occurrence of a value of weather or climate variable above or below a threshold value near the upper or lower ends of the range of observed values of the variable.
Climate risk	The likelihood of severe alteration in the normal functioning of a community or society due to hazardous climate events and their interaction with vulnerable socio-economic, environmental or material conditions.
Climate variability	Refers to the variation in the mean state and other statistics such as standard deviations, extremes of the climate at all spatial and temporal scale.
Determinism	Refers to a condition where evolution from one state to another is based on some set of know laws, equation or formulations.
Drought	a prolonged period of abnormally low rainfall, leading to a shortage of water.
El Niño-Southern Oscillation	The El Niño-Southern Oscillation is a recurring climate pattern involving changes in the temperature of waters in the central and eastern tropical Pacific Ocean which directly affects rainfall distribution in the tropics.

Exposure	The presence of people, livelihood, infrastructure, or economic, social or cultural assets in places that could be adversely affected by a climate hazard.
Hazard	The potential occurrence of a natural or human induced extreme climatic event that may cause loss of life, property, infrastructure and environmental resources.
Heat Wave	A period of abnormally high surface temperatures relative to those normally expected.
Indian Ocean Dipole	It is the difference in sea surface temperature between two poles- a western pole in the Arabia Sea and an eastern pole in the eastern Indian Ocean which contributes significantly to rainfall variability in the region in between.
Net Primary Productivity	Is the rate at which energy is transferred as biomass by autotrophs to the consumers in the terrestrial ecosystems . Alternatively, it can be defined as the rate of accumulation of biomass or energy.
Nonlinearity	A process is called nonlinear when there is no simple proportional relation between cause and effect.
Nontationarity	A time series is known to follow the principle of nonstationarity if the statistical characteristics of the distribution change with time.
North Atlantic Oscillation	It is a weather phenonom in the North Atlantic Ocean of fluctuations in the difference of atmospheric pressure at sea level between the Icelandic Low and Azores High.

Predictability	The extent to which the future states of a system may be predicted based on knowledge of current and past states of the system.
Resilience	The capacity of a system to anticipate, adjust, accommodate and recover from the impacts of a hazardous event
Return level	The return level is defined as a value that is expected to be equaled or exceeded on average once every interval of time.
Return period	An estimate of the average time interval between occurrences of an event of a given size or intensity.
Uncertainty	The degree to which a value or a relationship is unknown in form of quantifiable data errors, ambiguously defined concepts or terminology or uncertain projection of human influences.
Vulnerability	It refers to the degree to which people or things they are susceptible to damage or are unable to cope with, the adverse impacts of climate change.
Weather	State of atmosphere at a particular place or time with respect to wind, temperature, cloudiness, moisture, pressure etc.

Chapter 1

Introduction

1.1 Climate change and variability

The climate is usually defined as average weather conditions in terms of some statistical properties of variables such as precipitation, temperature or wind over a certain period of time. This particular period of time could range from months to hundreds, thousands, and millions of years. In general, a period of 30 years is considered for various statistical interpretations of the climate variables. The climate, in a broad sense, is the statistical accounting of the climate system. The climate system is composed of five main components – the atmosphere, hydrosphere, cryosphere, land and biosphere. This climate system is dynamic and is continuously changing due to several factors, such as internal and external forcings. The variations in the average state of different climatic variables at various temporal or spatial scale are called climate variability. These variations are basically anomalies or deviations from the average over a given scale of time (month, season or year). Whereas, climate change is a statistically significant deviation from the average state over a more extended period, preferably decades.

The human and natural climatic forcings induce internal variations in various components of the climate system of the Earth. The feedbacks which are generated by these are responsible, either for the intensifying or impairing the forcing. However, different components of the climate system respond differently to these forcings. This response time for the components such as land, atmosphere, ocean surface, vegetation and ice can range from hours to years. Similarly, the response time for the deep ocean, ice sheets, glaciers to exhibit the changes due to forcings can be 100 to 1000 years. Therefore, the Earth's climate system can take hours to centuries to respond to the external forcings.

The major reason, as suggested by the Fifth assessment report (AR5) affecting the climate system, has been the increasing concentration of the greenhouse gases causing global warming (IPCC 2014). The impacts of global warming can already be observed in the natural and human systems, which are of high interest. According to the Intergovernmental Panel on Climate Change (IPCC), climate change can be defined as the alteration in the mean and/ or the variability in its properties for a long period of time, generally considered in decades. The primary change is mainly due to a number of natural and anthropogenic factors. The natural factors may comprise of volcanic eruptions, ocean current changes, change in Earth's orbit, solar radiation variations and multiple internal variabilities. The major anthropogenic activity which defines the course of climate change has been burning of fossil fuels leading to an increase in greenhouse gas emissions. In this context, the IPCC's AR5 stated that 1983 to 2012, was most likely, the warmest 30 years' period in over the last 1400 years, particularly in the Northern Hemisphere. On average, the study of global temperature data set reveals that Earth in 2012 is 0.85 °C warmer as compared to 1880 (IPCC 2014).

1.2 Climate extremes and their impacts

Climate change has attracted much attention in the research community as the extreme behaviour of climate is more significant to human well-being than their average values. The changing climate conditions have led to changes in the intensity, duration, frequency and timing of unprecedented weather events. Primarily, extremes are defined in terms of changes in the location or the shape of probability distributions representing a climatic variable. However, some extreme events such as drought might not be directly represented by any extreme event, but, an accumulation of climatic events which are not extreme. Most of the extreme climatic events are considered as the result of natural climate variability along with the strong influence of increasing greenhouse gas emissions.

Extreme climatic events are rare, which means that the assessment of climate extreme is to be done by analysis limited quantity of data. In this sense, the rarer the event, the more difficult it is to identify its distribution and occurrence. However, more confident conclusions can be drawn by analyzing the changes in climatic extremes represented by those data which are available for a longer period of time. Based on such observations, it can be concluded that the number of cold days and nights have overall decreased and the number of warm days at a global scale has increased (Field et al. 2012). Medium confidence has been observed in the temperature extremes in the Asian continent. Further significant changes in the occurrence of heavy precipitation events have been witnessed in some parts of the world. Most of these changes have been in terms of an increase in the number of extreme precipitation events along with strong regional variations. Further, there are also evidences that climate factors have caused changes in the magnitude and frequency of floods and cyclones at the local scale (IPCC 2014).

With the occurrence of more extreme climatic events, the related disasters have also increased in terms of losses. These disasters have become more variable and significant in nature, leading to poor risk estimations. In general, the developed countries are likely to suffer more economic losses due to such events whereas, the risk to population in terms of fatalities and economic losses as compared to the proportion of gross domestic product (GDP) is higher in developing countries (Russo et al. 2015). According to the IPCC's special report on managing climate extremes, 95% of the fatalities from climate-induced disasters have occurred in the developing nations (Field et al. 2012). The exposure and vulnerability components of climate-induced disasters are the governing factors of the losses. Countries with an increasing trend in vulnerability and exposure elements tend to be at higher risk of damage. Proper risk estimation and assessment of extreme climatic events are necessary for deciding risk reduction strategies.

1.2.1 Climate extremes and their impacts in India

India's mean temperature has increased approximately by 0.7 °C in the past century (Hingane et al. 1985). The mean temperature over the country is projected to increase roughly around 4.4 °C as compared to 1976-2005 mean temperature (Krishnan et al. 2020). The increase in temperature over the past years can be observed in the projected frequencies of future warm days, warm nights and heatwaves. It is expected that summer heatwaves over India will increase by at least 3 times by the end of this century as compared to the 1976-2005 period (Krishnan et al. 2020). A similar trend is expected in the duration of summer heatwaves, however with more uncertainty in the estimates. Corresponding to the changes in temperature, the monsoon precipitation pattern has also changed particularly over the past 50 years (Guhathakurta and Rajeevan 2008). The frequency of dry spells has increased, and wet spells have become more intense (Singh and Ranade 2010). Moreover, the frequency of high rainfall intensities has increased by three-fourth during 1950-2015 (Roxy et al. 2017). Similarly, an overall decrease in the rainfall events has led to an increase in the propensity for frequent drought events in India. The later half of the 20th century has witnessed the increase in both duration and severity of the drought events (Samra 2004). In conclusion, the country has witnessed an increase in the mean temperature, decline in the monsoon rainfall and an increase in the extreme precipitation and rainfall events along with droughts. Most of this rise in the extreme climatic events have been attributed to the anthropogenic influence on climate systems. Since this anthropogenic influence is expected to become more significant in future; therefore, proper extreme climatic risk reduction strategies are required.

1.3 Assessment of extreme climate risk and resilience

As discussed, the extreme climate-related risks posing potential loss of property and lives have increased over the past. Researchers and policymakers around the globe agree that current adaptation and mitigation

policies might not be sufficient to deal with the implications of extreme climate. Therefore, a comprehensive climate risk assessment and management framework is required for minimizing the possible damage. This comprehensive risk assessment framework must be context-specific and should be able to produce region-based outputs. The risk due to extreme climatic events is governed by the driver hazard, exposure and vulnerability measure. The climate risk assessment involves the identification of the key components causing a high and low level of hazard. Moreover, the knowledge about a climatic hazard, variability and uncertainty in projections need to be taken into consideration. It is advisable to take the likelihood of severe disturbance in the normal functioning of the concerned subject as the measure of hazard. This hazard, when faced by a population with vulnerable socio-economic conditions, leads to high risk and subsequent loss of lives, property, economic and environmental impacts. By definition, a hazard is defined as the possible occurrence of a naturally occurring or human-influenced physical event which may cause the damages mentioned above. Whereas, the exposure denotes the presence of population, livelihood, ecosystem services, natural resources, infrastructure and property or social and economic assets, which could be possibly damaged due to the hazard. Under the exposed scenarios, the severity and level of the adverse impacts due to extreme climatic events depend on the socially governed circumstances known as vulnerability. In general, vulnerability is defined as the tendency to be severely impacted. This tendency, of course, is a characteristic of the exposed element. Particularly, in the extreme climate disaster risk estimation concept, the vulnerability is related to the properties of the concerned population and their ability to cope, resist and recover from the impact. More precisely, the vulnerability can be defined as the varied historical, economic, social, environmental, ecosystem services, governmental and institutional conditioning of the population which is under the influence of the possible extreme events.

Resilience is defined as the ability of a system to absorb, resist and recover from the perturbation caused by any disturbing event. In the context of climatic extremes, the resilience can be referred to as the ability of a system to absorb or recover from the shock of events such as floods, droughts, fires, cyclones and rising sea levels. Over the years, it has been observed that the economic losses due to natural calamities have been increasing. This also points out the fact that extreme climatic events are more severely hitting the poorest and those with high vulnerability. One of the major tools to minimise such losses is to increase the resilience of a highly vulnerable population. This requires a proper assessment of risk and innovative and effective response measures for adaptation. In recent contexts, the increasing risk of extreme climatic events has made us realize that existing vulnerability reduction and adaptation strategies are not up to the mark. Improving the resilience requires ensuring renovation and development of existing and new assessment techniques, infrastructural upgrading, institutional and policy interventions, and efforts at the individual levels.

1.4 Limitations and gaps in approaches for risk and resilience assessment

An ideal comprehensive extreme climate risk management approach should focus on instantaneous as well as the long term extreme climatic events. Therefore, the risk reduction strategy requires long term as well as short term goals. A top-down approach based on expert-to-individual based mechanism could play an important role in such cases. In this context, accurate extreme climate risk assessment is necessary. The likelihood of extreme events, generally, is denoted by the return period, which is the expected duration between two events of concern. These time intervals or return periods are inversely related to the annual exceedance probability, which is the likelihood of the event exceeding given magnitude in a particular year. The frequency of events which actually show a longer return period might not be reliable. Other climate data sources such as paleoclimate data denote that existing climate variables data might not

completely incorporate all aspects of natural variability (Zorita et al. 2003). Further, the stationary assumptions in existing practices might not be sufficient as the statistical characteristics of the climatic variables are not constant over the period of time. Therefore, improving qualitative methods for estimating the extreme climatic hazard requires acquiring suitable observational data, proper idea about the system's interconnections, incorporation of the natural and human factors, and estimation of uncertainties in the projected probabilities. Once this is achieved, inclusive estimates of the vulnerability and exposure elements combined with the hazard measure can be utilized for estimating proper risk and resilience. The complexity of climate systems, ecosystem-climatic interactions, interdependence of the extremes make the risk estimation and assessment process intricate. Further, the risk due to extreme climatic events does not only depend on the magnitude of extremes themselves but also different components of risk, such as exposure and vulnerability. The risk reduction and adaptation to climate change are significantly dependent upon the accurate estimation of hazardous physical events and their interaction with exposure and vulnerability parameters. Therefore, in context of climate change, a better understanding of the climate extremes in terms of their occurrence, dependence on different factors, dynamics and predictability is necessary to further evaluate the implications for risk and resilience in India.

1.5 Objectives of the study

The objectives of the study are as follows:

1. Assessment of the predictability of precipitation and temperature profiles in India in the past century.
2. Understanding the role of nonstationary global scale modes and its influence on extreme climate in India.
3. Probabilistic analysis of the dependence of ecosystem functioning on extreme climate.

4. Risk and resilience to extreme climate conditions: towards a comprehensive framework

1.6 Organization of the thesis

Literature relevant to various aspects of climate change, nonlinearity and predictability, the nonstationary influence of natural factors, the impact of extremes on terrestrial ecosystem functioning and existing practices in risk and resilience estimation are concisely reviewed in Chapter 2.

Chapter 3 discusses the detailed theory, methodology, results and discussion obtained from the first objective, i.e. assessment of nonlinearity and determinism in temperature and precipitation profiles in the past century in India. The study has been done by analyzing the district-wise profiles of climate data, and the degree of predictability was identified.

In Chapter 4, the influence of global scale modes on climate extremes in the country is investigated. The return levels of extreme precipitation indices in the stationary and nonstationary setting are estimated and characterised on the river basin scale. Further, the uncertainty in return levels is also estimated by using the Bayesian framework.

Chapter 5 discusses the joint dependence of extreme climatic variables and the ecosystem functioning parameters. The implication in terms of droughts are evaluated, and the impacts of extreme climatic condition on vegetation condition and ecosystem functioning have been recorded.

Chapter 6 provides a detailed analysis of the risk and resilience to extreme climatic conditions and discusses a possible framework for risk management and reduction. The risk due to extreme precipitation and droughts is discussed, and resilience of terrestrial ecosystems in recovering from hydroclimatic disturbances is estimated.

Chapter 7 presents the summary and conclusions of the work described in the thesis.

Chapter 2

Literature review

2.1 Introduction

Climate extremes are expected to have serious implications for risk and resilience. The subsequent sections in the chapter explain the physical understanding of climate extremes, past and future changes in extremes, probabilistic and multivariate approaches of understanding the extreme climate-induced hazards, the importance of nonstationarity and concept of risk and resilience. The chapter concludes with an outlook that explains the outputs of literature review in the context of the thesis objectives.

2.2 The predictability of Indian climate

Indian climate is extremely diverse and is influenced by a large number of factors (Rajeevan et al. 2012; Niranjan Kumar et al. 2013). Rainfall on Indian landmass is primarily contributed by the southwest monsoon, which is enormously vital for millions of people living in the Indian subcontinent (Kumar et al. 2005). Although the inter-annual variations in monsoon rainfall over the country are only about 10% of the long-term average, the nature of extremes in rainfall results in floods and droughts and can cause large scale economic and human losses (Shukla and Mooley 1987). It is well documented that variability of seasonal rainfall over India is associated with sea surface anomalies in the tropical Pacific Ocean, such as those related to El Niño and Southern Oscillation (ENSO), in the Indian Ocean, such as the Indian Ocean Dipole (IOD) and the Arabian sea (Rajeevan et al. 2012; Azad and Rajeevan 2016). These agents, in combination or independently affect the moisture transport dynamics, which in turn induces variability in precipitation patterns. For instance, Izumo (2008) discussed that a fall in Somalia-Oman upwelling supports the monsoon rainfall along the western coastal plains of India by intensifying the SST and hence, improving moisture transport towards the country. Shukla and Huang (2016) found

that pre-monsoon conditions in the Arabian sea may have significant implications for monsoon rainfall. The limitations and problems associated with existing modelling approach have been discussed in several studies which call for exploring alternative approaches for achieving better predictability of Indian monsoon rainfall (Kang et al. 2002; Rajeevan and Nanjundiah 2009).

Similarly, temperature over India is also highly variable due to natural as well as human influences (Gadgil and Dhorde 2005; Kothawale and Rupa Kumar 2005). Kothawale et al. (2010) found that ENSO has a significant influence on the temperature profiles over India. The change in diurnal temperature in north-east India was attributed to a decrease in sunshine duration in the region (Jhaharia and Singh 2011). (Arora et al. 2005) studied the trends of temperature in India and found that the change is temporally as well as spatially variable. The nonlinearity of precipitation and temperature over the country lead to poor risk assessment. In the context of climate change, better predictability of precipitation and temperature is necessary for accurate forecasting of extreme events and related risks

2.3 Climate extremes: past and future

The Fifth Assessment Report of the IPCC differentiates between the extreme weather and climatic event by describing a weather event as a rare event occurring at a particular time and place (Field et al. 2012). However, an extreme climatic weather event has been explained as the pattern of such events persisting for some time or season. There are many approaches available to investigate extreme climatic events. For instance, considering the record-breaking events (Coumou et al. 2013; Beniston 2015), deriving extremes from the percentile-based approaches (Russo et al. 2015; Schär et al. 2016), or utilising the extreme value theory to estimate the return levels of particular events. For understanding specifically, the extreme behaviour of temperature and precipitation, the Expert Team on Climate Change Detection and Indices (ETCCDI) came up with a set of extreme climate

indices which have been comprehensively utilised in a variety of studies around the world (Sillmann et al. 2013; Zhang and Zwiers 2013; Tebaldi and Wehner 2018). Many of the indices described by ETCCDI are comparatively moderate; however, further analysis, such as calculating the return levels on the block maxima data can be used to derive more extreme indices. Conventionally, the return level approach has been utilised to infer extreme climate data for temperature and precipitation extremes (Zhang et al. 2011; Ali et al. 2019; Ben Alaya et al. 2020).

The outputs from the studies based on observational data suggest, in high confidence, that high-temperature extremes have increased and low-temperature extremes have decreased after the 1950s globally (Field et al. 2012). At the continental level, the results show that such changes have occurred in most of the regions in North America, Europe, Asia and Australia (Portmann et al. 2009). However, the confidence in such inferences is lower in the case of the African and the South American continents. This low confidence or higher variability in these regions is primarily due to the low availability of accurate climate data. The study indicates that most of the land surface areas in the world depict rising occurrences of warm nights and declining cold nights. Similarly, the same areas show a rising occurrence of warm days and declining cold days apart from a few regions in the North and South America. Further, several studies suggest that this rise and fall in the extremes is mostly due to climate change rather than the influence of internal variability (Portmann et al. 2009; Fischer et al. 2014; Kim et al. 2016).

Apart from the observed data, the historical climate model simulations also confirm the extreme warming and cooling trends in the past (Sillmann et al. 2013). The model generated data, as opposed to the observed data sets, are more homogenous in nature. However, simulated data may lead to some inconsistencies in the climate estimates. For instance, most climate model data denote a rising occurrence of more severe hot extremes over the eastern part of the United States which is not valid for extremes derived from the

observed data (Dittus et al. 2018). Further, the Coupled Model Intercomparison Projects Phase 5 (CMIP5) data also reveal different behaviour of cold extremes as compared to the observational estimates (Field et al. 2012). The study also suggests that the alterations in the precipitation extremes are usually more spatially varied relative to the temperature extremes. The results obtained from the climate model simulations of the historical extremes also suggest rising rainfall extremes due to growing greenhouse gas emissions (Min et al. 2011). The observational data and the climate simulations represent a similar trend of rainfall extremes; however, the pattern represented over the land areas may vary. This is not surprising, as the regional trends, in general, are more significantly governed by the internal variability (King et al. 2015). As the increase in temperature trend has been recorded, it is expected that the heat stress might also increase. Moreover, regional heat stress is more affected by local humidity characteristics. Willett and Sherwood (2012) showed that even if the humidity is less in some regions, more intense heat stress can be still be observed. Moreover, Knutson and Ploshay (2016) suggested significant evidence of the role of global climate change in summer heat stress. The changing extreme climatic conditions have also impacted the occurrence of droughts. The drought events derived from the famous indices like Standard Precipitation Index (SPI) and Palmer Drought Severity Index (PDSI) reveal that the droughts events have been increasing globally (Sheffield et al. 2012). However, these indices often involve simplification of the physical processes, for instance, the evapotranspiration, which may lead to inaccuracies in the results. In the context of dry periods, the investigation of consecutive dry days (CDD) from the observation-based data reveals that there has been no significant trend. However, the results from the gridded data set indicate an increase in the dry durations in Africa and both North and South America after the 1950s (Donat et al. 2013).

The previously mentioned studies discussed the trend of past climate extremes. Moreover, understanding the future patterns of climate extremes

is equally important for proper risk estimation. The general circulation models (GCMs) are one of such sources which can be used to understand the future propagation of extremes. The mean projected warming in different Representative Construction Pathways (RCPs), by the end of 2099 as compared to 1986-2005, are given as 0.3°C -1.7°C (RCP 2.6), 1.1 °C - 2.6 °C (RCP 4.5), 2.6 °C - 4.8 °C (RCP 8.5) (Field et al. 2012). The results from CMIP5 simulations, in general, indicate a local rise in the intensity of temperature extremes with global warming (Seneviratne et al. 2016). Moreover, the trend in intensity appears to be stronger in the land areas than the oceans and vary significantly over different geographical areas. The cold temperature extremes, for instance, annual daily minimum temperature has increased over the northern part of the world. Whereas, the hot extreme, for instance, the daily maximum temperature has risen in most continents of the world (Dwyer and Cummer 2013). Analysis of temperature extremes derived from the percentile or heatwaves, in particular, suggest that warm days and warm nights may significantly increase in the tropics and subtropics (Russo et al. 2015). Precipitation extremes, as presented by the annual maximum 1-day precipitation (RX1day), are predicted to strengthen with the increasing average temperature in most parts of the world, excluding some subtropical regions (Min et al. 2011). Most of the regions indicate a rise in extreme rainfall; however, the results obtained from different models do not conclude the same (Pfahl et al. 2017). Further, the extremes in rainfall, as represented by the ETCDDI indices are mainly capable of daily, monthly or annual extremes are not suitable for representing the sub-daily extremes which are often a result of local processes as such as storms. The future projections of such extremes indicate that sub-daily extremes are expected to increase with rising average warming conditions (Martel et al. 2020).

2.3.1 Rainfall extremes in India and its association with oscillations

India's economy is mainly dependent upon the performance of summer monsoon, which accounts for nearly three-fourth of the annual rainfall (Kumar et al. 2010; Yadav 2013). The analysis of historical data suggests that the rainfall has remained stable over the past century. However, with the rise in global average temperature, the extreme events have also been rising (Goswami et al. 2006). Moreover, any significant long-term trend in the rainfall has not been recorded, but there exists inter-decadal variability in the monsoon rainfall (Goyal 2014). India, in the past, has witnessed several heavy rainfall events due to the underlying variability in southwest summer monsoon rains. For instance, in August 2019, a series of floods hit nine states in India, causing massive loss of lives and property. Over 40 million people were affected by widespread flooding in the Indian subcontinent during 2017, as suggested by the United Nations Office for the Coordination of Humanitarian Affairs (UN-OCHA) report (UN 2017). It was found that floods attributed to heavy rainfall events have caused a loss of \$3 billion in 2015 (Benfield 2017). The International Disaster Data Base (<http://www.emdat.be>) suggests that 268 major flooding events occurred in India during 1950-2015 costing 69,000 lives, making 17 million people homeless and affecting 825 million people. Roxy et al. (2017) found that there has been a threefold increase in the extreme rain events over India during 1950-2015. This indicates that extreme rainfall events have increased over time, and there is an urgent need to investigate the dynamics of their occurrence and their role in augmenting risks. There is a consensus among researchers that global climate change is altering extreme rainfall in India and which has given rise to environmental, economic and social risks (Singh and Ranade 2010; Krishnan et al. 2020). Therefore, a comprehensive analysis of the past rainfall extremes can aid to formulate strategies supporting mitigation, adaptation and preparedness measures in the context of both present and future climate-induced disasters. In the context of India,

there is enormous variability in the flood risk factors and studying the changes in heavy rainfall events is crucial from the perspective of extreme rainfall-induced disaster risk reduction. Heavy rainfall extremes could be a result of external forcings which include both human-induced and natural activities or/and internal forcings such as internal mechanisms within the climate system (IPCC 2014). However, there exists substantial debate in the recent literature about spatio-temporal distribution of extreme rainfall events over India and their relationship with various aspects of global climate change. For instance, Kulkarni (2012) suggested that there is a rising trend in rainfall extremes co-occurring along with decreasing moderate rainfall causing insignificant overall trend. However, percentile-based frequency and intensity analysis of extreme rainfall events showed no visible spatially uniform trends over India (Ghosh et al. 2012). These conflicting conclusions about extreme rainfall events in current research point out the necessity of a comprehensive evaluation of rainfall extremes.

Many studies have established that there is a significant association between the large-scale oscillations and regional or local precipitation extremes (Bracken et al. 2018; Das et al. 2019). The qualitative and quantitative assessment of the association between the climatic oscillations and heavy rainfall, in particular, could deliver an essential understanding of flood hazard prevention, mitigation and enhance the flood management strategy (Ward et al. 2014). Several oscillation indices have been extensively investigated to understand the variability of hydrological extremes. El Nino Southern Oscillation (ENSO) index is known to dominate the interannual variability of rainfall over Indian landmass (Gadgil et al. 2004; Azad and Rajeevan 2016). Yadav et al. (2009) suggested that there is an increasing influence of ENSO on winter precipitation in north-west India. Further, it has been found that the association between ENSO and north-east monsoon has become stronger over time (Kumar et al. 2007). However, the regional association between ENSO and Indian rainfall is strengthening as some studies show that global warming might have weakened the same (Kripalani

et al. 2003; Sooraj et al. 2015). Ashrit et al. (2001) recommended that the interannual correlation between ENSO and Indian summer monsoon rainfall might lead to reduced rainfall. Another critical sea surface temperature (SSTs) pattern, which affects the regional monsoon pattern in India is the Indian Ocean Dipole (IOD). Also, the IOD, often treated as a counterpart of ENSO, is a measure of the difference between SSTs between two 'oceanic poles' (the Arabian Sea and Eastern Indian ocean). Mishra et al. (2012) suggested that IOD variability during monsoon month induces significant changeability in the rainfall pattern over India. It has been found that positive IOD has enhanced precipitation in northern India (Behera et al. 2013). Such oscillations not only act independently to affect the regional precipitation patterns but also in combination to complicate the prediction process. For instance, it has been noted from the investigation of various SST anomalies that strong IOD events in the past might have resulted in the weakening of ENSO-monsoon relationship (Guan et al. 2003; Ashok et al. 2004). A critical phenomenon incorporating the teleconnection patterns in the pressure at sea level and the surface temperature is known as North Atlantic Oscillation (NAO) which also affects the monsoon activity over India. It has been observed that the NAO index measures in April are inversely related to the monsoon rainfall (Dugam and Kakade 1999; Kakade and Dugam 2000). Kar and Rana (2014) suggested that moisture transfer from the Arabian sea during active NAO phase and the presence of cyclonic anomaly causes heavy rainfall over north-west India. Similarly, NAO during winter months was found to be one of the primary reasons for variation in precipitation in the north-west Himalaya (Bhutiyan et al. 2010). Roy (2011) observed that the NAO had a major role in governing the regional precipitation during the peak rainy seasons and concluded that NAO had pronounced effect over most of the regions in the peninsular India. In light of the above discussion, it is worth considering that ENSO, IOD and NAO are amongst the important large-scale climatic factors governing rainfall pattern over India. In context of risks due to heavy precipitation

events, a comprehensive evaluation of the influence of ENSO, IOD and NAO over historical precipitation extreme events is necessary.

2.3.2 Climate extremes and their influence on terrestrial ecosystems

Climate change is one of the main factors which disturbs terrestrial ecosystem functioning (Hinzman et al. 2005; Grimm et al. 2013). Global warming may result in the intensified hydrological cycle, which can further give rise to more extreme events (Huntington 2006; Dai 2011). Dai (2013), from the analysis of soil-moisture, drought indices and precipitation-evaporation patterns, suggested that the chances of drought have increased in this century. Drought, which arises because of the long-term deficit in water availability, is an integral part of terrestrial ecosystem-climate interaction. A prolonged drought period influences the feedback processes between soil and atmosphere, resulting in a decline of soil moisture content. Plants depend solely on soil moisture to fetch required water for photosynthesis, which further controls the stem-water dynamics, stomatal regulation and transpiration losses (Bréda and Granier 1996). Moreover, the investigation of climate impact on terrestrial ecosystems needs the understanding of soil moisture conditions and variability associated with it (Brunner et al. 2009). Long term precipitation deficit and high-temperature cause an increase in atmospheric water demand which results in the depletion of moisture content in the root zone depth. This has the potential of severely impacting the terrestrial ecosystem functioning, especially because climate warming may result in more variable precipitation and evapotranspiration (Huntington 2006). A critical study by Allen et al. (2010) identified the increased risks of vegetation mortality due to soil moisture droughts and rising temperature. Several other studies can be referred, which underline the detrimental impact of drought on terrestrial ecosystem functioning in terms of vegetation distribution and growth (Peters et al. 2002; Wan et al. 2010; Vicente-Serrano et al. 2013). There are significant problems related to the assessment of the impact of extreme

climatic conditions and their impact on vegetation. Quantification of drought characteristics is difficult as we primarily identify droughts by its impact on different systems. Moreover, it is intricate to identify the starting and terminating point of a drought span (Nagarajan 2009). The complex nature of climate extremes introduces various elements of uncertainties in the response of different terrestrial ecosystem types (Vicente-Serrano et al. 2012). For instance, Zhang et al. (2017) in their work, suggested that it is essential to incorporate the duration, distribution, trends and severity as well as their complex interactions. Further, the assessment is constrained as the terrestrial ecosystem response to drought disturbances is a function of both vegetation type and climate conditions (Wu and Chen 2013). Sharma and Goyal (2017), in a comprehensive study of the impact of hydroclimatic disturbance on ecosystem resilience, found that every vegetation type, climate zone and river basin has a unique response to the extreme climate conditions which should be considered while studying the ecosystem-climate interactions.

Normalised difference vegetation index (NDVI) is one of the most frequently used vegetation index to assess the terrestrial ecosystem functioning. Li et al. (2010) suggested that a significant correlation exists between NDVI and different eco-climatic parameters for different vegetation types. Assessment of NDVI and climate variables may provide useful insights into the key factors which control changes in terrestrial ecosystems (Okin and Dong 2018). However, the mechanism of terrestrial ecosystem response to extreme climate disturbances is still unclear. Moreover, most of the studies about terrestrial ecosystem functioning and extreme climate are focused around analysing the characteristic of individual variables or indices. In relation to the studies involving the impact of extreme climatic conditions on terrestrial ecosystems, NDVI at times has been directly compared to precipitation or the drought indices (Mohler et al. 1986; Tucker and Choudhury 1987; Tucker 1989). Later, Vegetation Condition Index (VCI), Standardised Vegetation Index (SVI)

and Vegetation Drought Response Index (VegDRI) were derived to understand the vegetation drought dynamics (Peters et al. 2002; Brown et al. 2008; Sahoo et al. 2015). However, like any other indices, vegetation indices are also sensitive to environmental conditions which can result in misinterpretation of terrestrial ecosystem response to extreme climatic conditions. They provide a robust description of vegetation condition, but might not be sufficient in understanding the mechanism of extreme climate-related stresses on terrestrial ecosystem functioning (Brown et al. 2008).

Similarly, Net primary productivity (NPP), a key indicator of ecosystem functioning, is the rate at which energy is transferred as biomass by autotrophs to the consumers in the terrestrial ecosystems. Change in climatic conditions directly influence the NPP occurrence and distribution (Liang et al. 2015). Analysing the response of NPP to change in the extreme climatic conditions provides an insight into the risk and resiliency of the terrestrial ecosystem (Yin et al. 2018b). For instance, Grimm et al. (2013) found that change in climatic conditions results in biome shifts, forest growth and mortality, and ecosystem state changes which in turn contribute to the alteration in NPP. Pan et al. (2015) demonstrated that variation in the NPP in different regions of the world is attributed to variability in precipitation, temperature and several climatic factors. In a recent study, it was found that quantification of spatio-temporal variability in NPP is essential in determining how the ecosystem may respond to future changes in climate and land use (Gu et al. 2017). Conventional analysis of the climate-controlling factors on terrestrial ecosystem productivity involves the investigations based on the long-term variability in mean temperature and precipitation and their relationship with NPP. In relation to climate-ecosystem interactions, ecosystem functioning indicators such NPP and CO₂ fluxes at times have been directly compared to climate indices (Tucker and Choudhury 1987; Ji and Peters 2003; Wu et al. 2015) However, these studies, although, provide a robust description of ecosystem state, are often insufficient in understanding the mechanism of risks generated due to

climatic condition (Brown et al. 2008). Also, the interaction of climate-soil-plant systems for energy and material exchange is complex and involves many hydrological and biogeochemical processes (Zhao et al. 2018a). The dependence of NPP and mean annual precipitation has been widely studied in the past (La Pierre et al. 2011; Reichmann et al. 2013). A study by Hoepfner and Dukes (2012) indicates that the NPP is significantly related to the global temperature anomalies and there is substantial evidence of the linkage between NPP variability and temperature changes across different ecosystems in multiple climate zones (Gillman et al. 2015; Chu et al. 2016). Miranda et al. (2009) advocated that lower water availability significantly alters the vegetation cover and its productivity. A recent study by Zhao et al. (2019) indicates that that water-carbon cycle is closely coupled and water availability plays a crucial role in determining the distribution of NPP in a region. Sinha et al. (2019) pointed out that the water balance of a catchment is influenced by changes in vegetation and remains intricately coupled with several other regional characteristics. Water availability, especially for the rainfed agroecosystems need to be properly understood and managed to meet food security and climate change problems (Qiu et al. 2018).

2.4 Probabilistic and multivariate assessment of extremes

The last section of the chapter discussed the past and future of climate extremes using different indices, observational sources and model data sets. In this section, probabilistic as well as the multivariate assessment of extremes has been discussed. There are many methods which allow us to estimate the probabilistic characteristics of the extreme events, including parametric, non-parametric, stochastic methods and the Extreme Value Theory (EVT). The concept of the parametric method involves fitting specific distributions to given returns. This approach is also known as the percentile-based approach or the return period method (Hobaek et al. 2015). The main disadvantage of this method is that the estimated returns are incapable of incorporating the tail behaviour, often asymptotic, and cannot be used to produce estimates beyond the sample range. Further, the

stochastic approaches produce recurrent conditions which yield return periods based on the random traction from probabilistic projections (Goldstein et al. 2003). Also, these methods consider the Gaussian case; therefore, they do not accommodate the tail complexities. The EVT methods have been formulated particularly to incorporate the tail behaviour of the data (Naveau et al. 2005).

There are many studies which demonstrate the usability of EVT models in analysing the extremes. Towler et al. (2010) modelled the hydrologic and water quality extremes in changing climatic conditions using the EVT. Zamani et al. (2016) analysed the influence of precipitation deficit on atmospheric droughts in Belgium and established that EVT allowed inferring the dependence for even those points where data was scarce. In another important study, Gross et al. (2018) confirmed that daily temperature variability and their extreme values are sensitive to the data choices. Therefore, assessment of the alterations in temperature extremes should be performed with proper verification of the data choice. Further, EVT was utilized to find the trend and uncertainty in future extreme precipitation indices in a river basin under different warming scenarios (Thasneem et al. 2019). Similar to the above studies; there are several other works which show the applicability of the univariate probabilistic EVT approach in analysing extreme indices. These include, but are not limited to Lazoglou et al. (2019), Ragno et al. (2019), Ban et al. (2020), O'Sullivan et al. (2020), Whan et al. (2020).

The extremes have been discussed in the context of single variable extreme events, however, the joint occurrence of extremes can have a more devastating impact on the natural and human systems. For instance, the joint occurrence of high wind speed and high rainfall could lead to more catastrophic damage as compared to their individual occurrences (Yang and Qian 2019). Analysing the multivariate nature of climate extremes is a very intriguing field of research. The investigations of multivariate extremes first need the detection of the most important variables and then the assessment

of the correlation between these drivers. The estimation of the likelihood of joint extremes is highly sensitive to the dependence structure between the associated variables (Masina et al. 2015). A most significant problem, in this context, is the availability of adequately long data (Davison and Huser 2015). Generally, estimating the dependence of different spatiotemporal varying extreme variables require prior experience or knowledge about the process (Zscheischler et al. 2014; Sippel et al. 2018). For example, the compound drought and heatwave occurrences might be exclusively dependent on the seasonal properties of the existing weather conditions (Zscheischler et al. 2014). Further, the nonlinear interdependence and complexity of natural systems may lead to poor estimation of the association between the associated variables. The nature of dependence between two variables makes the return period sensitive, and this might lead to uncertain risk estimates. In addition, most of the conventional statistical and empirical approaches are formulated based on the assumption of stationarity, scale invariance which is not suitable in climate change studies (Khaliq et al. 2006; Sivakumar 2017).

The Copula is a useful tool to model multivariate distribution among random variables and is independent of individual probabilistic specifications (Sklar 1959). Copulas are capable of, up to a very good extent, capturing the nonlinear dependence between the selected variables (Hobaek et al. 2015; Nguyen-Huy et al. 2019). Copulas have been widely utilized in a variety of fields such as finance (Chiou and Tsay 2008; Ning 2010), hydrology (Zhang et al. 2012; Chen et al. 2016), signal processing (Iyengar et al. 2009; Lasmar and Berthoumieu 2014), medical (Winkelmann 2012; Emura and Chen 2018), climate studies (Jhong and Tung 2018; Yin et al. 2018a). Studies support the idea that Copulas provide a robust methodology for studying hydro-climatic events (Kao and Govindaraju 2010; Zhang et al. 2013). Copula was utilized in studying the concurrence of climate extremes during the California droughts (AghaKouchak et al. 2014). The study discussed a possible replicable methodology for risk

assessment for associated climate extremes such as floods and storms, droughts and extreme temperature. Li et al. (2015) explored the applicability of Copula in crop meteorological drought risk and found that the joint probabilistic approach offers greater versatility in the estimation of risk and associated uncertainties. Recently the joint behaviour of temperature and precipitation extremes was modelled using multivariate Copula approach, and it was concluded that the method is suitable for quantifying the dependence between extremes (Lazoglou et al. 2019; Mesbahzadeh et al. 2019; Mirakbari et al. 2020).

2.5 Nonstationary analysis of extremes

Most of the univariate and multivariate techniques associated with the analysis of extreme climatic conditions are based on the assumptions of stationarity. However, due to the significant impact from the anthropogenic and natural activities, the stationary assumption in extreme climate risk management and planning is not suitable (Milly et al. 2015). Therefore, in the prevailing adverse consequences of climate change, implementation of non-stationarity to model the extreme events of the climatic variables has gained popularity with the advancement of the computational facilities. Hence, recent studies aim at the inclusion of nonstationary approach in climate change analysis. For example, Katz et al. (2002) discussed the application of statistics for physically meaningful and improved analysis of the extreme climatic applications. These developments primarily relate to the maximum likelihood (ML) estimation of the parameters in the presence of physical covariates. Authors also illustrated the application with examples which include maximum precipitation and streamflow considering the trends and dependence structure with atmosphere-ocean circulation (El Niño phenomenon). Sugahara et al. (2009) modelled the historical (1933-2005) extreme precipitation over Sao Paulo, Brazil, under the nonstationary approach. The extracted extreme precipitation series using the peak over threshold (POT) method were fitted to the General Pareto distribution (GPD). The parameters of the GPD were computed

using the ML method. Keeping the shape parameter constant they used the annual cycle, and linear trend as time-varying covariates to examine the non-stationarity in extreme precipitation by constructing four different GPD models. Authors used the rescaled Akaike Information Criterion (AIC) with second-order bias correction as evaluation criteria to identify the best model among the four models. Based on the criteria, a model with a linear trend in scale parameter was considered as the best model. The result showed a significant increase in magnitude and frequency of high quantiles of daily rainfall (e.g. 40 mm increase between 1933 and 2005) in the city. Sillmann et al. (2011) examined the non-stationarity in monthly minima of European winter fitting the 6-hourly minimum temperature with General Extreme Value (GEV) distribution and considering North Atlantic atmospheric blocking as a covariate. The covariate was applied to the location and scale parameters of GEV distribution, and the model was able to improve the fitting of extreme minimum temperature in large regions of Europe. Based on the analysis, high quantiles of minimum temperature showed a decreasing trend. However, the cooling effect of the atmospheric blocking in future climate scenarios is weakened due to the enhanced greenhouse gases, and thus decreases the probability of occurrence of very cold winter in north-eastern parts of Europe. Westra et al. (2013) inspected the presence of trends in annual maximum daily precipitation between 1900 and 2009 from a global dataset 8326 high-quality land-based stations. Initially, a non-parametric Mann-Kendall trend test (M-K test) was used to evaluate the presence of any monotonic trends. Secondly, a nonstationary test was executed to determine the strength of association between the precipitation extremes and globally averaged near-surface temperature. Authors used GEV distribution having globally averaged temperature as a covariate in location parameter only. Precisely, the obtained results indicated a significant increasing trend of annual maximum precipitation over two-thirds of stations and the changing proportion of intensity of rainfall with respect to the changes in the global mean temperature varies at a rate of

between 5.9% and 7.7% K-1. Cheng and Aghakouchak (2014) modelled the nonstationary IDF curves for sustainable infrastructure design considering the maximum extreme rainfall series of five stations at the USA. Authors fitted a nonstationary model to annual maximum rainfall series using GEV distribution with time as a covariate at location parameter. Trend analysis using M-K test was performed to confirm the existence of the nonstationary component in term of a trend at 95% confidence level. Authors reported that extreme precipitation could be underestimated by 60% under the stationary assumption, which increases the flood risk and failure risk in infrastructure systems. Furthermore, they also implemented the Bayesian approach for uncertainty modelling of the nonstationary return levels and observed higher uncertainty in lower return level while modelling the nonstationary IDF curves. Mondal and Mujumdar (2015) detected the change in the extreme precipitation through nonstationary modelling over India using high resolution daily gridded dataset. In particular, authors extracted the extreme precipitation using POT method and modelled the non-stationarity by linking the parameter of the distribution with three physical covariates (i.e. global warming, local temperature changes, and El Niño-Southern Oscillation). Further, the authors modelled the intensity, duration, and frequency of extreme rainfall with GPD, Poisson, and Geometric distribution, respectively. They observed stationary condition in the duration of extreme precipitation at most of the locations, whereas intensity and frequency of extreme precipitation are primarily linked with local temperature changes at a large number of grids. The superiority of stationary and nonstationary models was examined by Yilmaz et al. (2017) over Victoria (Australia). GEV with stationary and nonstationary climate conditions was investigated using high-quality extreme rainfall data from 23 stations in Victoria. While developing the nonstationary GEV model, time and different indices of climate oscillations affecting the rainfall variability in Australia were used as covariates. From the results, they found that stationary model was superior to the nonstationary model and therefore

this model was used to determine the spatial variability of rainfall IDF relationships in Victoria. Recently, Cancelliere (2017) reviewed the framework, concepts, and available tools to model the nonstationary series. An extension of such methodology to model the drought length assuming non-stationarity either in hydrological variables or in-demand levels was also presented. The application to the new methodology was carried out to characterise drought length using four different annual precipitation series in Sicily with varying degree of a trend in the mean. Author suggested that the methodology can be extended for other drought characteristics such as severity, intensity and also to incorporate the inevitable uncertainty associated with the assessment of non-stationarity in hydrological series. Recently, many studies have approached the development of non-stationary models to understand the influence of natural variability in extremes (Bracken et al. 2018; Galiatsatou et al. 2018). Yin et al. (2019) examined the spatiotemporal changes and frequency of extreme precipitation in the Huai river basin during 1960 to 2014 and found that stationary assumptions lead to underestimation of future return levels. Song et al. (2020) developed a nonstationary Standardised Precipitation Index using nonlinear dependence model for Yangtze River Basin, China and suggested that extreme climatic conditions are better explained by nonstationary indices as compared to their stationary counterparts.

2.6 Extreme climate risk and resilience

Properly identifying and analysing the risk due to extreme climatic conditions is essential for formulating effective response measures. It is evident from the studies mentioned earlier that the investigation of climate extremes requires proper incorporation of variabilities and uncertainties. These uncertainties and variabilities put forth important challenges to risk and resilience estimation (Eiser et al. 2012). Research shows that more innovative tools and methods are needed for extreme climate risk assessment. Further, the understanding of risk inducing process and selecting a proper methodology is essential for deciding extreme climate-

induced disaster's response and mitigation plans. McEntire et al. (2010) introduced an integrated disaster response model based on the concepts of different social and scientific disciplines and suggested that a comprehensive approach is required for risk assessment. The IPCC AR5 framework has given an overall concept to estimate risk by combining the hazard, exposure and vulnerability estimates (Field et al. 2012). Over the years, this approach has been able to produce reliable estimates of extreme climate risk as it allows the integration of intrinsic vulnerability of the subjects rather than just observing at the impacts (Cavan and Kingston 2012). The risk due to extremes does not only depends on the severity of hazard and the vulnerability but also the other factors such as capacity, sensitivity and exposure to the hazard (Field et al. 2012). Therefore, the investigation of risk due to extreme climatic events considering all critical drivers of risk is crucial.

Several studies have approached the risk and resilience estimation based on the previously mentioned frameworks. For instance, Nicholls et al. (2008) ranked top cities of the world in terms of the net worth exposed to extreme climate disasters and found that USA, Japan and the Netherlands contain more than 50 percent of the net exposure. The impact of changing climatic conditions on flood risk and extreme rainfall in India events was investigated, and it was found that the risk has become more significant in the country (Guhathakurta et al. 2011). Harvey et al. (2014) detected the vulnerability of agriculture-dependent population in Madagascar to extreme weather events as well as the pest and disease outbreaks. A study focusing on the impact of global warming on freshwater availability and food security revealed that most developing countries might face many critical issues due to climate change (Betts et al. 2018). In another significant study, the impact of extreme climatic condition in the major wheat-producing regions in the world was estimated (Toreti et al. 2019). It was concluded that accurate assessment of exposure and vulnerability and its integration with the hazard measures is crucial in assessing the risk in these regions.

Chen et al. (2019) studied the compound hot temperature and drought events in terms of exceedance probabilities and characterised the results based on different vegetation and ecosystems. Moreover, the study of co-occurring hazards in context of global warming revealed that the risk due to such hazards may remain higher in future due to increased exposure and vulnerability of human population (AghaKouchak et al. 2020). The investigation suggested that proper understanding of hazards associated with individual extreme events as well as the joint extremes is necessary for proper risk estimation.

The concept of resilience becomes crucial when the understanding of the capacity of a system to absorb, rearrange and recover from the impact of some disturbance is required. Moreover, in the view of climate extremes, the understanding of the capacity of exposed population or infrastructure to cope up with the extremes risks and recover to an equilibrium state is important in framing extreme climate management policies. It has been observed that climate extremes have drastically affected the response and resilience of ecosystems in different parts of the world (Pérez et al. 2010). Therefore, it is essential that the decision-making bodies should work towards understanding and integrating the reliable estimates of the capacity of ecosystems to changing climatic conditions. Hoover et al. (2014) suggested that the response and recovery of the exposed subject are varied in terrestrial ecosystems and may depend on, for example, the species of grassland ecosystems. Different components in the existing system play an essential role in deciding the resilience characteristics. For example, Isbell et al. (2015) explained that biodiversity, without much human interfere, stabilizes the terrestrial ecosystems making them more resilient to the extreme conditions. Further, it was observed that extreme climatic events govern the terrestrial ecosystem functioning and chances of higher mortality and poor resilience are evident with increasing extreme events (Hutchison et al. 2018). Moreover, Rammig et al. (2020) pointed out the importance of considering the interlink between the ecosystems and society while

quantifying the resilience and suggested that an integrated approach including the ecological resilience and societal evolution is more suitable. In recent years, the resilience concept has been utilized to understand the response and recovery capacity of human society to a variety of extreme climatic events, some of which are floods (Bertilsson et al. 2019; Wang et al. 2019), cyclones (Islam et al. 2020; Uddin et al. 2020), droughts and heatwaves (Howe et al. 2019; Kamara et al. 2019; Mihunov and Lam 2020).

2.7 Conclusions

An overview of past and future climate extremes, probabilistic and multivariate approaches to investigate extremes, the importance and application of nonstationary analysis and the concept of risk and resilience has been presented in this chapter. The discussions about past and future extremes suggest that high-temperature extremes have increased over the past and low-temperature extremes have decreased. The changes in precipitation extremes have been more variable in nature due to the strong influence of regional factors. The future scenarios suggest that continuation and amplification of past trends could lead to more severe droughts and instantaneous rainfall events. The literature review discussed the advantages of EVT and Copula in analysing the extremes. The studies suggest that EVT and Copula based methods are one of the most reliable tools to examine the risk due to extremes. However, most of the previous studies have been performed under nonstationary assumptions. It was found from the past works that nonstationary approaches are more useful while modelling the extremes. Several works, after comparison of the nonstationary models to their stationary counterparts, suggested that nonstationary probabilistic models are more efficient in understanding and estimating the consequences of climate extremes. Further, the concept of risk and resilience in the context of climate extremes was discussed in the last section. The literature review indicates that proper assimilation of the hazard, vulnerability and exposure elements is necessary for estimating the

risk. Moreover, the selection of suitable methodology and integration of uncertainty in the estimates is also very crucial for the decision making process. Further, the resilience of different human and natural systems is a function of several factors. Therefore, the thesis, addressing the gaps pointed out in the literature review, aims to assess the climate extremes using an advanced nonstationary multivariate probabilistic approach and provide more reliable estimates of the risk and resilience for India.

Chapter 3

Predictability of temperature and precipitation in the past century

3.1 Introduction

Several studies show that climate change has caused alterations in precipitation and temperature profiles all across the globe (Li et al. 2011; Gobiet et al. 2014). This change is expected to continue in future and cause large-scale damage to property and lives (IPCC 2014). Classical approaches to assess climate predictability revolve around understanding the variability in climate components. However, the climate over a region is governed by many factors and the interconnections between them. Several processes in the climate system are nonlinear due to a chaotic or random component in the cause-effect relationship, which is difficult to detect and incorporate into current modelling practices. Therefore, more sensible techniques are required to understand the hidden mechanism in different climate processes and overcome the limitations of current approaches.

In this study, the investigation of the predictability of temperature and precipitation data from the perspective of a nonlinear dynamic system is performed by analysing 102 years' (1901-2002) mean monthly temperature and precipitation data at the district level using the delay vector variance (DVV) method (Gautama et al. 2004). This approach can be utilised to understand nonlinearity from both deterministic and stochastic perspectives. The method of DVV does not require prior knowledge about the time series, and it efficiently manages the essential aspects of nonlinearity such as time delay, embedding dimensions, behaviour in phase space and predictability (Jaksic et al. 2015). They suggested that this method is also robust to the presence of noise and produces results which are easier to interpret. Earlier, the concept of DVV has been utilised to study

biomedical signals, heart rate variability, tremor detection, electroencephalogram, functional magnetic resonance imaging, structural and mechanical vibrations, and financial time series (Gautama et al. 2003, 2004, Jaksic et al. 2015, 2016). Although the utilisation of DVV approach in climate data analysis has been rare, its applicability in a wide range of fields is encouraging. This study provides the district wise understanding of the temporal and spatial evolution of Indian climate predictability and provides essential inputs for achieving better climate predictions in future.

3.2 Data and methodology

As discussed, this study aims to investigate the nonlinear and deterministic characteristics of precipitation and temperature profile in India over the past century. Briefly, methodology involves understanding the nonlinear behavior of the data using the DVV approach. The DVV method is based on the comparison of the target variances of the original data and their linearized surrogate versions. This difference, which is quantified in terms of RMSE is a measure of nonlinearity and minimum target variance of the original data indicates the deterministic characteristics. Once the degree of nonlinearity was quantified, the memory persistency, and the statistical scale dependence was checked with the help of different Hurst exponent measures. The methods have been discussed in detail in the sections given below. The overall methodology has been discussed in Figure 3.1. The code utilized for this work was developed using the DVV toolbox developed by Mandic et al. (2008) in MATLAB.

3.2.1 Precipitation and temperature data

This study is performed over 566 stations in India, where each station represents a district-an administrative division of the country. 102 years' (1901-2002) mean monthly precipitation and temperature data is acquired from the 'India water portal' website (<http://www.indiawaterportal.org/metdata>). These stations are well spread over India and can be treated as representing the average weather conditions in

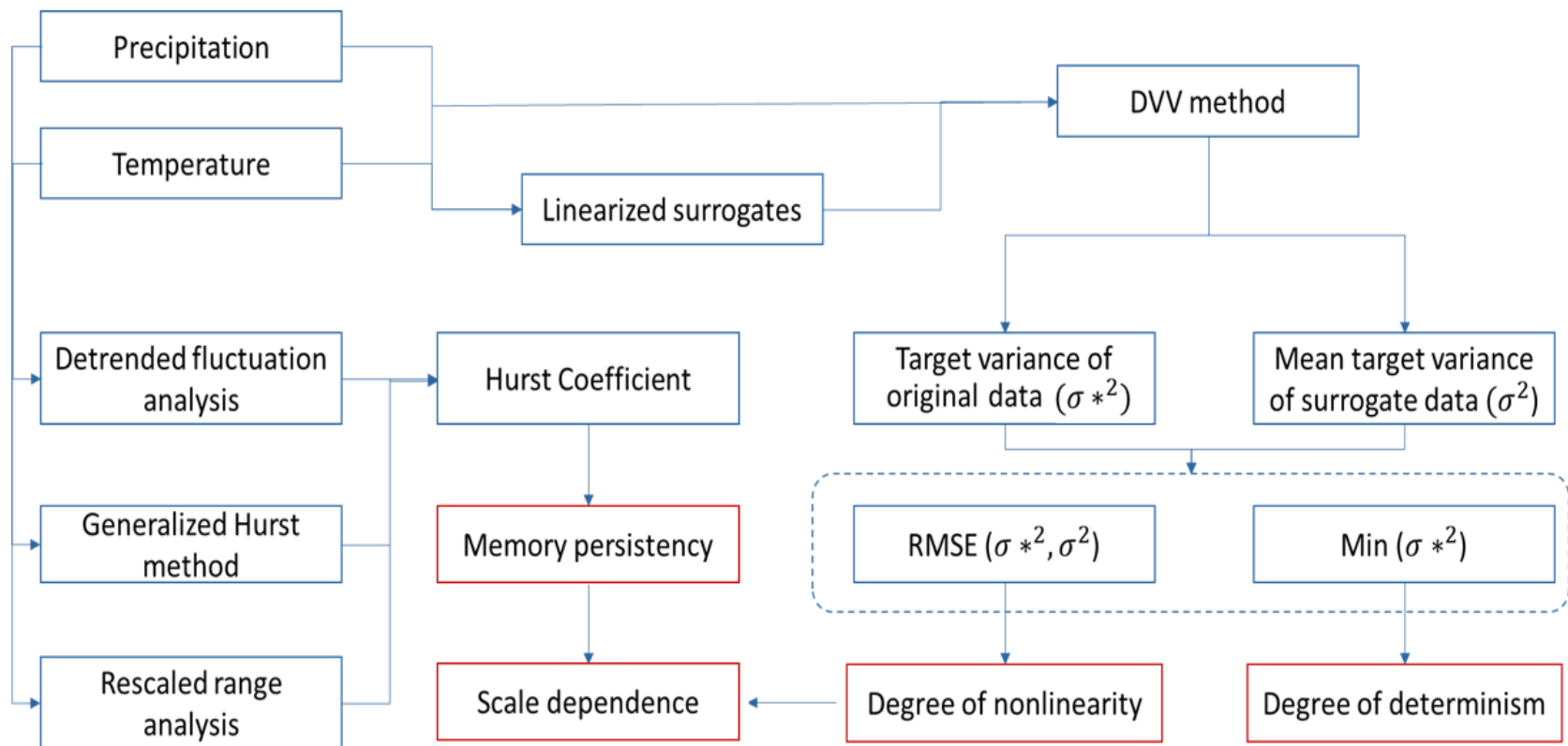


Figure 3.1 Flowchart of the methodology

their respective districts. For the demonstration of results, one district from six climatologically different regions of the country, namely north-west, north-east, interior peninsula, north-central, east-coast and west-coast, is chosen. Figure 3.2 can be referred to visualise the location of demonstrating stations and the boundaries of districts used in this study. Data of some districts are not available, for which, interpolation of the results from surrounding stations was performed to provide full-scale analysis of India. For properly analysing the evolution of determinism and nonlinearity over time, the meteorological data is subdivided into three 34 years (1901-1934, 1935-1968, and 1969-2002) subsets over which the investigation is performed.

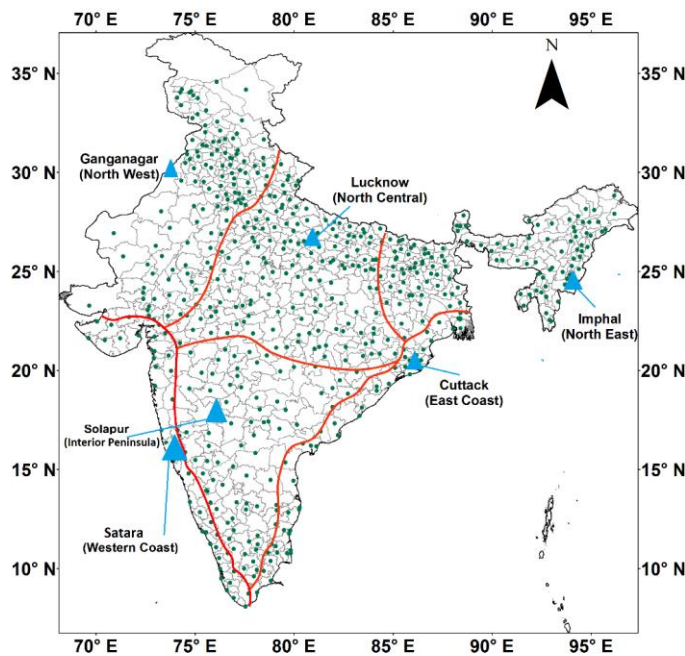


Figure 3.2 Location and details of demonstrating stations (blue triangles) and the coverage of districts used in this study (green dots). The boundaries of six different climatic zones have been given in red

3.2.2 Scaling properties and memory persistence

Here, the methodology adopted to study the scaling properties and memory carrying capacity of the temperature and precipitation profiles has been discussed. The method of Hurst exponent which have been widely utilised

in such studies is employed to check the scale dependence and memory persistency (Morales et al. 2012; Ray et al. 2016a). Hurst exponent $H(q) = 0$ indicates that the time series is composed of pure white noise and the autocorrelation function (ACF) lapses drastically with time. For a short-range dependent (SRD) behaviour, $0 < H(q) < 0.5$ and the ACF decreases exponentially, smoother than the previous case. Here, the time series adopts behaviour almost similar to Brownian motion (fBm). However, for a perfect Brownian motion time series, the value of $H(q)$ is equal to zero. For $H(q) > 0.5$, it can be assumed that the time series loses its SRD property and acquires long-range dependence (LRD) characteristics.

There are many methods available for calculations of Hurst exponent, and each of these methods has its own set of advantages and limitations. Since this study deals with the analysis of climate data, one method might not be sufficient to explain the variability. Therefore, three methods, namely, generalised Hurst method, detrended fluctuation analysis (DFA) and rescaled range (R/S) analysis were employed separately on all data sets to confirm the reliability of the results.

3.2.2.1 Generalised Hurst method

This method analyses the statistical properties of a time series $X(t)$ (with $t = v, 2v, \dots k \dots T$) for time resolution (v) and time period (T). This scaling is explained by estimation of an exponent (H) which is related to the long term dependence of a time series. The formula for q-order moments of the distribution of the increments is given by Di Matteo et al. (2003)

$$K_q(\tau) = \frac{\langle |X(t + \tau) - X(t)|^q \rangle}{\langle X(t) |^q \rangle} \quad (3.1)$$

This formula very well describes the progression of time series $X(t)$ regarding stochastic variation. The Hurst exponent $H(q)$ incorporating the scaling properties is estimated by the following relation

$$K_q(\tau) \sim \left(\frac{\tau}{\vartheta} \right)^{qH(q)} \quad (3.2)$$

The above equation gives rise to two cases, the case I, in which $H(q) = H$ and case II where $H(q)$ depends upon the order q . The case I describes the uni-scaling process and case II is meant for multi-scaling. When a data set exhibits different statistics in different time scales, it is said to be demonstrating multi-scaling properties. In this study, the generalised Hurst exponent values with $q=1,2,3,4$ and 5 are estimated. When the values of Hurst exponents did not change with the order of moment q , it was assumed that time series is uni-scaling. However, when the exponent values change nonlinearly with the order of moment q , the time series is considered as showing multi-scaling properties.

3.2.2.2 Detrended fluctuation analysis

Detrended Fluctuation Analysis (DFA) is one of the widely used approaches for studying the scaling properties and is useful in examining the self-similarity in time series. The methodology includes the construction of a cumulative time series (X_t) from the original series (x_t) transforming the underlying noise into respective random walks.

$$X_t = \frac{1}{N} \sum_{i=1}^t (x_i - \langle x \rangle) \quad (3.3)$$

This series is further subdivided into a number of ‘boxes’ containing n observations on which least square fitting is employed to detect the presence of a local trend if any. The procedure is followed for each box, and lastly, an average fluctuation function $F(n)$ is calculated which is based on the minimization of root mean squared error over the whole cumulative series (Peng et al. 1994; Kantelhardt et al. 2001):

$$F(n) = \left[\frac{1}{N} \sum_{t=1}^N (X_t - Y_t)^2 \right]^{\frac{1}{2}} \quad (3.4)$$

Here, Y_t is estimated as the local trend for a given box. The fluctuating function $F(n)$ finds proportionality with the scale n of the box which is further defined by an empirical power law equation as:

$$F(n) \propto n^\beta \quad (3.5)$$

Here, the exponent β is similar to the Hurst exponent. For a signal to be fractional Brownian motion (fBm), exponent $0 < \beta < 1$. If the value is greater than 1, the signal is considered to be a non-stationary time series, and then the Hurst exponent can be inferred from the relation $H = \beta - 1$.

3.2.2.3 Rescaled Range analysis

This method examines the standard deviation with changing ‘range’ of the time series. It gives an idea about the variability of the signal with respect to different scales. This variability is termed as ‘rescaled range (R/S)’ and which is the ratio of ‘range’ of signal to its standard deviation. For calculating the rescaled range, the values of range (R_n) and standard deviation (S_n) are calculated, which is later averaged over their respective lengths. These averaged rescaled ranges values, and scales are plotted on log-log axes, and the slope of this line gives Hurst exponent (Bassingthwaight and Raymond 1994):

$$\left(\frac{R_n}{S_n}\right)_{av} = \left(\frac{n}{2}\right)^H \quad (3.6)$$

Here, R_n is the range denoting the difference between the minimum and maximum values of x_n , while S_n is given by the sum of $x_i - \bar{x}_n$ over different lags till the scale is limited to a particular smaller value. Here n is the length of time series and \bar{x}_n is the average value. This method is considered to be robust with respect to the length of time series and proves to be efficient in analysing both large and small scale signals (Chamoli et al. 2007).

3.2.3 Analysis of nonlinearity and determinism

3.2.3.1 Delay Vector Variance method

For a standard time series $x(i) = \{x_1, x_2, x_3 \dots x_n\}$, a set of delay vectors (DVs) $[x(k) = \{x_{k-m\tau}, \dots, x_{k-\tau}\}]$, where $k = 1, 2, 3, 4 \dots N$ and τ and m are the time lag and embedding dimension, respectively, is generated by the simple process of delay coordinate embedding. Mean μ_d and standard deviation σ_d is calculated for all pairwise Euclidean distance between delay vectors. $\varphi_k(r_d)$ is defined by selecting a set of DVs from the generated DVs such that they lie within a specific Euclidean distance (r_d) to the delay vectors. For these sets of DVs, the variance of respective targets $\sigma_k^2(r_d)$ is calculated and normalised by the variance of the whole data set σ_x^2 . The target variance $\sigma^{*2}(r_d)$ which is a measure of unpredictability can be given as (Gautama et al. 2004):

$$\sigma^{*2}(r_d) = \frac{\frac{1}{N} \sum_{k=1}^N \sigma_k^2(r_d)}{\sigma_x^2} \quad (3.7)$$

It is suggested that a sufficient number of DVs should be considered to calculate the target variance (Mandic et al. 2008). In this study, only those sets of data which have at least 30 reference DVs were selected. To standardise the distance axis for further analysis with reference to target variance, the Euclidean distance (r_d) is replaced by $(r_d - \mu_d)/\sigma_d$ where, μ_d and σ_d are mean and standard deviation of all pairwise distance between delay vectors. The distribution of minimum target variance with standardized distance is utilized to interpret the presence of deterministic dynamics in a system. A strong deterministic component results in lower minimum target variance value hence, which can be considered as a sign of better predictability (Gautama et al. 2004; Ray et al. 2016b).

Comparison of original time series variance with its surrogate data sets enables us to examine the validity of the null hypothesis, i.e. the time series is a result of a linear stochastic process. For the generation of surrogate data

sets, inverse iterated amplitude adjusted Fourier transform (iAAFT) method is employed, which produces a linearised version of the original time series with similar amplitude spectrum (Theiler et al. 1992). The difference between test statistics of the surrogate and the original time series can be used to characterise the time series based on nonlinearity. In this study, the target variance of original time series is compared with the averaged variance of 99 surrogate data sets. For visualisation, both the target variances are plotted in ‘DVV plots’, and it is expected that the variance curve of a linear time series should overlap with the variance curve of surrogate series. For exact quantification of the nonlinear deviation, the difference between target variance of original time series and linearised surrogate sets is quantified in terms of root mean squared error (Hu and Yin 2009):

$$RMSE = \sqrt{\text{mean} \left\{ \sigma^{*2}(r_d) - \frac{\sum_{i=1}^{N_s} \sigma_{s,i}^{*2}(r_d)}{N_s} \right\}^2} \quad (3.8)$$

where, $\sigma_{s,k}^{*2}(r_d)$ is the target variance at distance r_d for i^{th} number of surrogates later averaged over full span incorporating only the acceptable values. The RMSE values are then plotted with respect to a bisector line in ‘DVV scatter plots’ which can be referred to visualise the degree of nonlinearity.

3.2.3.2 Selection of embedding parameters

It is important to note that proper representation of time series in phase space is necessary to investigate the nonlinear dynamics which depends upon the selection of optimum embedding dimension m and time lag τ (Kyoung et al. 2011). The values of m and τ should not be selected arbitrarily. A larger value of m not only causes more complex calculations but also increases the effect of noise in data (Zhang et al. 2014). At the same time, a large value of τ can significantly reduce the interdependence of two adjacently reconstructed state variables. Similarly, selecting considerably

smaller m and τ can lead to an incomplete representation of time series in phase space. (Gautama et al. 2004) pointed out that the DVV method is robust to the selection of parameters which is an added advantage for this study. However, considering the spatial and temporal coverage and variable nature of the data sets, a wide range of time lag and embedding dimensions has been tested. Since the main focus of the study is estimating the predictability of involved data sets; that particular combination of time lag and embedding dimension which produced maximum predictability is selected (Gautama et al. 2004). A similar method is used by (Jaksic et al. 2015) in the study of the dynamic behaviour of offshore wind floating substructures. For precipitation, a total of 280 combinations ($m = 2:8 \times \tau = 1:40$), and for temperature, 180 combinations ($m = 2:7 \times \tau = 1:30$) of embedding dimensions and time lags are examined.

3.3 Results

3.3.1 Optimum embedding dimensions and time lag

Figure 3.3 shows the distribution of optimum embedding dimension and time lag obtained for precipitation and temperature profile in different periods, respectively. The embedding dimension m , which is the number of previous time samples utilised for investigating predictability is generally larger for temperature as compared to precipitation. In the spatial plots, most of the regions except the north-west and extreme northern part of the country indicate that larger value of m is required for proper phase reconstruction of temperature data (Figure 3.4a). For the periods of 1901-1934, 1935-1968 and 1969-2002, the optimum value of $m > 5$ is obtained in 291, 261 and 316 out of 566 districts respectively. Although the maximum allowable value of m is 8 for precipitation data, most favourable range of m is 2-5 for 244, 257 and 288 districts in the three given periods (Table 3.1). Also, the most commonly preferred value of embedding dimensions is 2 irrespective of the time periods (Figure 3.3b). Surprisingly, this minimum value of m is observed in the regions of little precipitation.

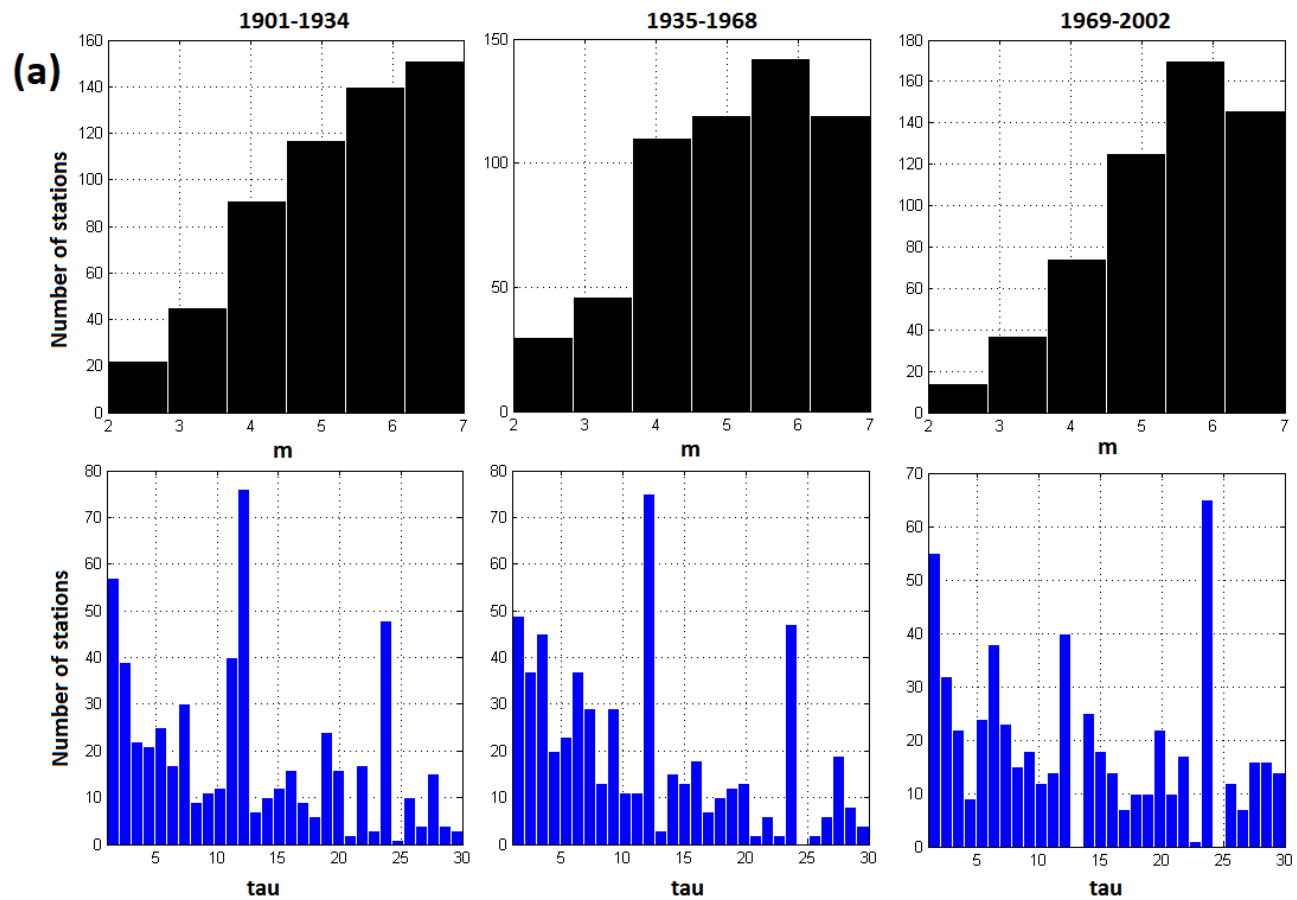


Figure 3.3a Distribution of optimal time lag and embedding dimensions for precipitation in different time periods

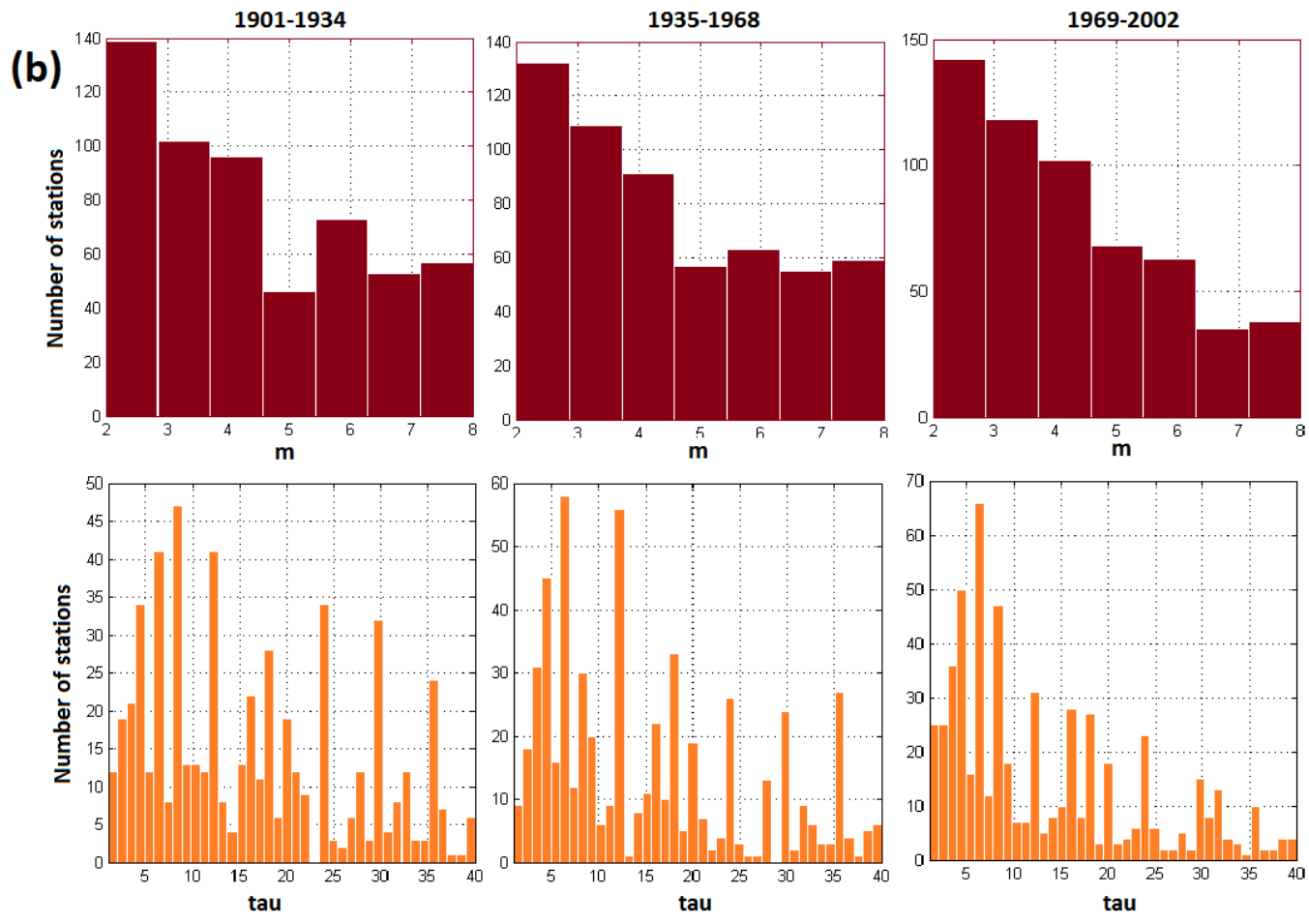


Figure 3.3b Distribution of optimal time lag and embedding dimensions for temperature in different time periods

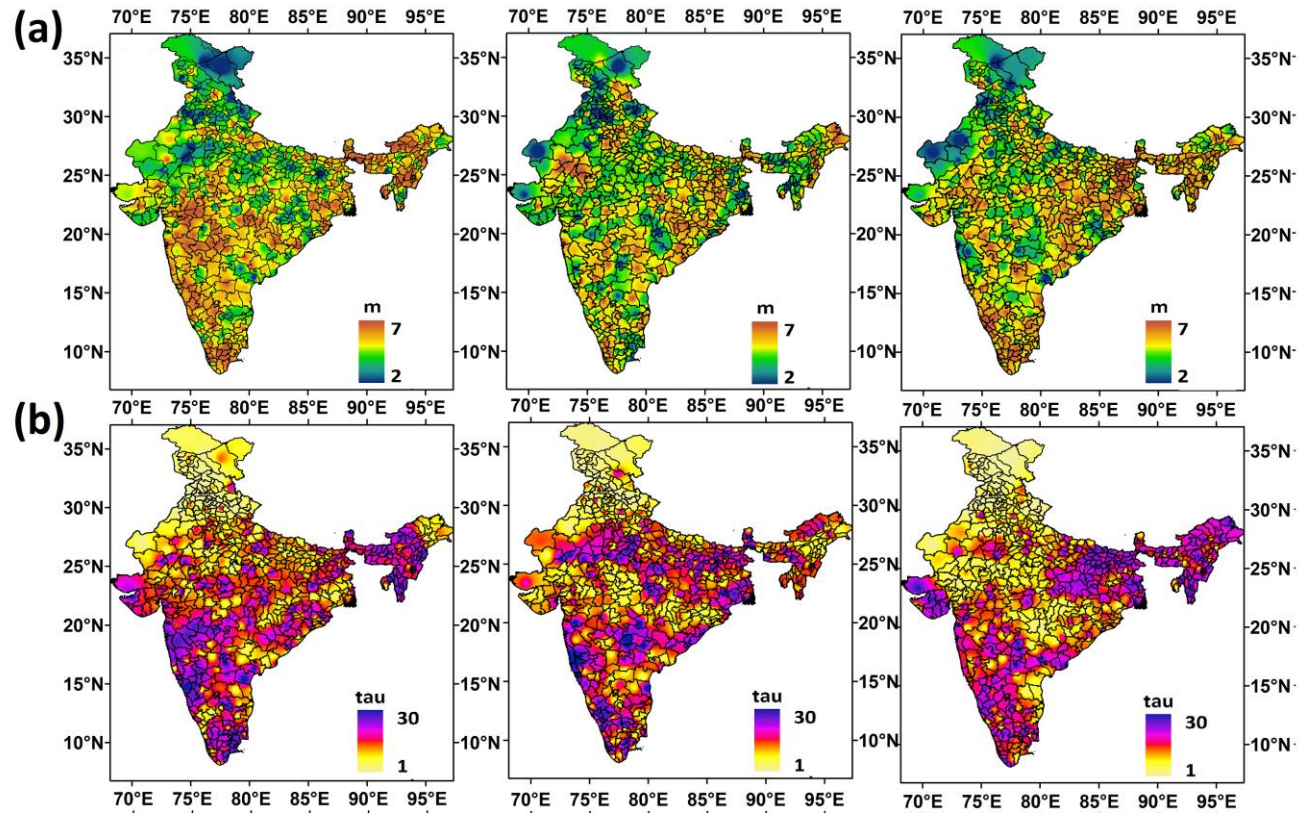


Figure 3.4ab District-wise spatial distribution of (a) embedding dimension and (b) time lag for temperature

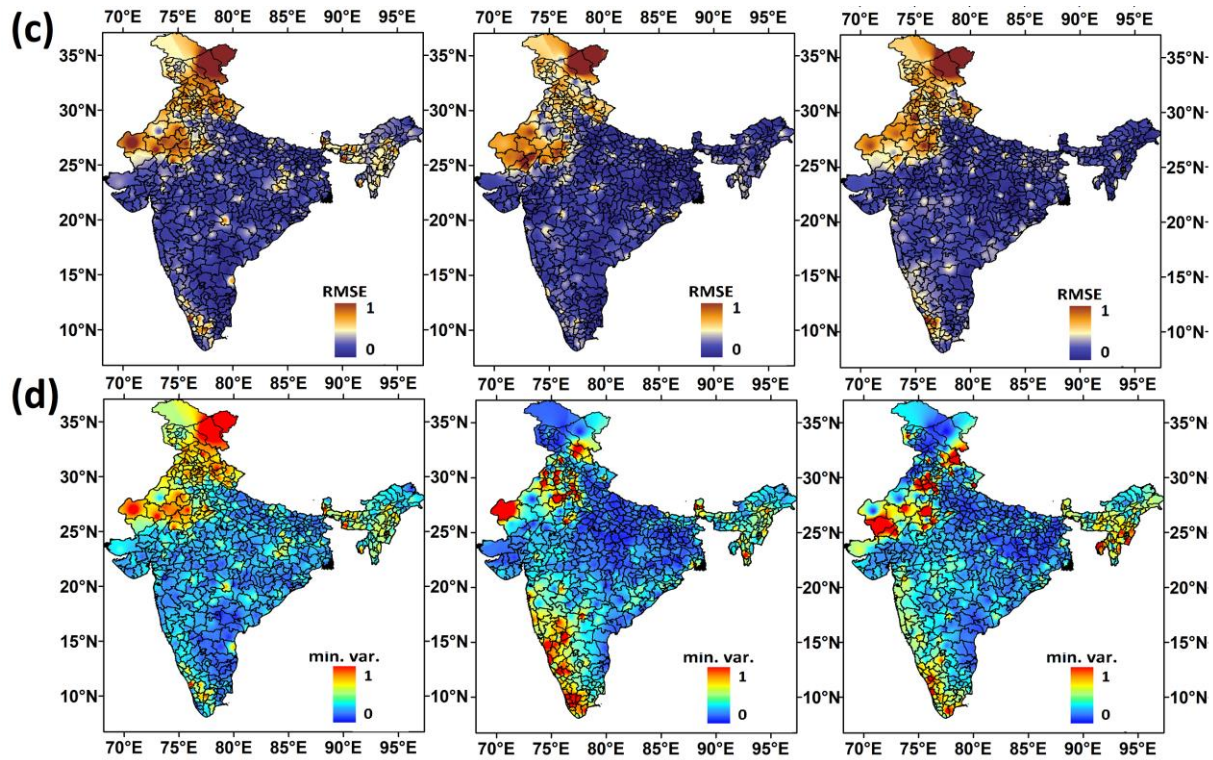


Figure 3.4cd District-wise spatial distribution of (c) normalised RMSE and (d) normalised minimum target variance for temperature

As compared to the embedding dimensions, optimum time lag (τ) values for precipitation are fairly distributed over the domain of 1 to 40. As the histogram plots indicate, this distribution of embedding parameters remains unchanged for both the variables in different time periods. Although, for precipitation, it is observed that lower τ is more preferred with the progress of time (Table 3.1). Optimal τ range is 1-6 across 139 districts in the initial 34 years; however, by the end of 1969-2002, this range becomes favourable for precipitation reconstruction across 218 districts. An opposite trend is observed in temperature as higher time lag ($\tau > 12$) values are more preferred with each passing time duration. During 1901-1934, the optimal time lag range for temperature is 1-6 for 181 districts, whereas, during 1969-

Table 3.1 Number of districts in different ranges of m and τ

	Temperature			Precipitation		
m	1901-1934	1935-1968	1969-2002	1901-1934	1935-1968	1969-2002
2	22	30	14	139	132	142
3-5	253	275	236	244	257	288
5-8	291	261	316	183	177	136
τ	Temperature			Precipitation		
1-6	181	211	180	139	177	218
7-12	178	168	122	134	133	122
13-24	170	148	199	166	148	143
24-40	37	39	65	127	108	83

Here, m is the optimum embedding dimensions and τ stands for optimum time lag

2002, $\tau=12-24$ is most preferred range covering a span of 199 districts. For precipitation, although, any particular trend in spatial variation preferred time lag values could not be specified, a good number of stations in the

central and northern are found to be turning towards lower τ values during 1969-2002 (Figure 3.5b). Moreover, districts in the low rainfall regions such as northwestern districts and the Himalayan regions require least time lag values. The analysis further shows that temperature profiles in regions of high precipitation, such as the north-east and west-coast required high time lag values for their proper representation in phase space (Figure 3.4a).

3.3.2. Assessment of nonlinearity

The evidence of nonlinearity can be fairly observed in the DVV scatter plots. The deviation of curves from the bisector line is a sign of the difference in target variances of the original time series and the averaged variance values of its surrogate data. This deviation is quantified in terms of RMSE, which represents the nonlinearity associated with the original data. DVV scatter plots for Satara (west-coast), Ganganagar (north-west), Imphal (north-east), Cuttack (east-coast), Solapur (interior peninsula) and Lucknow (north-central) are shown in Figure 3.6 to demonstrate the nonlinear behaviour of temperature and precipitation data in different regions and periods. It should be noted that one station might not represent the nonlinearity profiles of a whole region due to large temporal and spatial variability. The error bars in these plots are the difference in test statistics for original and its surrogate time series. It can be observed from the DVV scatter plots for temperature that significant deviation from bisector line is observed for Ganganagar district during 1901-1934, whereas, least deviation is observed for Satara district during 1969-2002 (Figure 3.6b). However, for precipitation, the deviation in DVV scatter plots are more random and a unique curve is obtained for each of the selected districts (Figure 3.6a). This deviation, i.e. RMSE, is calculated for all 566 districts using Equation 3.8 in all three different periods. For properly analysing the results, RMSE values are normalised on a scale of 0 to 1 and then categorised into moderately nonlinear (0-0.1), significantly nonlinear (0.1-0.25), highly nonlinear (0.25-0.5) and extremely nonlinear (0.5-1) classes.

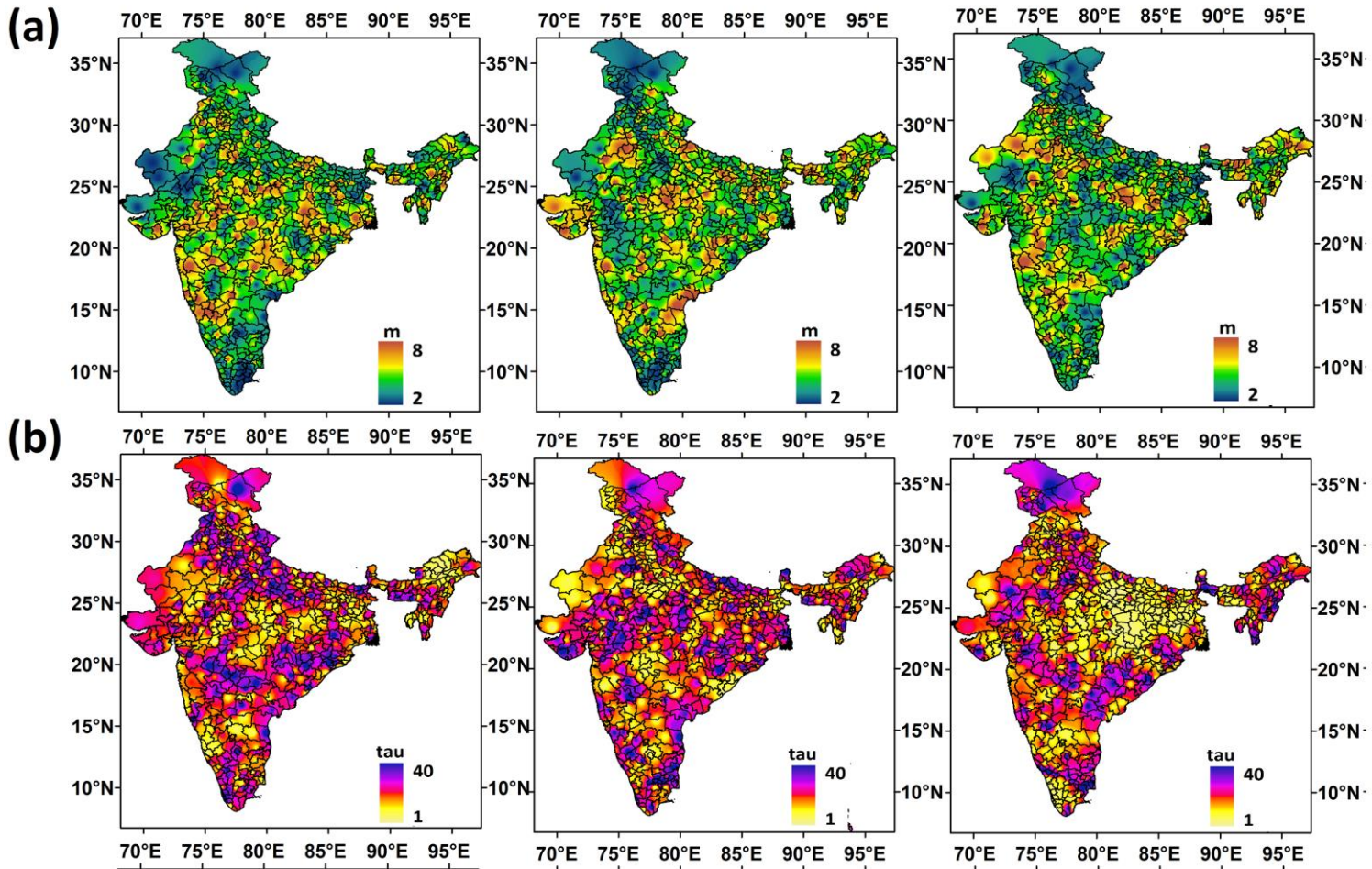


Figure 3.5ab District-wise spatial distribution of (a) embedding dimension, (b) for precipitation

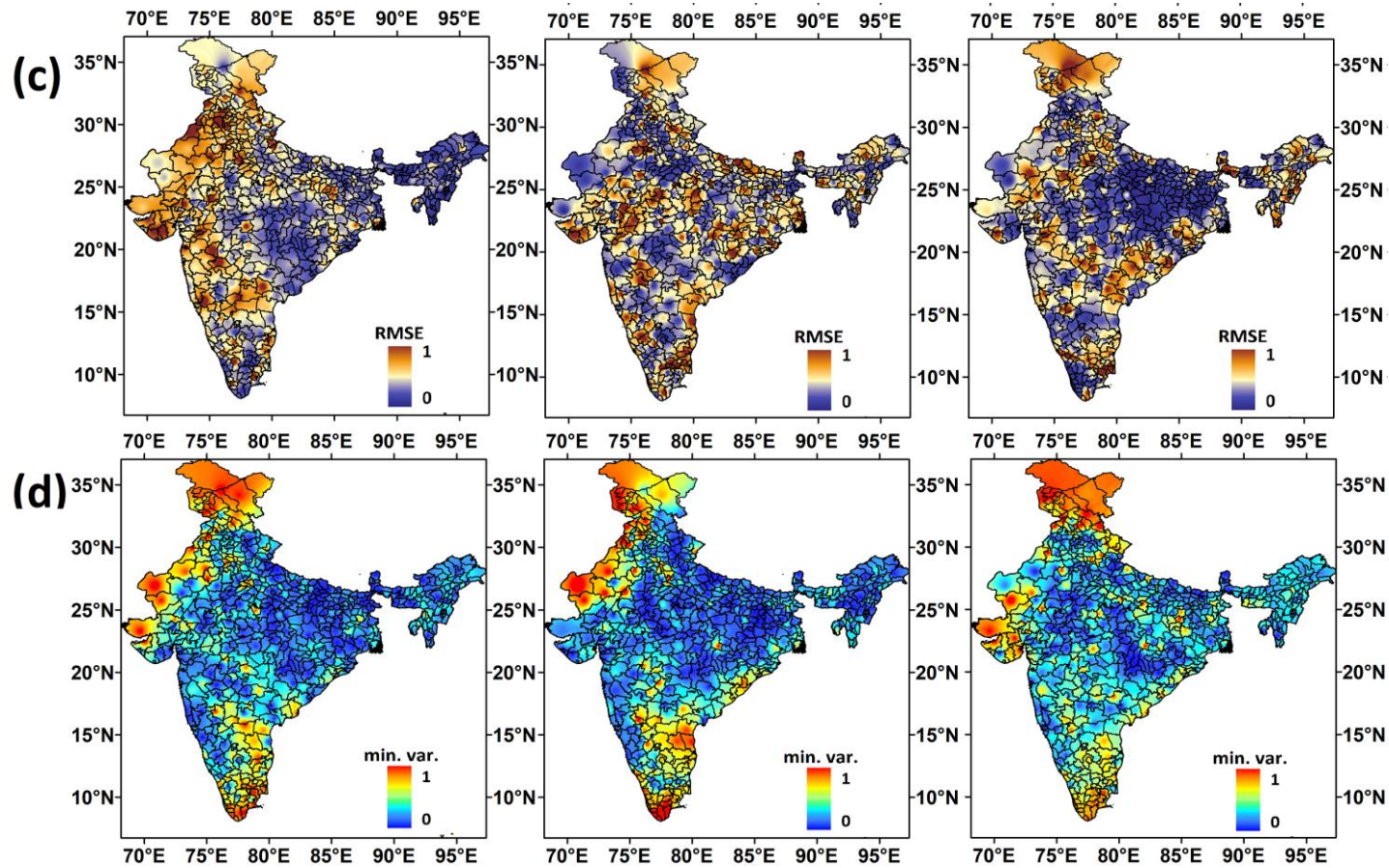


Figure 3.5cd District-wise spatial distribution of (c) normalised RMSE and (d) normalised minimum target variance for precipitation

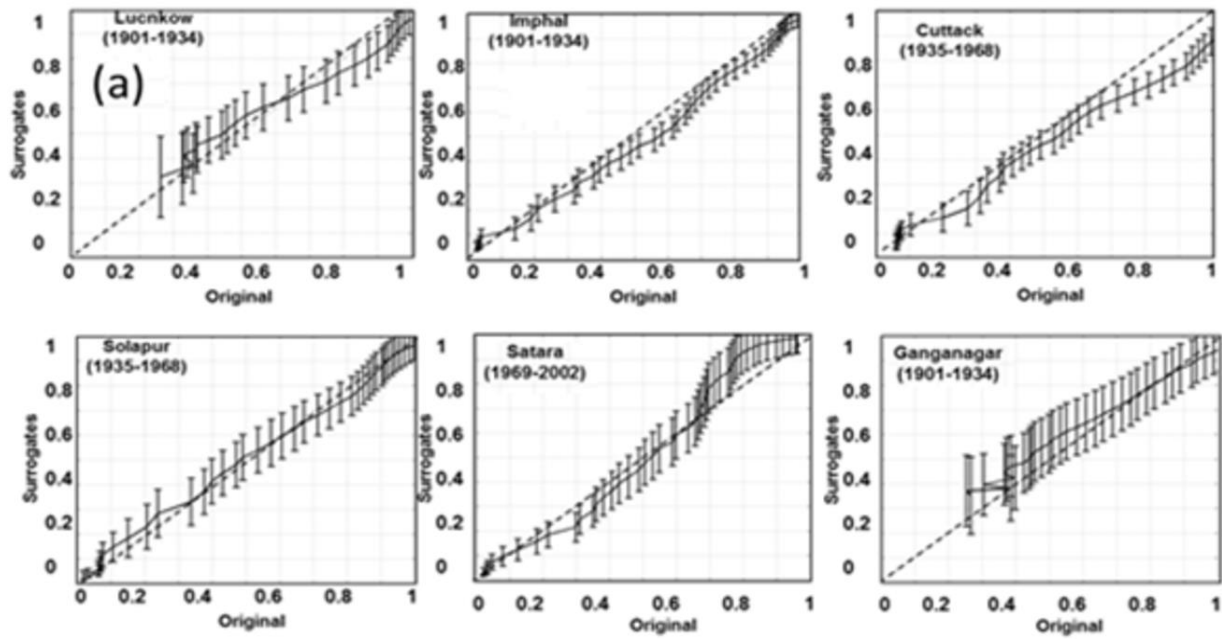


Figure 3.6a DVV scatter plots for six districts in different time periods for precipitation

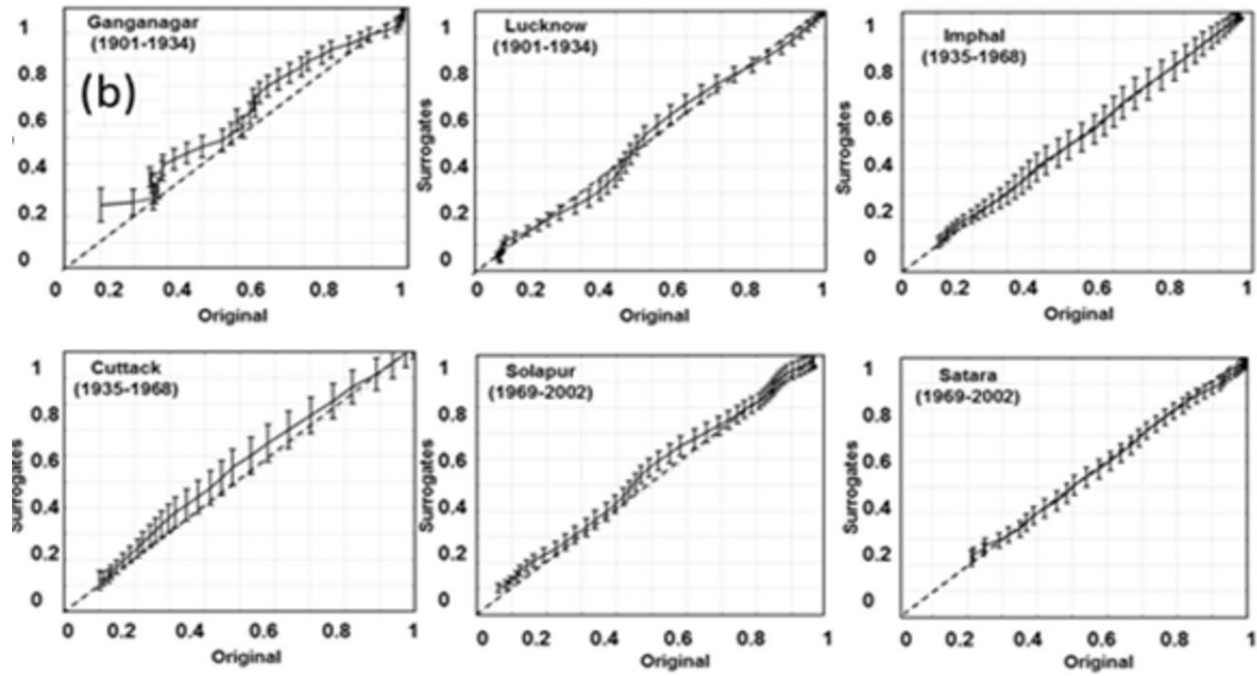


Figure 3.6b DVV scatter plots for six districts in different time periods for temperature

The results show that a large number of districts exhibit significant to extreme nonlinearity in its temperature and precipitation profiles irrespective of the period (Figure 3.7 and Table 3.2). It is also observed that the magnitude of nonlinearity in precipitation has intensified over time. For example, during 1969-2002, a total of 472 districts show signs of significant to extreme nonlinearity as compared to 449 and 458 districts during the years 1901-1934 and 1935-1968 respectively. In Figure 3.5c, the spatial variation of nonlinearity at all India scale is shown, which indicates that initially low precipitation districts of the country have the most significant nonlinear characteristics. However, significant changes in the nonlinearity profile of precipitation in the country in next time periods are observed. The north-east region which receives the heaviest rainfall in the country, initially, has least nonlinear districts. However, by the end of 2002, most of the districts in this region have become heavily nonlinear. For temperature, the RMSE values are much more clustered in nature, and not much of the spatial variation is observed in different periods (Figure 3.3c). Also, as compared to 341 significant to extremely nonlinear districts in the initial 34 years, only 223 and 279 districts have fallen in this category during 1935-1968 and 1969-2002 respectively (Table 3.2). The number of stations showing only moderate signs of nonlinearity is found to increase up to 225, 343 and 287 during respective periods of 1901-1934, 1935-1968 and 1969-2002. Strongest nonlinearity is observed in the north-west region for which Ganganagar was used as a representative district (Figure 3.5c). Unlike precipitation, a greater degree of nonlinearity is observed in the north-east region's temperature profile in initial 34 years, which is found to be weakening with the course of time and eventually becoming similar to the rest of regions. In addition to this, slight variations in the nonlinearity profile are also observed in a few districts in the western regions in the initial and last 34 years. It is also found that nonlinearity level in precipitation across 309 districts either increased or remained the same during the transition from 1901-1934 to 1935-1968. Again, in the next transition, i.e. 1935-1968

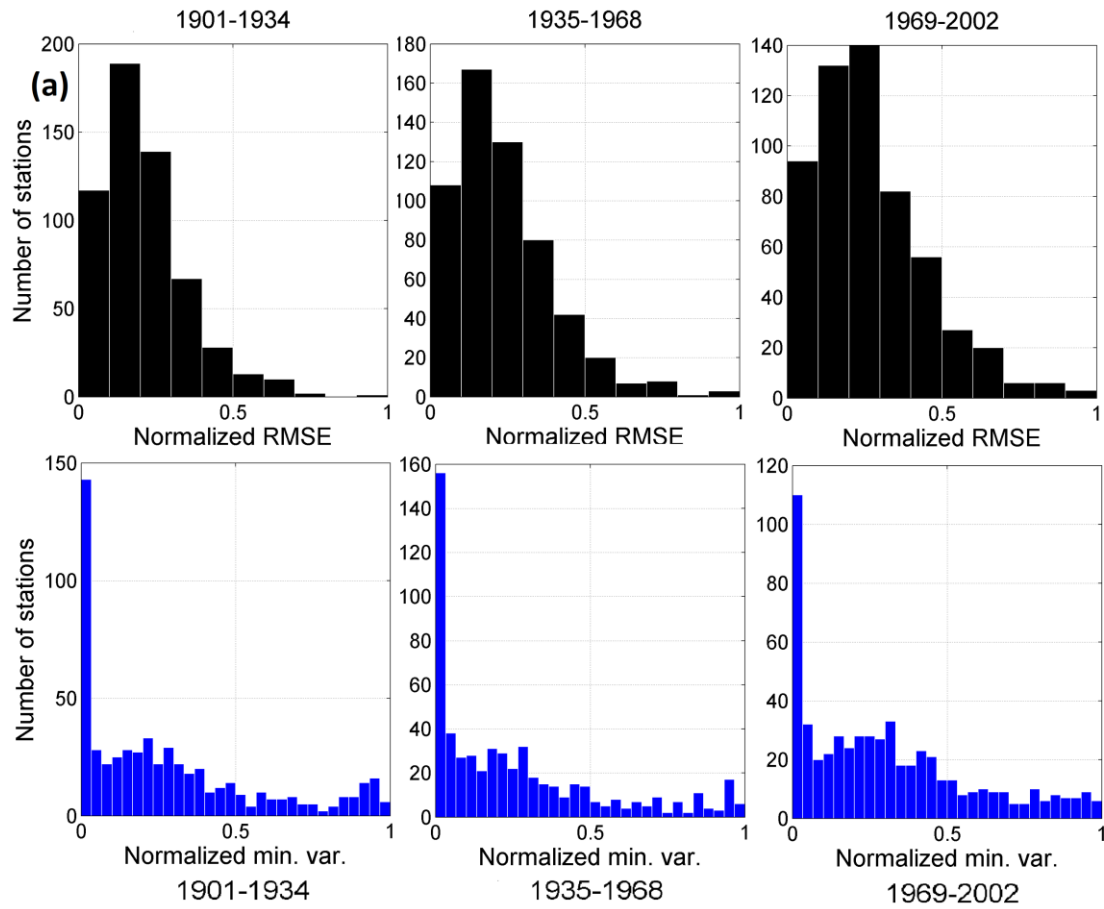


Figure 3.7a Distribution of normalised RMSE and normalised minimum variance values for precipitation in different time periods

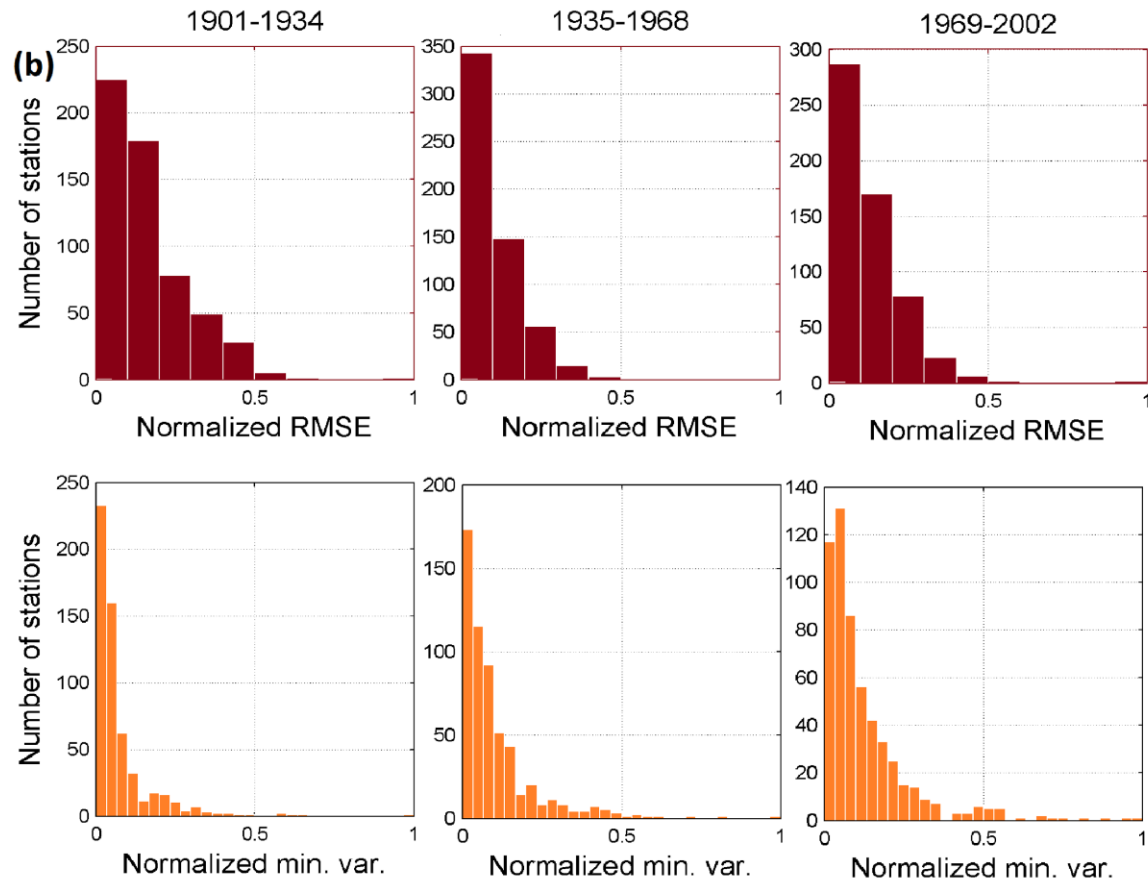


Figure 3.7b Distribution of normalised RMSE and normalised minimum variance values for temperature in different time periods

Table 3.2 Number of districts in different ranges of RMSE and minimum target variance

	Temperature			Precipitation		
RMSE	1901-1934	1935-1968	1969-2002	1901-1934	1935-1968	1969-2002
0.00-0.1	225	343	287	117	108	94
0.1-0.25	229	178	218	263	236	211
0.25-0.5	105	44	59	160	183	199
0.5-1.00	7	1	2	26	39	62
	Temperature			Precipitation		
min.var.	1901-1934	1935-1968	1969-2002	1901-1934	1935-1968	1969-2002
0.00-0.1	455	380	334	193	221	162
0.1-0.25	80	132	166	124	114	116
0.25-0.5	26	46	47	136	134	167
0.5-1.00	5	8	19	113	97	121

to 1969-2002, a similar trend is observed in 314 districts. Similarly, in the case of temperature, increasing or the same level of nonlinearity is observed in 305 districts during 1901-1934 and 1935-1968. However, when the RMSE values of 1935-1968 and 1969-2002 are considered, 329 out of 566 districts showed either equalled or increased degree of nonlinearity. In addition to this, the percentage change (with respect to 1) in nonlinearity by plotting the difference between the RMSE values of 1901-1934 and 1935-1968 on x-axis and 1935-1968 and 1969-2002 on y-axis (Figure 3.8) is also compared. Hence, the first quadrant (+,+) denotes increasing trend of nonlinearity throughout the century, second quadrant (-,+) denotes a decrease in the difference in RMSE values of 1935-1968 and 1901-1934, while an increase in RMSE during 1969-2002 and 1935-1968 and so on for the other quadrants. It is observed that nonlinearity in precipitation has continuously increased throughout the century in 120 districts and initially

decreased and then increased in 194 districts. Similarly, nonlinearity in temperature has continuously increased in 167 districts and lastly increased after initial decrement in 162 districts. More importantly, a constant decrease in nonlinearity in precipitation and temperature is observed only in 63 and 99 districts, respectively. It is also very clear from the plots that absolute percentage change in nonlinearity in precipitation is more significant and random than the temperature in which more drastic change is observed only in first transition periods as large number of values are clustered around x-axis (Figure 3.8a-d).

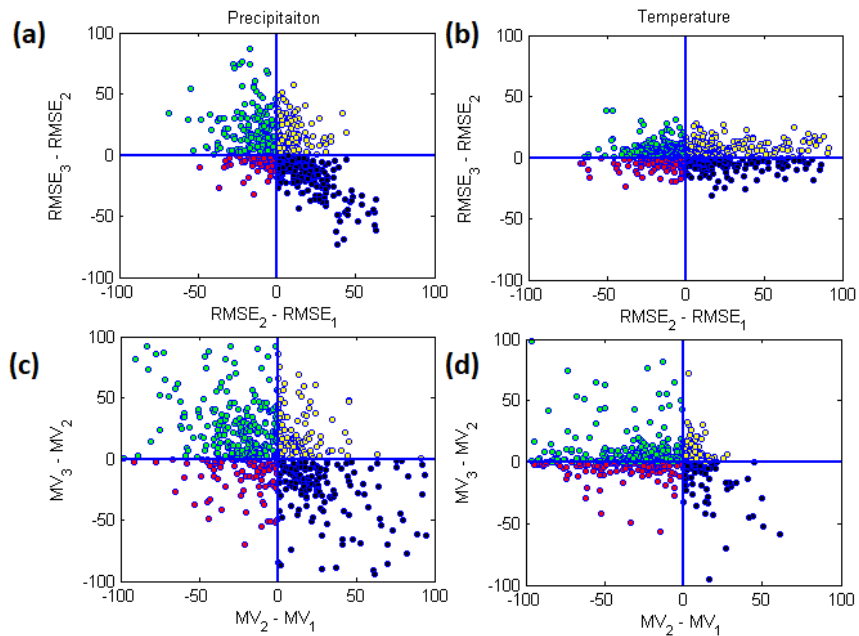


Figure 3.8 Absolute percentage change in nonlinearity and determinism for (a,c) precipitation and (b,d) temperature. $RMSE_{3/2} - RMSE_{2/1}$ represents the difference in normalised RMSE values of 2002-1969/1968-1935 - 1968-1935/1934-1901, respectively. Similarly, $MV_{3/2} - MV_{2/1}$ represents the difference in normalised minimum variance values of 2002-1969/1968-1935 - 1968-1935/1934-1901, respectively

3.3.3 Scale dependence and nonlinearity

Before analysing the deterministic behaviour of temperature and precipitation data, the memory persistency and scaling properties have been briefly discussed. It can be inferred from Hurst exponents values that both precipitation and temperature exhibit the properties of fractional Brownian motion irrespective of the time durations (Figure 3.9a,b). This behaviour can be validated by the Hurst exponent measures obtained from the three different methods. The Hurst exponent values from all three methods lie below 0.5, and it can be added to the conclusion that both the variables exhibit fractional Brownian motion with short-range dependence characteristics. The presence of SRD notion in Indian climate is not only confirmed but also indicates the existence of some feedback mechanism which keeps the values of temperature and precipitation relatively stable across the country. The anti-persistency in the climate data also stresses that there may be hidden periodicities in both the variables which need to be examined. Since the study is more concerned about the changes in scaling properties with respect to its dependence on nonlinearity, hence, instead of investigating more specifically about the scale dependence, the relationship between nonlinearity and scale dependence is analysed. For a more precise understanding, the $H(q)$ vs (q) plots for the previously selected different districts have been shown in Figure 3.9c,d which represent the generalised Hurst exponent $H(q)$ values plotted against increasing order of moment (q) . It can be clearly observed that most of the plots show nonlinearly varying values of $H(q)$ with changing order of moment (q) . Further, it can also be noticed that there is a significant correlation between the degree of nonlinearity and the $H(q)$ values. In most cases, higher the nonlinearity higher was the nonlinear relation of $H(q)$ and (q) (Figure 3.9c,d). For example, it is known from the DVV analysis, that temperature profile of Ganganagar is one of the most nonlinear out of six selected districts (Table 3.3,3.4). Here, the $H(q)$ vs (q) plots for north west's Ganganagar district's temperature time series appear to stand out from the

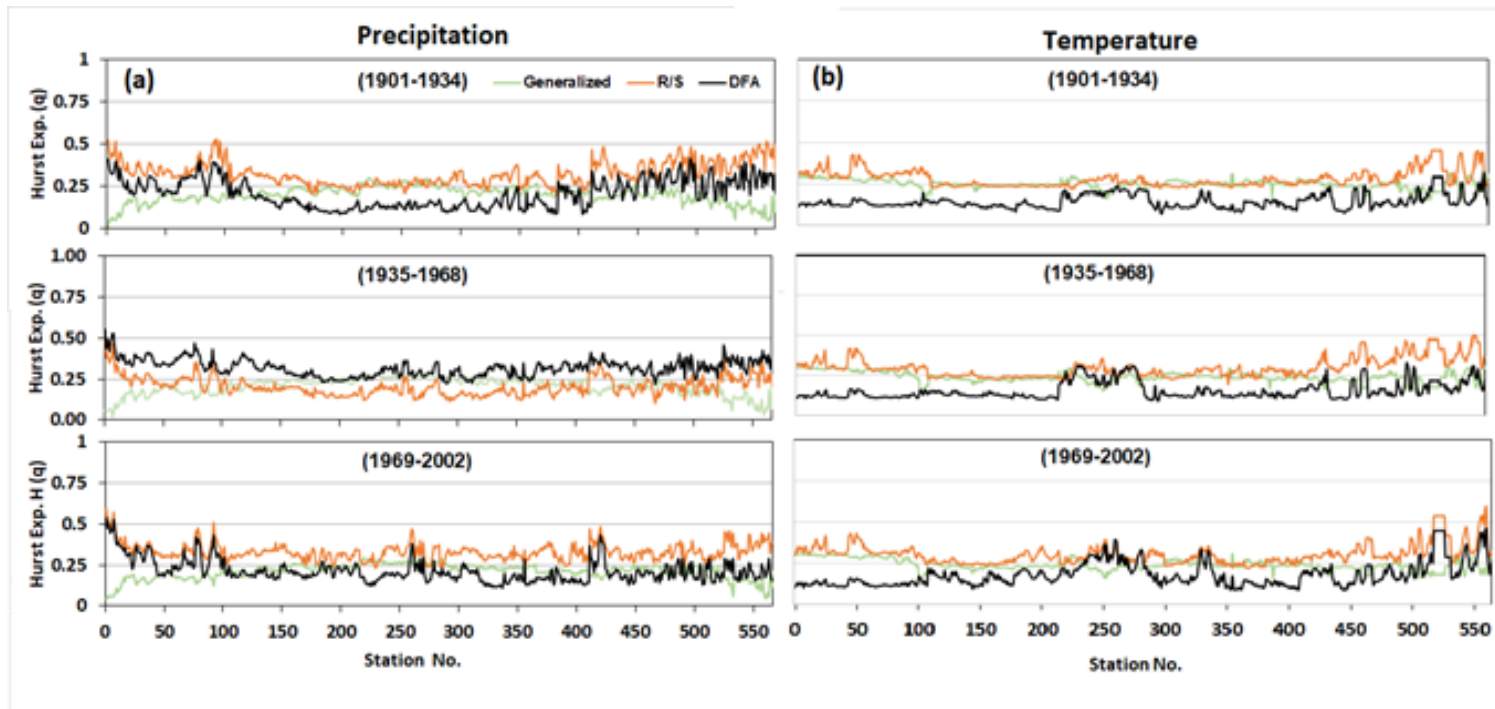


Figure 3.9ab Hurst exponents values for (a) precipitation and (b) temperature using generalised Hurst, rescaled range and detrended fluctuation analysis methods

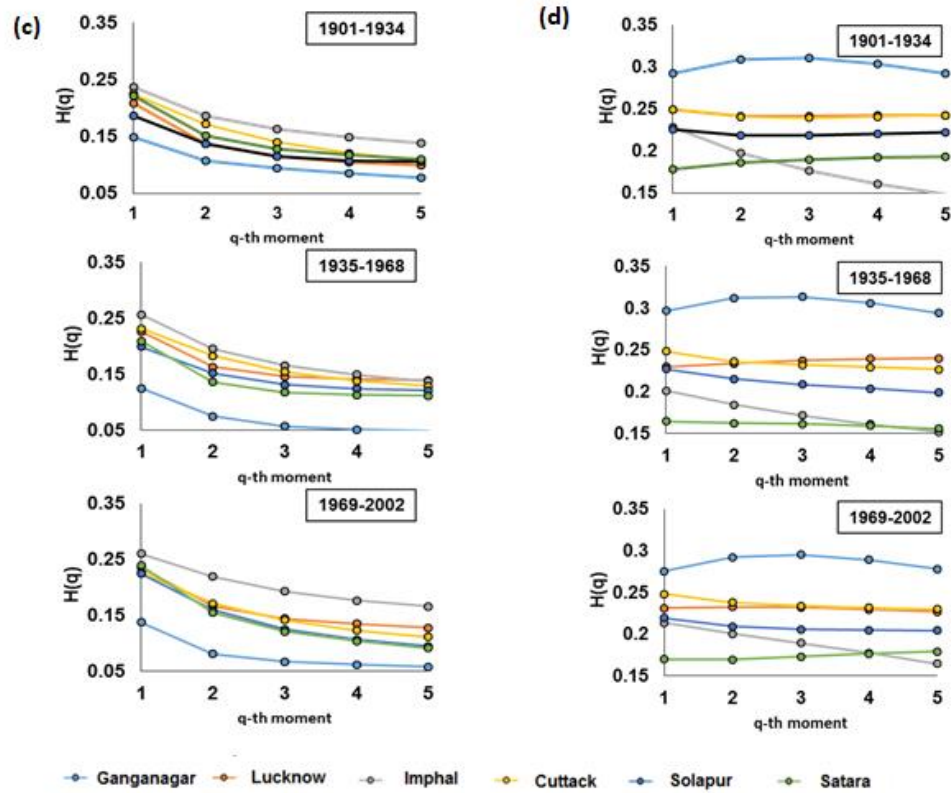


Figure 3.9cd (c) and (d) represent the change in Hurst exponent ($H(q)$) with changing orders of moment (q) for precipitation and temperature, respectively

Table 3.3 Optimal embedding dimension, time lag, RMSE, minimum target variance and Hurst exponent measures of sample stations in different time periods for temperature data

Station	m	tau	RMSE	min.var.	Hurst Exponent		
					Gen.	DFA	R/S
(1901-1934)							
Ganganagar	7	1	0.083	0.023	0.292	0.119	0.301
Lucknow	3	20	0.019	0.061	0.250	0.113	0.237
Imphal	7	10	0.053	0.052	0.228	0.206	0.283
Cuttack	3	8	0.021	0.065	0.249	0.191	0.266
Solapur	7	4	0.038	0.078	0.225	0.144	0.290
Satara	5	24	0.039	0.050	0.178	0.239	0.336
(1935-1968)							
Ganganagar	3	1	0.094	0.015	0.297	0.114	0.293
Lucknow	4	12	0.013	0.017	0.230	0.138	0.244
Imphal	3	24	0.032	0.076	0.201	0.245	0.283
Cuttack	5	5	0.041	0.101	0.248	0.165	0.290
Solapur	6	14	0.049	0.092	0.227	0.150	0.368
Satara	2	30	0.033	0.170	0.164	0.269	0.452
(1969-2002)							
Ganganagar	5	1	0.074	0.015	0.303	0.112	0.320
Lucknow	5	3	0.023	0.041	0.231	0.146	0.247
Imphal	6	19	0.071	0.234	0.214	0.299	0.324
Cuttack	5	12	0.057	0.044	0.248	0.310	0.348
Solapur	6	24	0.024	0.054	0.219	0.174	0.345
Satara	4	3	0.027	0.169	0.170	0.235	0.404

Here, 'Gen', 'DFA' and 'R/S' are abbreviations used for generalised Hurst method, detrended fluctuation analysis and rescaled range analysis respectively. min.var. denotes minimum target variance.

Table 3.4 Optimal embedding dimension, time lag, RMSE, minimum target variance and Hurst exponent measures of sample stations in different time periods for precipitation data

Station	m	Tau	RMSE	min. var.	Hurst Exponent*		
					Gen.	DFA	R/S
(1901-1934)							
Ganganagar	8	24	0.113	0.020	0.148	0.386	0.427
Lucknow	8	2	0.071	0.410	0.208	0.179	0.313
Imphal	5	24	0.081	0.015	0.236	0.14	0.283
Cuttack	7	12	0.072	0.052	0.225	0.172	0.315
Solapur	6	2	0.026	0.434	0.186	0.325	0.387
Satara	4	24	0.093	0.003	0.221	0.293	0.321
(1935-1968)							
Ganganagar	4	12	0.093	0.075	0.125	0.467	0.348
Lucknow	5	30	0.087	0.019	0.226	0.308	0.2
Imphal	5	12	0.052	0.011	0.256	0.327	0.206
Cuttack	8	12	0.041	0.030	0.231	0.329	0.182
Solapur	8	12	0.048	0.002	0.199	0.361	0.233
Satara	5	24	0.067	0.000	0.209	0.268	0.199
(1969-2002)							
Ganganagar	5	12	0.088	0.022	0.138	0.417	0.455
Lucknow	5	5	0.081	0.179	0.235	0.224	0.335
Imphal	7	12	0.083	0.018	0.26	0.203	0.366
Cuttack	8	24	0.050	0.038	0.227	0.112	0.303
Solapur	4	12	0.048	0.013	0.224	0.207	0.335
Satara	4	9	0.040	0.056	0.239	0.205	0.285

*Here, 'Gen', 'DFA' and 'R/S' are abbreviations used for generalised Hurst method, detrended fluctuation analysis and rescaled range analysis respectively. min.var. denotes minimum target variance.

rest following the most nonlinear trend. Moreover, $H(q)$ vs (q) plots of Lucknow and Cuttack districts whose RMSE values are comparable (0.019 and 0.021 respectively) in 1901-1934, have overlapping curves in Figure 3.9d. In addition to this, least nonlinearity is observed for Lucknow district's temperature profile during three subsequent periods, for which, the $H(q)$ vs (q) plots are almost linear with a little or no change. Moreover, $H(q)$ values for precipitation were changing more nonlinearly with increasing (q) . It should be noted that precipitation, in general, had larger RMSE values due to the presence of higher nonlinear components (Table 3.4). As suggested by Jaksic et al. (2016), a nonlinear change in $H(q)$ values with increasing order of moment (q) suggest that time-series carries multi-scaling behaviour. Hence, it can be firmly concluded that precipitation, being more nonlinear, is also carrying a stronger multi-scaling characteristics

3.3.4 Assessment of determinism

In the previous section, DVV scatter plots are utilised to visualise the presence of nonlinearity in a time series by observing the difference between original and surrogate data sets. Here, 'DVV plots' can be used to visualise the nonlinearity as well as the presence of deterministic component, which is estimated as the value of minimum target variance of the original time series. Figure 3.10 represents the DVV plots of six stations for temperature and precipitation. Original minimum target variance curves for precipitation are more disorderly as compared to its linearised surrogate versions, indicating significant nonlinearity. The minimum values of variance in the variance curve of original data can be utilised to understand the presence of deterministic component. In almost every plot, the presence of a strong deterministic component can be noticed. Also, to understand the variation over the three time periods, the DVV plots plots of some stations have also been shown (Figure 3.11ab). It can be noticed that the difference between the target variance of the surrogate and original data set of

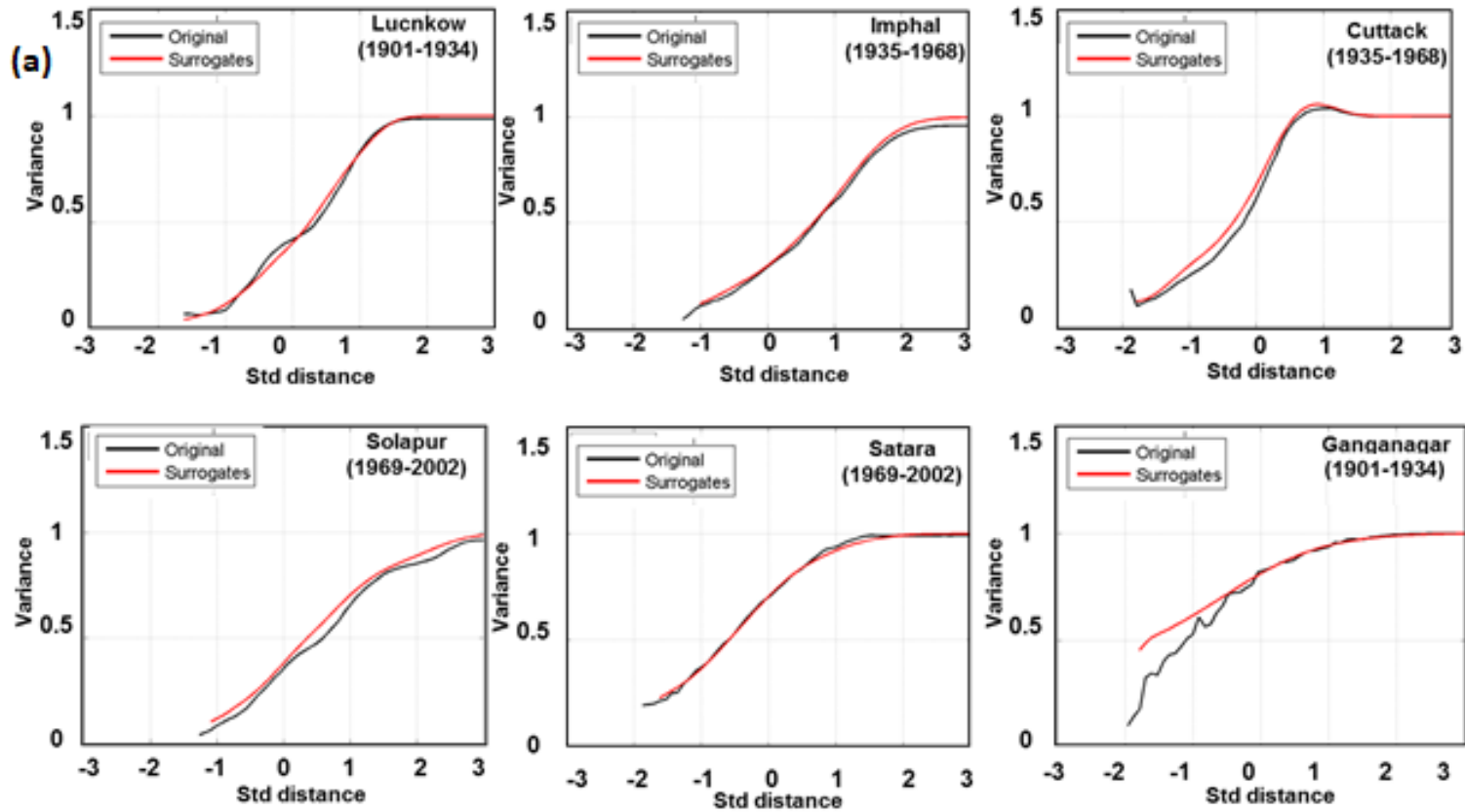


Figure 3.10a DVV plots for six districts in different time periods for temperature. Red and black lines denote target variance values for original and surrogate data sets

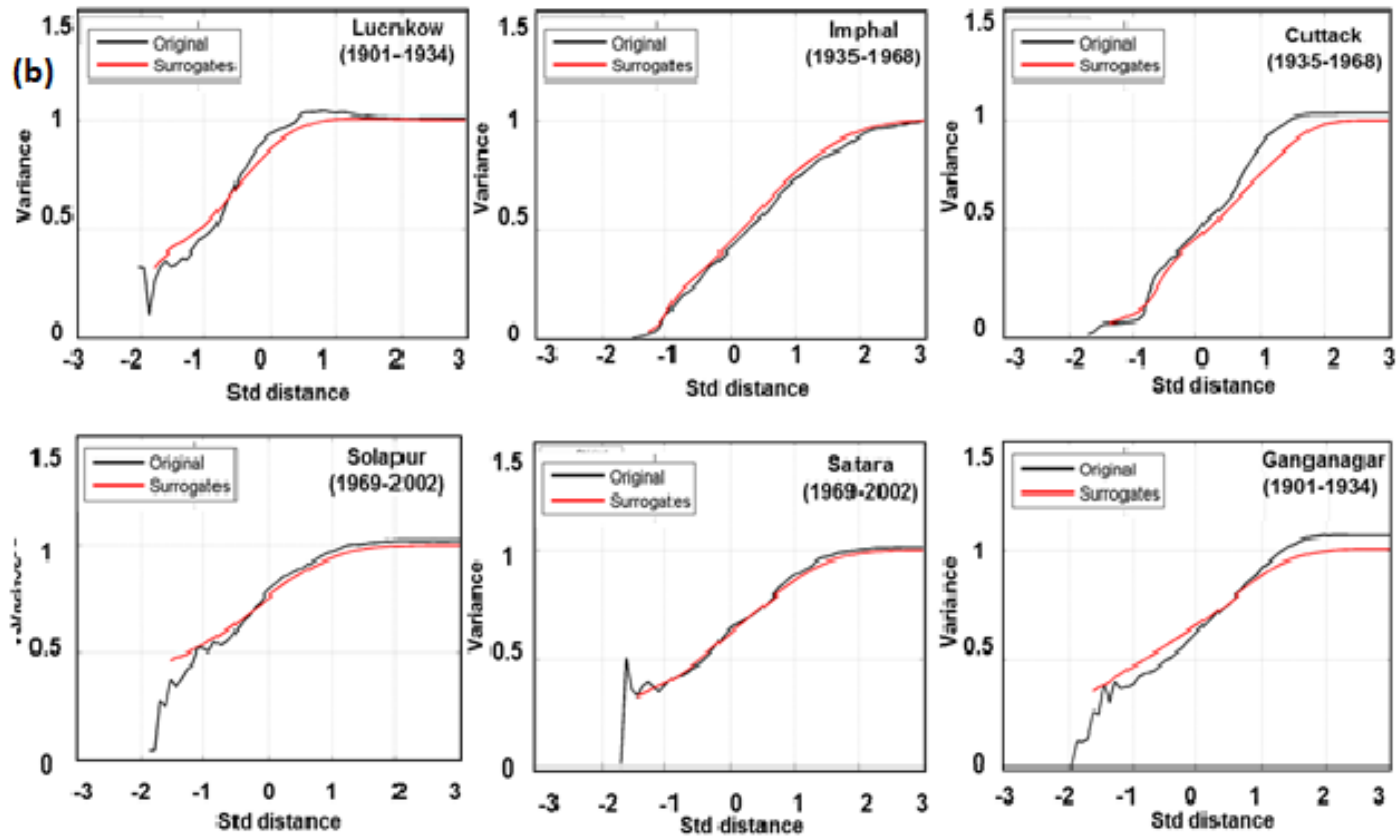


Figure 3.10b DVV plots for six districts in different time periods for precipitation. Red and black lines denote target variance values for original and surrogate data sets

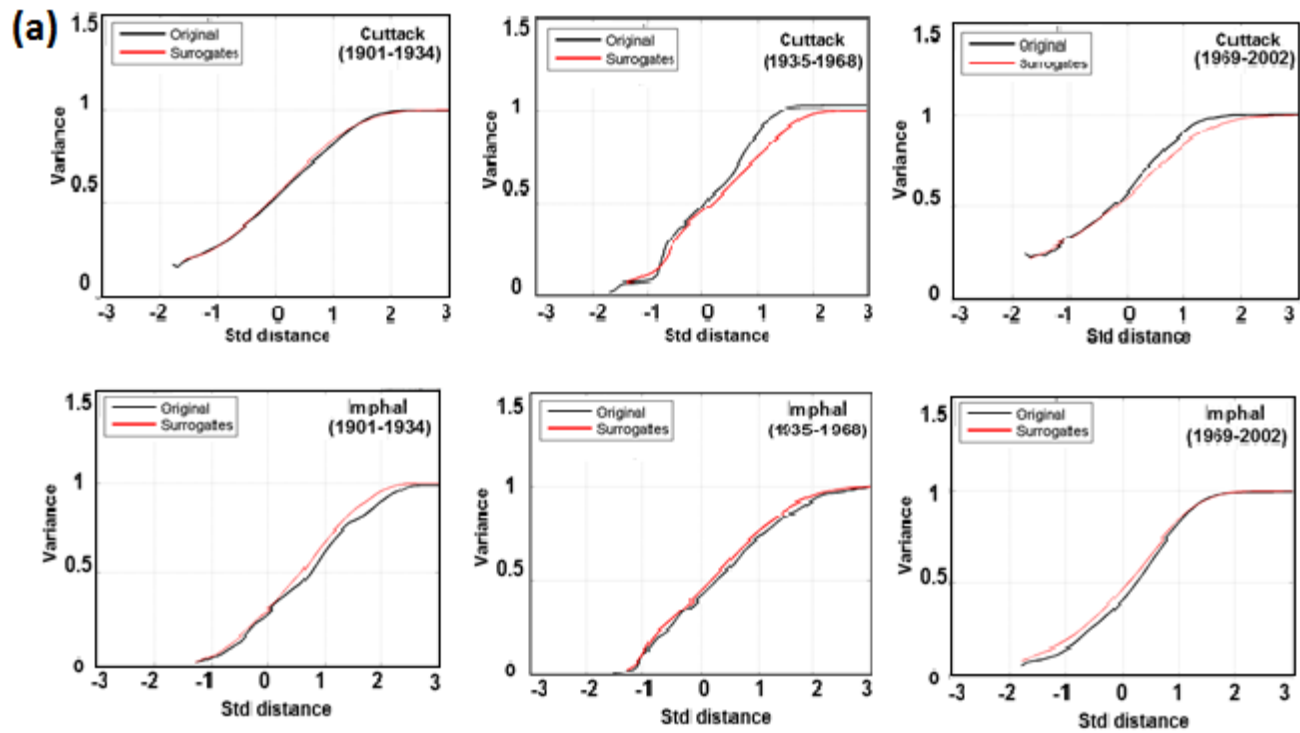


Figure 3.11a DVV plots for two representative stations during (1901-1934), (1935-1968) and (1969-2002) for temperature. Red and black lines denote target variance values for original and surrogate data sets

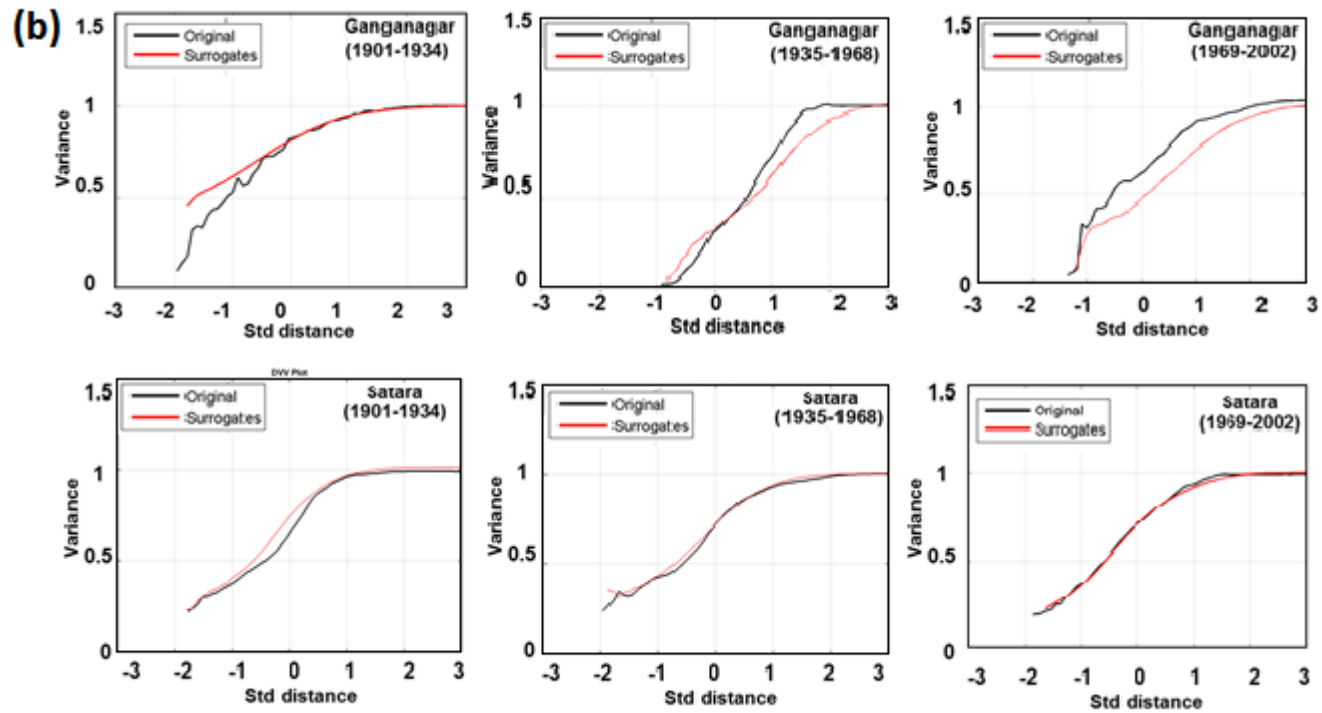


Figure 3.11b DVV plots for two representative stations during (1901-1934), (1935-1968) and (1969-2002) for precipitation. Red and black lines denote target variance values for original and surrogate data sets

Ganganagar keeps varying overtime which is an indicator of significant nonlinearity. Further, the less nonlinear stations, e.g. Satara, have not shown much deviation over time. To understand the determinism, minimum target variance values for all 566 stations are computed and normalised over a scale of 0 to 1 for proper comparison. Normalised minimum target variance values are classified as highly deterministic (0-0.1), significantly deterministic (0.1-0.25), moderately deterministic (0.25-0.5) and non-deterministic (0.5-1). For precipitation, it is observed that initially, 193 out of 566 districts are highly deterministic, which later gets reduced to 162 districts by the end of 2002 (Table 3.2). Further, the number of significantly deterministic stations is 124 during 1901-1934, which are limited to 114, and 116 during 1935-1968 and 1969-2002 respectively. At the same time, the increase in the number of moderately deterministic stations is also observed. The distribution of absolute percent change in the deterministic behaviour of districts during the last century can be observed in Figure 3.7c,d. Only, 88 and 135 out of 566 districts witnessed a continuous rise in determinism in their precipitation and temperature profiles throughout the century. However, a total of 210 and 247 districts exhibit a trend of rising and then fall in determinism in their precipitation and temperature profiles. Individually, during the transition from 1901-1934 to 1935-1968 time period, determinism is observed to decrease in temperature profiles across 186 districts in the country. Whereas, during 1935-1968 to 1969-2002, determinism in temperature has decreased in 336 districts across the country. Similarly, determinism in precipitation has also decreased in 268 (1901-1934 to 1935-1968) and 317 (1935-1968 to 1969-2002) districts.

The spatial distribution of normalised minimum variance suggests that both precipitation and temperature, in general, carry strong deterministic components (Figure 3.4d, 3.5d). For initial 34 years, all districts except a few in the north-west, north-east and west-coast region exhibit strong deterministic properties in their respective temperature profiles. However, with time, districts in the west-coast region have become less deterministic.

Moreover, precipitation data, which is found to be more nonlinear than the temperature, is also significantly deterministic in most parts of the country except the low precipitation zones. The districts in the north-west, extreme north and southern part of the country are found to be consistently non-deterministic throughout the century. It should be noted that the presence of nonlinearity should not always be related to unpredictability. If the underlying nonlinearity is accompanied by strong determinism, the chances of better predictability prevail.

3.4 Discussions

The main aim of this study is to detect the presence of underlying nonlinearity and determinism in the Indian climate from a predictability point of view. For this purpose, the temperature and precipitation profiles of 566 districts of the country are analysed using the DVV approach which is supposed to be robust to the presence of noise, length of data and choice of embedding parameters. The analysis shows that both temperature and precipitation are highly nonlinear. For precipitation, the normalised RMSE values are found to be significantly increased in subsequent periods which indicate that precipitation in India is becoming increasingly nonlinear. Quantitatively, precipitation profiles in about 80% out of 566 districts are found to be significant to extremely nonlinear throughout the century. At the same time, the number of non-deterministic to moderately deterministic districts have increased (66% in 1901-1934 to 71% in 1969-2002) over the century, and the number of significantly deterministic districts have decreased (34% in 1901-1934 to 28% in 1969-2002). If this trend continues, the chances of better predictability of precipitation are supposed to be grim in future. Similarly, temperature profiles in about 60% (341) out of 566 districts are found to be significant to extremely nonlinear in the initial 34 years which counts up to 279 (50%) districts in 1969-2002. Although, there was a decrease in the number of significant to extremely nonlinear districts, however, the decrease in the number of highly deterministic stations is also observed to decrease with time (455 in 1901-1934, 380 in 1935-1968 and

334 in 1969-2002). This is not encouraging as loss of determinism is evidence of decreasing predictability. Moreover, considerable spatial changes in the nonlinearity profile are observed in different periods.

It is further concluded that the nonlinearity associated with rainfall is both time and scale-dependent. This finding of scale and time dependence of Indian rainfall is in agreement with other such studies (Subash et al. 2011; Subash and Sikka 2014). A nonlinear precipitation input in hydrological cycle further increases the chances of uncertainty in remaining components. Hence, knowledge about the nonlinearity in rainfall pattern can provide crucial inputs in deciding policies and plans for efficient water resource management practices in this region which has witnessed several droughts and floods in the past years. Unlike the precipitation data where large variation in the temporal and spatial distribution of nonlinearity is observed, large RMSE values for temperature profiles are found to be clustered in the north-west region. This part of the country experiences one of the most significant variations in daily maximum and minimum temperature and receives scanty rainfall. Detection of long term nonlinearity in these circumstances further increases the chances of poor predictability hence, increased risks. Initially, a few stations in north-east India are found to be nonlinear, also, in the last 34 years, some districts in the western coastal region are found to be turning nonlinear. Considering all the time periods and spatial distribution of rainfall, it is likely that precipitation extremes are closely related to the distribution of nonlinearity in temperature profiles which further needs to be explored. In addition to this, for precipitation, nonlinearity is higher, and determinism is lower than of temperature. For both, regions of extreme precipitation and temperature (either higher or lower) are significantly non-deterministic in all time periods. As most of the districts in extreme climate zones are also found to be nonlinear as well as non-deterministic, the prediction of extreme climate events in these regions might remain least predictable in future. Moreover, a shift in the nonlinear dynamics is not only observed with time but also with scale. Hurst exponent

values obtained from three methods discussed earlier disclosed that both the variables show properties of anti-persistent process with short-range dependence. For precipitation, exponent values are observed to be changing more nonlinearly with the order of the moment, leading to the conclusion that precipitation is more significantly multi-scaling than temperature. Further, the presence of nonlinearity, as well as strong determinism in the climate, is a strong indication of hidden chaotic dynamics which may be explored in future studies. Since this study provides a characterization of nonlinearity and determinism in different spatial and temporal scale, possible interconnections between both is also a significant issue to be examined.

3.5. Conclusions

This study presents the analysis of the predictability of the Indian climate of the past century (1901-2002) by investigating the nonlinear and deterministic dynamics of the precipitation and temperature data of India at the district level. The evidence of nonlinearity or randomness and associated determinism are utilised as the measure of predictability. It is found that districts in the extreme rainfall or temperature zone are least deterministic and highly nonlinear. Precipitation profiles in the majority of districts are significant to extremely nonlinear, especially in the north-west and arid zones of the country. In addition to this, the predictability of precipitation in the majority of districts has decreased due to the deterioration in deterministic characteristics. Although, nonlinearity in temperature is found to be somewhat lesser as compared to precipitation, the trend of determinism suggests that temperature profiles also remains increasingly unpredictable. It is observed that precipitation, being more nonlinear is more sensitive to changes in spatial and temporal variations. Moreover, the analysis of scaling properties suggests that all the variables show characteristics of fractional Brownian motion (fBm), anti-persistent, short-range dependent time series. The extent of nonlinearity is observed to be strongly related to multi-scaling properties. The analysis on a few sample

stations revealed that a significantly nonlinear precipitation profile is also significantly multi-scaling in nature. It is found that districts in the extreme climate zones are highly nonlinear and least deterministic which induces a poor state of climate predictability in these regions. The trend of nonlinearity and determinism indicates that chances of better climate predictability in these sensitive zones might be more significantly affected in future.

Chapter 4

Low-frequency global-scale modes and their influence on rainfall extremes

4.1 Introduction

As discussed in the literature review section, the inclusion of physical processes as covariates under the changing climate is crucial. Subsequently, it is also vital to have reliable estimates of the return levels for optimal design purposes. Ignoring the uncertainty associated with the distribution's parameters may lead to under/overestimation of designs that subsequently can cause catastrophic damages (Coles et al. 2003). Specifically, the classical approach uses the point estimate of the parameters obtained using different methods such as L-moments (Saf 2009; Haddad et al. 2011), method of moments(Lück and Wolf 2016), and maximum likelihood estimation (MLE) (Das and Umamahesh 2017). Moreover, Coles et al. (2003) reaffirmed that the classical approach does not encompass the model uncertainty comprehensively and is confined to produce an overly positive assessment of extremes. The Bayesian method is one of such methods to overcome this issue. With this approach, it is possible to obtain the posterior distribution of the parameters by integrating it over the parameter space. Moreover, the introduction of Markov Chain Monte Carlo (MCMC) methodology allows the approximation of the integrals by employing a Markov chain with the posterior distribution (Chandra et al. 2015).

In this study, the risks due to heavy precipitation in India is investigated by employing nonstationary EVT in the Bayesian framework. The major objective of the work can be given as identifying the linkage of large-scale climate oscillation to historical (1951-2013) extreme precipitation and examining the uncertainty related to the parameters by employing the Bayesian approach. Specifically, the parameters of the probability distribution are analysed to ascertain the associated uncertainty

incorporating the prior distribution and likelihood function. The MCMC algorithm is employed to obtain the parameter samples from the posterior distribution using the Bayes rule. Further, high-resolution spatial maps and underlying uncertainties in return level and parameters over India have been prepared, and the results have been characterised on the river basin scale. The findings have critical applications on the understanding of how ENSO, IOD and NAO influence extreme precipitation in different parts of the country and would enable a more rigorous theoretical foundation for assessment of risks due to heavy rainfall.

4.2 Data and methodology

4.2.1 Study area and data

Many major rivers basins across the globe have witnessed changes in their natural ability to absorb the impacts of climate change. In this context, river basins have a distinctive geographical, geological, hydrological characteristic. Therefore, analysis on a river basin scale could give a proper framework for managing water resources in the context of the risks due to extreme rainfall. This study is performed over 24 major river basins of the country for appropriate characterisation of the regions of high risks. Figure 4.1 can be referred for the location of river basins and their corresponding IDs.

In this study, gridded daily precipitation data for 1951-2013 is extracted from a high spatial resolution ($0.5^\circ \times 0.5^\circ$) IMD (India Meteorological Department) data set which has been prepared using daily rainfall from a network of 6955 rain-gauge stations in the country (Pai et al. 2014). The IMD states that these data had been prepared by assuring quality control of rain gauge stations and verified using existing data sets. This data is known to capture the variability in the Indian monsoon rainfall most efficiently among those obtained from similar sources (Mishra et al. 2014).

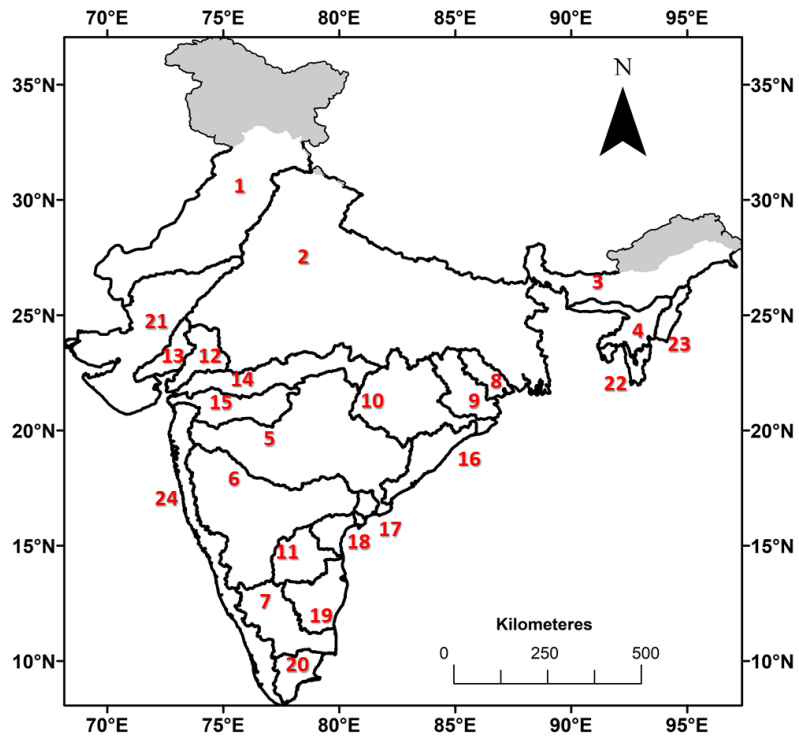


Figure 4.1 River basins and their IDs used in the study. The details of basin IDs are : 1-Indus,2-Ganga,3 Brahmaputra,4-Barak, 5- Godavari,6-Krishna,7-Cauvery,8-Subernrekha,9-Brahmani and Baitarani, 10 Mahanadi, 11-Pennar,12-Mahi, 13-Sabarmati, 14-Narmada, 15-Tapi, 16-East flowing rivers between Mahanadi and Godavari basins (EFRMGB), 17- East flowing rivers between Godavari and Krishna basins (EFRGKB),18- East flowing rivers between Krishna and Pennar basins (EFRKPB) ,19- East flowing rivers between Pennar and Cauvery basins (EFRPCB),20-East flowing rivers between Subernrekha and Cauvery basins (EFRSCB), 21-Luni ,22- Minor rivers flowing into Bangladesh (MRFB) ,23-Minor rivers flowing into Myanmar (MRFM) ,24- Western Ghats (WG)

Four precipitation indices, namely, monthly maximum one-day precipitation (Rx1 day), annual count of days when precipitation is more than or equal to 10mm (R10), maximum number of consecutive wet days (CWD) and simple daily precipitation intensity index (SDII) which is total annual rainfall divided by the number of wet days are calculated based on the recommendations of Expert Team on Climate Change Detection and Indices (ETCCDI) (Zhang and Zwiers 2013). The indices were developed using the Climdex package in R (Bronaugh 2014). These indices have been extensively utilized, and their investigation has produced significant results in the analysis of extreme rainfall over India and the world (Revadekar and Preethi 2012; Rao et al. 2014; Pfahl et al. 2017). It is to be noted that the annual maximum values of the extremes are considered during the analysis.

As discussed, ENSO, IOD and NAO are used as covariates for analysing the nonstationary impact on extreme rainfall. Several studies have utilised the SSTs to understand the variability in monsoon rainfall in India (Gershunov et al. 2001; Revadekar and Kulkarni 2008). The monthly mean anomaly of SST with respect to 1981-2010, averaged over the NINO3.4 (17°E-120°W, 5°S-5°N), is calculated. Since annual precipitation indices are taken into account, therefore, the SST anomalies during their dominant period (November to March) have been considered. The monthly SST anomalies are obtained from the National Oceanic and Atmospheric Administration (NOAA) Centre for Weather and Climate Prediction (<https://www.cpc.ncep.noaa.gov/data/indices/>) website. IOD is measured as Dipole Mode Index (DMI) encompassing the dipole mode in the tropical the Indian Ocean. The DMI is described as the difference between SST anomaly between tropical western Indian Ocean and the tropical south-eastern Indian Ocean. The DMI data is downloaded from the Japan Agency for Marine-Earth Science and Technology (JAMSTEC) website (<http://www.jamstec.go.jp/frcgc/research/d1/iod/>). The NAO index is given as the difference between sea pressure between the sub-tropical high and sub-polar low. NAO has been recognised as one of the major modes of rainfall

variability in India specifically in the winter season in the northern hemisphere. The NAO data is obtained from the Climate Research Unit (CRU) website (<https://crudata.uea.ac.uk/cru/data/nao/>).

4.2.2 Methods

The overall methodology employed in this study has been represented with the help of a flowchart in Figure 4.2. In the very first step, the extreme precipitation indices (Rx1 day, SDII, R10 and CWD) from historical (1951-2013) precipitation data are computed and analysed for their spatio-temporal distribution, variability and trends. Eventually, the stationary and nonstationary modelling of extreme indices are performed, and the best fit model is obtained. The results obtained in this step is used as the initial setting for Bayesian analysis to obtain the posterior distribution parameters. Subsequently, parameters and return levels in different return periods are estimated along with their uncertainties. The extreme value analysis was done using the extRemes 2.0 package in R (Gilleland and Katz 2016).

4.2.2.1 Trend analysis of the extreme precipitation indices

World Meteorological Organization (WMO) guidelines recommend many methods for trend detection in hydro-climatic variables (Kundzewicz and Robson 2000; Hannaford and Marsh 2006). In this study, Mann- Kendall (MK) test is used to detect the existence of a linear trend in the extreme precipitation indices. The MK test is a nonparametric test for the detection of trends in a time series. MK test is simple, robust and has the advantage of dealing with data inconsistency such as missing values in a time series. Hence, in this study, the nonparametric MK test is used to analyse the temporal behaviour of Rx1 day, SDII, R10 and CWD over India. For the sake of brevity, the MK test has not been discussed in detail here, and there are several works available (Cao et al. 2015; Gao et al. 2016) which can be followed to understand the test in detail.

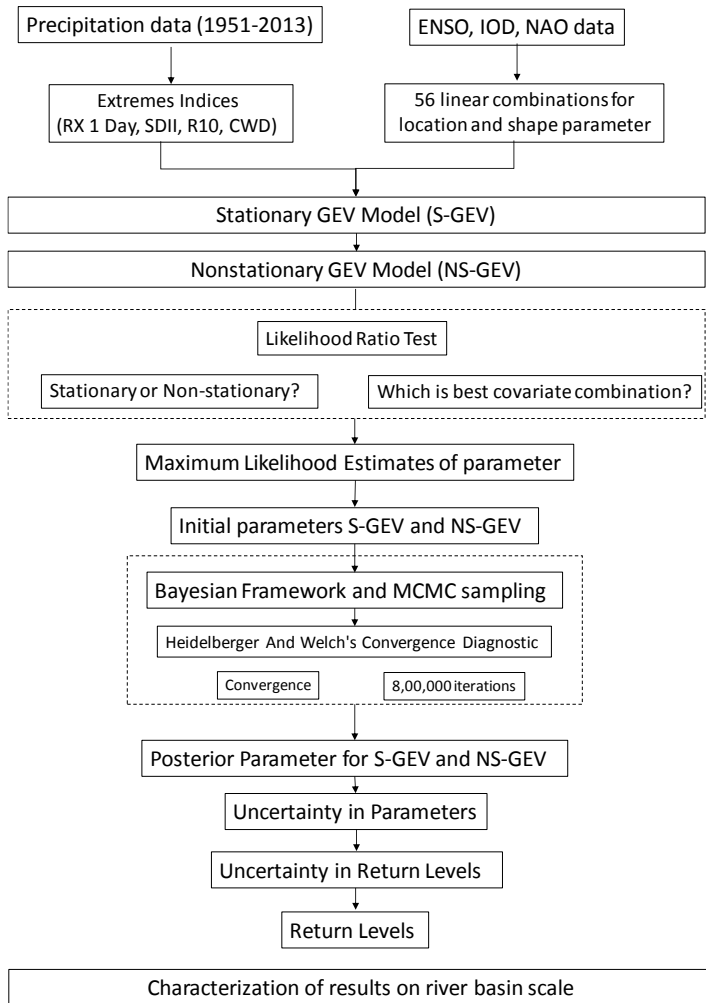


Figure 4.2 Methodological flowchart

4.2.2.2 Nonstationary modelling of extreme precipitation indices

Two of the majorly used probability distributions to study the extreme climate variables are the Generalized Extreme Value (GEV) distribution and Generalized Pareto (GP) distribution (Cooley 2009). The probability distribution of extreme precipitation indices is considered as GEV. It should be noted that all four extreme precipitation indices have been modelled using the GEV distribution, assuming that all are continuous random variables. The cumulative probability distribution function for GEV distribution can be given by Equation 4.1.

$$F(x; \mu, \sigma, \xi) = \begin{cases} \exp\left\{-\left[1 + \frac{\xi(x-\mu)}{\sigma}\right]^{-1/\xi}\right\}, & \sigma > 0, 1 + \frac{\xi(x-\mu)}{\sigma} > 0, \xi \neq 0 \\ \exp\left\{-\exp\left[-\frac{(x-\mu)}{\sigma}\right]\right\}, & \sigma > 0, \xi = 0 \end{cases} \quad (4.1)$$

where, x corresponds to the annual extreme precipitation indices and $\theta = [\mu, \sigma, \xi]$ represents the location, scale and scale parameters. The GEV distribution parameters mentioned in Equation 4.1 correspond to the stationary assumption. Further, nonstationarity in the GEV distribution is introduced by the expressing these parameters as linear functions of the large-scale oscillation indices which are ENSO (to be read as C_1), IOD (C_2) and NAO (C_3). Considering the shape parameter as a function of time is often not advised (Coles 2001; Yilmaz and Perera 2014). Hence, for the sake of simplicity, the shape parameter ξ is assumed to be constant and only location and scale parameters are varied. Further, Gilleland and Katz (2016) suggested that varying the scale parameter without changing the location parameter might not be appropriate in modelling the influence of covariates. Therefore, in view of these criteria, 56 (M1, M2, M3...) linear combinations considering the linear dependence of location and shape parameters on climate indices for the nonstationary modelling are considered. Please see Table 4.1 for details about the covariate combination equations. The ID for stationary model is given by M0 in which the values of covariates is zero

representing constant parameters. The coefficients μ_1, μ_2, μ_3 and $\sigma_1, \sigma_2, \sigma_3$ in the nonstationary models denote the trend in location and shape parameters depicting the influence of physical covariates C_1, C_2 and C_3 respectively. Based on the comparison of nonstationary models with its stationary counterpart, the impact of related large-scale oscillations on the extreme precipitation can be assessed.

For parameter estimation, maximum likelihood (ML) approach is adopted, which is known to incorporate the nonstationary characteristics of parameter distribution (Towler et al. 2010). The ML estimates are the values of $\theta = [\mu, \sigma, \xi]$ on which the likelihood function attains maximum value. Lets, define $X = x_1, x_2, x_3, \dots, x_{(n-1)}, x_{(n)}$ be the series of any selected extreme indices with n number of observations. The log-likelihood can be defined as:

$$L(\theta|X) = -n \log \sigma - (1 + 1/\xi) \sum_{i=1}^n \log \left[1 + \xi \left(\frac{x_i - \mu}{\sigma} \right) \right] - \sum_{i=1}^n \left[1 + \xi \left(\frac{x_i - \mu}{\sigma} \right) \right]^{-1/\xi} \quad (4.2)$$

$$, 1 + \xi \left(\frac{x_i - \mu}{\sigma} \right) > 0$$

where $L(\theta)$ is the likelihood function of the parameter vector θ . Precisely, the likelihood function is the measure of how likely the datasets are as a function of the unknown parameters of GEV distribution, and the MLE evaluates the values of parameters those maximize the likelihood function (Katz 2013). The MLE estimation in the context of this study can be defined by, e.g. for M1 where the location parameter is linked with covariate C_1 (ENSO), function $L(\mu(C_1), \sigma, \xi|X)$ based on four parameters μ_0, μ_1, σ , and ξ . Optimization is performed to obtain these four parameters so that the likelihood function is maximized.

Table 4.1 Description of the models used in the present study

Model ID	Description
M0	$X \sim GEV[\mu, \sigma, \xi]$
M1	$X \sim GEV[(\mu_0 + \mu_1 C_1), \sigma, \xi]$
M2	$X \sim GEV[(\mu_0 + \mu_2 C_2), \sigma, \xi]$
M3	$X \sim GEV[(\mu_0 + \mu_3 C_3), \sigma, \xi]$
M4	$X \sim GEV[(\mu_0 + \mu_1 C_1 + \mu_2 C_2), \sigma, \xi]$
M5	$X \sim GEV[(\mu_0 + \mu_2 C_2 + \mu_3 C_3), \sigma, \xi]$
M6	$X \sim GEV[(\mu_0 + \mu_3 C_3 + \mu_1 C_1), \sigma, \xi]$
M7	$X \sim GEV[(\mu_0 + \mu_1 C_1 + \mu_2 C_2 + \mu_3 C_3), \sigma, \xi]$
M8	$X \sim GEV[(\mu_0 + \mu_1 C_1), (\sigma_0 + \sigma_1 C_1), \xi]$
M9	$X \sim GEV[(\mu_0 + \mu_1 C_1), (\sigma_0 + \sigma_2 C_2), \xi]$
M10	$X \sim GEV[(\mu_0 + \mu_1 C_1), (\sigma_0 + \sigma_3 C_3), \xi]$
M11	$X \sim GEV[(\mu_0 + \mu_2 C_2), (\sigma_0 + \sigma_1 C_1), \xi]$
M12	$X \sim GEV[(\mu_0 + \mu_2 C_2), (\sigma_0 + \sigma_2 C_2), \xi]$
M13	$X \sim GEV[(\mu_0 + \mu_2 C_2), (\sigma_0 + \sigma_3 C_3), \xi]$
M14	$X \sim GEV[(\mu_0 + \mu_3 C_3), (\sigma_0 + \sigma_1 C_1), \xi]$
M15	$X \sim GEV[(\mu_0 + \mu_3 C_3), (\sigma_0 + \sigma_2 C_2), \xi]$
M16	$X \sim GEV[(\mu_0 + \mu_3 C_3), (\sigma_0 + \sigma_3 C_3), \xi]$
M17	$X \sim GEV[(\mu_0 + \mu_1 C_1 + \mu_2 C_2), (\sigma_0 + \sigma_1 C_1), \xi]$
M18	$X \sim GEV[(\mu_0 + \mu_2 C_2 + \mu_3 C_3), (\sigma_0 + \sigma_1 C_1), \xi]$
M19	$X \sim GEV[(\mu_0 + \mu_3 C_3 + \mu_1 C_1), (\sigma_0 + \sigma_1 C_1), \xi]$
M20	$X \sim GEV[(\mu_0 + \mu_1 C_1 + \mu_2 C_2), (\sigma_0 + \sigma_2 C_2), \xi]$
M21	$X \sim GEV[(\mu_0 + \mu_2 C_2 + \mu_3 C_3), (\sigma_0 + \sigma_2 C_2), \xi]$
M22	$X \sim GEV[(\mu_0 + \mu_3 C_3 + \mu_1 C_1), (\sigma_0 + \sigma_2 C_2), \xi]$

M23	$X \sim GEV[(\mu_0 + \mu_1 C_1 + \mu_2 C_2), (\sigma_0 + \sigma_3 C_3), \xi]$
M24	$X \sim GEV[(\mu_0 + \mu_2 C_2 + \mu_3 C_3), (\sigma_0 + \sigma_3 C_3), \xi]$
M25	$X \sim GEV[(\mu_0 + \mu_3 C_3 + \mu_1 C_1), (\sigma_0 + \sigma_3 C_3), \xi]$
M26	$X \sim GEV[(\mu_0 + \mu_1 C_1 + \mu_2 C_2 + \mu_3 C_3), (\sigma_0 + \sigma_1 C_1), \xi]$
M27	$X \sim GEV[(\mu_0 + \mu_1 C_1 + \mu_2 C_2 + \mu_3 C_3), (\sigma_0 + \sigma_2 C_2), \xi]$
M28	$X \sim GEV[(\mu_0 + \mu_1 C_1 + \mu_2 C_2 + \mu_3 C_3), (\sigma_0 + \sigma_3 C_3), \xi]$
M29	$X \sim GEV[(\mu_0 + \mu_1 C_1), (\sigma_0 + \sigma_1 C_1 + \sigma_2 C_2), \xi]$
M30	$X \sim GEV[(\mu_0 + \mu_1 C_1), (\sigma_0 + \sigma_2 C_2 + \sigma_3 C_3), \xi]$
M31	$X \sim GEV[(\mu_0 + \mu_1 C_1), (\sigma_0 + \sigma_3 C_3 + \sigma_1 C_1), \xi]$
M32	$X \sim GEV[(\mu_0 + \mu_2 C_2), (\sigma_0 + \sigma_1 C_1 + \sigma_2 C_2), \xi]$
M33	$X \sim GEV[(\mu_0 + \mu_2 C_2), (\sigma_0 + \sigma_2 C_2 + \sigma_3 C_3), \xi]$
M34	$X \sim GEV[(\mu_0 + \mu_2 C_2), (\sigma_0 + \sigma_3 C_3 + \sigma_1 C_1), \xi]$
M35	$X \sim GEV[(\mu_0 + \mu_3 C_3), (\sigma_0 + \sigma_1 C_1 + \sigma_2 C_2), \xi]$
M36	$X \sim GEV[(\mu_0 + \mu_3 C_3), (\sigma_0 + \sigma_2 C_2 + \sigma_3 C_3), \xi]$
M37	$X \sim GEV[(\mu_0 + \mu_3 C_3), (\sigma_0 + \sigma_3 C_3 + \sigma_1 C_1), \xi]$
M38	$X \sim GEV[(\mu_0 + \mu_1 C_1), (\sigma_0 + \sigma_1 C_1 + \sigma_2 C_2 + \sigma_3 C_3), \xi]$
M39	$X \sim GEV[(\mu_0 + \mu_2 C_2), (\sigma_0 + \sigma_1 C_1 + \sigma_2 C_2 + \sigma_3 C_3), \xi]$
M40	$X \sim GEV[(\mu_0 + \mu_3 C_3), (\sigma_0 + \sigma_1 C_1 + \sigma_2 C_2 + \sigma_3 C_3), \xi]$
M41	$X \sim GEV[(\mu_0 + \mu_1 C_1 + \mu_2 C_2), (\sigma_0 + \sigma_1 C_1 + \sigma_2 C_2), \xi]$
M42	$X \sim GEV[(\mu_0 + \mu_1 C_1 + \mu_2 C_2), (\sigma_0 + \sigma_2 C_2 + \sigma_3 C_3), \xi]$
M43	$X \sim GEV[(\mu_0 + \mu_1 C_1 + \mu_2 C_2), (\sigma_0 + \sigma_3 C_3 + \sigma_1 C_1), \xi]$
M44	$X \sim GEV[(\mu_0 + \mu_2 C_2 + \mu_3 C_3), (\sigma_0 + \sigma_1 C_1 + \sigma_2 C_2), \xi]$
M45	$X \sim GEV[(\mu_0 + \mu_2 C_2 + \mu_3 C_3), (\sigma_0 + \sigma_2 C_2 + \sigma_3 C_3), \xi]$
M46	$X \sim GEV[(\mu_0 + \mu_2 C_2 + \mu_3 C_3), (\sigma_0 + \sigma_3 C_3 + \sigma_1 C_1), \xi]$
M47	$X \sim GEV[(\mu_0 + \mu_3 C_3 + \mu_1 C_1), (\sigma_0 + \sigma_1 C_1 + \sigma_2 C_2), \xi]$
M48	$X \sim GEV[(\mu_0 + \mu_3 C_3 + \mu_1 C_1), (\sigma_0 + \sigma_2 C_2 + \sigma_3 C_3), \xi]$

M49	$X \sim GEV[(\mu_0 + \mu_3 C_3 + \mu_1 C_1), (\sigma_0 + \sigma_3 C_3 + \sigma_1 C_1), \xi]$
M50	$X \sim GEV[(\mu_0 + \mu_1 C_1 + \mu_2 C_2 + \mu_3 C_3), (\sigma_0 + \sigma_1 C_1 + \sigma_2 C_2 + \sigma_3 C_3), \xi]$
M51	$X \sim GEV[(\mu_0 + \mu_1 C_1 + \mu_2 C_2), (\sigma_0 + \sigma_1 C_1 + \sigma_2 C_2 + \sigma_3 C_3), \xi]$
M52	$X \sim GEV[(\mu_0 + \mu_2 C_2 + \mu_3 C_3), (\sigma_0 + \sigma_1 C_1 + \sigma_2 C_2 + \sigma_3 C_3), \xi]$
M53	$X \sim GEV[(\mu_0 + \mu_3 C_3 + \mu_1 C_1), (\sigma_0 + \sigma_1 C_1 + \sigma_2 C_2 + \sigma_3 C_3), \xi]$
M54	$X \sim GEV[(\mu_0 + \mu_1 C_1 + \mu_2 C_2 + \mu_3 C_3), (\sigma_0 + \sigma_1 C_1 + \sigma_2 C_2), \xi]$
M55	$X \sim GEV[(\mu_0 + \mu_1 C_1 + \mu_2 C_2 + \mu_3 C_3), (\sigma_0 + \sigma_2 C_2 + \sigma_3 C_3), \xi]$
M56	$X \sim GEV[(\mu_0 + \mu_1 C_1 + \mu_2 C_2 + \mu_3 C_3), (\sigma_0 + \sigma_3 C_3 + \sigma_1 C_1), \xi]$

The MLE estimation is performed both for the stationary as well as nonstationary models. To compare the significance between stationary and nonstationary models, the likelihood ratio test (LR test) is used (Coles 2001). In the present study, the nonstationary model (NS-GEV) with a linear trend in the parameters and the stationary model (S-GEV) with no trend in the parameters are tested for the validity. In this test, a stationary model is considered as the null hypothesis and nonstationary model as the alternate one. The hypothesis testing is carried out using the minimised negative likelihood function ($nllh$) of the S-GEV model with NS-GEV model at any particular significance level α . Twice the difference between $nllh_{S-GEV}$ and $nllh_{NS-GEV}$ is computed which is supposed to have an approximate Chi-squared distribution for large sample size (Katz 2013) (Equation 4.3). Mathematically,

$$2[nllh_{(S-GEV)} - nllh_{(NS-GEV)}] > c_\alpha \quad (4.3)$$

Where, c_α is the $(1 - \alpha)$ quantile of the Chi-squared distribution. In this investigation, a 5% significance level (i.e. 95% confidence level) is utilised. It should be noted that after selecting the nonstationary and stationary distribution using the LR test, the best fit nonstationary model if obtained, is selected using the least p-value. In the present study, the LR test is

performed for all the 56 nonstationary combinations and compared with the stationary model.

4.2.2.3 Bayesian framework for parameter uncertainty

As discussed in the previous section, the parameters of the stationary and nonstationary methods are obtained through the MLE. However, MLE provides only the point estimate of the parameters and does not accommodate the uncertainty associated with them. To solve this issue and quantify the uncertainty, Bayesian analysis proves to be an efficient framework (Coles et al. 2003; Huard et al. 2010). Moreover, analysis of extreme events requires a large sample of data which is one of the main limitations in hydrology (Das and Umamahesh 2017). Furthermore, with the availability of limited dataset, parameter estimation using the classical approach is questionable (Coles and Tawn 1996). In the context of engineering design, the return levels under higher return periods are of paramount importance. If the parameter uncertainty is overlooked, then the designed return levels may provide erroneous inputs to the design criteria. Moreover, Lins and Cohn (2011) stated that the nonstationarity characteristics in hydrology are extremely uncertain, which cannot be computed using the deterministic approach. In view of the above, the Bayesian analysis is used to model the parameter uncertainty.

The central principle of Bayesian approach lies in upgrading the uncertainty associated with the parameter which is expressed in terms of prior distribution using the Bayes rule. The ability of the Bayesian analysis to incorporate the additional information in the form of prior makes it more popular (Eli et al. 2012). While discussing the usefulness of the Bayesian approach, Coles and Tawn (1996) stated that the period of data used for any extreme data analysis might not represent the complete behaviour and Bayesian framework is a solution to this limitation. The Bayes theorem combines inputs from the prior distribution and likelihood function of the

data into the posterior distribution. The posterior distribution can be found by multiplying the likelihood function and prior distribution of parameters

$$p(\theta|x) \propto p(x|\theta)p(\theta) \quad (4.4)$$

where, $p(\theta|x)$ presents the posterior distribution of the parameter vector $\theta = (\mu, \sigma, \xi)$, $p(\theta)$ is the prior distribution, $p(x|\theta)$ defines the likelihood function equal to $\prod_{i=1}^n p_{GEV}(x_i|\mu, \sigma, \xi)$, n is the number of observation, and $p_{GEV}(x_i|\mu, \sigma, \xi)$ is the probability distribution function of the GEV distribution evaluated at x_i .

Selection of the prior distribution is the matter of extensive debate in the research fraternity (Clark 2005; Gelman 2008) and the approaches those are frequently used in the hydrological analysis include (i) the prior distribution which is defined based on the expert's knowledge. Example: the "geophysical prior" for the shape parameter of the GEV distribution based on the experience of the hydrological studies (Martins and Stedinger 2000); (ii) based on the similarities among the different sites and using the regional information, the prior distribution from one location can be used for the other location (Ribatet et al. 2007); (iii) due to the lack of knowledge the non-informative prior (e.g., normal distribution with large variance) can be used (Jeffreys 1946). It is impossible to solve Equation 4.4 analytically; hence, the numerical method, namely Markov Chain Monte Carlo (MCMC) sampler, is adopted to create a large number of realisations from the posterior distribution (Martins and Stedinger 2000). For instance, utilising the prior distribution and likelihood of parameter, the MCMC algorithm draws a large sample of parameter vector (e.g., $\theta_1, \theta_2, \dots, \theta_m$) and using each set of parameter vector return levels for a given probability of occurrence (p) which can be obtained using Equation 4.5

$$Z_p(\hat{\mu}, \hat{\sigma}, \hat{\xi}) = \hat{\mu} - \frac{\hat{\sigma}}{\hat{\xi}} \left\{ 1 - [-\log(1-p)]^{-\hat{\xi}} \right\} \quad \text{for } \xi \neq 0 \quad (4.5)$$

$$Z_p(\hat{\mu}, \hat{\sigma}) = \hat{\mu} - \hat{\sigma} \log [-\log(1-p)] \quad \text{for } \xi = 0$$

The sampling of the parameter vector with the specified prior and likelihood function is accomplished using the Metropolis-Hastings algorithm (Metropolis et al. 1953; Hastings 1970). Each parameter from the parameter vector is updated through the random walk Metropolis algorithm. However, the convergence of the MCMC chain towards the posterior distribution should be monitored. Precisely, a poor choice of the initial parameter vector may lead to drawing realisations those are not from the equilibrium distribution during the initial runs. Therefore to determine the length of each simulation, in the present study, Heidelberger and Welch's convergence diagnostic (Heidelberger and Welch 1981, 1983) is used. Details of MCMC and Metropolis-Hastings algorithms can be obtained from (Renard et al. 2013; Chandra et al. 2015).

4.3 Results

4.3.1 Temporal variability of extreme precipitation

Figure 4.3a represents the spatial variation of the mean maximum one-day precipitation (Rx1 day), annual count of days when precipitation is more than or equal to 10mm (R10), maximum number of consecutive wet days (CWD) and simple daily precipitation intensity index (SDII) extreme precipitation for the period 1951-2013. The maximum and minimum value of Rx1day and SDII were around 13mm to 133mm, and 0.31mm/day to 38.75 mm/day respectively. Similarly, the range of R10 and CWD were 0.93 days and 100.22 day, and 0.17 to 77.40 days respectively. It is evident that extreme rainfall events are most dominantly observed over the river basins in the west coast, north-east and followed by central India. Compared to the SDII and CWD, the high values of Rx1day and R10 are somewhat more noticeable in the Indo-Gangetic plain as well as river basins such as the Godavari, Brahmani and Baitarani. Figure 4.3b shows the temporal variation in the extreme precipitation indices over the past 63 years. Most significant variability in Rx1 day is observed in river basins such as Luni, Mahi and Brahmaputra where the standard deviation is above 10 mm.

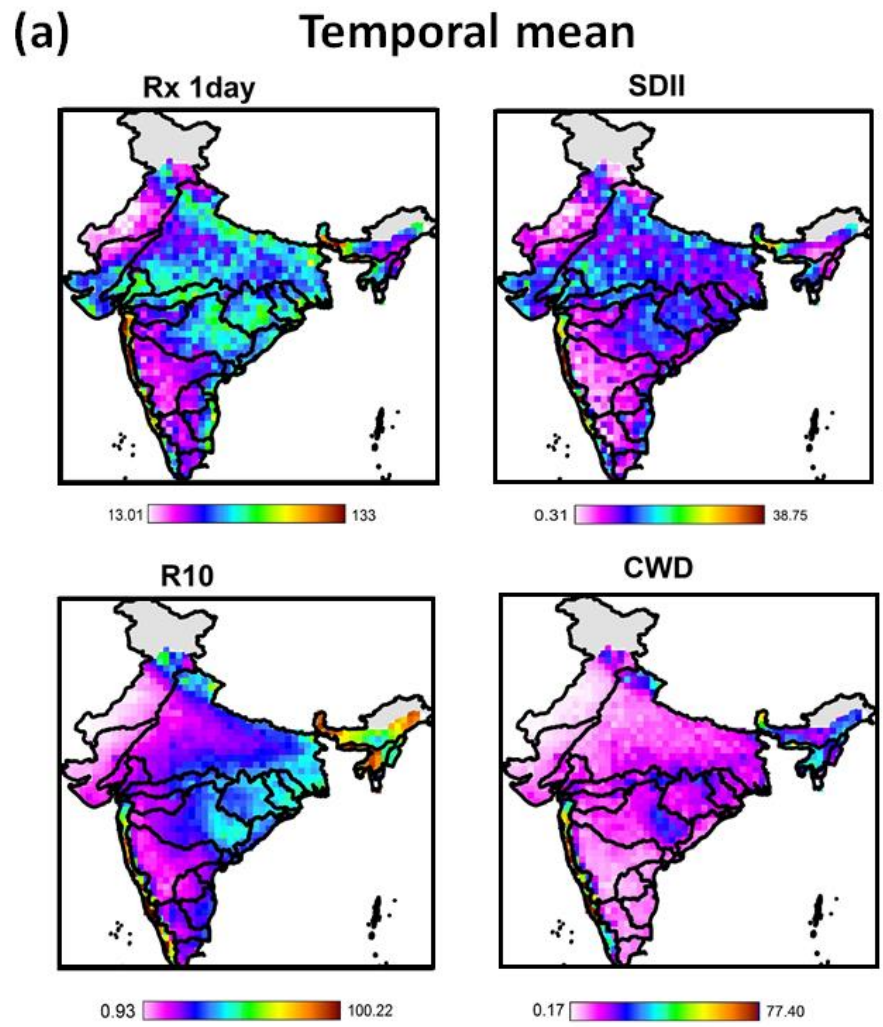


Figure 4.3a The spatial map of annual mean of extreme precipitation indices over 1951-2013

(b) Temporal standard deviation

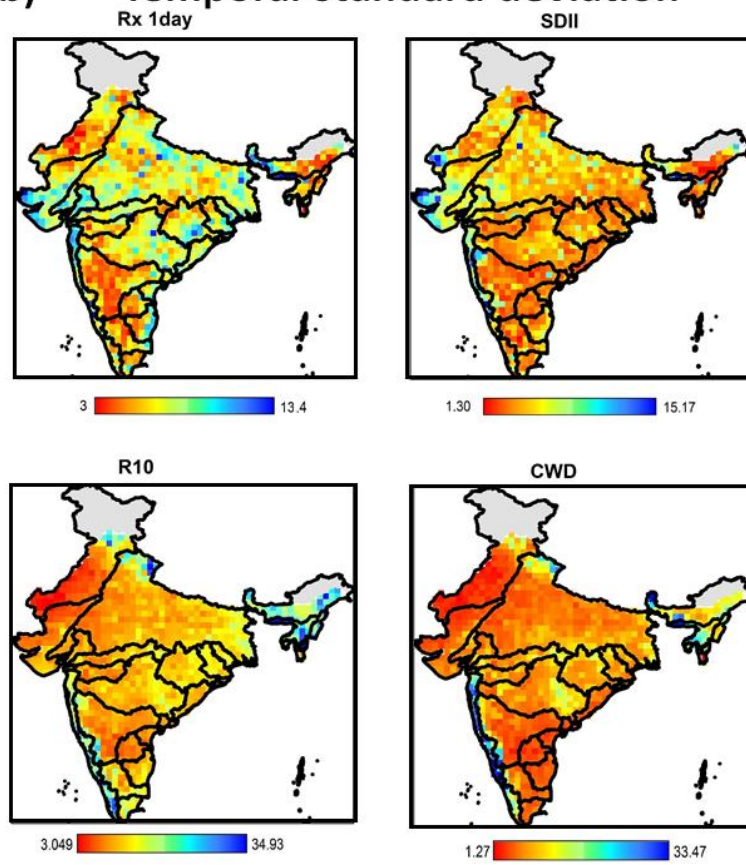


Figure 4.3b The spatial map of standard deviation of extreme precipitation indices over 1951-2013

Whereas, the extreme rainfall in arid river basins such as Pennar and Indus are found to be insignificantly variable. However, the variability in precipitation intensity was ranging from 1.30 mm/day to 15.17 mm/day. Similarly, in the northwest region, the standard deviation was below 5 days for both R10 and CWD. To visualize the evolution of extreme precipitation during 1951-2013, trend analysis is performed using nonparametric Mann Kendall (MK) test at 5% significance level. The outputs of the analysis are categorised into four different classes based on the value of Z statistics which are: significantly increasing ($Z > 1.96$), significantly decreasing ($Z < -1.96$), increasing ($0 < Z < 1.96$) and decreasing ($-1.96 > Z > 0$). The Rx1 day and SDII indices are found to be increasing whereas, the R10, as well as CWD indices, are mostly increasing in most of the river basins (Figure 4.3c).

4.3.2 Parameters and their uncertainty

As discussed, the parameters of the best-fit model for different indices are calculated using the MLE approach. After processing the models through the Markov chain based on the convergence criteria for S-GEV and NS-GEV models, a set of parameters from the posterior distribution are obtained. Thereafter, the return levels at different return periods for stationary as well as nonstationary models using the sample of parameters are calculated. Figure 4.4 represents the spatial distribution of the mean and standard deviation of the samples from the posterior distribution, respectively. It should be noted that the location parameter, scale parameter and the shape parameter is represented by P1, P2 and P3, respectively. It can be observed from the figure that high values of mean in cases of location parameter for SDII, R10 and CWD are obtained mostly in the river basins which receive high rainfall. The maximum value (220.98mm) of mean location parameter for Rx1day was obtained for the western ghats river basin, whereas minimum

(c) Historical trend analysis

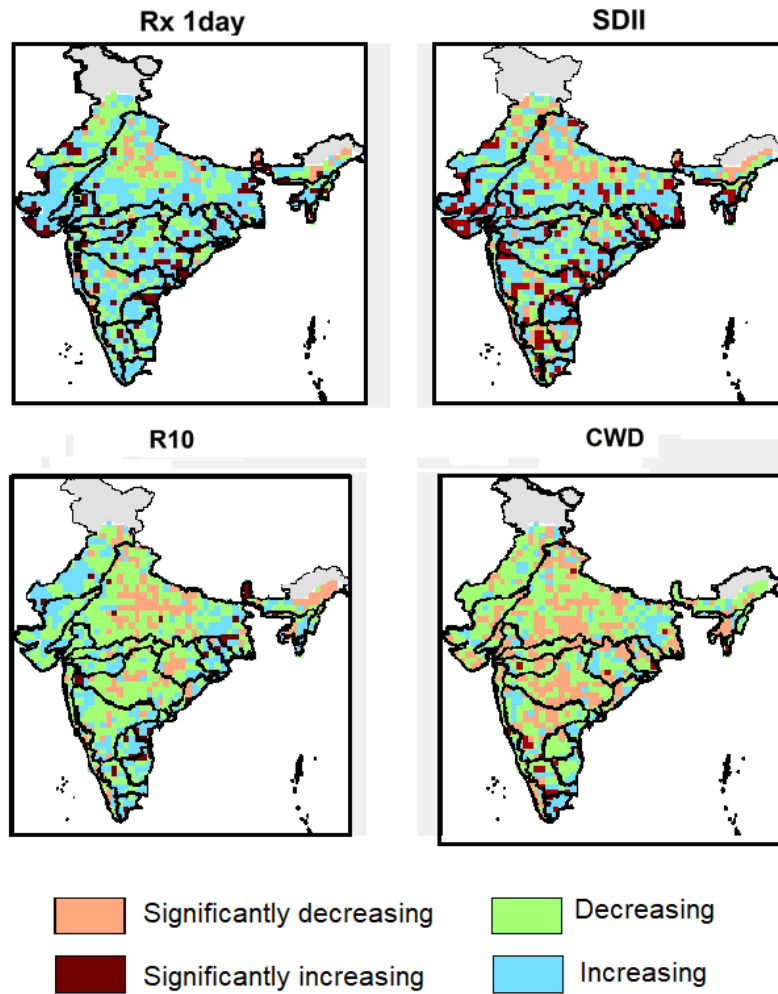


Figure 4.3c The spatial map of trend significance (Z statistics) of extreme precipitation indices over 1951-2013

value (17.84mm) was obtained for the northwest region (Figure 4.4a-i). The trend of variation in the scale parameter was also very similar to the location parameter and the range of mean scale parameter was 10.50-92.6mm. The mean of location parameter for Rx1 day, in general, is higher in most parts of the country except the arid regions like in the north-west. Similarly, the mean of the scale parameter could also be characterised on the basis of high and low rainfall zones of the country. Similar inferences can be drawn for R10 and CWD (Figure 4.4a-ii). However, unlike the results obtained for mean parameters, the standard deviation of the parameter samples is not characterisable on the basis of rainfall zones. The variability of location, scale and shape parameters is more randomly distributed over the country (Figure 4.4b-i,ii).

4.3.3 Return levels, magnitude and variability of extreme precipitation

The return levels at different return periods are estimated from parameter samples of the posterior distribution obtained from the Bayesian analysis. Under the stationary assumption, i.e. for S-GEV models, the return levels throughout the temporal duration of the time series remain the same. However, the return levels obtained from NSE-GEV models are time-varying, since, they were assumed to be time-dependent on ENSO, IOD and NAO. Figure 4.5 shows the spatial distribution of return levels both for the nonstationary and stationary cases at 10, 20, 50, and 100 year return periods. It should be noted that for the nonstationary case, the temporal mean of the return levels has been shown. It is evident from the spatial patterns of the return levels that with the increase in the return periods, the return level intensifies and the area under extreme rainfall also increases. The quantification of return levels and their temporal variability is related to the

Mean of parameter samples (Rx1day and SDII)

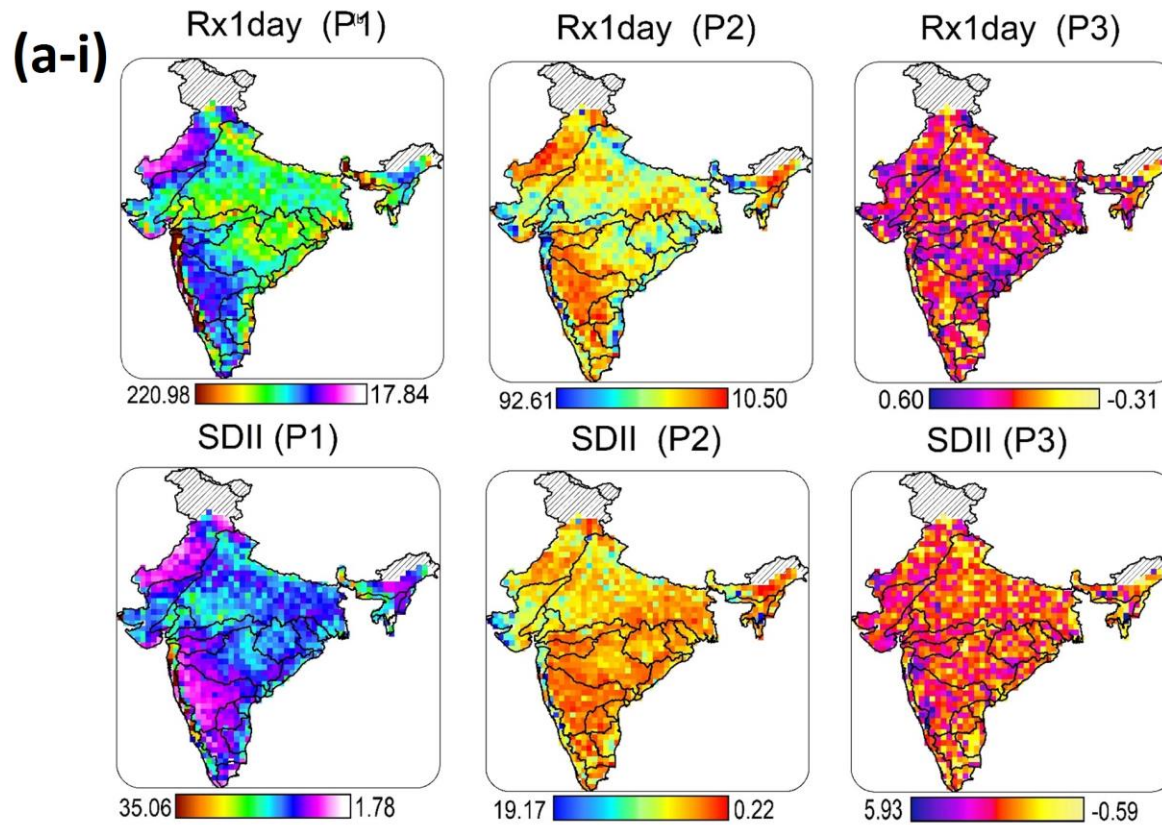


Figure 4.4a-i Spatial distribution of the mean parameter samples from the posterior distribution for Rx1day and SDII. Here, P1, P2 and P3 represent the location, scale and shape parameters respectively

Mean of parameter samples (R10 and CWD)

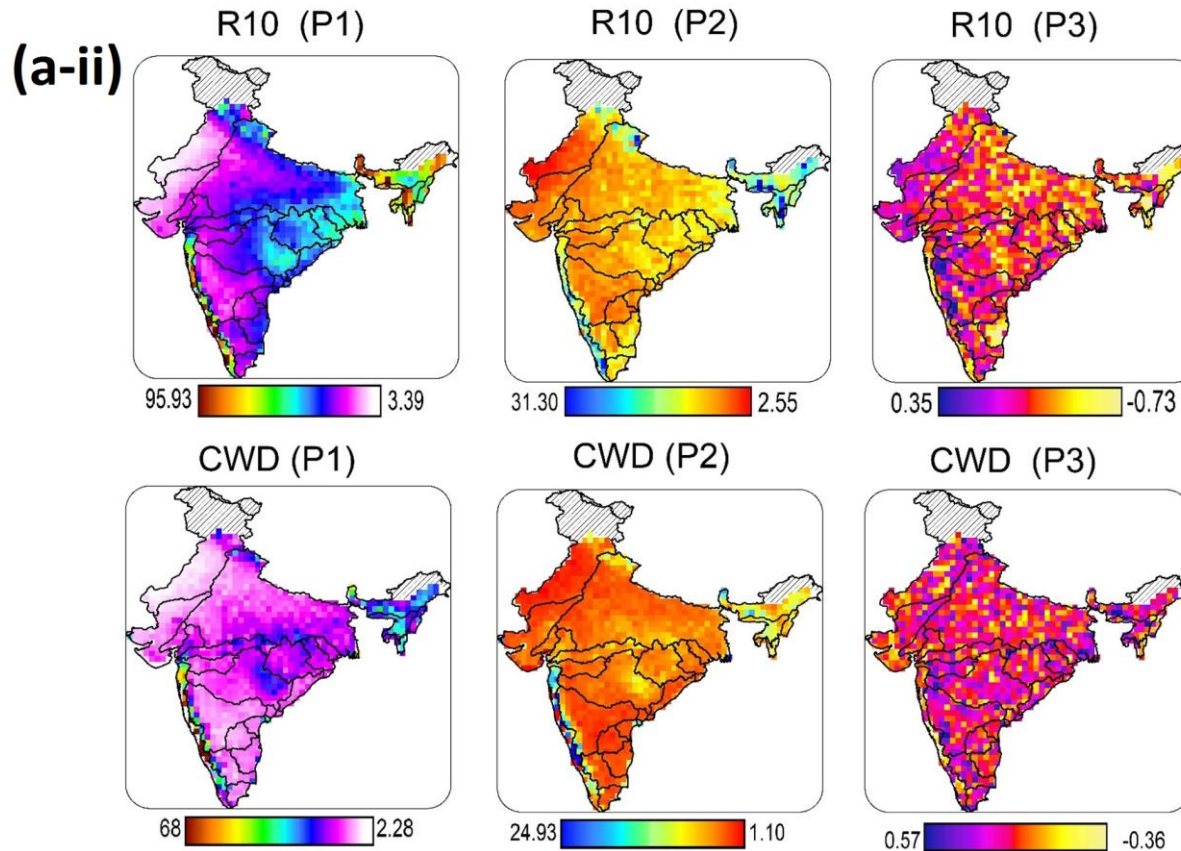


Figure 4.4a-ii Spatial distribution of the mean parameter samples from the posterior distribution for R10 and CWD. Here, P1, P2 and P3 represent the location, scale and shape parameters respectively

Standard dev. of parameter samples (Rx1day and SDII)

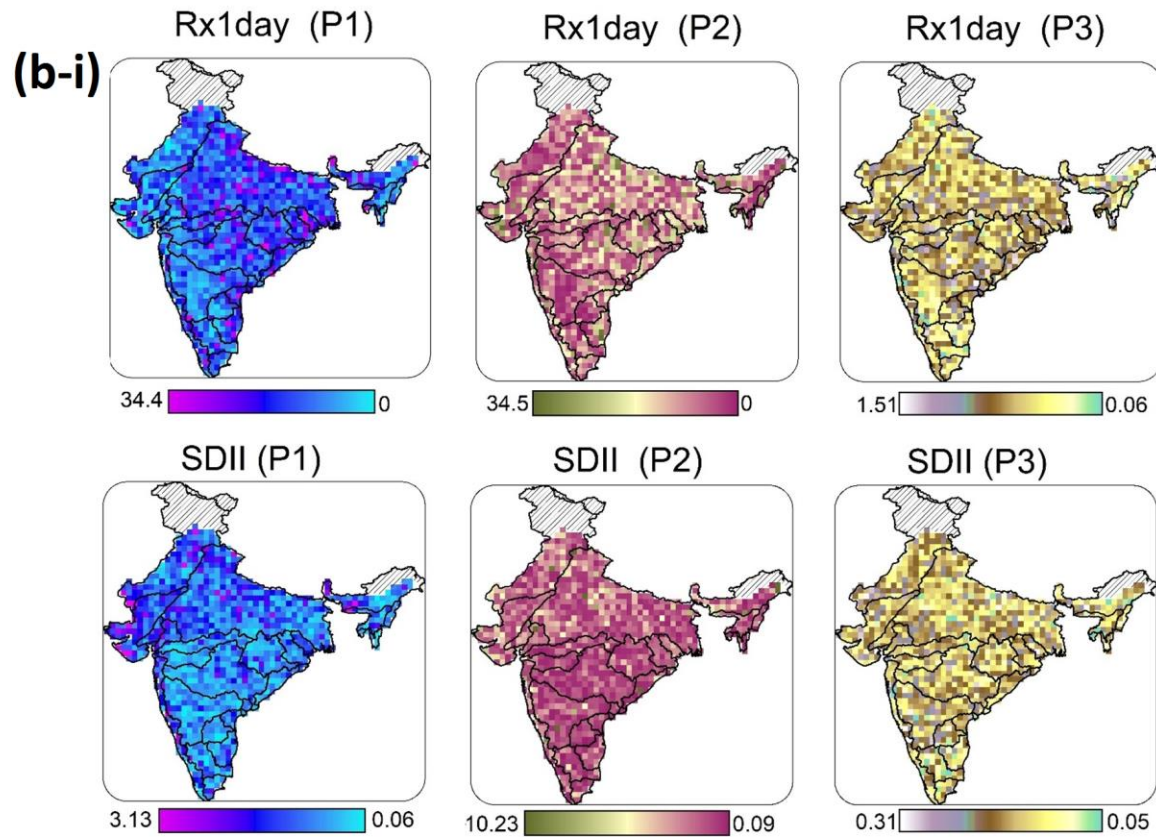


Figure 4.4b-i Spatial distribution of the standard deviation of parameter samples from the posterior distribution for Rx1day and SDII. Here, P1, P2 and P3 represent the location, scale and shape parameters, respectively

Standard dev. of parameter samples (R10 and CWD)

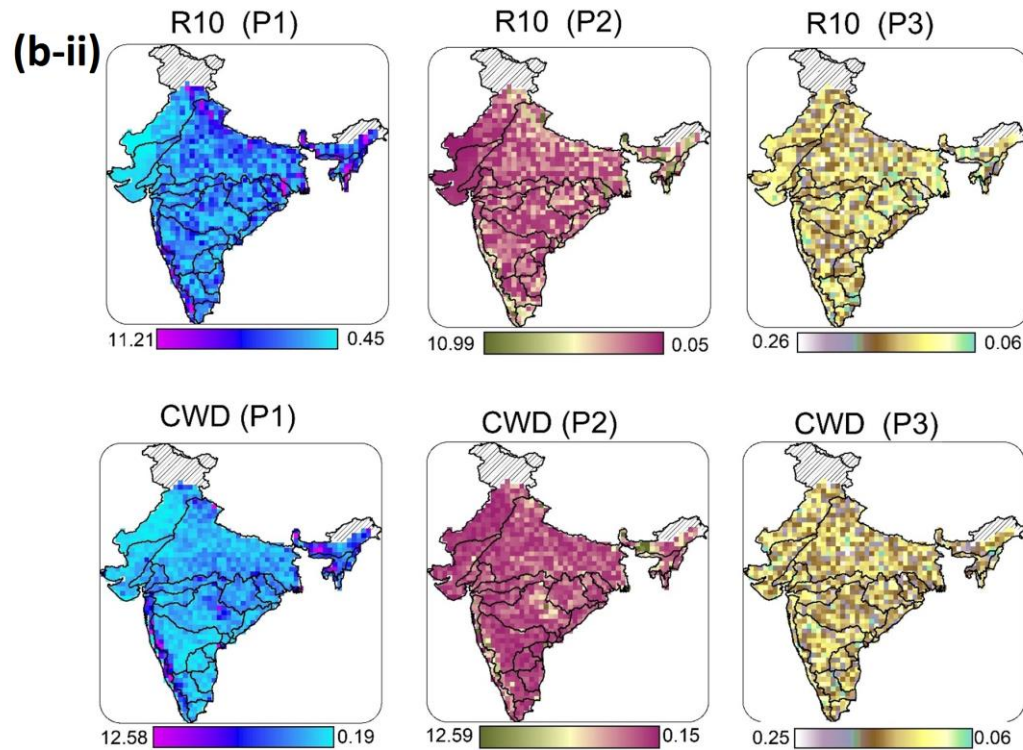


Figure 4.4b-ii Spatial distribution of the standard deviation of parameter samples from the posterior distribution for Rx1day and SDII. Here, P1, P2 and P3 represent the location, scale and shape parameters, respectively

river basins. Please refer to Figure 4.6a-d for the river basin-wise return level estimates for stationary and nonstationary cases. River basins in the east-coast, western ghats and the north-east exhibit highest return levels. The river basins in the less precipitation zones such as Luni and Mahi show high return levels at 100 years return period. The river basins with least return levels are MRFM, EFRSCB, Indus, Krishna and Pennar river basin. The nonstationary return levels are greater as compared to the stationary return levels. This difference is most significantly observed in high rainfall river basins such as Brahmaputra and MRFB as well as low rainfall river basins such as Mahi and Luni.

A little overestimation of return levels by the stationary models is observed in the Barak and MRFB river basins. Similarly, the return levels mapping of SDII shows similar spatial characteristics as Rx1day. However, the regions of extremely low-intensity rainfall are more clearly defined. High-intensity return levels are observed in the western ghats, Barak and Brahmaputra river basins, as well as Luni, Mahi and Sabarmati river basins. Least intensity is observed in the river basins of the east-coast and the interior peninsula (Figure 4.6). In general, the nonstationary return levels are found to be higher in magnitude than the stationary return levels. The most significant disparity is observed in the EFRMGB, Luni, MRFB, Brahmaputra river basins and the western ghats. For R10, high and low return levels region are more clearly characterisable. The increase in return levels over different return periods is comparatively smaller as compared to other indices. Brahmaputra, Barak, MRFB, MRFM river basins and the western ghats are the regions where higher return levels are observed in both stationary and nonstationary cases. Although the spatial pattern of return levels is similar in both cases, stationary models are found to be underestimating the return levels. It can be noted that the influence of large-scale oscillations as captured by nonstationary models is poorly represented by the stationary models in Barak, WG and MRFM basins. The spatial pattern of mean return levels for CWD reveals that stationary models have

overestimated the return levels, especially when higher return period, such as 50 and 100 are considered (Figure 4.5). It can be observed that the area under $CWD > 20$ has significantly increased in the north-central part of the country with higher return periods. Similar to other indices, highest return levels are observed in the Brahmaputra, western ghats and Barak river basins in both the cases (Figure 4.6). The nonstationary stationary mean return levels are higher than the stationary return levels, in Barak, MRFM and MRFB basins. The difference between mean nonstationary and stationary return level of five river basins (Brahmaputra, Mahi, EFRGKB, EFRPKB and MRFB) have is greater than 100 mm at 100 year return period and only two river basins (Barak and MRFM) have relatively lesser return levels in the nonstationary cases. Similarly, the precipitation intensity return levels was geater in nonstationary case only in two river basins (Barak and MRFB). The R10 nonstationary return levels at 100 year return period were differing with a magnitude above 10 days for river basins like Barak, Subernrekha, MRFM and WG. Whereas, the overestimated nonstationary return levels were observed for Barak, MRFB and MRFM of around 5 days for CWD.

Figure 4.7 represents the return period-wise variability of the return levels of different extreme indices. Overall, the figure denotes that the temporal variability due to the influence of climatic oscillations in the return levels in all indices is significant. This variability is most significant in Rx1 day followed by CWD, R10 and SDII, particularly at higher return periods. For Rx1 day, average variability is highest in EFRGKB and EFRPKB, and lowest in MRFM, Krishna and Barak river basins. The river basins which receives the least rainfall, e.g. Luni, Subernrekha and Mahi are found to be experiencing high variability in the rainfall intensity. Only western ghats, out of high rainfall river basins, is found to be experiencing variability of such magnitude. Further, variability in R10 return levels is highest in the Subernrekha and EFRSCB river basins. Interestingly variability in CWD return levels is lowest in Subernrekha and EFRSCB river basins.

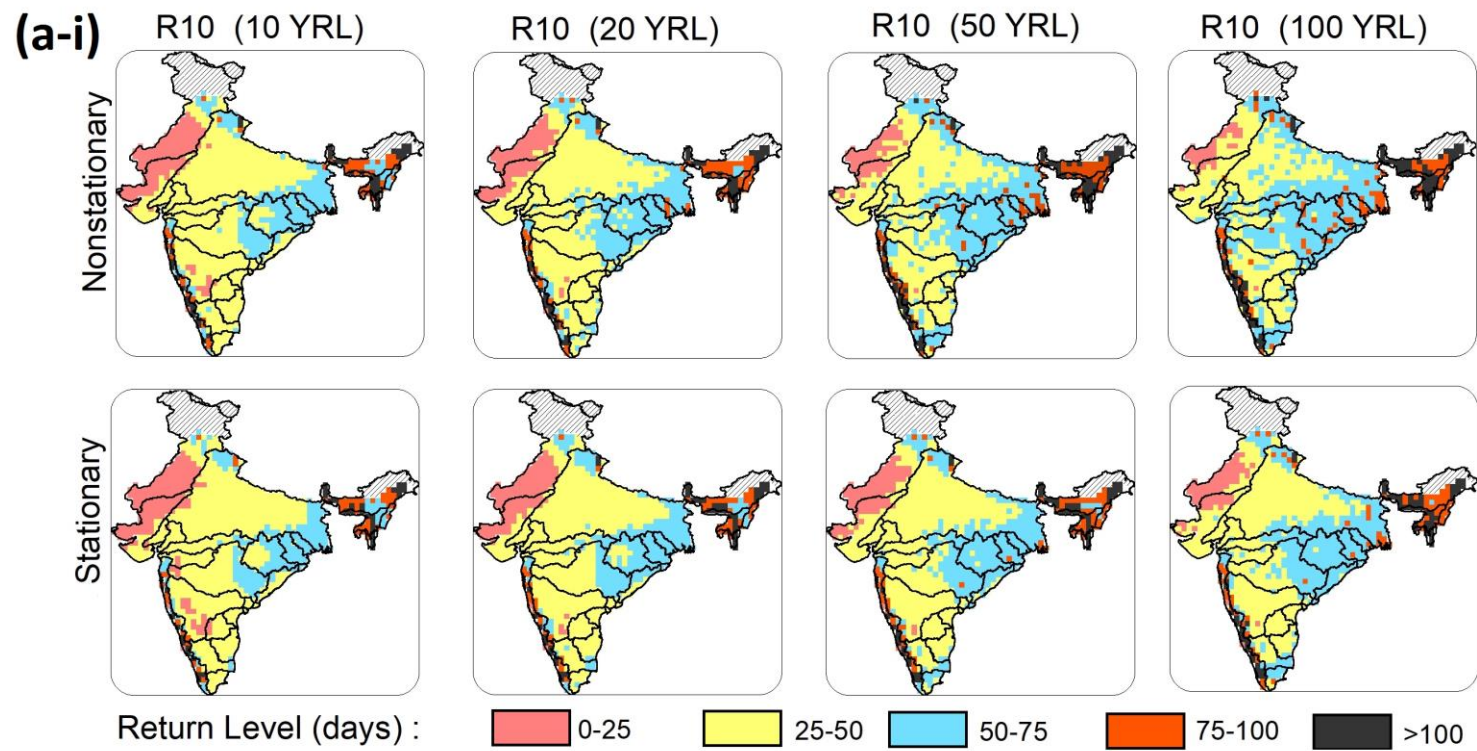


Figure 4.5a-i Spatial distribution of return levels both for the nonstationary and stationary cases for R10 at different return periods

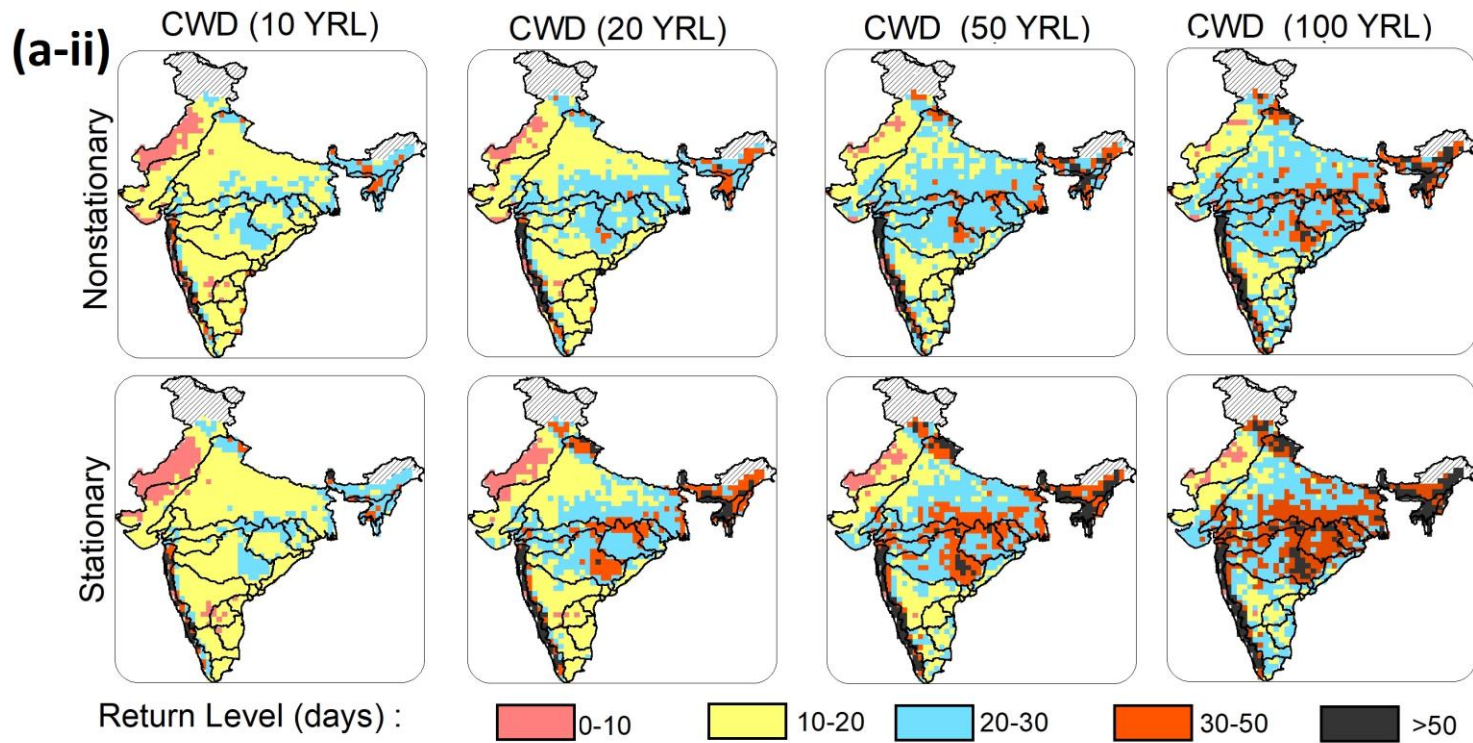


Figure 4.5a-ii Spatial distribution of return levels both for the nonstationary and stationary cases for CWD at different return periods

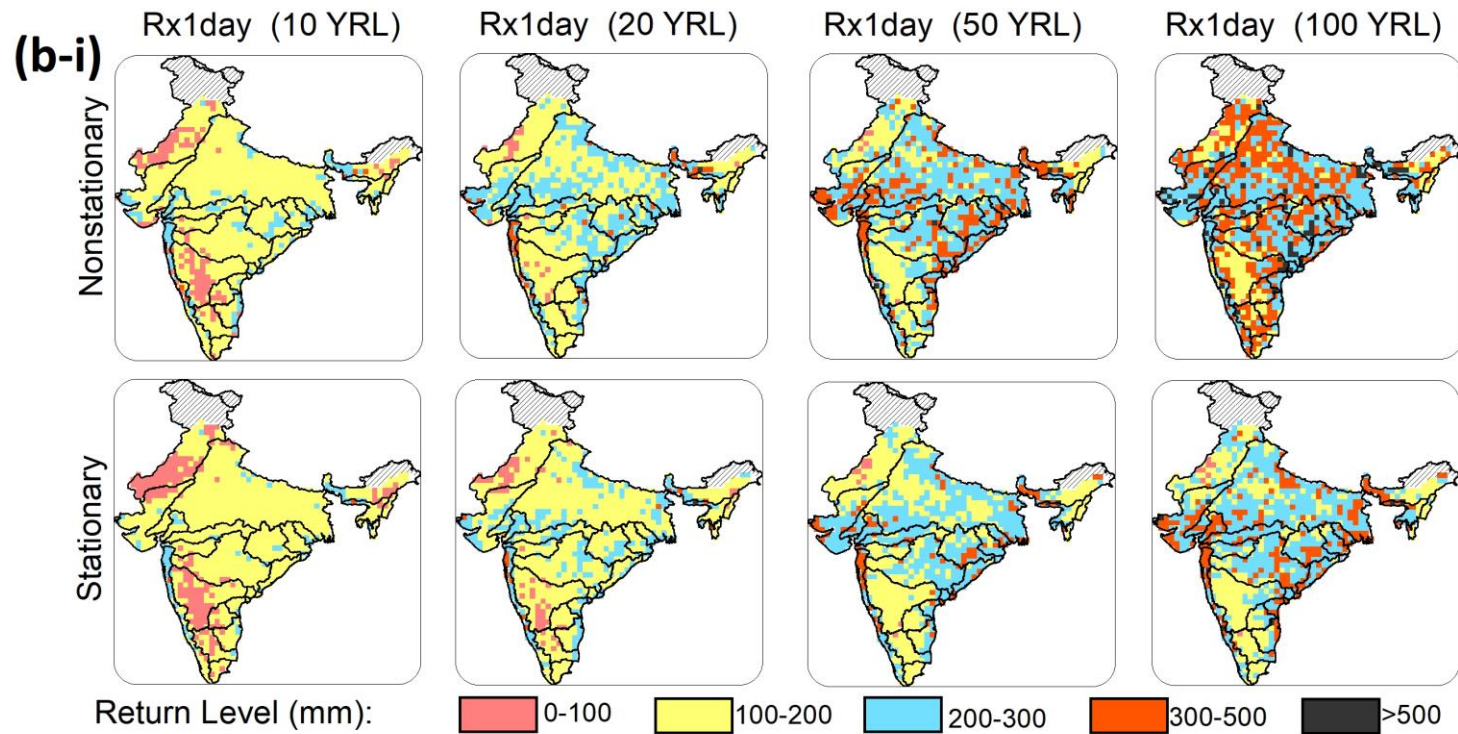


Figure 4.5b-i Spatial distribution of return levels both for the nonstationary and stationary cases for Rx1day at different return periods

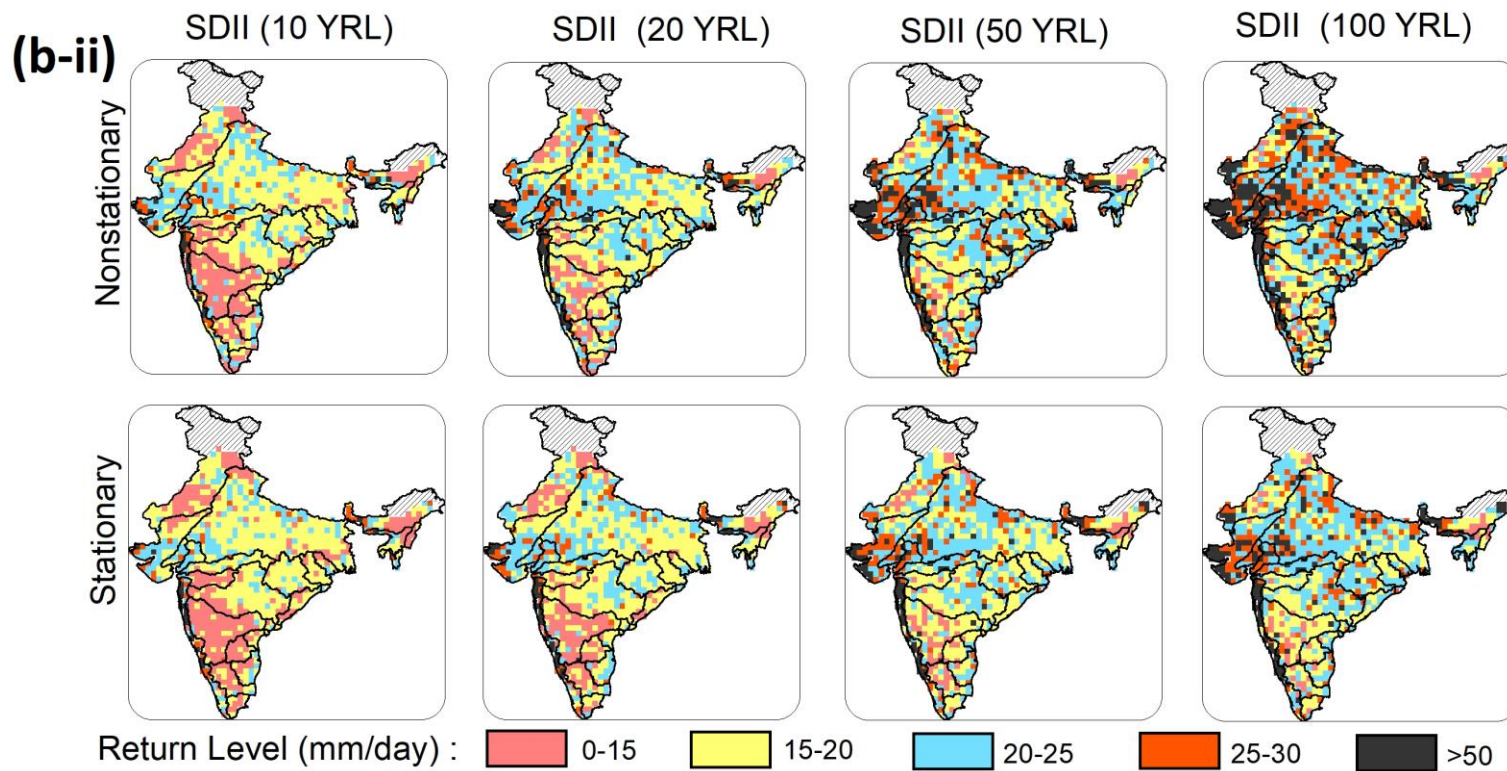


Figure 4.5b-ii Spatial distribution of return levels both for the nonstationary and stationary cases for SDII at different return periods

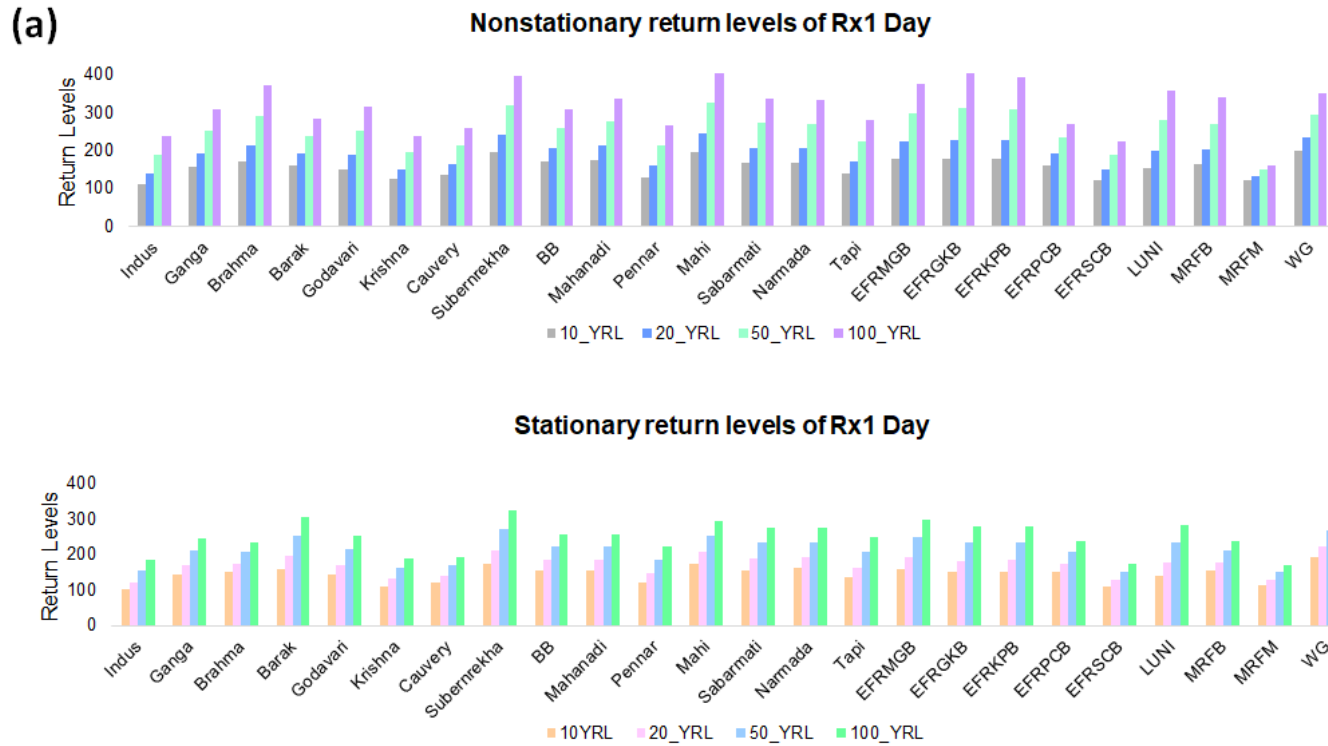


Figure 4.6a The nonstationary and stationary return levels of Rx1 Day for different return periods

(b)

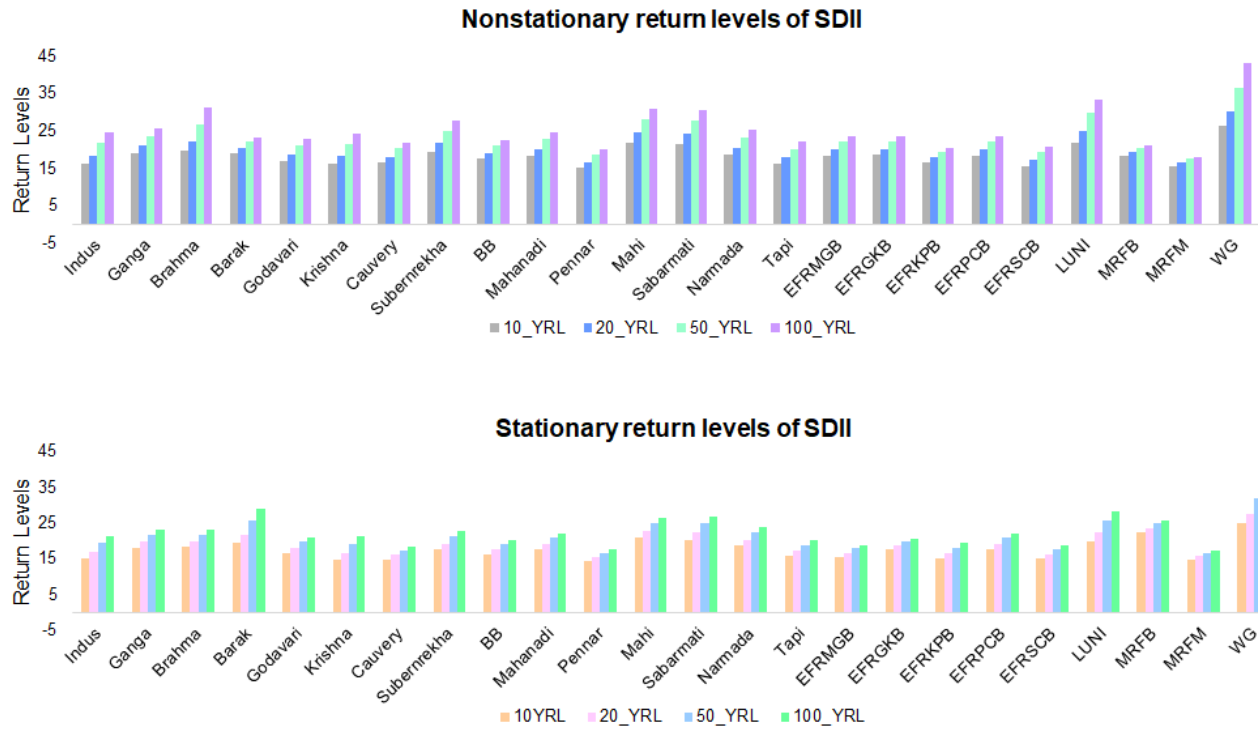


Figure 4.6b The nonstationary and stationary return levels of SDII for different return periods

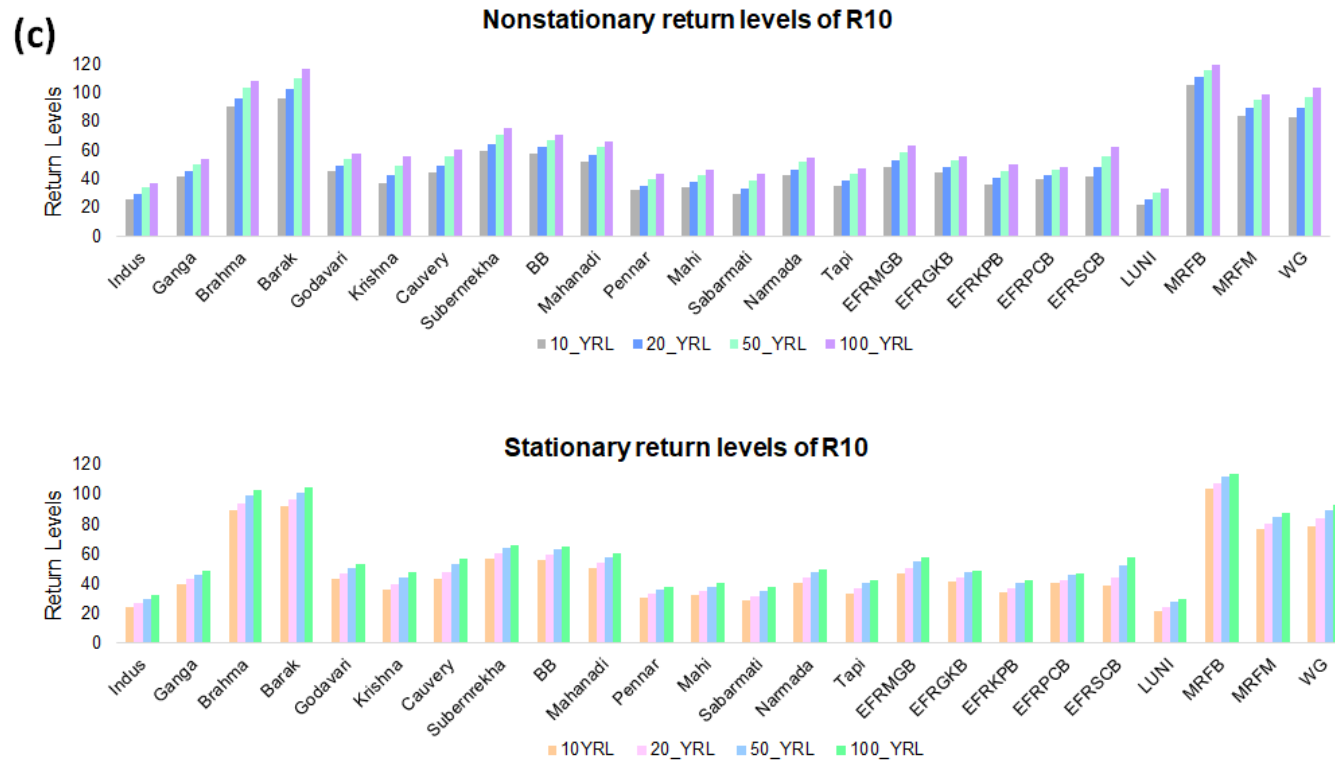


Figure 4.6c The nonstationary and stationary return levels of R10 for different return periods

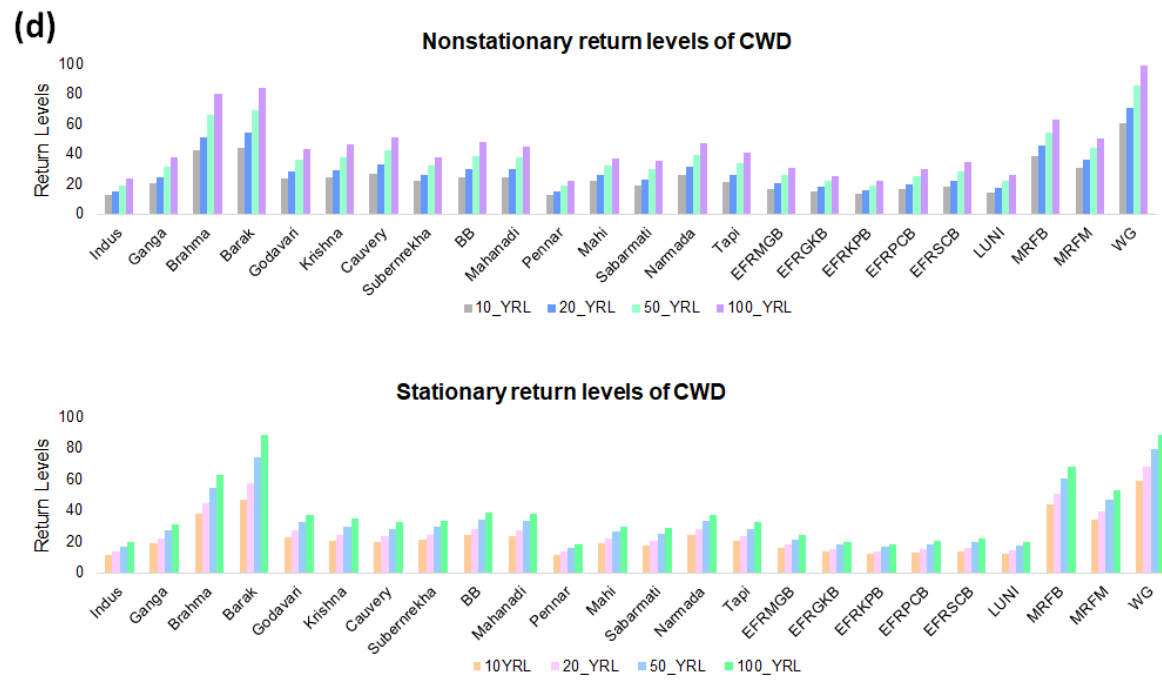


Figure 4.6d The nonstationary and stationary return levels of CWD for different return periods

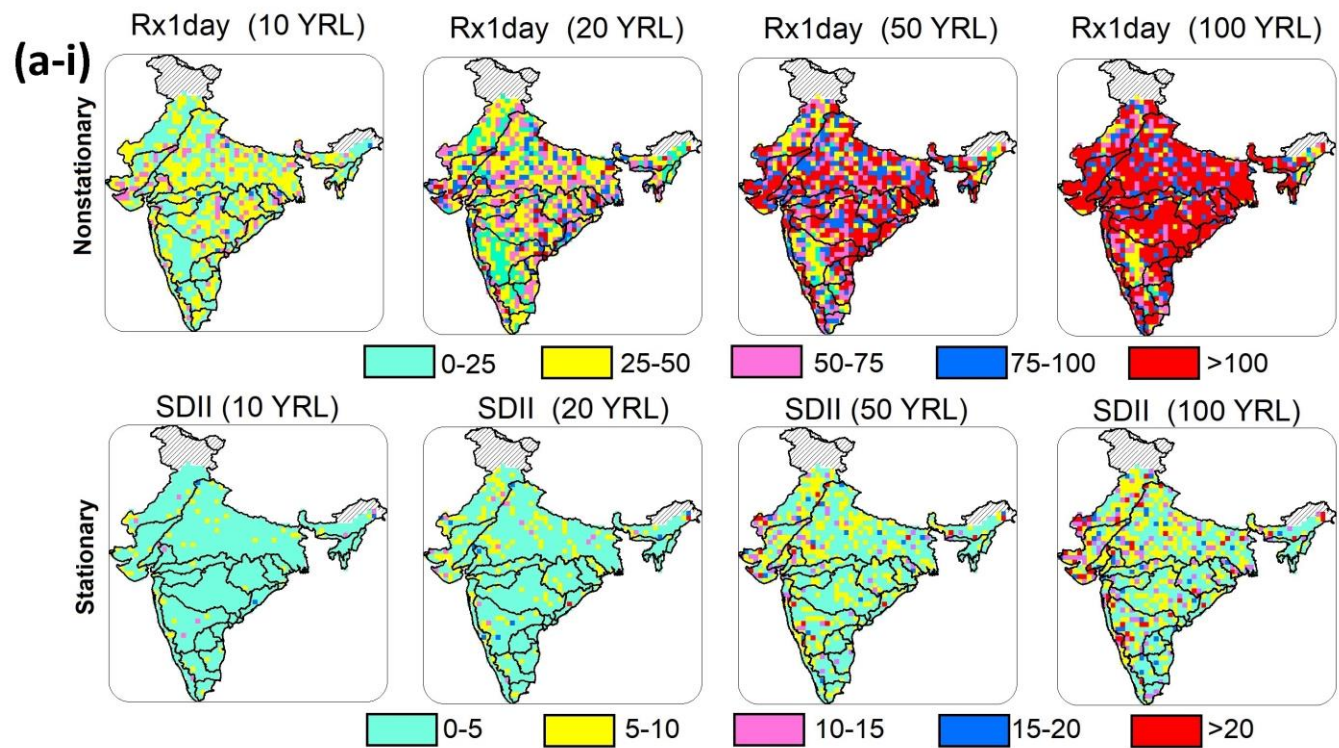


Figure 4.7a Spatial variability in the return levels for Rx1day and SDII. The variability is defined in terms of standard deviation over 1951-2013

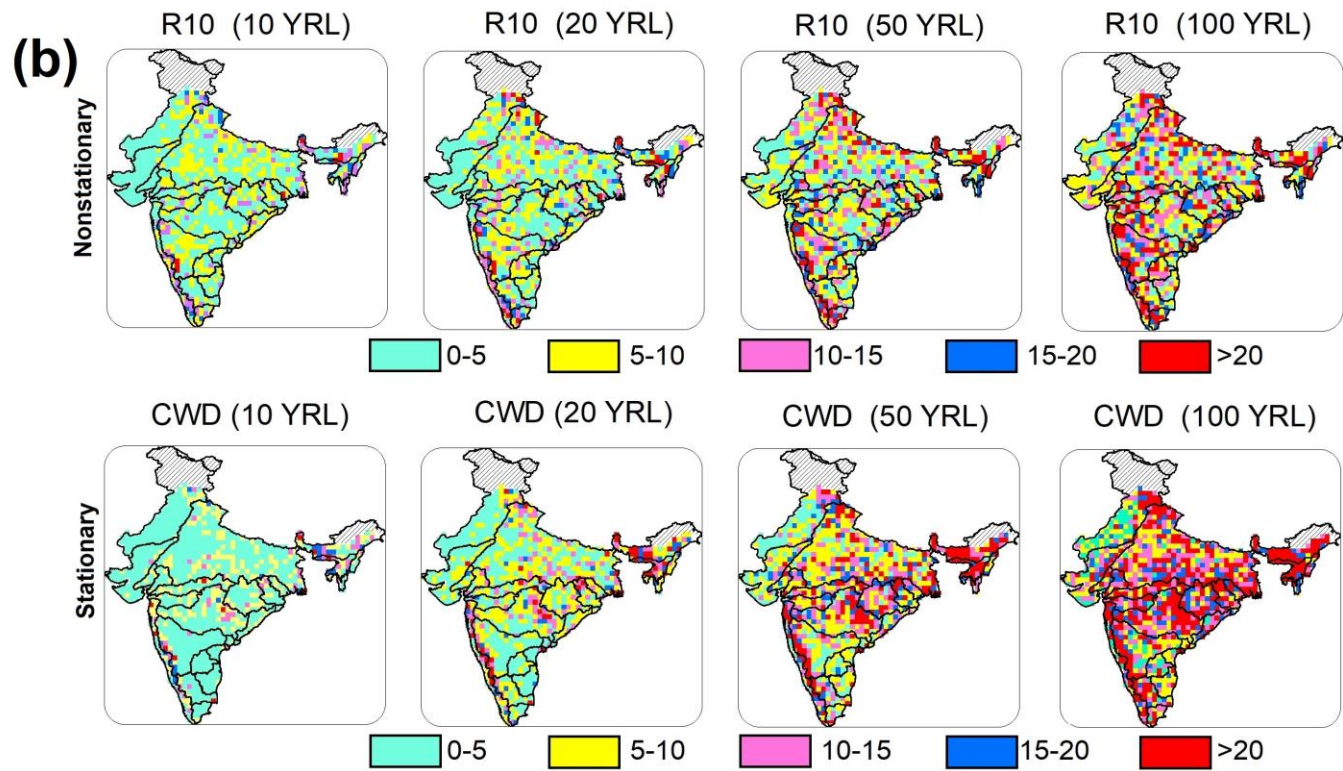


Figure 4.7b Spatial variability in the return levels for R10 and CWD. The variability is defined in terms of standard deviation over 1951-2013

4.4 Discussion

The present study is focused on estimating the return levels and the variability of extreme precipitation indices under the changing relationship with three large scale climatic oscillations ENSO, IOD and NAO. The behaviour of four historical extreme precipitation indices which are Rx 1 day, SDII, R10 and CWD during the period of 1951-2013 are analysed. The historical trend in the extreme precipitation indices over India is found to have distinct spatial patterns. The trend analysis of these indices suggests that maximum one-day precipitation intensity, as well as the rainfall intensity, have increased in the past Whereas, the number of consecutive wet days and number of days having at least 10 mm rainfall has decreased over the period of time. This indicates that the extreme precipitation over India has become more intense as well as heavy downpours events have increased. These results are generally consistent with those found in past research (Endo et al. 2009; Kumar et al. 2010). The increasing trend of Rx1 day and SDII is observed in all major parts of the country except the north-east and some parts of northern India. Significant decrease in R10 and CWD is noticed mainly in the north-central part of the country.

As discussed in the previous studies, the extreme precipitation indices over India have exhibited significant variability in the past (Rajeevan et al. 2008; Vittal et al. 2013; Ganguli and Reddy 2014). The possible governing factors include internal natural variability and external and anthropogenic climate forcings (Zhang et al. 2007; Marvel et al. 2017; Dai and Bloecker 2019). It is well established that the large scale climatic oscillations are fundamental influences over precipitation variability (Gao et al. 2017; Xiao et al. 2017). In this study, extreme value analysis in a nonstationary setting along with the Bayesian framework is employed to assess the influence of large-scale oscillations on precipitation indices over India. Based on the best stationary and nonstationary models obtained by the likelihood ratio test, it is found that all four indices exhibit significant nonstationary behaviour. It is noticed

from the analysis that nonstationary models, which vary linearly with both location and scale parameters, are found to perform better in most of the cases. Therefore, it can be argued that the changeability in the extreme precipitation indices is highly influenced by the climate oscillations over India. It should be noted that the regional characteristics of the basin may influence the change; however, these investigations are not carried out in the present analysis. It is also observed that uncertainty in return levels is higher in case of the higher return period; this suggests that special attention should be given while selecting the design return levels in extreme rainfall areas. The spatial mapping of uncertainty in parameters and return levels over different river basins is intended to enable the policymakers to frame decisions for different regions more precisely. The quantification of uncertainty in return levels, especially in the climatologically sensitive river basins is crucial in understanding the influence of large-scale factors in augmenting extreme risks. Studies suggest that arid regions are more vulnerable to climate change (Interests et al. 2016; Sinha et al. 2019). In this study, it is observed that variability in return levels is high not only in the regions where rainfall is abundant but also in the drought-prone areas. It is likely that these regions may experience short spells of heavy downpours in the form of high-intensity rainfall. This may lead to the simultaneous occurrence of flash floods and droughts in the regions. Previous studies suggest that there have been occurrences of such compound events in western India, leading to a huge loss of property and lives (Jayan 2012; Ganguli and Reddy 2013). In this context, the study aids the decision-makers in framing productive extreme rainfall induced disaster response measures.

4.5 Conclusions

This study facilitates the understanding of the nonstationary influence of ENSO, IOD and NAO on high precipitation in the region. It is found that extreme precipitation events in the country are dominated by these oscillations, especially in central India. Moreover, the return levels of high

rainfall are found to be intensifying with increasing return period. Also, it is observed that uncertainty in return levels is significant in almost every river basin. Despite the association, there remains a significant amount of uncertainty in the relationships between extreme precipitation indices and ENSO, IOD and NAO. One possible reason behind this uncertainty can be our assumption of linearly varying covariation combination for nonstationary models. Moreover, we have studied the dependence of extreme precipitation only on three large-scale oscillations. Nonlinear combination of other global factors can be pursued for future studies. However, the analysis provides in-depth identification and characterization of the magnitude and variability in return levels and delivers crucial inputs for understanding the time-varying risks of high precipitation. The study put forward the all-India assessment of the regional impact of global climatic factors to understand the complex behaviour of high precipitation over the country.

Chapter 5

Dependence of terrestrial ecosystem functioning on extreme climatic conditions

5.1 Introduction

Conventionally, studying the response of terrestrial ecosystem productivity to the extreme climatic conditions involved the experimental investigation of ecosystem variables (such as plant diversity, vegetation cover, nutrient concentration) as well as statistical or empirical-based analysis (Saseendran et al. 2000; Li et al. 2014; Sakschewski et al. 2015; Gang et al. 2017). The existing experimental approaches have limited applicability as it is challenging to incorporate the wide spatio-temporal variability in ecosystem functioning. The knowledge about specific impacts of climate extremes such as severe drought, prolonged precipitation deficit and extreme temperature on the terrestrial ecosystems has become critical to society and science. Modelling the behaviour of ecosystems during and after climate extremes at larger spatial scales and over longer periods requires more in-depth knowledge on possible response mechanisms. Therefore, more efficient techniques are required to understand the association between the dynamics of the ecosystem's response to extreme climatic conditions and its implication to the society.

Since the significant nonlinear correlation between climate variables and ecosystem functioning indicators might not be captured during univariate analysis, many researchers have recommended the use of joint distribution to describe the characteristics of such events (Kao and Govindaraju 2010; Chen et al. 2012; Huang et al. 2014).. In this regard, Copula is a useful tool to model multivariate distribution among random variables (Sklar 1959). There are several studies which support the idea that Copulas provide a robust methodology for studying hydro-climatic (Kao and Govindaraju 2010; Zhang et al. 2013; Bracken et al. 2018).

Here, a study, integrating climate data (precipitation, temperature and soil moisture content) and remote sensing observations (NDVI/NPP) using bivariate Copula-based approach to quantify the impact of extreme climatic conditions over terrestrial ecosystem functioning has been performed. This study estimates the extent of terrestrial ecosystems likely to be affected by extreme climatic conditions at vegetation type and river basin scales. Further, it identifies the most influencing extreme climatic factor capable of inducing severe damage to terrestrial ecosystem functioning.

5.2 Data and methodology

5.2.1 River basins of India and land cover types

The changes in climate conditions lead to alterations in the water balance of a river basin driving changes in rainfall-runoff relationships. The hydrological variables, which depend on the physical and geological characteristics of a river basin, govern the response of terrestrial ecosystems to climate disturbances. To understand the impact of extreme climatic conditions on terrestrial ecosystem functioning, 24 river basins across India as classified by India-WRIS (2014) are selected. Figure 5.1 describes the river basin ID, location and nomenclature. Vegetation distribution is also one of the primary factors which govern the terrestrial ecosystem functioning. Moreover, India's vegetation significantly changes at different temporal and spatial scales. To investigate the ecosystem dynamics in the context of vegetation types, 10 major land covers types from the of 5.1 MCD12Q1 data of Land Cover Institute (LCI, https://landcover.usgs.gov/global_climatology.php) are utilised (Broxton et al. 2014). Among the significant land cover classes, Croplands (CL) is one of

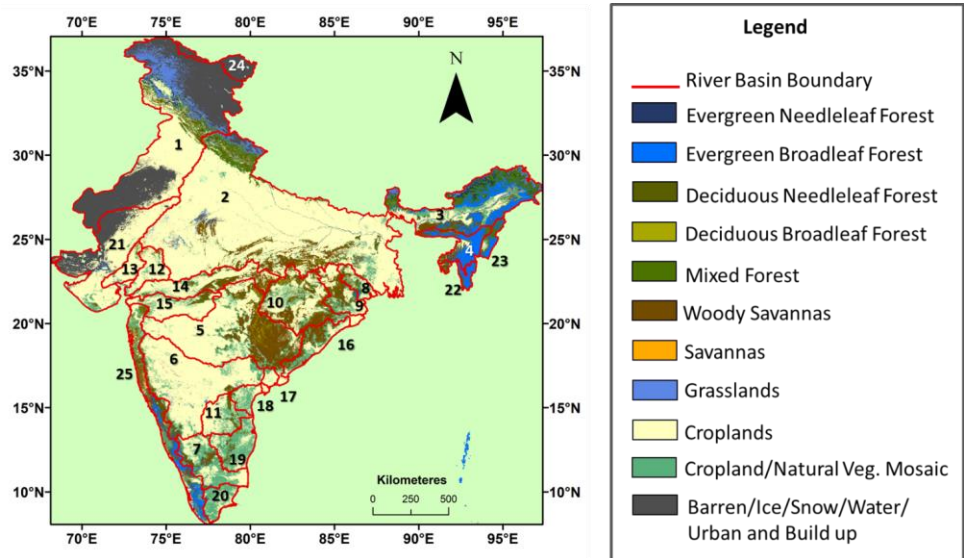


Figure 5.1. River basins IDs and details of Land Cover types considered for analysis. The details of basin IDs are : 1-Indus, 2-Ganga, 3 Brahmaputra, 4-Barak, 5-Godavari,6-Krishna,7-Cauvery,8-Subernrekha,9-Brahmani and Baitarani, 10 Mahanadi, 11-Pennar,12-Mahi, 13-Sabarmati, 14-Narmada, 15-Tapi, 16-East flowing rivers between Mahanadi and Godavari basins (EFRMGB), 17- East flowing rivers between Godavari and Krishna basins (EFRGKB),18- East flowing rivers between Krishna and Pennar basins (EFRKPB) ,19- East flowing rivers between Pennar and Cauvery basins (EFRPCB),20-East flowing rivers between Subernrekha and Cauvery basins (EFRSCB), 21-Luni ,22-Minor rivers flowing into Bangladesh (MRFB) ,23- Minor rivers flowing into Myanmar (MRFM) ,24- Western Ghats (WG)

the most dominant vegetation types covering more than 50% of the total area of the country (Yue et al. 2014). Major forest cover types are Deciduous Broadleaf and Deciduous Needleleaf Forests (DBF and DNF) which are known to follow seasonal pattern of leaf-on and leaf-off periods. These forest types are found irregularly in all parts of the country except Rajasthan and Himalayan region (Reddy et al. 2015). The EvergreenNeedleleaf Forests and Evergreen Broadleaf forests (ENF and EBF), found mainly in the coastal plains with limited spread over lower

slopes of north-east, Aravalli and the Western Ghats are known to remain green most of the times in the year (Joshi et al. 2011).

5.2.2 Climate data

Gridded data of mean monthly temperature, precipitation and soil moisture content for the period of 1982-2010 are analysed. The precipitation data has been extracted at a spatial resolution ($0.25^\circ \times 0.25^\circ$) from the India Meteorological Department 4 (IMD-4) data set (Pai et al. 2014). Temperature data for the period of 1982-2010 is also obtained from IMD, which is developed using Shepard's angular distance method from 395 observational stations in the country (Srivastava et al. 2009). The soil moisture data is extracted from the Climate Prediction Centre (CPC) soil moisture product developed by the Earth System Research Laboratory of National Oceanic Atmospheric Administration (ESRL-NOAA) (<http://www.esrl.noaa.gov/psd/data/gridded/data.cpcsoil.html>). The data validation and its application in various sectors suggest that both interannual and annual variability of soil moisture is well captured and produce excellent results in soil-climate interaction studies (Fan and van den Dool 2004; Prasad et al. 2006; Koster et al. 2016).

5.2.3 NDVI and NPP data

NDVI data is extracted from the Global Inventory Modelling and Mapping Studies (GIMMS) (<http://ecocast.arc.nasa.gov/data/pub/gimms/3g/>) source with a spatial and temporal scale of 8×8 km and 15 days, respectively. This data set is considered ideal for monitoring the changes in vegetation productivity and has been widely used to analyse the relationship between climate and terrestrial ecosystem interaction (Tan and Gan 2016). The GIMMS data set from the Advanced Very High-Resolution Radiometer (NOAA-AVHRR) sensor has been corrected for orbital drift errors and vegetation change (Liu et al. 2016).

Similarly, the NPP data is obtained from the NASA-Earth Observation System (EOS) program's MOD17A2 dataset. The Moderate Resolution

Imaging Spectroradiometer (MODIS) net primary productivity data is available from the year 2000 at 8-day, monthly and annual time steps. The data has been prepared by after performing a number of quality assurance, calibration and validation activities. Several works using MODIS data has been performed, which validates its suitability. For instance, Nayak and Dadhwal (2010) in a significant study, checked the consistency of NPP estimates from the CASA model (Carnegie–Ames–Stanford Approach), field-based observations, and MODIS data. It was found that the CASA-based annual NPP, NPP from MODIS data and ground-based NPP were in good agreements with each-other.

The NDVI, soil moisture, temperature and soil moisture data are regridded at a resolution of $(0.25^\circ \times 0.25^\circ)$ using the Inverse Distance Weightage (IDW) algorithm. Further, the NPP data is available for a relatively lesser temporal duration (2000-2010). Therefore, for the sake of computational simplicity, the analysis using NPP is performed at a resolution of $(0.50^\circ \times 0.50^\circ)$. The investigation is performed on monsoon, nonmonsoon and annual scale considering seasonal variations as one of the key factors in ecosystem climate interaction.

5.2.4 Copula based bivariate probabilistic model

Figure 5.2 gives the overview of the methodology adopted in this study. The Copula is a flexible approach to represent multivariate joint distribution (Nelson 2006). Although Copula theory was tabled in the mid of 20th century by Sklar (1959), the wide applicability of Copula in different fields has come into picture only in recent years. Conventional bivariate approaches suffer from many limitations and have limited efficiency because of various limitations (Zhang 2005). Most approaches do not incorporate essential aspects such as stationarity and scaling properties in current bivariate models. However, Copula based approach offers an alternative to overcome these limitations. The complexity of dependence can be modelled with the help of many existing Copula families and their

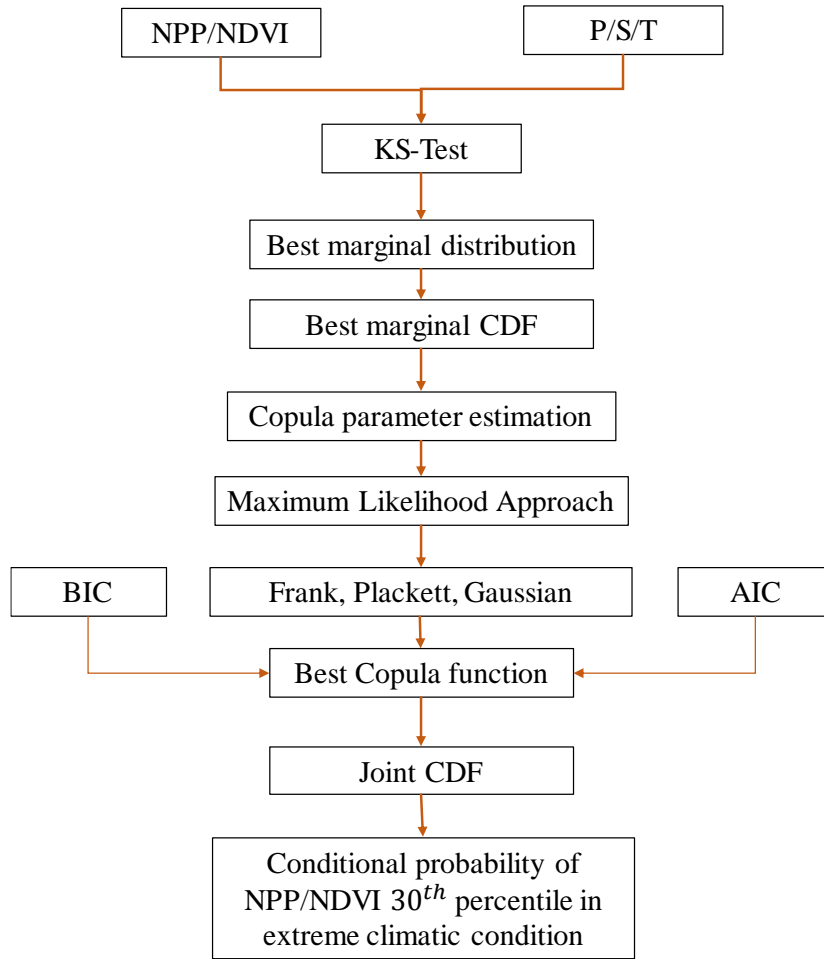


Figure 5.2 The Copula based methodology utilized in the analysis.

associated parameters. Briefly, according to Sklar’s theorem (Sklar 1959), a multivariate distribution $F(x_1, x_2 \dots x_n)$ can be expressed by a Copula as

$$F(x_1, x_2, \dots, x_n) = C[F_{X_1}(x_1), F_{X_2}(x_2) \dots F_{X_n}(x_n)] = C(u_1, u_2 \dots u_n) \quad (5.1)$$

Where, $F_{X_i}(x_i)$, denoted by u_i in the Copula definition denotes the CDF of i^{th} variable, and C is the cumulative Copula distribution function. Of the many existing Copula families, Copulas from the Elliptical family (Gaussian and t) carry several properties of the multivariate Gaussian distributions (Favre et al. 2004). Archimedean Copulas (Gumbel, Clayton and Frank) are another widely used Copula class as they offer greater

versatility modelling data with inconsistent dependencies (Chiou and Tsay 2008). In this study, Frank Copula from the Archimedean Copula families has been chosen. Additionally, Plackett Copula types are also used to accommodate more flexibility in modelling joint behaviour of the data. There are many advantages to selecting the mentioned Copula types. Firstly, the density of Frank and Plackett Copula types offer great versatility to incorporate a variety of marginal processes (Chiou and Tsay 2008). Secondly, the parameter for these Copulas is single in number; hence, the methodology involved to model the dependence structure of variables is relatively more straightforward and flexible (Ganguli and Reddy 2014). Moreover, the Copulas chosen in this study are capable of modelling a wide range of dependence including positively and negatively correlated variables, which may be the case considering the type of datasets used in this study (Zhang and Singh 2007).

It is necessary to find the most suitable marginal probability distribution for each random variable before modelling their joint structure. For this purpose, five different probability distributions (Gaussian, Gamma, Lognormal, Weibull and Generalised Extreme Value distributions) are compared based on their goodness-of-fit (Kolmogorov-Smirnov) statistics (Wilcox 2005). After finding the best fit marginal distribution function for all the four variables on a seasonal and annual scale, best-fit Copula function out of Plackett, Gaussian and Frank is decided by log-likelihood approach (Gomez et al. 2017). Best Copula and Copula parameters for all the cases are found using Akaike Information Criterion (AIC) and Bayesian Information Criterion (BIC) which estimate the relative performance of considered models (Cong and Brady 2012; Lasmar and Berthoumieu 2014). Once the best Copula function and parameter is decided, the joint

distribution is formulated. Further, the response of terrestrial ecosystem productivity to extremes is estimated by analysing the conditional probability of ecosystem functioning indicators (NDVI/NPP) with respect to stressed climatic condition (precipitation, temperature and soil moisture

content). Calculation of the conditional probability distribution, in such case, for the set of variables NDVI- Precipitation (NDVI-P), NDVI-Soil Moisture content (NDVI-S) and NDVI-Temperature (NDVI-T) as $N_1 \leq n_1$ and $N_2 \leq n_2$ can be given as

$$F_{N_1 \leq n_1 | N_2 \leq n_2}(n_1, n_2) = \frac{C(F_{n_1}(N_1), F_{n_2}(N_2))}{F_{n_2}(N_2)} = \frac{C(u_1, u_2)}{u_2} \quad (5.2)$$

To fulfil the criteria of extreme climatic conditions, the conditional probability distribution of NDVI/NPP in stressed scenarios of temperature, precipitation and soil moisture content is computed. These stressed scenarios represent the non-exceedance of the 20th ($n \leq 20^{th}$) percentile of the climate variables. To quantify the stress induced, a threshold NDVI/NPP value corresponding to less than 30th percentile ($n_{NDVI} \leq 30^{th}$) is identified. The conditional probabilities are calculated for each season and annual scale for all the grid points across the country. The selection of threshold is necessary to investigate and demarcate the temporal and spatial risk to ecosystem functioning. By considering the lower thresholds of climate variable, the likelihood of extreme changes in ecosystem functioning triggered by extreme climate conditions can be observed. The Copula based analysis was done by developing code in MATLAB and the plots were prepared using ArcGIS 10.6

5.3 Results

5.3.1 Selection of suitable thresholds

The threshold is selected such that the sensitivity of terrestrial ecosystem functioning to extreme climatic conditions could be captured. A demonstrative case illustrates the threshold selection process. For instance, the thresholds of 10 to 50 percentiles for soil moisture, precipitation and temperature are tried against the NPP thresholds. It is found that if climatic constraints are eased, i.e., by selecting higher percentiles of climate data, the conditional probabilities are reduced, depicting lower likelihood of a

drastic reduction in NPP (Figure 5.3-5.6). Similarly, to evaluate the likelihood of extreme damage to NPP, first, a threshold as low as 10th percentile is selected. The results show that likelihood of $NPP \leq 10^{th}$ percentile is very low, and most parts of the country are safe under stressed climate. The likelihood estimates suggested that even if the climatic condition is highly constrained, the bivariate models showed very minimum chances of $NPP \leq 10^{th}$ percentile (Figure 5.3, 5.5). This means that $NPP \leq 10^{th}$ percentile is way too unrealistic even for the highly stressed climatic condition; hence, it cannot be selected as a suitable threshold for the analysis. Similar results are observed for $NPP \leq 20^{th}$ percentile threshold, which gives almost moderate or safe likelihood values for all thresholds of precipitation, temperature and soil moisture (Figure 5.4, 5.6). Therefore, it can be concluded that neither an eased climatic condition nor too stressed NPP is suitable for analysing the sensitivity of terrestrial ecosystem functioning to extreme climatic conditions. Therefore, a threshold of $NPP_{30^{th}}$ percentile (not too stressed) and soil moisture, precipitation and temperature $\leq 20^{th}$ percentile (not too eased) is selected.

5.3.2 Risk to terrestrial ecosystem functioning

5.3.2.1 Impact on vegetation condition

As discussed, the joint distribution of NDVI-temperature, NDVI-precipitation and NDVI-soil moisture content is estimated on both seasonal and annual scales. Once, the joint probabilities are obtained, the conditional probability of NDVI value with the suitable threshold ($n_{NDVI} \leq 30^{th}$) percentile, which represents risk condition is evaluated using Equation 5.2 at each grid point in different stressed scenarios of climate variable ($n \leq 20^{th}$) percentile. The results for the first scenario ($n_{NDVI} \leq 30^{th}$) percentile is shown in Figure 5.7. The conditional probability values

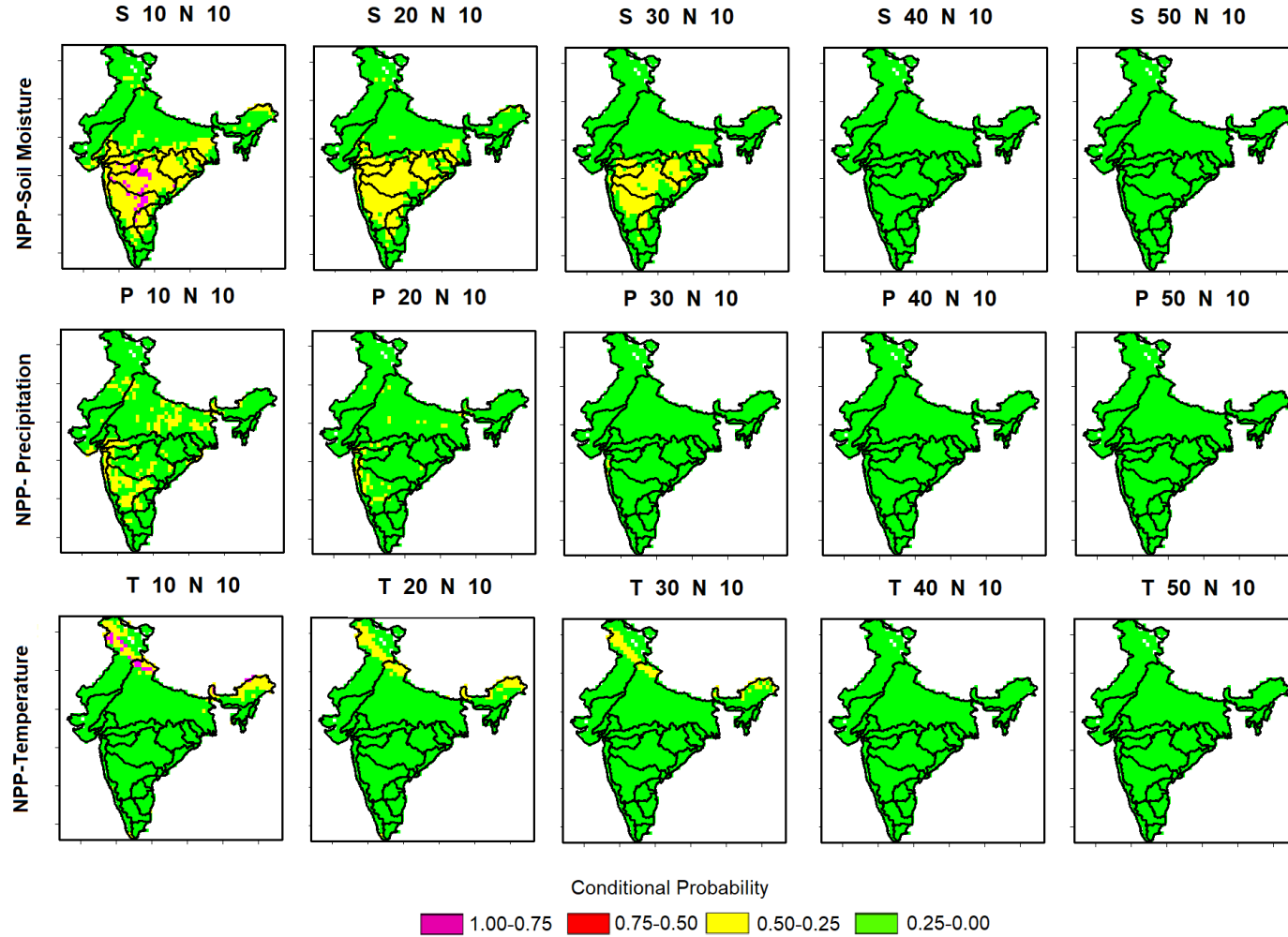


Figure 5.3 Conditional likelihood of $n_{NPP} \leq 10^{th}$ percentile in different scenarios of S/P/T in nonmonsoon season to understand the best possible threshold of NPP and climatic data

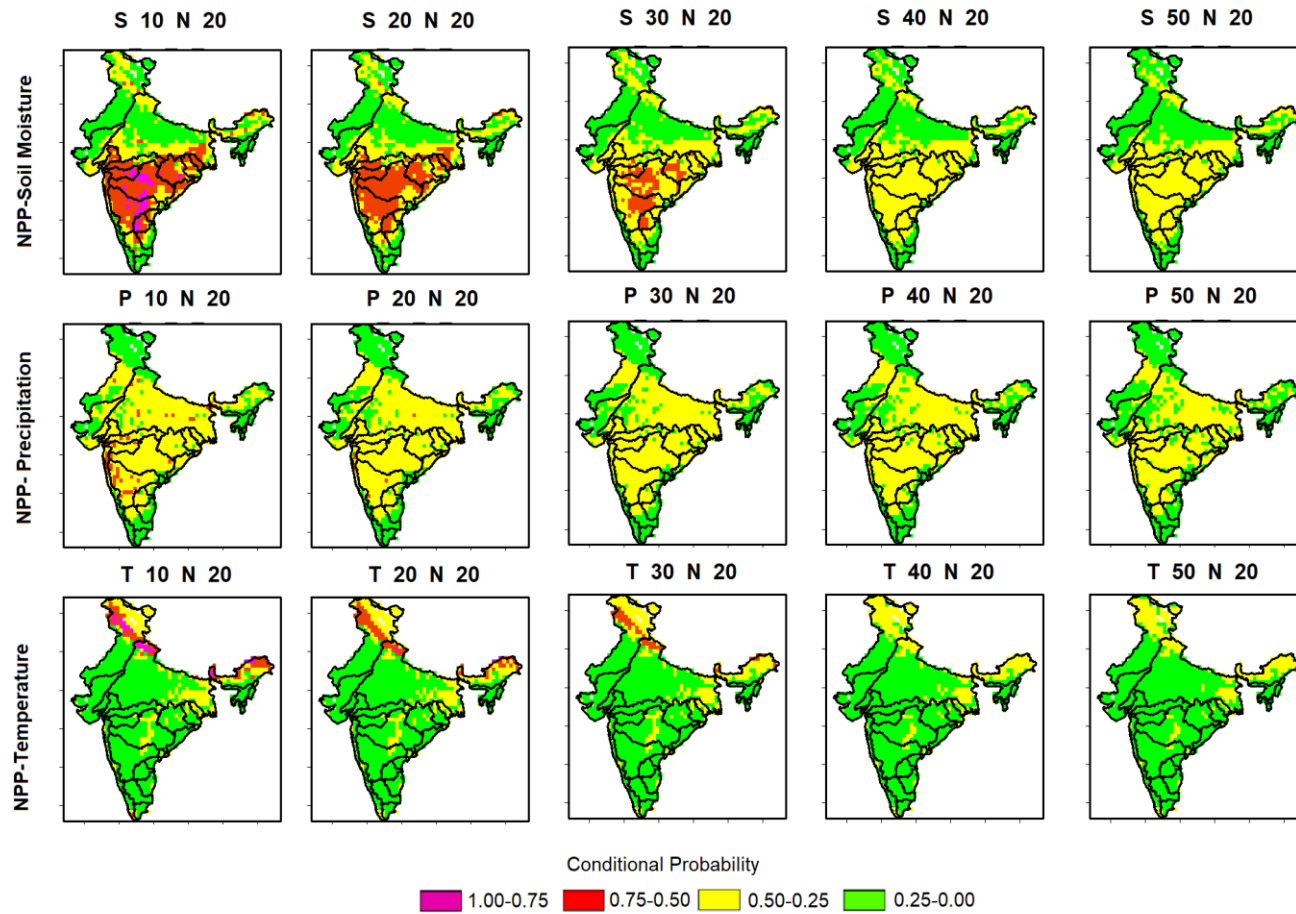


Figure 5.4 Conditional likelihood of $n_{NPP} \leq 20^{th}$ percentile in different scenarios of S/P/T in nonmonsoon season to understand the best possible threshold of NPP and climatic data

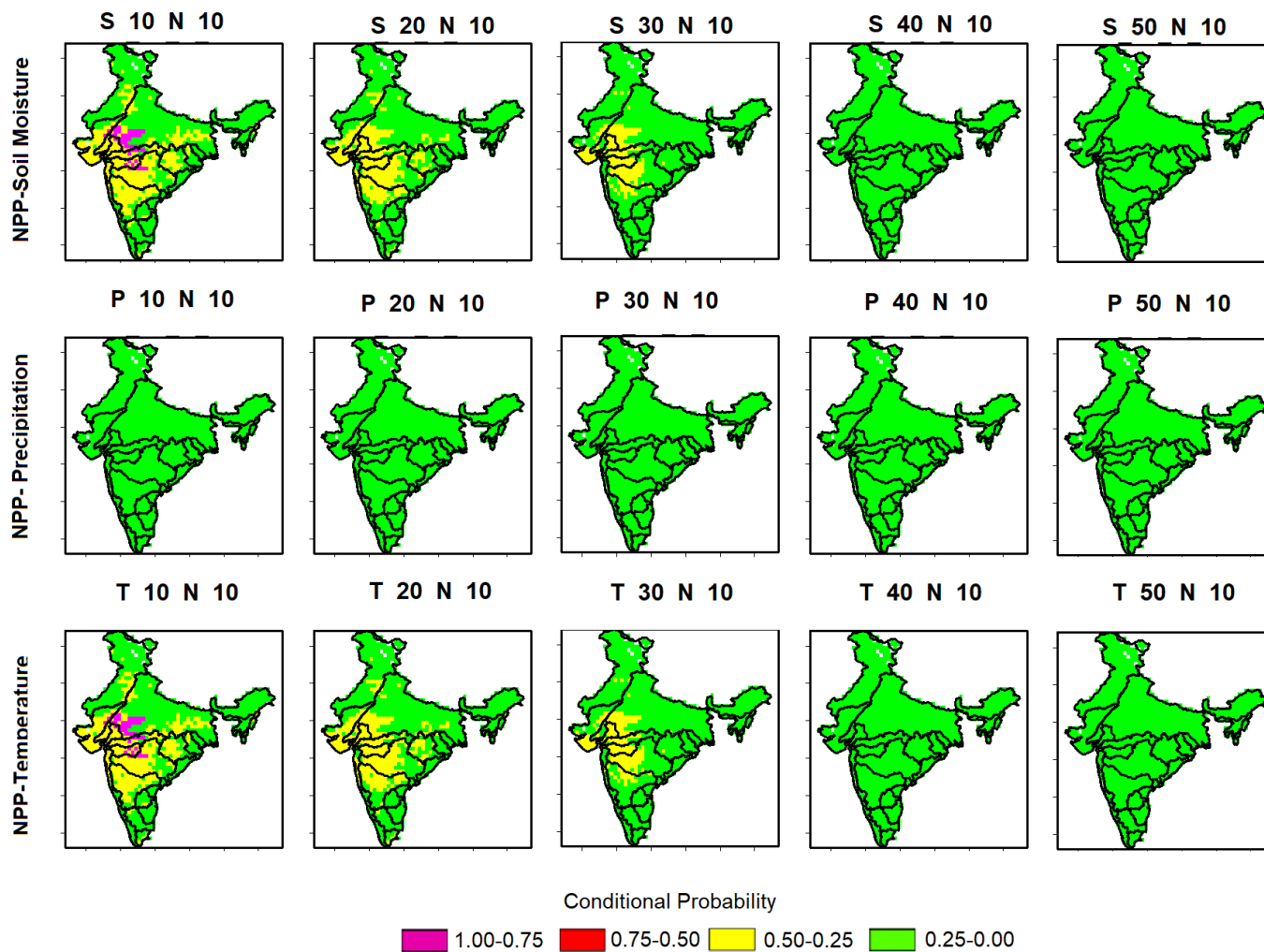


Figure 5.5 Conditional likelihood of $n_{NPP} \leq 20^{th}$ percentile in different scenarios of S/P/T in monsoon season to understand the best possible threshold of NPP and climatic data

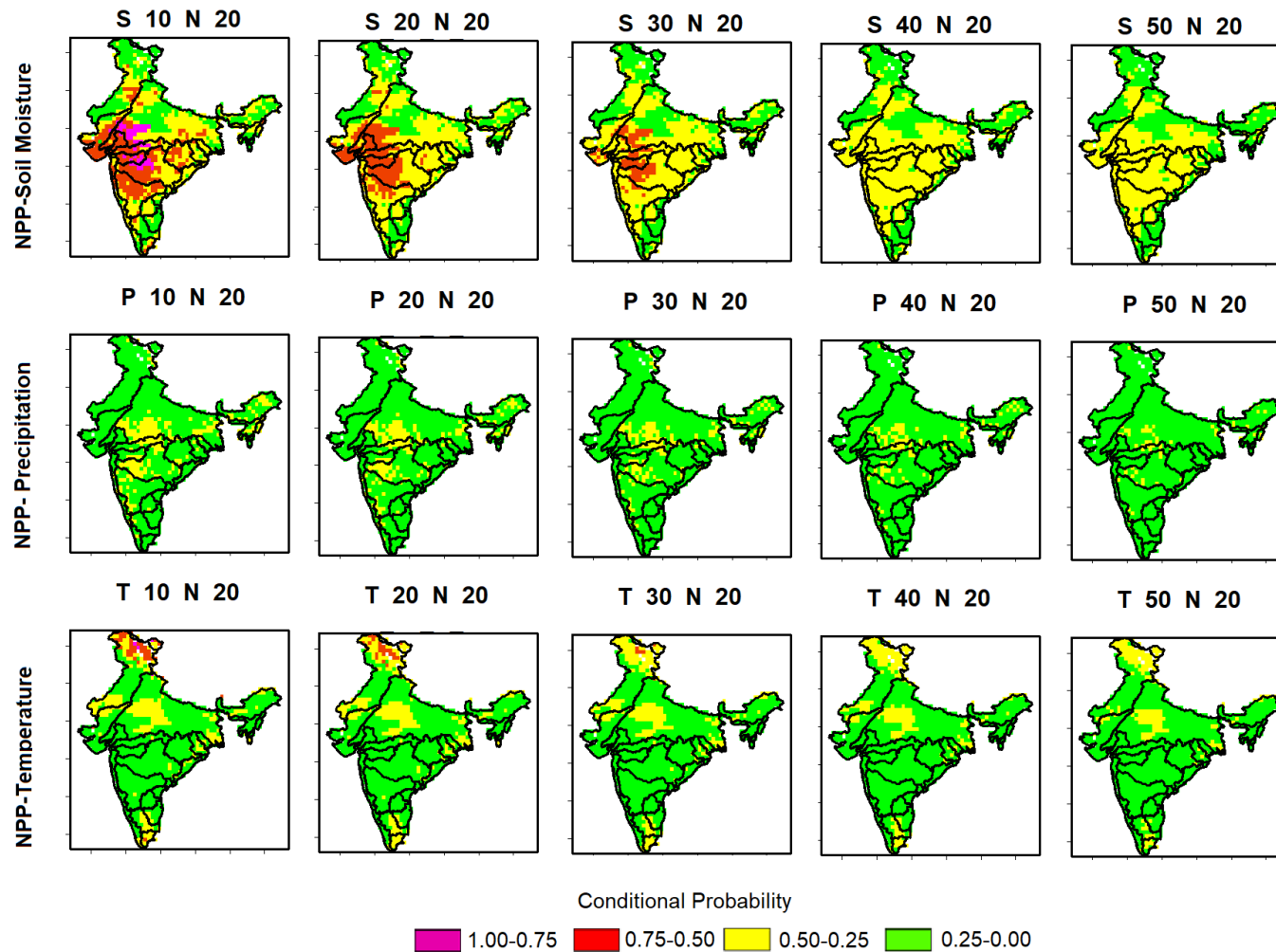


Figure 5.6 Conditional likelihood of $n_{NPP} \leq 20^{th}$ percentile in different scenarios of S/P/T in monsoon season to understand the best possible threshold of NPP and climatic data

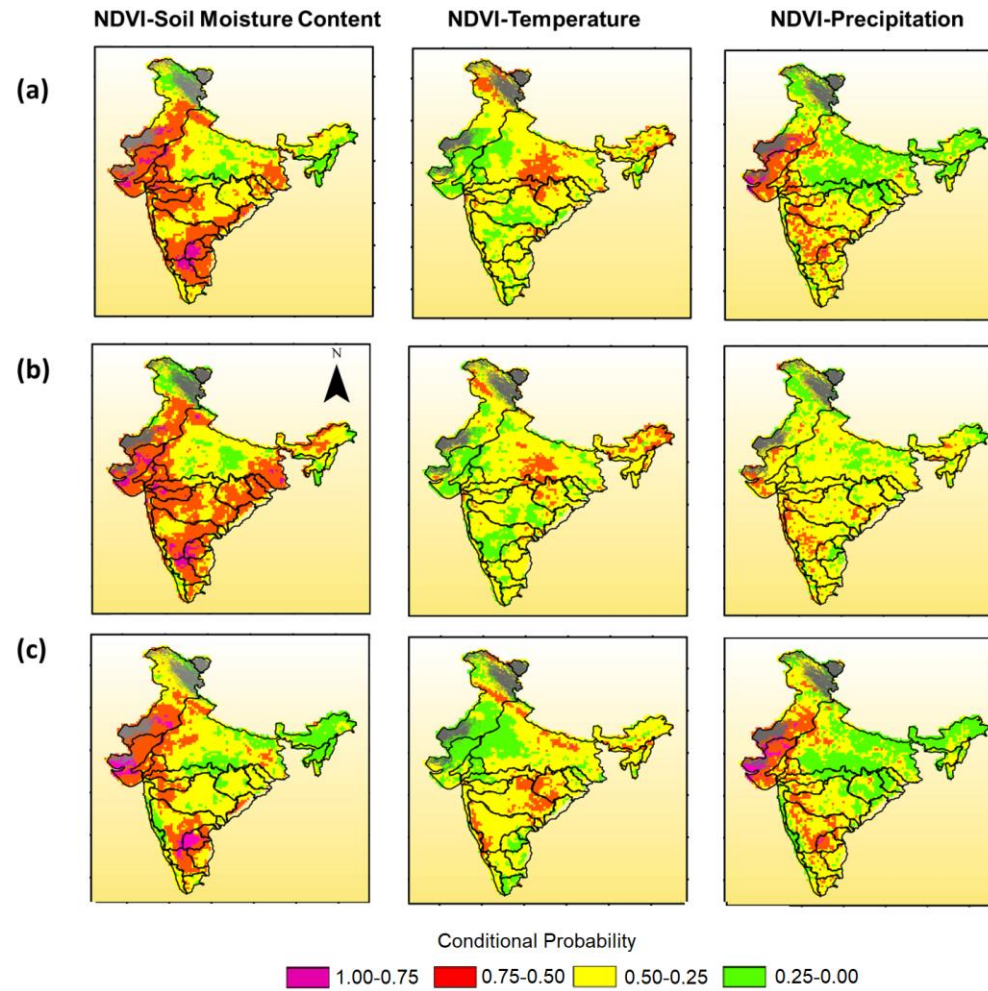


Figure 5.7 Conditional probabilities of $n_{NDVI} \leq 30^{th}$ percentile at (a) annual (b) nonmonsoon and (c) monsoon season scale

are classified to define the risks as extreme (0.75-1), high (0.50-0.75), moderate (0.25-0.50) and low (0.25-0.00). On an annual scale, most of the basins in the country except some in the north-east region (e.g. Barak) are susceptible to moderate or high risk. High likelihood of risk is observed from the NDVI-soil moisture content analysis, which indicates that soil moisture deficit is the biggest threat to existing vegetation cover (Figure 5.7c). Significant areas of river basins like Pennar, Krishna, Mahi, Sabarmati and Luni showed the high or extreme likelihood of risk when lower precipitation scenario ($n \leq 20^{th}$) percentile is considered. However, lower soil moisture conditions ($n \leq 20^{th}$) percentile worsens the situation and the extent of areas under high drought likelihood further increases (Table 5.1). This indicates that these river basins are unable to hold the incident precipitation for a longer duration to ensure enough soil moisture for their vegetation. Although a significant percentage of the above-mentioned river basins are facing high risks, it is important to note that even smaller percentage (7.03%) in large river basins like Ganga accounts for a huge area of 56,089.53 km² which also needs to be addressed. On a seasonal scale, higher risks are observed in nonmonsoon season than the monsoon season, which is shown in Figure 5.8. The river basins in the north-east region are least susceptible to risk in lowered precipitation and soil moisture conditions. However, lower temperature scenarios do induce some risks in these areas. This may have caused due to the lack of necessary warmth or sunshine for plant growth in cold regions (Figure 5.7). Hence, the increase in temperature in these regions may lower the risks to terrestrial ecosystems. Moreover, low-temperature scenarios do not have any significant impact on most of the other river basins. Detailed results at seasonal scales for all river basins have been given in Table 5.1-5.3.

Table 5.1 Area under high risk at annual scale in stressed climate at river basin level

Sl No.	Basin	NDVI-S		NDVI-P		NDVI-T	
		(%)	Sq. km.	(%)	Sq. km.	(%)	Sq. km.
		Area (1000 km ²)					
1	Indus	37.51	171.90	24.04	110.17	14.02	64.26
2	Ganga	23.32	186.08	7.03	56.09	14.90	118.93
3	Brahmaputra	3.13	5.92	0.35	0.66	21.54	40.79
4	Barak	0.00	0.00	0.00	0.00	1.55	2.93
5	Godavari	42.08	119.26	18.50	52.43	5.09	14.44
6	Krishna	57.42	134.99	40.82	95.96	1.74	4.10
7	Cauveri	82.72	64.64	16.08	12.57	0.00	0.00
8	Subarnarekha	29.75	7.09	2.19	0.52	0.00	0.00
9	BB	33.91	17.07	0.00	0.00	3.38	1.70
10	Mahanadi	3.42	4.32	1.30	1.64	31.82	40.25
11	Pennar	96.72	44.84	46.11	21.37	0.00	0.00
12	Mahi	90.74	34.25	37.51	14.16	0.00	0.00
13	Sabarmati	86.32	24.58	45.56	12.97	0.00	0.00
14	Narmada	33.99	29.49	13.51	11.72	27.25	23.64
15	Tapi	82.76	52.07	18.87	11.87	5.09	3.20
16	EFRMGB	62.57	29.42	16.20	7.62	4.02	1.89
17	EFRGKB	73.20	6.30	15.38	1.32	61.54	5.30
18	EFRKPB	98.37	23.45	44.45	10.60	0.00	0.00
19	EFRPCB	85.64	45.94	9.60	5.15	0.00	0.00
20	EFRSCB	14.45	4.31	6.67	1.99	0.00	0.00
21	Luni	91.75	169.53	81.56	150.69	0.00	0.00
22	MRBB	3.44	0.50	0.00	0.00	0.00	0.00
23	MRMB	0.00	0.00	0.00	0.00	33.82	4.93
24	WG	29.74	30.53	5.43	5.57	0.65	0.66

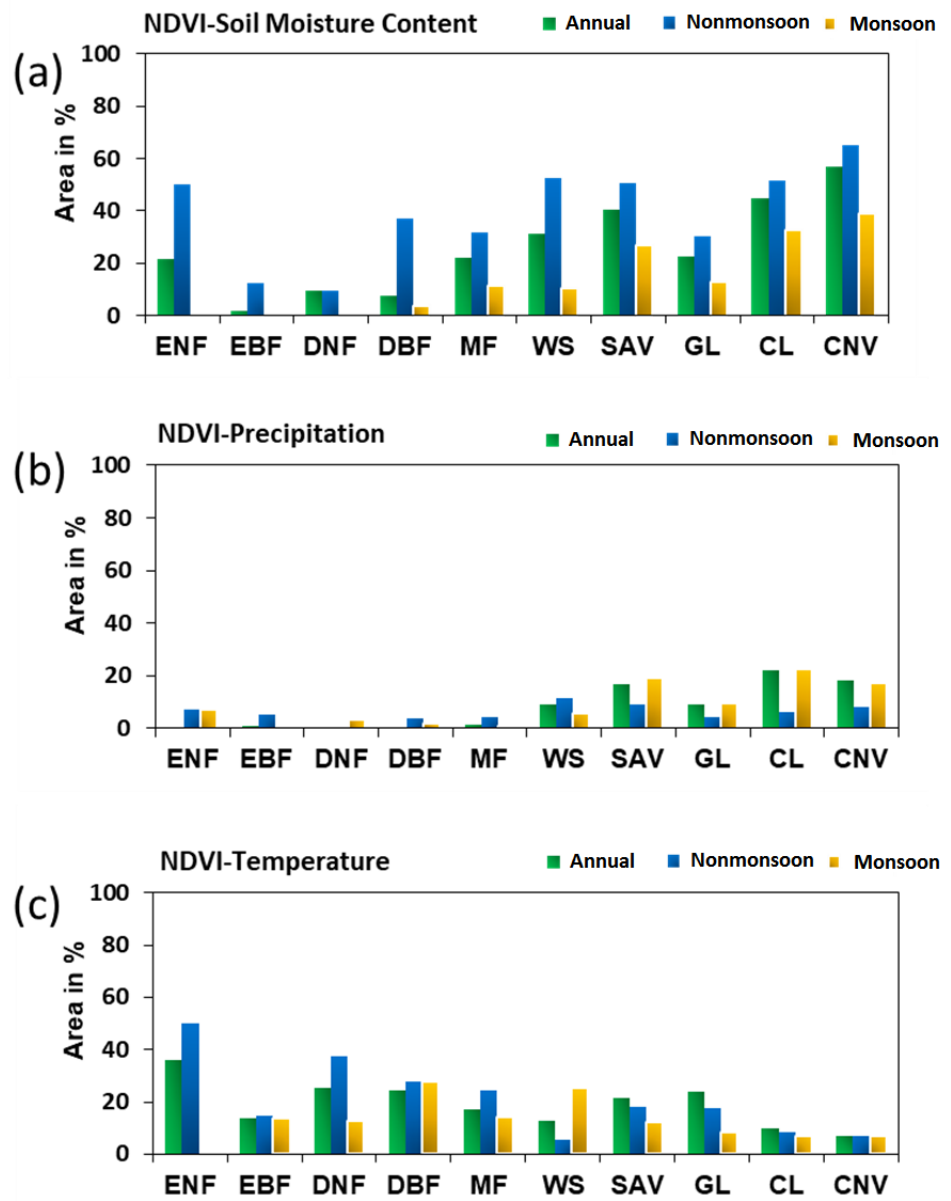


Figure 5.8 Percent areas of land cover types showing high likelihood risk for (a) NDVI-Soil Moisture Content, (b) NDVI-Temperature and (c) NDVI-Precipitation

Table 5.2 Vegetation area under high risk in nonmonsoon season in stressed climate at river basin level

SI No.	Basin	NDVI-S		NDVI-P		NDVI-T	
		(%)	Sq. km.	(%)	Sq. km.	(%)	Sq. km.
		Area (1000 km²)					
1	Indus	36.42	166.92	1.68	7.69	6.25	28.63
2	Ganga	26.49	211.36	0.96	7.63	10.91	87.09
3	Brahmaputra	27.23	51.58	4.84	9.17	34.82	65.94
4	Barak	0.00	0.00	3.18	6.00	0.50	0.95
5	Godavari	61.84	175.27	9.41	26.67	2.77	7.86
6	Krishna	62.33	146.53	19.44	45.70	1.08	2.54
7	Cauveri	71.51	55.88	9.32	7.28	0.00	0.00
8	Subarnarekha	83.79	19.97	0.00	0.00	0.00	0.00
9	BB	85.33	42.95	0.00	0.00	0.00	0.00
10	Mahanadi	49.91	63.12	1.05	1.32	24.36	30.82
11	Pennar	93.87	43.51	14.07	6.52	0.00	0.00
12	Mahi	93.28	35.21	0.00	0.00	0.00	0.00
13	Sabarmati	86.32	24.58	2.33	0.66	0.00	0.00
14	Narmada	43.12	37.40	0.76	0.66	13.35	11.58
15	Tapi	92.70	58.32	10.04	6.32	5.15	3.24
16	EFRMGB	63.04	29.64	9.82	4.62	1.41	0.66
17	EFRGKB	50.12	4.31	7.69	0.66	23.08	1.99
18	EFRKPB	70.78	16.87	0.00	0.00	5.56	1.32
19	EFRPCB	50.15	26.90	1.23	0.66	0.00	0.00
20	EFRSCB	39.93	11.90	6.67	1.99	0.00	0.00
21	Luni	92.40	170.73	24.46	45.20	1.43	2.65
22	MRBB	7.12	1.04	0.00	0.00	0.00	0.00
23	MRRMB	0.00	0.00	0.00	0.00	18.18	2.65
24	WG	36.03	36.99	23.30	23.92	0.22	0.23

Table 5.3 Vegetation area under high risk in monsoon season in stressed climate at river basin level.

		NDVI-S		NDVI-P		NDVI-T	
		Area (1000 km ²)					
Sl No.	Basin	(%)	Sq. km.	(%)	Sq. km.	(%)	Sq. km.
1	Indus	38.12	174.67	31.26	143.23	5.63	25.82
2	Ganga	17.91	142.88	7.78	62.11	6.48	51.74
3	Brahmaputra	0.00	0.00	0.00	0.00	9.31	17.63
4	Barak	0.00	0.00	0.00	0.00	3.39	6.40
5	Godavari	11.92	33.77	12.14	34.41	26.58	75.33
6	Krishna	37.75	88.75	33.33	78.35	12.00	28.20
7	Cauveri	65.13	50.90	15.25	11.92	0.85	0.66
8	Subarnarekha	0.00	0.00	2.41	0.57	0.00	0.00
9	BB	0.00	0.00	0.00	0.00	0.00	0.00
10	Mahanadi	0.00	0.00	1.43	1.81	36.19	45.78
11	Pennar	88.15	40.86	62.44	28.94	0.00	0.00
12	Mahi	66.25	25.01	28.96	10.93	0.00	0.00
13	Sabarmati	84.17	23.97	43.73	12.45	0.00	0.00
14	Narmada	19.04	16.52	9.37	8.13	4.76	4.13
15	Tapi	41.79	26.29	17.80	11.20	2.01	1.27
16	EFRMGB	29.69	13.96	0.00	0.00	11.16	5.25
17	EFRGKB	0.00	0.00	0.00	0.00	23.08	1.99
18	EFRKPB	68.57	16.35	41.01	9.78	0.00	0.00
19	EFRPCB	40.59	21.77	9.61	5.15	0.00	0.00
20	EFRSCB	11.09	3.30	19.21	5.73	0.00	0.00
21	Luni	94.09	173.84	85.27	157.55	0.00	0.00
22	MRBB	0.00	0.00	0.00	0.00	0.00	0.00
23	MRMB	0.00	0.00	0.00	0.00	8.50	1.24
24	WG	1.28	1.31	0.64	0.65	14.45	14.83

Most dominant land cover type in the country is Croplands, which majorly contributes to agricultural production. Soil moisture content remains the most significant factor affecting the Croplands (Figure 5.8). Further, lowered precipitation scenario augments the chances of vegetation drought more severely than lowered temperature scenario. While lowered precipitation has negligible impact on evergreen forests and deciduous forests types, the role of temperature is significant in these forest types and lowering the temperature profile increases the chances of high risk (Figure 5.8). On seasonal scales, as obtained in the study at river basins level, extreme or high risks are more evident in the nonmonsoon season. More than 50% of the Croplands fall under high or extreme drought risks in nonmonsoon season in low soil moisture scenario. Evergreen forest is almost undisturbed in the monsoon season and remains safe from the risks probably because of improved water availability in the monsoon months. However, about 33% and 39% of Cropland and Cropland/natural vegetation mosaic respectively fall under high or extreme risks in the same season, raising serious concerns about India's food security.

5.3.2.2 Impact on net primary productivity

In the context of net primary productivity, the investigation at annual time scale reveals that terrestrial ecosystems in a majority of the river basins come under high-risk category when subjected to very low soil moisture values (Figure 5.9). Lowering the temperature is least disturbing to the ecosystem productivity except in high-altitude cold regions. The high risks due to stressed temperature at annual scale are observed only in 4 out of 24 river basins which collectively add up to less than 10% of the country's area (Table 5.4). However, reducing the precipitation induces moderate risks of severe damage to productivity in most of the river basins. Small areas of the Western Ghats, river basins in the eastern coast such as FRMGP, EFRGKB and EFRPCB and north-east region namely, Barak and Brahmaputra are

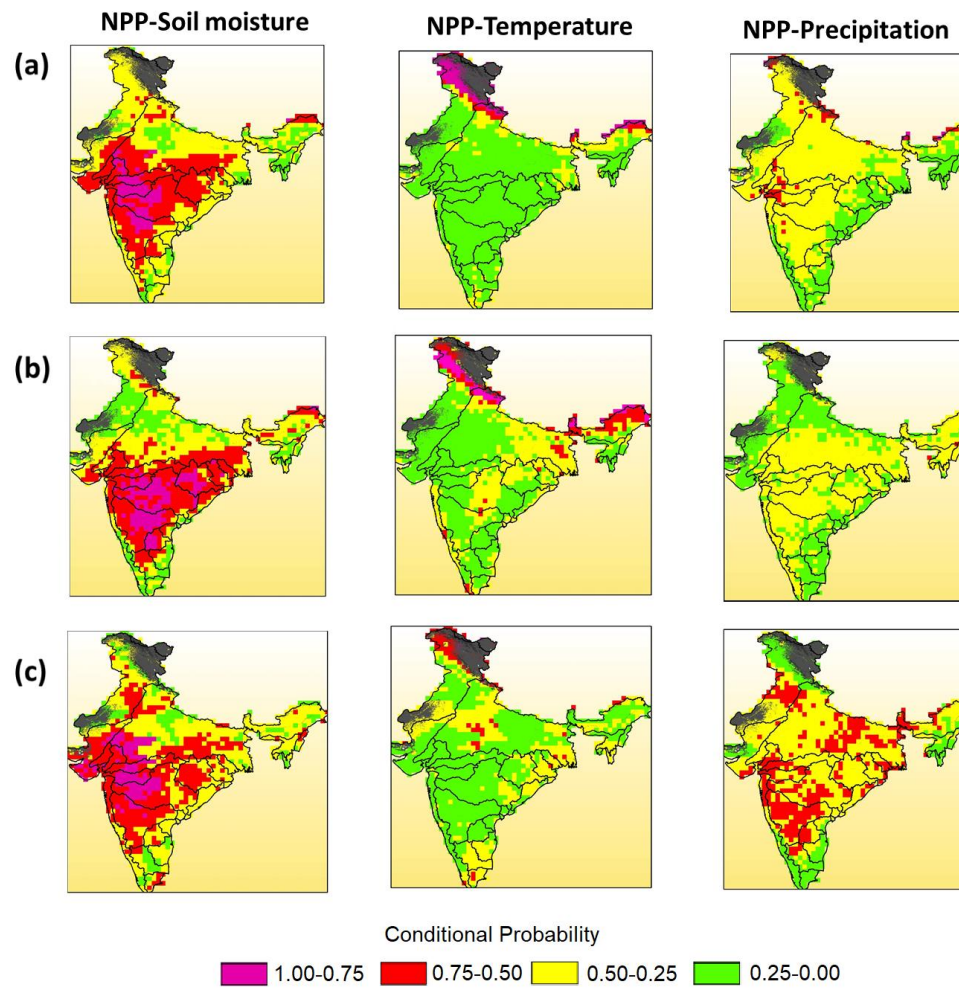


Figure 5.9 Conditional probabilities of $n_{NPP} \leq 30^{th}$ percentile at (a) annual (b) nonmonsoon and (c) monsoon season scale

Table 5.4 NPP area under high risk at annual scale in stressed climate at river basin level

		NPP-S		NPP-P		NPP-T	
		Area (1000 km ²)					
SI No.	Basin	(%)	Sq. km.	(%)	Sq. km.	(%)	Sq. km.
1	Indus	2.89	13.24	5.92	27.15	44.80	205.29
2	Ganga	29.46	235.09	4.23	33.77	5.98	47.68
3	Brahmaputra	13.29	25.16	6.64	12.58	21.33	40.40
4	Barak	0.00	0.00	0.00	0.00	0.00	0.00
5	Godavari	85.28	241.71	0.70	1.99	0.00	0.00
6	Krishna	80.56	189.40	2.25	5.30	0.00	0.00
7	Cauveri	20.34	15.89	0.00	0.00	0.00	0.00
8	Subarnarekha	25.00	5.96	0.00	0.00	0.00	0.00
9	BB	28.95	14.57	0.00	0.00	0.00	0.00
10	Mahanadi	76.44	96.68	0.00	0.00	0.00	0.00
11	Pennar	44.29	20.53	0.00	0.00	0.00	0.00
12	Mahi	100.00	37.75	21.05	7.95	0.00	0.00
13	Sabarmati	100.00	28.48	2.33	0.66	0.00	0.00
14	Narmada	97.71	84.76	13.74	11.92	0.00	0.00
15	Tapi	100.00	62.91	22.11	13.91	0.00	0.00
16	EFRMGB	1.41	0.66	0.00	0.00	0.00	0.00
17	EFRGKB	0.00	0.00	0.00	0.00	0.00	0.00
18	EFRKPB	0.00	0.00	0.00	0.00	0.00	0.00
19	EFRPCB	0.00	0.00	0.00	0.00	0.00	0.00
20	EFRSCB	0.00	0.00	0.00	0.00	0.00	0.00
21	Luni	46.59	86.09	2.15	3.97	0.00	0.00
22	MRBB	0.00	0.00	0.00	0.00	0.00	0.00
23	MRMB	0.00	0.00	0.00	0.00	0.00	0.00
24	WG	37.42	38.41	2.58	2.65	0.00	0.00

prone to high risks. Productivity in the river basins such as Mahi and Tapi is most likely to be hit by extreme changes in the annual precipitation as 22.11% and 21.05% of their area exhibit high risks, respectively. More importantly, the analysis of annual NPP and soil moisture levels reveals that 100% area of three river basins (Mahi, Sabarmati and Tapi) are prone to high risks. However, the river basins in the east-coast and the north-east region are relatively safer. Similar to results at the annual scale, stressed temperature scenario is not a major threat in monsoon season, and only about 6.5% of country's area is at high risk (Table 5.5 and Figure 5.9). However, it is observed that extreme reduction in soil moisture even in the monsoon season might cause severe damage to the ecosystem productivity of about 38% area of the country. More than 50% area of 8 out of 24 river basins is prone to severe damage due to lower soil moisture levels. In addition, reducing the precipitation, soil moisture and temperature to the same level more significantly damages the productivity in the nonmonsoon season. The temperature in nonmonsoon months may bring more substantial risks to the ecosystem productivity in high-altitude basins as compared to the annual scale and monsoon season (Table 5.6). It can be observed that about 61.54% area of the Brahmaputra basin is under high risk followed by the Indus river basin's 28.18%. Further, ecosystem productivity in about 24% area of the country is at high risks in lowered precipitation scenario in the nonmonsoon season as compared to 1% in the monsoon season. Productivity in the Krishna river basin is found to be most vulnerable as 68.17% of its area is at high risks in the nonmonsoon season.

Table 5.7 shows the areas under the high-risk class at different vegetation type levels in the monsoon, nonmonsoon season and annual scale. Stressed temperature scenario induces such high risks in 57.14% of ENF at the annual scale. Further, ecosystem productivity of 45.30% of the Croplands is at high risks in lower temperature scenario. It is found that the ENF is most sensitive to the extreme climate conditions as 28.57% and 35.71% of their areas are likely to touch the 30th percentile threshold in stressed soil

Table 5.5 NPP area under high risk in monsoon season in stressed climate
at river basin level

Sl No.	Basin	NPP-S		NPP-P		NPP-T	
		(%)	Sq. km.	(%)	Sq. km.	(%)	Sq. km.
		Area (1000 km²)					
1	Indus	14.02	64.24	0.00	0.00	29.77	136.42
2	Ganga	33.20	264.89	0.00	0.00	5.56	44.37
3	Brahmaputra	3.50	6.62	0.35	0.66	1.75	3.31
4	Barak	9.86	4.64	5.63	2.65	0.00	0.00
5	Godavari	76.87	217.87	0.00	0.00	0.00	0.00
6	Krishna	82.54	194.03	0.00	0.00	0.00	0.00
7	Cauveri	16.95	13.24	0.00	0.00	0.00	0.00
8	Subarnarekha	19.44	4.64	0.00	0.00	8.33	1.99
9	BB	21.05	10.60	0.00	0.00	5.26	2.65
10	Mahanadi	63.35	80.13	0.00	0.00	0.00	0.00
11	Pennar	25.71	11.92	0.00	0.00	0.00	0.00
12	Mahi	100.00	37.75	0.00	0.00	0.00	0.00
13	Sabarmati	100.00	28.48	0.00	0.00	0.00	0.00
14	Narmada	78.63	68.21	0.00	0.00	0.00	0.00
15	Tapi	98.95	62.25	0.00	0.00	0.00	0.00
16	EFRMGB	4.23	1.99	0.00	0.00	0.00	0.00
17	EFRGKB	0.00	0.00	0.00	0.00	0.00	0.00
18	EFRKPB	0.00	0.00	0.00	0.00	0.00	0.00
19	EFRPCB	0.00	0.00	0.00	0.00	0.00	0.00
20	EFRSCB	44.44	13.24	0.00	0.00	17.78	5.30
21	Luni	69.18	127.81	0.00	0.00	1.08	1.99
22	MRBB	0.00	0.00	0.00	0.00	0.00	0.00
23	MRMB	36.36	5.30	0.00	0.00	0.00	0.00
24	WG	0.00	0.00	0.00	0.00	60.00	0.00

Table 5.6 NPP area under high risk in nonmonsoon season in stressed climate at river basin level

Sl No.	Basin	NPP-S		NPP-P		NPP-T	
		(%)	Sq. km.	(%)	Sq. km.	(%)	Sq. km.
		Area (1000 km²)					
1	Indus	4.05	18.54	14.45	66.22	28.18	129.13
2	Ganga	18.67	149.00	27.14	216.55	10.04	80.13
3	Brahmaputra	25.17	47.68	17.83	33.77	61.54	116.55
4	Barak	5.63	2.65	0.00	0.00	0.00	0.00
5	Godavari	96.96	274.82	33.64	95.36	1.40	3.97
6	Krishna	92.39	217.21	68.17	160.26	1.13	2.65
7	Cauveri	44.07	34.44	21.19	16.56	0.00	0.00
8	Subarnarekha	88.89	21.19	44.44	10.60	8.33	1.99
9	BB	78.95	39.73	23.68	11.92	5.26	2.65
10	Mahanadi	89.01	112.58	16.23	20.53	0.52	0.66
11	Pennar	81.43	37.75	42.86	19.87	0.00	0.00
12	Mahi	92.98	35.10	43.86	16.56	0.00	0.00
13	Sabarmati	48.84	13.91	2.33	0.66	0.00	0.00
14	Narmada	80.92	70.20	31.30	27.15	0.00	0.00
15	Tapi	97.89	61.59	48.42	30.46	0.00	0.00
16	EFRMGB	70.42	33.11	22.54	10.60	0.00	0.00
17	EFRGKB	0.00	0.00	0.00	0.00	0.00	0.00
18	EFRKPB	58.33	13.91	8.33	1.99	0.00	0.00
19	EFRPCB	22.22	11.92	0.00	0.00	0.00	0.00
20	EFRSCB	0.00	0.00	0.00	0.00	0.00	0.00
21	Luni	16.85	31.12	8.60	15.89	0.00	0.00
22	MRBB	0.00	0.00	4.54	0.65	4.55	0.66
23	MRMB	0.00	0.00	0.00	0.00	0.00	0.00
24	WG	30.97	31.79	26.45	27.15	7.10	7.28

Table 5.7 NPP area under high risk in different seasons and annual scale
in stressed climate at LULC level

		NPP-S		NPP-P		NPP-T	
		Area (1000 km ²)					
Sl No.	LULC	(%)	Sq. km.	(%)	Sq. km.	(%)	Sq. km.
		Annual					
1	ENF	28.57	2.65	35.71	3.31	57.14	5.30
2	EBF	3.27	3.31	0.65	0.66	4.58	4.64
3	DNF	15.63	3.31	6.25	1.32	28.13	5.96
4	DFB	35.19	12.58	3.70	1.32	16.67	5.96
5	MF	26.24	24.50	10.64	9.93	42.55	39.73
6	WS	43.15	110.59	1.03	2.65	4.39	11.26
7	SAV	37.08	21.85	10.11	5.96	13.48	7.95
8	GL	32.60	39.07	13.81	16.56	45.30	54.30
9	CL	49.61	760.89	2.89	44.37	1.42	21.85
10	CNV	24.92	54.96	3.60	7.95	4.50	9.93
		Monsoon					
1	ENF	0.00	0.00	0.00	0.00	36.02	3.34
2	EBF	6.54	6.62	0.00	0.00	0.64	0.66
3	DNF	15.63	3.31	3.12	0.66	9.38	1.99
4	DFB	14.81	5.30	3.52	1.26	5.56	1.98
5	MF	10.64	9.93	0.70	0.65	4.26	3.97
6	WS	35.14	90.06	0.00	0.00	2.07	5.30
7	SAV	38.20	22.52	0.00	0.00	6.74	3.97
8	GL	28.73	34.44	0.00	0.00	27.07	32.45
9	CL	54.58	837.05	0.09	1.32	2.55	39.07
10	CNV	27.33	60.26	0.00	0.00	5.41	11.92
		Nonmonsoon					
1	ENF	28.57	2.65	28.57	2.65	85.71	7.95
2	EBF	5.23	5.30	3.27	3.31	18.30	18.54
3	DNF	21.88	4.64	6.25	1.32	43.75	9.27
4	DFB	48.15	17.22	7.41	2.65	31.48	11.26
5	MF	29.08	27.15	8.51	7.95	56.03	52.32
6	WS	65.89	168.87	18.60	47.68	6.72	17.22
7	SAV	38.20	22.52	19.10	11.26	20.22	11.92
8	GL	35.36	42.38	16.57	19.87	46.96	56.29
9	CL	43.83	672.15	36.83	564.87	5.01	76.82
10	CNV	42.94	94.70	16.52	36.42	10.21	22.52

moisture and precipitation condition, respectively. Possible reduction in annual soil moisture levels is highly threatening to the productivity of about half (49.61%) of the Croplands. This threat to the Croplands is more intensified in the monsoon season, and 54.58% of its area comes under high-risk zones. However, extremely stressed precipitation could cause high risks only in a small portion of DNF (3.12%) and DBF (3.52%). However, the lower temperature remains a threat to Evergreen Needleleaf Forest even in monsoon season. The nonmonsoon season, as discussed, is found to be the most unfavourable period for the smooth functioning of terrestrial ecosystems in the country. An enormous 85.71% of the ENF is found to be at high risk in lower temperature scenario. Furthermore, lower soil moisture content causes the maximum amount of risks in the WS (65.89%), followed by DBF (48.15%), Croplands (43.83%), Croplands/Natural Vegetation Mosaic (42.94%), Savannas (38.20%), Grasslands (35.36%), Mixed Forests (29.08%), DNF (21.88%) and EBF (5.23%). Stressed precipitation in the nonmonsoon season is found to be affecting Croplands the most (36.83%).

5.4 Discussions

This study is aimed at investigating the possible changes in terrestrial ecosystem functioning under the influence of extreme climatic conditions. Modelling this dependence is complex and requires an efficient framework for estimating the risk to terrestrial ecosystems (Twine and Kucharik 2009; Chu et al. 2016). The likelihood of NPP dropping down to the 30th percentile threshold in stressed scenarios of precipitation, soil moisture content and temperature using a multivariate probabilistic approach in different seasons and annual scale is performed. The results agree with previous studies that variations in the terrestrial ecosystem is strongly governed by changing climatic conditions (Tian et al. 2010; Kyoung et al. 2011; Singh et al. 2011). It is found that stressed soil moisture levels are the most crucial in governing the ecosystem productivity in many regions. This conclusion is in accordance with the previous findings indicating that soil moisture strongly dominates the functioning of terrestrial ecosystems

(Norby et al. 2004; Falloon et al. 2011; Xu et al. 2012). Terrestrial ecosystems in the nonmonsoon season are most susceptible to damage under extreme conditions. This is logical, as the nonmonsoon season is also the drought-prone duration in the country where inadequate water availability limits the productivity of plants (Bhuiyan 2004). In stressed soil moisture conditions, the river basins in the peninsular as well as the north-western regions are highly vulnerable. The high risk in Luni, Mahi and Pennar river basins is due to the fact that these are one of the most drought-prone basins of the country (Gosain et al. 2006; Prabhakar and Shaw 2008). The threat to productivity in these regions directs towards the risks to vegetation growth and activity. The nonmonsoon season also comprises of months in which temperature is at its lowest value which makes the season most unfavourable for ecosystems in high-altitude zones. Kusre and Lalringliana (2014) have shown that winter droughts in the Himalayan region of India are a major cause of concern calling for urgent management measures in the region. It is observed that lowering the temperature has the least impact on the NPP and NDVI in other areas. This result asserts that NPP and NDVI have the least coherence with temperature in India (Nayak et al. 2013). The rate of biomass yield is a product of the growth duration and mass accumulation which is primarily influenced by the amount of sunlight intercepted by plants over an optimum range of temperature (Ritchie and Nesmith 1991). It is well known from very early studies that low light conditions may severely affect primary productivity (Davey 1989; Davison 1991). Therefore, extreme or high risks in these regions during lower temperature are reasonable. The effect of highly stressed precipitation is less severe as compared to stressed soil moisture content. Research shows that the Godavari river basin experience very high rainfall and temperature variability; hence, it is susceptible due to changing climatic conditions (Jhajharia et al. 2014; Das and Umamahesh 2015). The tendency of soil moisture being more dominant factor than precipitation in causing extreme damage to the ecosystem productivity is observed in 18 out of 24 river

basins. This indicates that most of the river basins in India lack the mechanism to hold incident precipitation.

5.5 Conclusions

The study facilitates the understanding of the impacts of extreme climatic conditions on terrestrial ecosystem functioning across India. The analysis is performed to identify the sensitive regions and time during the year in which the maximum threat to ecosystem functioning may occur. The study on river basins and land cover scales provides in-depth identification and characterisation of the risk factors and delivers crucial inputs for terrestrial ecosystem management and sustainable policymaking. The study puts forward all-India assessment of the regional impact of global climate change over ecosystem functioning across different river basins and land cover types. It can be concluded that there is a significant threat to the terrestrial ecosystem functioning due to extreme climatic conditions, especially in the western and southernmost parts. Large areas in most of the river basins are susceptible to high chances of risk due to possible deficit in required soil moisture levels. The investigation also covers the seasonal aspects of the vegetation response and finds that monsoon season is relatively more favourable for terrestrial ecosystem growth and productivity. Despite the relatively limited availability of data, the proposed approach performs reasonably well.

Chapter 6

Risk and resilience to climate extremes: inferences from the analysis

6.1 Introduction

Changing climate extremes have attracted much attention in the research community as the extreme behaviour of climate is more significant to the human well being than their average values. Recent years have witnessed several extreme weather events causing large scale loss of life and property. For instance, the economic loss due to extreme weather such as extreme cold, heat and hurricanes in the United States in 2018 was estimated at \$155 billion (Fritz 2018). Further, Japan's summer heatwaves in 2018 resulted in the hospitalisation of 22,000 people due to heat strokes (Mania et al. 2018). California, Greece and Australia experienced some of the most devastating wildfires of their histories in the same year (Levin and Tirpak 2018). It is noteworthy that over 40 million people were affected by widespread flooding in the Indian subcontinent during 2017 (UN 2017). Similar events were recorded in 2015, 2016 and 2018 and 2019 in many states of India, resulting in substantial loss of human lives and property (Doshi 2016; Dash and Punia 2019; Rai 2019; Sudheer et al. 2019). Moreover, there have been 22 major drought events in India from 1871 to 2002, and five of them were severe (Samra 2004). A prolonged drought event poses a significant implication to the country's water and food security. Further, the Intergovernmental Panel on Climate Change (IPCC) Special Report on climate extremes stressed that continued warming of Earth would lead to further variability in the spatial and temporal pattern of extremes (Field et al. 2012).

In the context of India, climate change, the persistent extreme weather events namely, droughts, floods, heatwaves have a significant role in shaping the natural ecosystems and impose challenges to the human society

(Easterling et al. 2000; Trenberth et al. 2014; Mann et al. 2017; Sisco et al. 2017). In the present scenario, the climate change is imposing huge challenges to food security and water resources of 1.2 billion population in India and the expected waiting time of the extreme events has been reduced significantly in the recent decades (Goyal and Surampalli 2018). The adverse consequences of extremes events may alter the spatio-temporal characteristics (e.g., frequency, intensity, and duration) and the water availability (Li et al. 2015a; Singh et al. 2018) causing threats to an agrarian country like India (Chattopadhyay 2010). In this view, it is of paramount importance to investigate the risk and resilience in the context of extreme weather events for suitable adaptation strategies and disaster mitigation policies.

Multifaceted effort should be conducted to understand the occurrence of extreme events and to figure out the implications for risk and resilience. However, understanding the mechanism of changes in extremes and their impacts due to the complex interdependence of various climate components essentially requires the utilisation of more advanced and inclusive framework. Previous studies primarily focused their attention on the long-term temporal trends of extremes and climate change; however, the nonstationarity in extremes related to climate change and associated uncertainty has not been extensively addressed (Vittal et al. 2013). Moreover, Coles et al. (2003) reiterated that the classical approaches do not include the model uncertainty comprehensively and is limited to produce an overly optimistic assessment of climate extreme. Further, the vulnerability and exposure to extreme climatic events are a function of factors such as social status, infrastructure in the region and economic capacity. These factors, in combination with the highly complex occurrence and distribution of extreme events, call for an integrated approach which would provide an estimation of risk and resilience

The studies shown in Chapter 3, 4 and 5 demonstrate the nonlinear evolution of climate and different aspects of its extreme behaviour. This chapter

presents a study investigating the risk and resilience to extreme climatic conditions. The results of this chapter have the conceptual foundation based on studies carried out in Chapter 4 and 5. Here, the risk due to extreme precipitation (based on Chapter 4) and resilience of terrestrial ecosystems to extreme climatic conditions (based on Chapter 5) have been discussed.

6.2 Data and Methodology

6.2.2 Methodology for extreme rainfall risk estimation

Using the steps discussed in the Chapter 4, the nonstationary and stationary return levels of the extreme rainfall indices are calculated. For calculating the risk, the 100-year return levels of Rx1 day and CWD are computed using the mean posterior parameters obtained during the Bayesian operation. The nonstationary return levels computed using the mean posterior parameters and the stationary return levels using MLE parameters are compared to observe the influence of selected oscillations (NAO, ENSO and IOD) on the extreme precipitation. The IMD's classification of rainfall intensity describes a one-day rainfall equal to or greater than 244.5 mm as an extremely heavy rain event (Guhathakurta et al. 2011). In this study, the return level of Rx1 day greater than 244.5 mm is considered as hazardous. Similarly, CWD duration of 20.2 days is a threshold for an extremely long wet spell, as suggested by Singh and Ranade (2010). The chance of hazardous Rx1 day and CWD return level in a district is computed as the percentage of grid points receiving rainfall return levels above these thresholds. This computation is performed for both the stationary and nonstationary processes at the district level. Once the degree of hazard, i.e., the percentage of each district's exhibiting return levels greater than the threshold values is estimated, two other elements of risks - exposure and vulnerability, are computed.

The measure of exposure is considered as the percentage of district area with population densities of children or the elderly greater than the national average. The national average of 109 for children population and 33 for old

population density (per square kilometre) is considered based on Census 2011 data. The percentage area of a district that shows the child and elderly population to be greater than 109 and 33, respectively, is estimated.

For the vulnerability part, the night-time lights and road availability indicators as two major infrastructure parameters are selected. The percentage of grid points with significant economic activity as represented by NASA's Visible Infrared Imaging Radiometer Suite (VIIRS) Day/Night Bands (DNB) data is calculated. This dataset delivers the estimates of surface upward radiance from the artificial nighttime light sources. Zhao et al., (2018b) in the study of the applicability of VIIRS/DNB data set in disaster risk assessment suggested that night time light data sets are useful in estimating the social-economic status. Stokes and Seto, (2019) utilized the data in understanding the urban infrastructural transitions in Asia, Latin America and Sub-Saharan Africa. In this study, we use the VIIRS/DNB radiances at 3 km resolution as a proxy to economic activities, urban land pattern, human activities and infrastructure at a very fine resolution. We filter the data based on the recommendation of Elvidge et al., (2017) so that only artificial lights from human settlement and electric lightings are considered.

The quality and location of transportation systems, particularly road network, plays a vital role in amplifying or reducing the risk of an extreme climatic event Cutter et al., (2000). The productivity of post hazard measures, especially during the response and mitigation processes depends upon the quality and density of transportation systems. Roads are one of the crucial elements that can be representative of the physical infrastructure indicator (Adger et al. 2005) In this study, we use the Global Roads Inventory Project-Version 4 (GRIP v4) data, which is a harmonized global dataset of about 222 countries comprising 21 million Km of roads (Meijer et al. 2018). Meijer et al., (2018) suggest that the error in spatial positional accuracy is a maximum of 500 metres based on the validations based on

VMAP data, digital and paper atlases, official topographic maps and remote sensing images from Google Maps, ESRI base maps and other available sources(2018). The suitability of these data can be surmised from a substantial body of literature (Kleinschroth et al. 2019; Koks et al. 2019; Schipper et al. 2019; Sloan et al. 2019; Stewart et al. 2019).

The overall methodology has been shown in Figure 6.1. Based on the hazard, exposure and vulnerability measures, the risk of extreme rainfall hazard based on the recommendations of IPCC (*i.e. Risk = Hazard × Exposure × Vulnerability*) is calculated for each district separately to assess the risk due to heavy downpour as well as extremely long rainfall duration (Oppenheimer et al. 2015). Mathematically,

$$Risk_D = P_{DTR} \times (P_{DCN} + P_{DON}) \times \frac{1}{(P_{DRA} + P_{DEA})} \quad (6.1)$$

Here,

$Risk_D$: District-wise Risk index value.

P_{DTR} : The hazard measure i.e., percentage of district pixels where Rx1 day or CWD is above threshold return levels of 244.5 mm and 20.2 days respectively.

P_{DCN} : The exposure measure i.e., percentage of district pixels where children population density is above the national average of 109.

P_{DON} : The exposure measure i.e., percentage of district pixels where the elderly population density is above the national average of 33.

P_{DRA} : The vulnerability measure i.e., percentage of district pixels on which road density is detected.

P_{DEA} : The vulnerability measure, i.e., the percentage of district pixels where economic activity/infrastructure is detected.

6.2.3 Methodology for terrestrial ecosystem resilience estimation

The basic idea behind estimating the resilience is to understand the ability of an ecosystem to absorb alterations in its state and recover from it (Holling

1973). In the context of this study, resilience has been viewed as the strength of terrestrial ecosystems of the country to return to an equilibrium position after a hydroclimatic disturbance. As discussed, droughts severely alter the hydrological equations and leading to alterations in water balance equations. The water balance equation between land and atmosphere govern

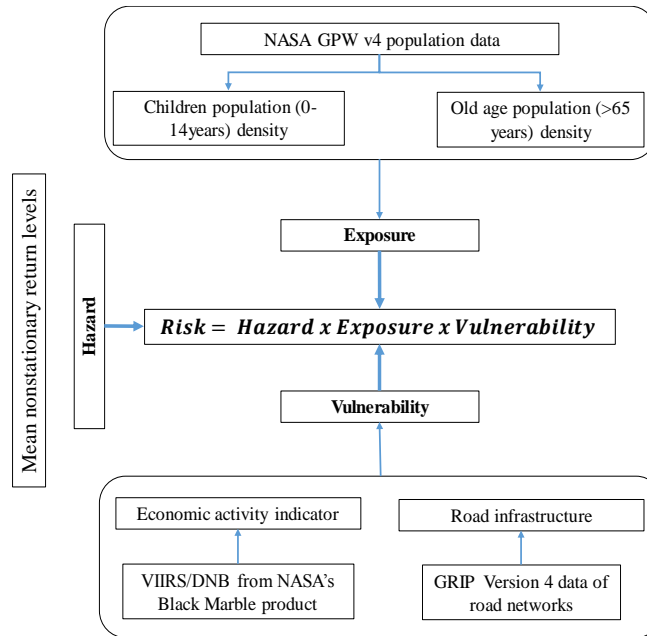


Figure 6.1 Overall methodology for estimating the risk due to extreme precipitation

the variation of forest biomass (Stegen et al. 2011). In Chapter 5, the impact of extreme climatic conditions on terrestrial ecosystem functioning has been discussed. Here, the resilience of terrestrial ecosystem functioning has been estimated by assessing the response of NDVI to dry conditions. The analysis is performed at both the river basin scale and the land cover type scale. The details about nomenclature and basin boundaries have been given in Chapter 5. The conclusions derived from Chapter 5 suggest that possible soil moisture deficit could lead to severe damage to the terrestrial ecosystem functioning. This possible condition has been identified as a drought event. One of the most widely used tools for identifying and monitoring droughts

all over the world has been Standardised Precipitation Index (SPI) which incorporates the information about drought history at a particular point (Radzka 2015). To estimate the impact of droughts on vegetation ecosystems from resilience point of view, the driest year during the period of 1982-2010 based on long term climate data is detected by deriving the SPI (Mckee et al. 1993; Vicente-Serrano et al. 2010). It has been assumed that a resilient ecosystem will recover quickly against a dry condition and maintain its vegetation vigour. The vegetation distribution at a particular point, which showed relatively undisturbed NDVI value in the driest year ($NDVI_d$) is considered as resilient. Most of the resilience studies suggest that for a fully resilient ecosystem the ratio of disturbed to a given baseline state approaches to 1, indicating complete recovery (Ingrisch and Bahn 2018). Here, an index, R_i is defined to measure resilience as a ratio of NDVI in the driest year to its temporal mean ($NDVI_m$) value calculated over the period of 1982-2010 as give by

$$R_i = \frac{NDVI_d}{NDVI_m} \quad (6.2)$$

6.3 Results

6.3.1 Risk due to heavy downpour and extremely long wet spells

The nonstationary return levels computed using the mean posterior parameters and the stationary return levels using MLE parameters are compared to observe the influence of selected oscillations on extreme precipitation. This computation is performed for both the stationary and nonstationary processes. Under the nonstationary condition, it is found that 456 (~72%) and 571 (~90%) out of 637 districts have more than 50% of their grid points witnessing rainfall return levels above the previously mentioned hazardous thresholds of Rx1 day and CWD respectively. However, under the stationary condition, rainfall in only 312 (~49%) and 524 (~82%) districts are detected which are experiencing such return levels. This points out the incapability of stationary GEV models to capture the

influence of oscillations in the return levels. Earlier, the results of LR test (see methods of Chapter 4) suggest that NS-GEV models are best-fit in 711 (~68%) and 764 (~74%) out of 1038 grids for Rx1 day and CWD respectively. The nonstationarity in GEV distribution is introduced by using 56 different linear combinations of physical covariates which are ENSO, IOD and NAO (See Table 4.1 in Chapter 4). It can be inferred from Figure 6.2 that ENSO is the most dominating covariate governing the location parameter in more than 400 (~38%) grid points for both the indices. However, the scale parameter is most significantly represented by the linear combination of all three covariates. It should be noted that first 7 out of the

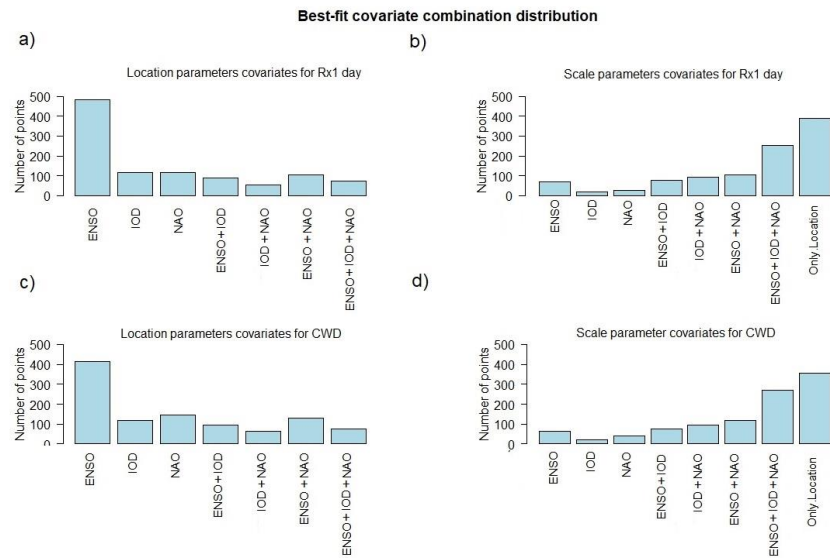


Figure 6.2 Distribution of optimal covariate combination for location and scale parameters of NS-GEV models for (a,b) Rx1 day and (c,d) CWD indices. The x-axis labels represent the linear combination of individual, double and all three covariates

56 models represent the variation in the location parameter only. Figure 6.2 b,d shows the variation in the scale parameter. It can be concluded that the variability of extreme climate, i.e., scale parameter of both Rx1day and CWD is majorly governed by the combined action of ENSO, NAO and IOD

phenomenon. After the assessment of the existing nonstationarity and obtaining the best covariate combination, the GEV distribution parameters for both nonstationary and stationary models are obtained using the maximum likelihood approach. Using these parameters as the initial setting for Bayesian analysis and employing the Markov Chain Monte Carlo (MCMC) algorithm sampler, the posterior parameter distribution is obtained for each grid point. The district-wise values of parameters are computed by extracting and averaging the mean posterior parameter distributions. Once the best combination and parameters are obtained, the return levels are estimated for hazard measure. Combining the hazard, exposure and vulnerability estimates, the risk is finally calculated. The index ($Risk_D$) estimated using Equation 6.1 is divided into five different classes of safe (0-0.25), low (0.25-0.50), moderate (0.50-0.75), high (0.75-1) and extreme (>1) risks. Figure 6.3 represents the distribution of districts

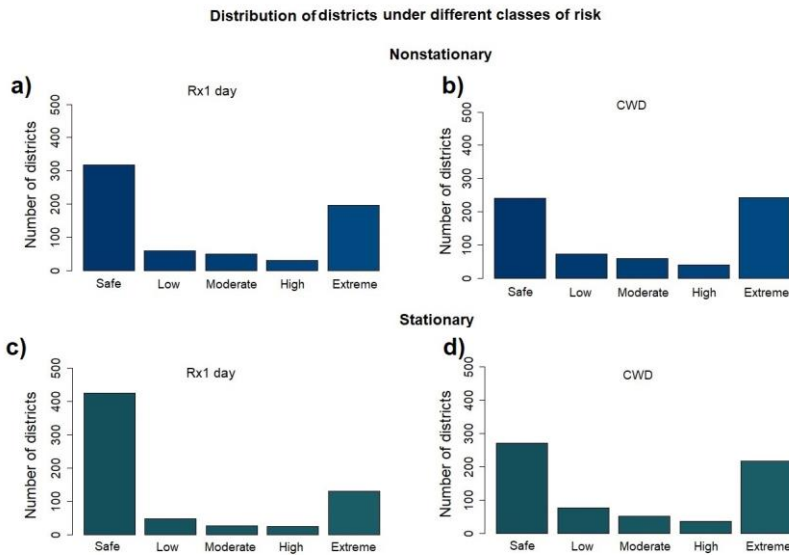


Figure 6.3 Distribution of districts under different classes of risk due under (a,b) nonstationary and (a,b) stationary scenarios

under different classes of risk in stationary and nonstationary conditions. 198 (~31%) out of 637 districts are identified to be experiencing extreme risks of severe one-day rainfall when nonstationarity is considered whereas,

only 132 (~21%) of the districts is extremely risked under the assumption of stationary. Similarly, extreme risk of long consecutive wet days is evident only in 219 (~34%) districts under stationarity, whereas, 244 (~39%) districts are identified as extreme using nonstationary models. Moreover, Figure 6.4 depicts the spatial distribution of risk classes for both Rx1 day and CWD.

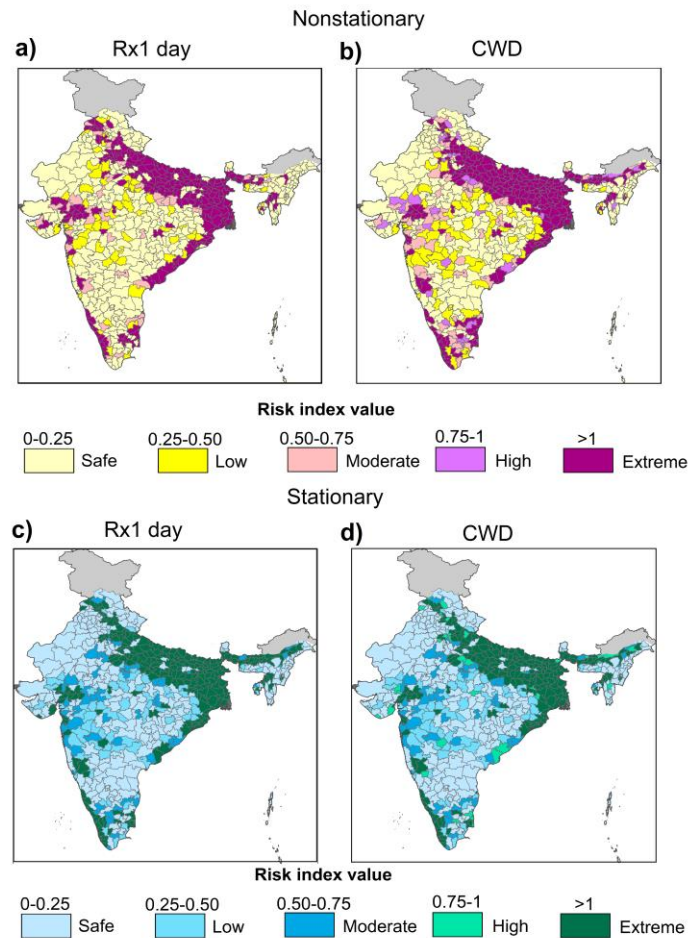


Figure 6.4 District-wise distribution of risk in (a,b) nonstationary and (c,d) stationary scenarios of extreme downpour (Rx1 day) and extremely long wet days (CWD)

The results are related to states considered in the study, and it is found that at least fifty percent districts in 8 out of 29 states are at high risk (Figure 6.5).

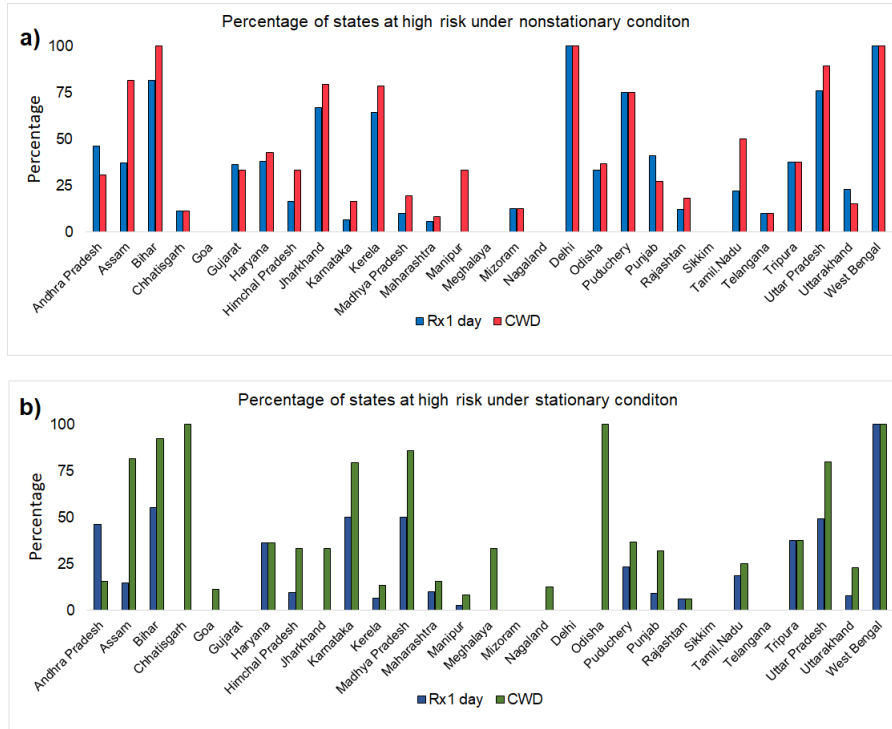


Figure 6.5 Percentage of districts in different states at high risk due to heavy downpour and extremely long wet spells

6.3.2 Resilience of terrestrial ecosystems to dry conditions

Figure 6.6 represents the resilience values obtained by Equation 6.2 across India. The maximum and minimum value of R_i are 1.41 and 0.29 respectively. River basins in the arid zones of India such as Mahi, Sabarmati, Luni and EFRKPB are detected to be severely non-resilient (Figure 6.7a). Not only the arid zones, the river basins which are known to be the lifelines of Indian agricultural systems are also found to be highly vulnerable in dry conditions. Area-wise, Ganga and Indus river basins are observed to be most non-resilient ones. Both of these river basins have a significant fraction of land under agricultural use, and a large population is dependent on them. The results clearly indicate that crop production in these

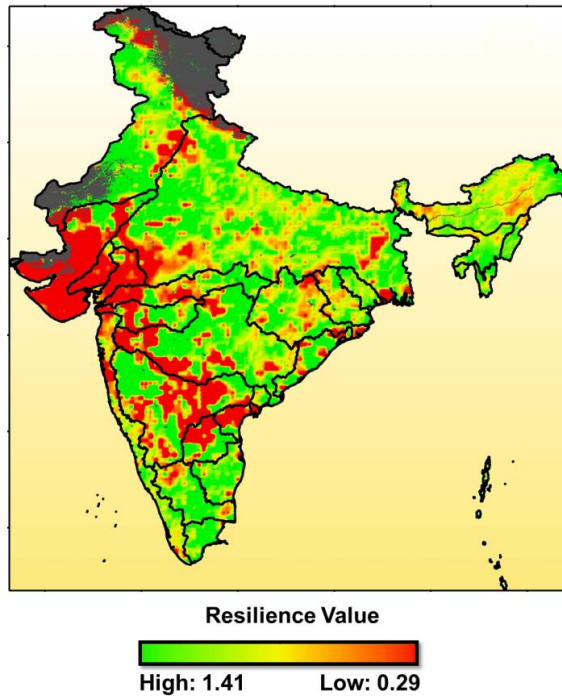


Figure 6.6 Spatial distribution of resilience (R_i) values

river basins may not be able to sustain the extreme conditions. Large river basins of southern India also face similar risks. Krishna and Godavari are the found to be two of the most fragile river basins in the southern part of the country. Both the river basins are highly stressed in terms of water availability, and non-resilient vegetation distribution increases the chances of high risk to the terrestrial ecosystems. Investigation of the resilience on different vegetation scale indicates that more than half of all vegetation types are non-resilient to vegetation droughts. India has the highest net Cropland area in the whole world, which makes up more than 50% of the country (Figure 6.7). The huge extent of non-resilient Cropland aggravates the challenges to Indian agriculture. Furthermore, about 74% of MF (Mixed forests) and 72% of SAV (Savanna) type vegetation cover is non-resilient. Mixed forest ecosystems which comprise of both coniferous and deciduous forest types are also observed to be highly insecure against drought

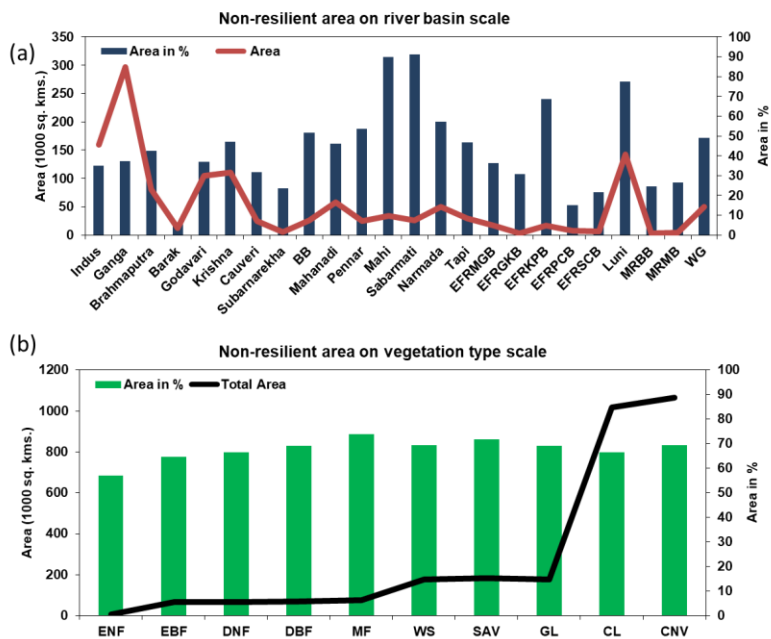


Figure 6.7 Non-resilient area at (a) river basins and (b) vegetation types scales

conditions. These forests are found in regions with a distinctly cool and warm season which sums up to a relatively moderate annual temperature. In India, these are majorly distributed in the Himalayan range along with other forest types, and it is alarming to see that even forest covers of these ecologically favourable zones are not safe from dry conditions. Deciduous forests are the most widespread forests of India and are heavily dependent on monsoons. The distribution of these forests is based on dry and moist conditions. It is found that a possible dry condition is capable of altering more than 65% of deciduous vegetation of the country. It is surprising that irrespective of its type, more than half of every vegetation cover is non-resilient. Hence, a possible vegetation drought scenario is expected to impact all vegetation types, which is a clear indicator of the threatened status of Indian vegetation ecosystem. The evergreen forests, which are found in high precipitation zones in the country such as north-east and west-coast, are expected to be least affected by such disturbances. Unlike the

deciduous forests, they do not shed their leaves all together during any part of a year. But, it was observed that both Evergreen Needleleaf and Evergreen Broadleaf Forests are unable to recover from the driest conditions and 50-60% of the total area of these forests show non-resilient behaviour in their respective driest years. The non-resilience of such forest ecosystems means that even the greenest forest cover in the country is not stable against drought disturbances.

6.4 Discussions

This chapter illustrates one example each of the risk and resilience estimation based on studies shown in previous chapters. In Chapter 3, the importance of incorporating nonstationarity and uncertainty has been discussed. The risk due to extreme precipitation is calculated. It is well known that the risk is not only determined by the characteristic of a hazard but also by the exposure and vulnerability components. Therefore, the degree of hazard caused by extreme precipitation is combined with the exposure and vulnerability components to get the measure of district-wise risk. Significant research in the past has shown that considering multivariate dimensions such as social, economic, infrastructural aspects can improve our strategies to minimise climate risk (Cardona et al. 2012; Field et al. 2012). The northern plains, which is one of the highly-dense regions of the country, is found to be most exposed because of the high density of children and the elderly population. The states of Bihar, Uttar Pradesh and West Bengal, which are most significantly exposed are also one of the most impoverished states of India (India 2016). These regions in the past have experienced several climatic disasters and have been found to be vulnerable to extreme climatic conditions. The vulnerability of an area which is exposed to some hazard can be reduced if the capacity to manage the disaster is present. In this sense, the infrastructure and economy of a region play a crucial role in determining the adaptive capacity. The availability of infrastructure is least in the north-east region as well as the north-west

region. It should be noted that districts in these regions are also one of the least populated and least developed. The risk estimates from the nonstationary models indicate that more than one-third of India's districts are experiencing either high or extreme risk from possible heavy rainfall downpour. Similarly, about 44% of the districts are at either high or extreme risk of the possible occurrence of extremely long consecutive wet spells. In general, the extreme risk is most significantly observed in the relatively poorer districts where the population density is high and economic activity indicator or infrastructure indicator is low. Further, the majority of districts in the east-coast reveal extreme risk of high chances of rainfall hazard, poor economic state and high exposure in terms of population. The north-east region, which receives the highest amount of rainfall in the world is not entirely at high risk despite being backwards in terms of economy and infrastructure. The results are related to states considered in the study, and it is found that at least fifty percent districts in 8 out of 29 states are at high risk. All districts of West Bengal depicted high risk of heavy downpour as well as extremely long spells under both stationary and nonstationary conditions.

Further, resilience is estimated in terms of the ability of terrestrial ecosystems to maintain their NDVI (vegetation vigour) in the driest year as compared to the mean NDVI during the time period 1982-2010. This study shows that none of the river basins is resilient to vegetation droughts and at least one-third area of 18 out of 24 river basins is fragile against such disturbances. Moreover, at least three-fourth areas of river basins situated in the arid zones in the country such as Mahi, Luni, and Sabarmati are found to be non-resilient. More importantly, some of the river basins which receive a high amount of rainfall are also found to be poorly capable of maintaining their productivity as more than 40% area of Barak and western ghats are non-resilient. These river basins already have scarce vegetation distribution and are highly prone to vegetation droughts. The non-resilience of such river basins essentially points towards their inability to achieve the

essential moisture condition for vegetation regrowth after a dry period. Barak river basin, which lies in India's one of the most ecologically rich regions is most efficient in supporting its vegetation cover in a dry year. Further, the ecosystem resilience based on the land cover scale is also checked to understand the capability of different vegetation types to recover from a drought condition. Area-wise, Evergreen Needleleaf and Evergreen Broadleaf Forests are the most resilient vegetation types. However, the analysis showed that more than half of every single vegetation type in the country is incapable of fighting dry conditions.

6.5 Conclusions

Studies demonstrated in the previous chapters deal with understanding the evolution of climate, the role of large scale oscillations in causing uncertainty in the extreme precipitation return levels, the joint dependence of climate extremes and the terrestrial ecosystem functioning. However, this study demonstrates the risk and resilience analysis to conclude the last objective of the overall research goal through two studies. This study enables the understanding of the influence of low-frequency global scale modes on the risk of extreme rainfall at the smallest administrative division level. The results reveal that these factors have a strong association with the extreme rainfall, and due to this connection, significant variability in return level exists. The characterisation of district-wise risks on the basis of return levels combined with exposure and vulnerability data are intended to aid the decision-makers in deciding effective disaster risk reduction plans and policies. Further, the resilience analysis, which is performed to understand the ability of terrestrial ecosystems of India in recovering from a dry condition shows that extreme climate conditions might have serious implications. The non-resilient state of Cropland raises a serious question to India's food security. The analysis points out that even if there is ample rainfall in a region, there might not be adequate soil moisture to ensure smooth terrestrial ecosystem functioning.

Chapter 7

Conclusions and scope for future work

7.1 Summary

The present study has been performed to deliver a comprehensive assessment of extreme climatic conditions over India and their implications for risk and resilience. Indian climate is extremely diverse and influenced by a large number of factors. The underlying nonlinearity in climate profiles is one of the major factors which contribute to poor predictability in the extreme climate zones. The complexity of climate systems, intricate ecosystem-climatic interactions, inter-dependence of the climate extremes and prevailing nonstationarity make the risk and resilience assessment a challenging task. Besides, the risk due to extreme climatic events does not only depend on the magnitude of extreme hazards but also different components of risk, such as exposure and vulnerability. The risk reduction and adaptation to climate change are significantly dependent upon the accurate estimation of these hazardous events and their interaction with exposure and vulnerability parameters. The following paragraphs give a summary and conclusions of the study presented in the thesis.

The climate over a region is governed by many factors. The underlying nonlinearity and complexity in climatic components limit the accuracy of climate predictions. The presence of strong determinism in a time series is an indication that a finite set of equations drive the process and a set of fixed laws explains its dynamic evolution from one state to another. The predictability of the Indian climate during the past century (1901-2002) is analysed using the DVV method. The results show that both precipitation and temperature exhibit a high degree of nonlinearity, multi-scaling, non-stationary and anti-persistent fractional Brownian motion (fBm) behaviour with short-range dependence (SRD) characteristics. Out of 566 selected districts, precipitation time series in 449 (80%), 458 (81%), and 472 (84%)

districts are found to be in the category of significant to extremely nonlinear during 1901-1934, 1935-1968, and 1969-2002, respectively. Whereas, the temperature profiles of 341 (60%), 223 (40%) and 279 (50%) districts are categorised into significant to extremely nonlinear during the same periods. The outcomes from the investigation suggested that the predictability of both temperature and precipitation has decreased over the period. Moreover, the decrease in the determinism is accompanied by increasing nonlinearity in most of the districts. This study allows the understanding of the nonlinear dynamics of the Indian climate and provides crucial inputs for examining the changes in spatial and temporal predictability in the country.

The low-frequency global-scale modes are widely considered as the significant drivers of inter-annual variability of the Indian rainfall pattern and extreme rainfall events. The qualitative and quantifiable assessment of the association between the climatic oscillations and heavy rainfall, in particular, could deliver an essential understanding of flood hazard prevention, mitigation and enhance the flood management strategy. The influence of ENSO, IOD and NAO on extreme precipitation during 1951-2013 over 24 major river basins of India using the non-stationary extreme value analysis is investigated. In addition, the uncertainty in the parameters of the fitted non-stationary extreme value distribution is assessed using Bayesian inference. It is found that extreme precipitation events in the country are dominated by these oscillations, especially in central India. Moreover, the return levels of high rainfall are found to be intensifying with increasing return period. In this study, it is observed that variability in return levels is high not only in the regions where rainfall is abundant but also in the drought-prone areas. It is likely that these regions may experience short spells of heavy downpours in the form of high-intensity rainfall. This may lead to the simultaneous occurrence of flash floods and droughts in these areas. The results presented here contribute to a better understanding of the large-scale climate variability and its impact on high rainfall pattern, which

would provide essential inputs for deciding rainfall-induced hazard prevention measures.

The above paragraphs represent the outputs of the investigations based on univariate analysis of climate data. As discussed in Chapter 5, the dependence of extreme climate with terrestrial ecosystems might not be suitably determined using the existing univariate approaches. Currently, modelling the response of the ecosystem to climate change is mostly based on assessing the impact of climatic trends such as changes in precipitating, temperature warming and increase in Carbon concentration or other parameters. Further, ecosystem-climatic interaction is complex; therefore, modelling the possible influence of extreme climate on ecosystem productivity from joint likelihood point of view is more suitable. In view of this, a study integrating climate data (precipitation, temperature and soil moisture content) and remote sensing observations (NDVI/NPP) using bivariate Copula-based approach is performed to quantify the impact of extreme climatic conditions over terrestrial ecosystem functioning. It is observed that at least half the area of 16 out of 24 major river basins is facing high risk due to possible lowered soil moisture levels. It can be concluded that there is a significant threat to the terrestrial ecosystem functioning due to extreme climatic conditions, especially in the western and southernmost parts. Large areas of most river basins are susceptible to high chances of risk due to soil moisture levels in the nonmonsoon season. The outputs of the analysis serve to the mapping of climatic factors influencing the ecosystem functioning at a multi-spatial and temporal scale.

The last chapter of the thesis presents an investigation involving the quantification of the risk due to extreme precipitation (based on Chapter 4) and resilience of terrestrial ecosystems to extreme climatic conditions (based on Chapter 5). The nonstationary extreme value theory, along with Bayesian uncertainty analysis, is employed to investigate the influence of ENSO, IOD and NAO in augmenting high rainfall risks in all districts across

29 states of India. The location and scale parameters of the Generalised Extreme Value (GEV) distribution are modelled through linear functions of the large-scale oscillations. The risks from high rainfall and extremely long wet spells are calculated by incorporating the socio-economic characteristics of districts such as population density of children and the elderly, economic activity and infrastructure. It is found that at least 50% of the districts in 8 out of 29 states are at high risk. Extreme risk is observed in 198 (~31%) and 249 (~39%) districts caused by heavy downpour and extremely long wet spells respectively. Moreover, it is also observed that the risk is underestimated using conventional stationary models. The resilience of terrestrial ecosystems to a dry condition is also investigated. The examination suggests that at least one-third area of 18 river basins is non-resilient to dry conditions. Moreover, more than fifty percent of each vegetation type is non-resilient, which points out the fragility of the country's terrestrial ecosystems. These findings provide useful insights for the policymakers to develop effective strategies for effective extreme climate risk mitigation and management strategies.

7.2 Future scope of work

As discussed earlier, the present research is devoted to understanding climate extremes and their implications for risk and resilience. However, there are many challenges that still exist in the field of climate extremes risk and resilience assessment. Hence, the following would be possible future works.

- The study provides the quantification of the degree of predictability in the Indian climate. Detection and attribution study to investigate the causes of lower predictability could be performed, which would be crucial in understanding the underlying mechanism behind the existing nonlinearity.
- The nonstationary analysis of rainfall extremes is done to identify the influence of global climatic oscillations. The study can be extended to different extremes incorporating the investigation of the role of the global as well as local factors.

- The extreme value analysis on rainfall extremes is performed by considering continuous GEV distributions. A more comprehensive analysis may be carried out using discrete distributions and then combining them with exposure and vulnerability parameters to estimate the risk.
- The dependence structure of climate variables and terrestrial ecosystem functioning is estimated using bivariate Copula models. Instead of using bivariate, other multivariate Copulas may be utilised in future studies to model the joint dependence of more than two variables.
- The risk due to extreme precipitation is investigated by combining the hazard measures with the population's exposure and vulnerability. The study can be extended to analyse the risk by integrating more socio-economic, perception-based and behavioural indicators.

REFERENCES

- Adger, W. N., Brooks, N., Bentham, G., Agnew, M., & Eriksen, S. (2005). *New indicators of vulnerability and adaptive capacity*. Norwich: Tyndall Centre for Climate Change Research.
- AghaKouchak A, Cheng L, Mazdiyasni O, Farahmand A (2014) Global warming and changes in risk of concurrent climate extremes: Insights from the 2014 California drought. *Geophys Res Lett* 41:8847–8852
- AghaKouchak A, Chiang F, Huning LS, et al (2020) Climate Extremes and Compound Hazards in a Warming World. *Annu Rev Earth Planet Sci* 48: 529-548
- Ali H, Modi P, Mishra V (2019) Increased flood risk in Indian sub-continent under the warming climate. *Weather Clim Extrem* 25:100212
- Allen CD, Macalady AK, Chenchouni H, et al (2010) A global overview of drought and heat-induced tree mortality reveals emerging climate change risks for forests. *For Ecol Manage* 259:660–684
- Arora M, Goel NK, Singh P (2005) Evaluation of temperature trends over India/Evaluation de tendances de température en Inde. *Hydrol Sci J* 50:81-93
- Ashok K, Guan Z, Saji NH, Yamagata T (2004) Individual and combined influences of ENSO and the Indian Ocean dipole on the Indian summer monsoon. *J Clim* 17:3141–3155
- Ashrit RG, Kumar KR, Kumar KK (2001) ENSO-monsoon relationships in a greenhouse warming scenario. *Geophys Res Lett* 28:1727–1730
- Azad S, Rajeevan M (2016) Possible shift in the ENSO-Indian monsoon rainfall relationship under future global warming. *Sci Rep* 6:20145
- Ban N, Rajczak J, Schmidli J, Schär C (2020) Analysis of Alpine precipitation extremes using generalized extreme value theory in convection-resolving climate simulations. *Clim Dyn* 55:61–75

- Bassingthwaite JB, Raymond GM (1994) Evaluating Rescaled Range Analysis for Time Series. *Ann Biomed Eng* 22:432–444
- Behera S, Brandt P, Reverdin G (2013) Ocean Circulation and Climate: The Tropical Ocean Circulation and Dynamics. Elsevier Inc. pp-385-393
- Ben Alaya MA, Zwiers F, Zhang X (2020) An Evaluation of Block-Maximum-Based Estimation of Very Long Return Period Precipitation Extremes with a Large Ensemble Climate Simulation. *J Clim* 33:6957–6970
- Benfield A (2017) 2016 Annual Global Climate and Catastrophe Report. <http://thoughtleadership.aonbenfield.com> Accessed March 2018, 2020
- Beniston M (2015) Ratios of record high to record low temperatures in Europe exhibit sharp increases since 2000 despite a slowdown in the rise of mean temperatures. *Clim Change* 129:225–237
- Bertilsson L, Wiklund K, de Moura Tebaldi I, et al (2019) Urban flood resilience—A multi-criteria index to integrate flood resilience into urban planning. *J Hydrol* 573:970–982
- Betts RA, Alfieri L, Bradshaw C, et al (2018) Changes in climate extremes, fresh water availability and vulnerability to food insecurity projected at 1.5 C and 2 C global warming with a higher-resolution global climate model. *Philos Trans R Soc A Math Phys Eng Sci* 376:20160452
- Bhuiyan C (2004) Various drought indices for monitoring drought condition in Aravalli terrain of India. In: Proceedings of the XXth ISPRS Congress, Istanbul, Turkey. pp 12–23
- Bhutiyani MR, Kale VS, Pawar NJ (2010) Climate change and the precipitation variations in the northwestern Himalaya: 1866–2006. *Int J Climatol A J R Meteorol Soc* 30:535–548
- Blumenthal MB (1991) Predictability of a Coupled Ocean–Atmosphere Model. *J Clim* 4:766–784

- Bracken C, Holman KD, Rajagopalan B, Moradkhani H (2018) A Bayesian Hierarchical Approach to Multivariate Nonstationary Hydrologic Frequency Analysis. *Water Resour Res* 54:243–255
- Bréda N, Granier A (1996) Intra-and interannual variations of transpiration, leaf area index and radial growth of a sessile oak stand (*Quercus petraea*). In: *Annales des sciences forestières*. EDP Sciences, pp 521–536
- Bronaugh, D. (2014). R package climdex. Pcic: PCIC implementation of climdex routines, Pacific Climate Impact Consortium, Victoria. British Columbia, Canada.
- Brown JF, Wardlow BD, Tadesse T, et al (2008) The Vegetation Drought Response Index (VegDRI): A new integrated approach for monitoring drought stress in vegetation. *GIScience Remote Sens* 45:16–46
- Broxton PD, Zeng X, Sulla-Menashe D, Troch PA (2014) A global land cover climatology using MODIS data. *J Appl Meteorol Climatol* 53:1593–1605
- Brunner I, Pannatier EG, Frey B, et al (2009) Morphological and physiological responses of Scots pine fine roots to water supply in a dry climatic region in Switzerland. *Tree Physiol* 29:541–550
- Cancelliere A (2017) Non stationary analysis of extreme events. *Water Resour Manag* 31:3097–3110
- Cao Q, Wang R, Zhang H, et al (2015) Distribution of organic carbon in the sediments of Xinxue River and the Xinxue River Constructed Wetland, China. *PLoS One* 10:1–12
- Cardona O-D, van Aalst MK, Birkmann J, et al (2012) "Determinants of risk: exposure and vulnerability." *Managing the Risks of Extreme Events and Disasters to Advance Climate Change Adaptation: Special Report of the Intergovernmental Panel on Climate Change*. Cambridge University Press, pp 65–108

- Cavan G, Kingston R (2012) Development of a climate change risk and vulnerability assessment tool for urban areas. *Int J Disaster Resil Built Environ* 3:253–269
- Chamoli A, Ram Bansal A, Dimri VP (2007) Wavelet and rescaled range approach for the Hurst coefficient for short and long time series. *Comput Geosci* 33:83–93
- Chandra R, Saha U, Mujumdar PP (2015) Model and parameter uncertainty in IDF relationships under climate change. *Adv Water Resour* 79:127–139
- Chattopadhyay N (2010) Climate Change and Food Security in India. In: *Climate Change and Food Security in South Asia*. Springer Netherlands, Dordrecht, pp 229–250
- Chen L, Chen X, Cheng L, et al (2019) Compound hot droughts over China: Identification, risk patterns and variations. *Atmos Res* 227:210–219
- Chen L, Singh VP, Guo S, et al (2012) Drought analysis using Copulas. *J Hydrol Eng* 18:797–808
- Chen YD, Zhang Q, Xiao M, et al (2016) Probabilistic forecasting of seasonal droughts in the Pearl River basin, China. *Stoch Environ Res Risk Assess* 30:2031–2040
- Cheng L, Aghakouchak A (2014) Nonstationary precipitation intensity-duration-frequency curves for infrastructure design in a changing climate. *Sci Rep* 4:1–6
- Cheng L, Aghakouchak A, Gilleland E, Katz RW (2014) Nonstationary extreme value analysis in a changing climate. *Clim Change* 127:353–369
- Chiou SC, Tsay RS (2008) A copula-based approach to option pricing and risk assessment. *J Data Sci* 6:273–301
- Chu C, Bartlett M, Wang Y, et al (2016) Does climate directly influence NPP globally? *Glob Chang Biol* 22:12–24

- Clark JS (2005) Why environmental scientists are becoming Bayesians. *Ecol Lett* 8:2–14
- Coles S (2001) *An Introduction to Statistical Modeling of Extreme Values*. Springer, London, pp 209-210
- Coles S, Pericchi LR, Sisson S (2003) A fully probabilistic approach to extreme rainfall modeling. *J Hydrol* 273:35–50
- Coles SG, Tawn JA (1996) A Bayesian Analysis of Extreme Rainfall Data. *Appl Stat* 45:463
- Cong R, Brady M (2012) The Interdependence between Rainfall and Temperature : Copula Analyses. *The Sci W J* 2012:1–11
- Cooley D (2013) Return Periods and Return Levels Under Climate Change. In: AghaKouchak A, Easterling D, Hsu K, et al. (eds) *Extremes in a Changing Climate: Detection, Analysis and Uncertainty*. Springer, Netherlands, pp 97–114
- Cooley D (2009) Extreme value analysis and the study of climate change. *Clim Change* 97:77–83
- Coumou D, Robinson A, Rahmstorf S (2013) Global increase in record-breaking monthly-mean temperatures. *Clim Change* 118:771–782
- Cutter SL, Mitchell JT, Scott MS (2000) Revealing the vulnerability of people and places: a case study of Georgetown County, South Carolina. *Ann Assoc Am Geogr* 90:713–737
- Dai A (2011) Drought under global warming: A review. *Wiley Interdiscip Rev Clim Chang* 2:45–65
- Dai A (2013) Increasing drought under global warming in observations and models. *Nat Clim Chang* 3:52–58
- Dai A, Bloecker CE (2019) Impacts of internal variability on temperature and precipitation trends in large ensemble simulations by two climate models. *Clim Dyn* 52:289–306
- Das J, Jha S, Goyal MK (2019) Non-stationary and Copula-Based Approach to Assess the Drought Characteristics Encompassing Climate Indices over the Himalayan States in India. *J Hydrol* 580:124356

- Das J, Umamahesh N V. (2017) Uncertainty and Nonstationarity in Streamflow Extremes under Climate Change Scenarios over a River Basin. *J Hydrol Eng* 22:04017042
- Das J, Umamahesh N V (2015) Multisite downscaling of monsoon precipitation over the Godavari River Basin under the RCP 4.5 Scenario. In: *World Environmental and Water Resources Congress 2015*. pp 1066–1075
- Dash P, Punia M (2019) Governance and disaster: Analysis of land use policy with reference to Uttarakhand flood 2013, India. *Int J Disaster Risk Reduct* 36:101090
- Davey MC (1989) The effects of freezing and desiccation on photosynthesis and survival of terrestrial Antarctic algae and cyanobacteria. *Polar Biol* 10:29–36
- Davison AC, Huser R (2015) Statistics of extremes. *Annu Rev Stat its Appl* 2:203–235
- Davison IR (1991) Environmental effects on algal photosynthesis: temperature. *J Phycol* 27:2–8
- De Keersmaecker W, Lhermitte S, Tits L, et al (2015) A model quantifying global vegetation resistance and resilience to short-term climate anomalies and their relationship with vegetation cover. *Glob Ecol Biogeogr* 24:539–548
- Di Matteo T, Aste T, Dacorogna MM (2003) Scaling behaviors in differently developed markets. *Phys A Stat Mech its Appl* 324:183–188
- Dittus AJ, Karoly DJ, Donat MG, et al (2018) Understanding the role of sea surface temperature-forcing for variability in global temperature and precipitation extremes. *Weather Clim Extrem* 21:1–9
- Donat MG, Alexander L V, Yang H, et al (2013) Global land-based datasets for monitoring climatic extremes. *Bull Am Meteorol Soc* 94:997–1006
- Doshi V (2016) Flooding in India affects 1.6m people and submerges national park. *Guardian*

<https://www.theguardian.com/world/2016/jul/27/> Accessed December 3 2019

- Dugam SS, Kakade SB (1999) Interactive mechanism between ENSO and NAO and its relationship with Indian summer monsoon variability. In: Proc. National Symposium on “Meteorology beyond 2000”, TROPMET. pp 53–58
- Easterling DR, Meehl G a, Parmesan C, et al (2000) Climate extremes: observations, modeling, and impacts. *Science* 289:2068–2074
- Eiser JR, Bostrom A, Burton I, et al (2012) Risk interpretation and action: A conceptual framework for responses to natural hazards. *Int J Disaster Risk Reduct* 1:5–16
- Eli A, Shaffie M, Zin WZW (2012) Preliminary Study on Bayesian Extreme Rainfall Analysis: A Case Study of Alor Setar, Kedah, Malaysia. *Sains Malaysiana* 41:1403–1410
- Elvidge CD, Baugh K, Zhizhin M, et al (2017) VIIRS night-time lights. *Int J Remote Sens* 38:5860–5879. <https://doi.org/10.1080/01431161.2017.1342050>
- Emura T, Chen Y-H (2018) Analysis of Survival Data with Dependent Censoring: Copula-based Approaches. Springer Singapore
- Endo N, Matsumoto J, Lwin T (2009) Trends in Precipitation Extremes over Southeast Asia. *Sola* 5:168–171
- Falloon P, Jones CD, Ades M, Paul K (2011) Direct soil moisture controls of future global soil carbon changes: An important source of uncertainty. *Global Biogeochem Cycles* 25: 1–14
- Fan Y, Van Den Dool H (2004) Climate Prediction Center global monthly soil moisture data set at 0.5° resolution for 1948 to present. *J Geophys Res D Atmos* 109:1–8
- Favre A-C, El Adlouni S, Perreault L, et al (2004) Multivariate hydrological frequency analysis using copulas. *Water Resour Res* 40:1–12

- Field CB, Barros V, Stocker TF, Dahe Q (2012) Managing the risks of extreme events and disasters to advance climate change adaptation: special report of the intergovernmental panel on climate change. Cambridge University Press
- Fischer EM, Knutti R (2016) Observed heavy precipitation increase confirms theory and early models. *Nat Clim Chang* 6:986–991
- Fischer EM, Sedláček J, Hawkins E, Knutti R (2014) Models agree on forced response pattern of precipitation and temperature extremes. *Geophys Res Lett* 41:8554–8562
- Franzke CLE, O’Kane TJ, Berner J, et al (2015) Stochastic climate theory and modeling. *Wiley Interdiscip Rev Clim Chang* 6:63–78
- Fritz A (2018) The cost of natural disasters this year: \$155 billion. *The Washington Post*
<https://www.washingtonpost.com/weather/2018/12/26> Assessed
 January 16 2019
- Gadgil A, Dhorde A (2005) Temperature trends in twentieth century at Pune, India. *Atmos Environ* 39:6550–6556
- Gadgil S, Vinayachandran PN, Francis PA, Gadgil S (2004) Extremes of the Indian summer monsoon rainfall, ENSO and equatorial Indian Ocean oscillation. *Geophys Res Lett* 31:2–5
- Galiatsatou P, Makris C, Prinos P, Kokkinos D (2018) Nonstationary joint probability analysis of extreme marine variables to assess design water levels at the shoreline in a changing climate. *Nat Hazards* 98:1051–1089
- Gang C, Zhang Y, Wang Z, et al (2017) Modeling the dynamics of distribution, extent, and NPP of global terrestrial ecosystems in response to future climate change. *Glob Planet Change* 148:153–165
- Ganguli P, Reddy MJ (2014) Evaluation of trends and multivariate frequency analysis of droughts in three meteorological subdivisions of western India. *Int J Climatol* 34:911–928

- Ganguli P, Reddy MJ (2013) Analysis of ENSO-based climate variability in modulating drought risks over western Rajasthan in India. *J earth Syst Sci* 122:253–269
- Gao M, Mo D, Wu X (2016) Nonstationary modeling of extreme precipitation in China. *Atmos Res* 182:1–9
- Gao T, Wang HJ, Zhou T (2017) Changes of extreme precipitation and nonlinear influence of climate variables over monsoon region in China. *Atmos Res* 197:379–389
- Gautama T, Mandic DP, Van Hulle MM (2004) A novel method for determining the nature of time series. *Ieee Trans Biomed Eng* 51:728–736
- Gautama T, Mandic DP, Van Hulle MM (2003) Indications of nonlinear structures in brain electrical activity. *Phys Rev E* 67:046204
- Gelman A (2008) Objections to Bayesian statistics. *Bayesian Anal* 3:445–449
- Gershunov A, Schneider N, Barnett T (2001) Low-Frequency Modulation of the ENSO–Indian Monsoon Rainfall Relationship: Signal or Noise? *J Clim* 14:2486–2492
- Ghosh S, Das D, Kao S-C, Ganguly AR (2012) Lack of uniform trends but increasing spatial variability in observed Indian rainfall extremes. *Nat Clim Chang* 2:86–91
- Gilleland E, Katz RW (2016) extRemes 2.0: An Extreme Value Analysis Package in R. *J Stat Softw* 72:1–39
- Gillman LN, Wright SD, Cusens J, et al (2015) Latitude, productivity and species richness. *Glob Ecol Biogeogr* 24:107–117
- Gobiet A, Kotlarski S, Beniston M, et al (2014) 21st century climate change in the European Alps-A review. *Sci Total Environ* 493:1138–1151
- Goldstein J, Mirza M, Etkin D, Milton J (2003) J2. 6 hydrologic assessment: Application of extreme value theory for climate extremes scenarios construction. In: 14th Symposium on Global Change and

Climate Variations, American Meteorological Society 83rd Annual Meeting Canada pp 1-5

- Gomez M, Concepción Ausín M, Carmen Domínguez M, Island G (2017) Seasonal copula models for the analysis of glacier discharge at King George Island, Antarctica. *Stoch Environ Res Risk Assess* 31:1107–112
- Gosain AK, Rao S, Basuray D (2006) Climate change impact assessment on hydrology of Indian river basins. *Curr Sci* 90:346–353
- Goswami BN, Venugopal V, Sangupta D, et al (2006) Increasing trend of extreme rain events over India in a warming environment. *Science* 314:1442–1445
- Goyal MK (2014) Statistical Analysis of Long Term Trends of Rainfall During 1901-2002 at Assam, India. *Water Resour Manag* 28:1501–1515
- Goyal MK, Surampalli RY (2018) Impact of Climate Change on Water Resources in India. *J Environ Eng* 144:04018054
- Grimm NB, Pairis A, Chapin FS, et al (2013) The impacts of climate change on ecosystem structure and function. *Front Ecol Environ* 11:474–48.
- GRIP (2018), Global Roads Inventory Project. In: ESRI. https://wwf-sightmaps.org/arcgis/rest/services/Global/Global_Roads_GRIP4/MapServer. Accessed 21 Dec 2019
- Gross MH, Donat MG, Alexander L V, Sisson SA (2018) The sensitivity of daily temperature variability and extremes to dataset choice. *J Clim* 31:1337–1359
- Gu F, Zhang Y, Huang M, et al (2017) Climate-driven uncertainties in modeling terrestrial ecosystem net primary productivity in China. *Agric For Meteorol* 246:123–132
- Guan Z, Ashok K, Yamagata T (2003) Summertime response of the tropical atmosphere to the Indian Ocean dipole sea surface temperature anomalies. *J Meteorol Soc Japan Ser II* 81:533–561

- Guhathakurta P, Rajeevan M (2008) Trends in the rainfall pattern over India. *Int J Climatol* 28:1453–1469
- Guhathakurta P, Sreejith OP, Menon PA (2011) Impact of climate change on extreme rainfall events and flood risk in India. *J Ear Sys Sci* 120:359–373
- Haddad K, Rahman A, Green J (2011) Design rainfall estimation in Australia: a case study using L moments and Generalized Least Squares Regression. *Stoch Environ Res Risk Assess* 25:815–825
- Hannaford J, Marsh T (2006) An assessment of trends in UK runoff and low flows using a network of undisturbed catchments. *Int J Climatol A J R Meteorol Soc* 26:1237–1253
- Harvey CA, Rakotobe ZL, Rao NS, et al (2014) Extreme vulnerability of smallholder farmers to agricultural risks and climate change in Madagascar. *Philos Trans R Soc B Biol Sci* 369:20130089
- Hasselmann K (1976) Stochastic climate models part I. Theory. *Tellus* 28:473–485
- Hastings WK (1970) Monte Carlo sampling methods using Markov chains and their applications. *Biometrika* 57:97–109
- Heidelberger P, Welch PD (1981) A spectral method for confidence interval generation and run length control in simulations. *Commun ACM* 24:233–245
- Heidelberger P, Welch PD (1983) Simulation run length control in the presence of an initial transient. *Oper Res* 31:1109–1144
- Hingane LS, Rupa Kumar K, Ramana Murty B V (1985) Long-term trends of surface air temperature in India. *J Climatol* 5:521–528
- Hinzman LD, Bettez ND, Bolton WR, et al (2005) Evidence and implications of recent climate change in northern Alaska and other arctic regions. *Clim Change* 72:251–298
- Hobaek H, Frigessi A, Maraun D (2015) How well do regional climate models simulate the spatial dependence of precipitation? An application of pair-copula constructions. *J Geophys Res Atmos* 120:2624–2646

- Hoeppe SS, Dukes JS (2012) Interactive responses of old-field plant growth and composition to warming and precipitation. *Glob Chang Biol* 18:1754–1768
- Holling CS (1973) Resilience and stability of ecological systems. *Annu Rev Ecol Syst* 4:1–23
- Hoover DL, Knapp AK, Smith MD (2014) Resistance and resilience of a grassland ecosystem to climate extremes. *Ecology* 95:2646–2656
- Howe PD, Marlon JR, Wang X, Leiserowitz A (2019) Public perceptions of the health risks of extreme heat across US states, counties, and neighborhoods. *Proc Natl Acad Sci* 116:6743–6748
- Hu H, Yin F (2009) Diesel Engine Fault Information Acquisition Based on Delay Vector Variance Method. 2009 Second Int Symp Knowl Acquis Model 199–202 Second International Symposium on Knowledge Acquisition and Modeling, IEEE pp. 199-202.
- Huang S, Hou B, Chang J, et al (2014) Copulas-based probabilistic characterization of the combination of dry and wet conditions in the Guanzhong Plain, China. *J Hydrol* 519:3204–3213
- Huard D, Mailhot A, Duchesne S (2010) Bayesian estimation of intensity-duration-frequency curves and of the return period associated to a given rainfall event. *Stoch Environ Res Risk Assess* 24:337–347
- Huntington TG (2006) Evidence for intensification of the global water cycle: review and synthesis. *J Hydrol* 319:83–95
- Hutchison C, Gravel D, Guichard F, Potvin C (2018) Effect of diversity on growth, mortality, and loss of resilience to extreme climate events in a tropical planted forest experiment. *Sci Rep* 8:1–10
- India-WRIS (2014) Watershed Atlas of India. New Delhi, India
- GOI (2016) Economic survey 2015–16. Government of Bihar. Patna
- Ingrisch J, Bahn M (2018) Towards a Comparable Quantification of Resilience. *Trends Ecol Evol* 1–9
- IPCC (2014) Climate Change 2014: Synthesis Report. Contribution of Working Groups I, II and III to the Fifth Assessment Report of the

- Intergovernmental Panel on Climate Change [Core Writing Team, R.K. Pachauri and L.A. Meyer (eds.)]. IPCC, Geneva, Switzerland, 151
- Isbell F, Craven D, Connolly J, et al (2015) Biodiversity increases the resistance of ecosystem productivity to climate extremes. *Nature* 526:574–577
 - Islam MA, Paull DJ, Griffin AL, Murshed S (2020) Assessing ecosystem resilience to a tropical cyclone based on ecosystem service supply proficiency using geospatial techniques and social responses in coastal Bangladesh. *Int J Disaster Risk Reduct* 2020:101667
 - Iyengar SG, Varshney PK, Damarla T (2009) A parametric copula based framework for multimodal signal processing. In: *Acoustics, Speech and Signal Processing, ICASSP 2009*. IEEE, pp 1893–1896
 - Izumo T (2008) The Role of the Western Arabian Sea Upwelling in Indian Monsoon. *J Clim* 21:5603–5623
 - Jaksic V, Mandic DP, Karoumi R, et al (2016) Estimation of nonlinearities from pseudodynamic and dynamic responses of bridge structures using the Delay Vector Variance method. *Phys A Stat Mech its Appl* 441:100–120
 - Jaksic V, O’Shea R, Cahill P, et al (2015) Dynamic response signatures of a scaled model platform for floating wind turbines in an ocean wave basin. *Philos Trans R Soc A Math Phys Eng Sci* 373:20140078–20140078
 - Jayan T V (2012) Floods in Western Rajasthan. *Agon Floods Flood Induc Water Conflicts India* <http://m.water-wheel.net> Assessed February 12 2019
 - Jeffress S, Haine T (2015) SST dynamics from a stochastic linear inverse method. In: *EGU General Assembly Conference Abstracts* 2015:5071
 - Jeffreys H (1946) An Invariant Form for the Prior Probability in Estimation Problems. *Proc R Soc A Math Phys Eng Sci* 186:453–461

- Jhajharia D, Dinpashoh Y, Kahya E, et al (2014) Trends in temperature over Godavari river basin in southern peninsular India. *Int J Climatol* 34:1369–1384
- Jhajharia D, Singh VP (2011) Trends in temperature, diurnal temperature range and sunshine duration in Northeast India. *Int J Climatol* 31:1353–1367
- Jhong B-C, Tung C-P (2018) Evaluating Future Joint Probability of Precipitation Extremes with a Copula-Based Assessing Approach in Climate Change. *Water Resour Manag* 32:4253–4274
- Ji L, Peters AJ (2003) Assessing vegetation response to drought in the northern Great Plains using vegetation and drought indices. *Remote Sens Environ* 87:85–98
- Joshi AK, Pant P, Kumar P, et al (2011) National Forest Policy in India: Critique of Targets and Implementation. *Small-scale For* 10:83–96
- Kakade SB, Dugam SS (2000) The simultaneous effect of NAO and SO on the monsoon activity over India. *Geophys Res Lett* 27:3501–3504
- Kamara JK, Agho K, Renzaho AMN (2019) Understanding disaster resilience in communities affected by recurrent drought in Lesotho and Swaziland—A qualitative study. *PLoS One* 14:0212994
- Kang I-S, Jin K, Wang B, et al (2002) Intercomparison of the climatological variations of Asian summer monsoon precipitation simulated by 10 GCMs. *Clim Dyn* 19:383–395
- Kantelhardt JW, Koscielny-Bunde E, Rego HH., et al (2001) Detecting long-range correlations with detrended fluctuation analysis. *Phys A Stat Mech its Appl* 295:441–454
- Kantz H, Schreiber T (2005) *Nonlinear Time Series Analysis*. *Technometrics* 47:381–381
- Kao SC, Govindaraju RS (2010b) A copula-based joint deficit index for droughts. *J Hydrol* 380:121–134

- Kar SC, Rana S (2014) Interannual variability of winter precipitation over northwest India and adjoining region: impact of global forcings. *Theor Appl Climatol* 116:609–623
- Katz RW (2013) *Statistical Methods for Nonstationary Extremes* Springer Netherlands, Dordrecht, pp 15–37
- Katz RW, Parlange MB, Naveau P (2002) Statistics of extremes in hydrology. *Adv Water Resour* 25:1287–1304
- Khaliq MN, Ouarda TBMJ, Ondo JC, et al (2006) Frequency analysis of a sequence of dependent and/or non-stationary hydro-meteorological observations: A review. *J Hydrol* 329:534–552
- Kim Y-H, Min S-K, Zhang X, et al (2016) Attribution of extreme temperature changes during 1951–2010. *Clim Dyn* 46:1769–1782
- King AD, Donat MG, Fischer EM, et al (2015) The timing of anthropogenic emergence in simulated climate extremes. *Environ Res Lett* 10:94015
- Knutson TR, Ploshay JJ (2016) Detection of anthropogenic influence on a summertime heat stress index. *Clim Change* 138:25–39
- Koster RD, Brocca L, Crow WT, et al (2016) Precipitation estimation using L-band and C-band soil moisture retrievals. *Water Resour Res* 52:7213–7225
- Kothawale D, Munot AA, Kumar K (2010) Surface air temperature variability over India during 1901–2007, and its association with ENSO. *Clim Res* 42:89–104
- Kothawale DR, Rupa Kumar K (2005) On the recent changes in surface temperature trends over India. *Geophys Res Lett* 32:18714
- Koutsoyiannis D, Montanari A (2007) Statistical analysis of hydroclimatic time series: Uncertainty and insights. *Water Resour Res* 43:1–9
- Kravtsov S, Sugiyama N, Roebber P (2018) Role of Nonlinear Dynamics in Accelerated Warming of Great Lakes. In: *Advances in Nonlinear Geosciences*. Springer, pp 279–295

- Kripalani RH, Kulkarni A, Sabade SS, Khandekar ML (2003) Indian monsoon variability in a global warming scenario. *Nat hazards* 29:189–206
- Krishnan R, Sanjay J, Gnanaseelan C, et al (2020) Assessment of Climate Change over the Indian Region: A Report of the Ministry of Earth Sciences (MoES), Government of India. New Delhi
- Kulkarni A (2012) Weakening of Indian summer monsoon rainfall in warming environment. *Theor Appl Climatol* 109:447–459
- Kumar P, Kumar KR, Rajeevan M, Sahai AK (2007) On the recent strengthening of the relationship between ENSO and northeast monsoon rainfall over South Asia. *Clim Dyn* 28:649–660
- Kumar R, Singh RD, Sharma KD (2005) Water resources of India. *Curr Sci* 89:794–811
- Kumar V, Jain SK, Singh Y (2010) Analysis of long-term rainfall trends in India. *Hydrol Sci J* 55:484–496
- Kundzewicz Z, Robson A (2000) Detecting trend and other changes in hydrological data. World Meteorological Organization
- Kusre BC, Lalringliana J (2014) Drought characterization and management in the east district of Sikkim, India. *Irrig Drain* 63:698–708
- Kyoung MS, Kim HS, Sivakumar B, et al (2011) Dynamic characteristics of monthly rainfall in the Korean Peninsula under climate change. *Stoch Environ Res Risk Assess* 25:613–625
- La Pierre KJ, Yuan S, Chang CC, et al (2011) Explaining temporal variation in above-ground productivity in a mesic grassland: the role of climate and flowering. *J Ecol* 99:1250–1262
- Lasmar N-E, Berthoumieu Y (2014) Gaussian Copula multivariate modeling for texture image retrieval using wavelet transforms. *IEEE Trans Image Process* 23:2246–61
- Lazoglou G, Anagnostopoulou C, Tolika K, Kolyva-Machera F (2019) A review of statistical methods to analyze extreme precipitation and

temperature events in the Mediterranean region. *Theor Appl Climatol* 136:99–117

- Levin K, Tirpak D (2018) 2018: A Year of Climate Extremes. World Resource Institute <https://www.wri.org/blog/2018/12/2018-year-climate-extremes> Assessed January 19 2020
- Li B, Tao S, Dawson RW (2010) Relations between AVHRR NDVI and ecoclimatic parameters. *Int J Rem Sens* 23:37–41.
- Li J, Zhang Q, Chen YD, Singh VP (2015a) Future joint probability behaviors of precipitation extremes across China: Spatiotemporal patterns and implications for flood and drought hazards. *Glob Planet Change* 124:107–122.
- Li M, Zhou X, Zhang Q, Cheng X (2014) Consequences of afforestation for soil nitrogen dynamics in central China. *Agric Ecosyst Environ* 183:40–46
- Li Y, Chen B-M, Wang Z-G, Peng S-L (2011) Effects of temperature change on water discharge, and sediment and nutrient loading in the lower Pearl River basin based on SWAT modelling. *Hydrol Sci J* 56:68–83
- Li Y, Gu W, Cui W, et al (2015b) Exploration of copula function use in crop meteorological drought risk analysis: a case study of winter wheat in Beijing, China. *Nat Hazards* 77:1289–1303
- Liang W, Yang Y, Fan D, et al (2015) Analysis of spatial and temporal patterns of net primary production and their climate controls in China from 1982 to 2010. *Agric For Meteorol* 204:22–36
- Lins HF, Cohn TA (2011) Stationarity: Wanted Dead or Alive? *J Am Water Resour Assoc* 47:475–480
- Liu Z, Li C, Zhou P, Chen X (2016) A probabilistic assessment of the likelihood of vegetation drought under varying climate conditions across China. *Nat Publ Gr* 1–10
- Lück A, Wolf V (2016) Generalized method of moments for estimating parameters of stochastic reaction networks. *BMC Syst Biol* 10:98

- Mandic D., Chen M, Gautama T, et al (2008) On the characterization of the deterministic/stochastic and linear/nonlinear nature of time series. *Proc R Soc A Math Phys Eng Sci* 464:1141–
- Mania GK, Ponnusamy D, Tsuchiya K (2018) Ultrafast Fabrication of Microneedle Array for Transdermal Ion Detection. In: 2018 International Symposium on Micro-Nano Mechatronics and Human Science (MHS). IEEE, pp 1–3
- Mann ME, Rahmstorf S, Kornhuber K, et al (2017) Influence of Anthropogenic Climate Change on Planetary Wave Resonance and Extreme Weather Events. *Sci Rep* 7:45242
- Martel J-L, Mailhot A, Brissette F (2020) Global and regional projected changes in 100-yr subdaily, daily, and multiday precipitation extremes estimated from three large ensembles of climate simulations. *J Clim* 33:1089–1103
- Martins ES, Stedinger JR (2000) Generalized maximum-likelihood generalized extreme-value quantile estimators for hydrologic data. *Water Resour Res* 36:737–744
- Marvel K, Biasutti M, Bonfils C, et al (2017) Observed and projected changes to the precipitation annual cycle. *J Clim* 30:4983–4995
- Masina M, Lamberti A, Archetti R (2015) Coastal flooding: A copula based approach for estimating the joint probability of water levels and waves. *Coast Eng* 97:37–52
- McEntire D, Crocker CG, Peters E (2010) Addressing vulnerability through an integrated approach. *Int J Disaster Resil Built Environ* 53: 1–19
- Mckee TB, Doesken NJ, Kleist J (1993) The relationship of drought frequency and duration to time scales. In: AMS 8th Conference on Applied Climatology. American Metrological Society, Boston MA, pp 179–184
- Mesbahzadeh T, Miglietta MM, Mirakbari M, et al (2019) Joint modeling of precipitation and temperature using copula theory for

current and future prediction under climate change scenarios in arid lands (Case Study, Kerman Province, Iran). *Adv Meteorol* 2019:6848049

- Metropolis N, Rosenbluth AW, Rosenbluth MN, et al (1953) Equation of State Calculations by Fast Computing Machines. *J Chem Phys* 21:1087–1092
- Mihailović DT, Mimić G, Arsenić I (2014) Climate predictions: The chaos and complexity in climate models. *Adv Meteorol* 2014:878259
- Mihunov V V, Lam NSN (2020) Modeling the dynamics of drought resilience in South-Central United States using a Bayesian Network. *Appl Geogr* pp.102224
- Milly PCD, Betancourt J, Falkenmark M, et al (2015) On critiques of “Stationarity is dead: Whither water management?” *Water Resour Res* 51:7785–7789
- Min S-K, Zhang X, Zwiers FW, Hegerl GC (2011) Human contribution to more-intense precipitation extremes. *Nature* 470:378–381
- Mirakbari M, Mesbahzadeh T, Soleimani Sardoo F, et al (2020) Observed and projected trends of extreme precipitation and maximum temperature during 1992–2100 in Isfahan province, Iran using REMO model and copula theory. *Nat Resour Model* 33:12254
- Miranda JDD, Padilla FM, Lázaro R, Pugnaire FI (2009) Do changes in rainfall patterns affect semiarid annual plant communities? *J Veg Sci* 20:269–276
- Mishra V, Shah R, Thrasher B (2014) Soil Moisture Droughts under the Retrospective and Projected Climate in India. *J Hydrometeorol* 2267–2292
- Mishra V, Smoliak B V, Lettenmaier DP, Wallace JM (2012) A prominent pattern of year-to-year variability in Indian Summer Monsoon Rainfall. *Proc Natl Acad Sci* 109:7213–7217
- Mohler RRJ, Wells GL, Hallum CR, Trenchard MH (1986) Monitoring vegetation of drought environments. *Bioscience* pp. 478–483

- Mondal A, Mujumdar PP (2015) Modeling non-stationarity in intensity, duration and frequency of extreme rainfall over India. *J Hydrol* 521:217–231
- Morales R, Matteo T Di, Gramatica R, Aste T (2012) Dynamical generalized Hurst exponent as a tool to monitor unstable periods in financial time series. *Physica A* 391:3180–3189
- Nagarajan R (2009) *Drought Assessment*. Springer Netherlands
- Naveau P, Nogaj M, Ammann C, et al (2005) Statistical methods for the analysis of climate extremes. *Comptes Rendus Geosci* 337:1013–1022
- Nayak RK, Patel NR, Dadhwal VK (2010) Estimation and analysis of terrestrial net primary productivity over India by remote-sensing-driven terrestrial biosphere model. 170:195–213
- Nayak RK, Patel NR, Dadhwal VK (2013) Inter-annual variability and climate control of terrestrial net primary productivity over India. 142:132–142
- Nelson RB (2006) *An introduction to Copulas*. Springer Science and Business media, New York
- Nguyen-Huy T, Deo RC, Mushtaq S, et al (2019) Copula statistical models for analyzing stochastic dependencies of systemic drought risk and potential adaptation strategies. *Stoch Environ Res Risk Assess* 33:779–799
- Nicholls RJ, Hanson S, Herweijer C, et al (2008) Ranking port cities with high exposure and vulnerability to climate extremes: exposure estimates. Environment Directorate. Organisation for Economic Co-operation and Development pp. 1–6
- Ning C (2010) Dependence structure between the equity market and the foreign exchange market—a copula approach. *J Int Money Financ* 29:743–759
- Niranjana Kumar K, Rajeevan M, Pai DS, et al (2013) On the observed variability of monsoon droughts over India. *Weather Clim Extrem* 1:42–50

- Norby RJ, Ledford J, Reilly CD, et al (2004) Fine-root production dominates response of a deciduous forest to atmospheric CO₂ enrichment. *Proc Natl Acad Sci* 101:9689–9693
- O’Sullivan J, Sweeney C, Parnell AC (2020) Bayesian spatial extreme value analysis of maximum temperatures in County Dublin, Ireland. *Environmetrics* 31:2621
- Okin GS, Dong C (2018) The Impact of Drought on Native Southern California Vegetation: Remote Sensing Analysis Using MODIS-Derived Time Series. *J Geo Res* 123:1927–1939.
- Oppenheimer M, Campos M, Warren R, et al (2015) Emergent risks and key vulnerabilities. In: *Climate Change 2014 Impacts, Adaptation and Vulnerability: Part A: Global and Sectoral Aspects*. Cambridge University Press, pp. 1039–1100
- Pai DS, Sridhar L, Rajeevan M, et al (2014b) Development of a new high spatial resolution (0.25× 0.25) long period (1901–2010) daily gridded rainfall data set over India and its comparison with existing data sets over the region. *Mausam* 65:1–18
- Pan S, Tian H, Dangal SRS, et al (2015) Impacts of climate variability and extremes on global net primary production in the first decade of the 21st century. *J Geogr Sci* 25:1027–1044
- Peng CK, Buldyrev S V., Havlin S, et al (1994) Mosaic organization of DNA nucleotides. *Phys Rev E* 49:1685–1689
- Pérez AA, Fernández BH, Gatti RC (2010) *Building Resilience to Climate Change: Ecosystem-based adaptation and lessons from the field*. IUCN
- Peters AJ, Waltershea EA, Ji L, et al (2002) Drought Monitoring with NDVI-Based Standardized Vegetation Index. *Pho E Rem S* 68:71–75
- Pfahl S, O’Gorman PA, Fischer EM (2017) Understanding the regional pattern of projected future changes in extreme precipitation. *Nat Clim Chang* 7:423

- Portmann RW, Solomon S, Hegerl GC (2009) Spatial and seasonal patterns in climate change, temperatures, and precipitation across the United States. *Proc Natl Acad Sci* 106:7324–7329
- Prabhakar SVRK, Shaw R (2008) Climate change adaptation implications for drought risk mitigation: A perspective for India. *Clim Change* 88:113–130
- Prasad AK, Chai L, Singh RP, Kafatos M (2006) Crop yield estimation model for Iowa using remote sensing and surface parameters. *Int J Appl Earth Obs Geoinf* 8:26–33
- Qiu L, Wu Y, Hao M, et al (2018) Simulation of the irrigation requirements for improving carbon sequestration in a rainfed cropping system under long-term fertilization on the Loess Plateau of China. *Agric Ecosyst Environ* 265:198–208
- Radzka E (2015) The assessment of atmospheric drought during vegetation season (according to standardized precipitation index SPI) in central-eastern Poland. *J Ecol Eng* 16:1
- Ragno E, AghaKouchak A, Cheng L, Sadegh M (2019) A generalized framework for process-informed nonstationary extreme value analysis. *Adv Water Resour* 130:270–282
- Rai D (2019) State, Bihar flood chaos: Satellite images show severity of flooding in the. *India Today* <https://www.indiatoday.in/diu/story/bihar-flood-satellite-images-flooding-1604831-2019-09-30> Assessed February 9 2020
- Rajeevan M, Bhate J, Jaswal AK (2008) Analysis of variability and trends of extreme rainfall events over India using 104 years of gridded daily rainfall data. *Geophys Res Lett* 35:1–6
- Rajeevan M, Nanjundiah RS (2009) Coupled model simulations of twentieth century climate of the Indian summer monsoon. *Platin Jubil Spec Vol Indian Acad Sci* 537–568
- Rajeevan M, Unnikrishnan CK, Bhate J, et al (2012) Northeast monsoon over India: Variability and prediction. *Meteorol Appl* 19:226–236

- Rammig A, Bahn M, Vera C, et al (2020) Adaptive capacity of coupled social-ecological systems to absorb climate extremes. *Climate Extremes and Their Implications for Impact and Risk Assessment*. Elsevier, pp 257–278
- Rao KK, Patwardhan SK, Kulkarni A, et al (2014) Projected changes in mean and extreme precipitation indices over India using PRECIS. *Glob Planet Change* 113:77–90
- Ray R, Khondekar MH, Ghosh K, Bhattacharjee AK (2016a) Memory persistency and nonlinearity in daily mean dew point across India. *Theor Appl Climatol* 124:119–128
- Ray R, Khondekar MH, Ghosh K, Bhattacharjee AK (2016b) Scaling and nonlinear behaviour of daily mean temperature time series across India. *Chaos, Solitons and Fractals* 84:9–14
- Reddy CS, Jha CS, Diwakar PG, Dadhwal VK (2015) Nationwide classification of forest types of India using remote sensing and GIS. *Env Mon Asses* 187:777
- Reichmann LG, Sala OE, Peters DPC (2013) Precipitation legacies in desert grassland primary production occur through previous-year tiller density. *Ecology* 94:435–443
- Renard B, Sun X, Lang M (2013) Bayesian Methods for Non-stationary Extreme Value Analysis. In: AghaKouchak A, Easterling D, Hsu K, et al. (eds) *Extremes in a Changing Climate: Detection, Analysis and Uncertainty*. Springer Netherlands, Dordrecht, pp 39–95
- Revadekar J V., Kulkarni A (2008) The El Nino-Southern Oscillation and winter precipitation extremes over India. *Int J Climatol* 28:1445–1452
- Revadekar J V, Preethi B (2012) Statistical analysis of the relationship between summer monsoon precipitation extremes and foodgrain yield over India. *Int J Climatol* 32:419–429

- Ribatet M, Sauquet E, Grésillon J-M, Ouarda TBMJ (2007) A regional Bayesian POT model for flood frequency analysis. *Stoch Environ Res Risk Assess* 21:327–339
- Ritchie JT, Nesmith DS (1991) Temperature and crop development. *Model plant soil Syst* 31:5–29
- Roxy MK, Ghosh S, Pathak A, et al (2017) A threefold rise in widespread extreme rain events over central India. *Nat Commun* 8:70
- Roy S Sen (2011) The role of the North Atlantic Oscillation in shaping regional-scale peak seasonal precipitation across the Indian subcontinent. *Earth Interact* 15:1–13
- Russo S, Sillmann J, Fischer EM (2015) Top ten European heatwaves since 1950 and their occurrence in the coming decades. *Environ Res Lett* 10:124003
- Saf B (2009) Regional flood frequency analysis using L-moments for the West Mediterranean region of Turkey. *Water Resour Manag* 23:531–551
- Sahoo RN, Dutta D, Khanna M, et al (2015) Drought assessment in the Dhar and Mewat Districts of India using meteorological, hydrological and remote-sensing derived indices. *Nat Hazards* 77:733–75
- Sakschewski B, von Bloh W, Boit A, et al (2015) Leaf and stem economics spectra drive diversity of functional plant traits in a dynamic global vegetation model. *Glob Chang Biol* 21:2711–2725
- Salas JD, Fu C, Cancelliere A, et al (2005) Characterizing the severity and risk of drought in the Poudre River, Colorado. *J Water Resour Plan Manag* 131:383–393
- Samra JS (2004) Review and analysis of drought monitoring, declaration and management in India, IWMI
- Saseendran SA, Sinha SK, Singh KK, et al (2000) Effects of climate change on rice production in the tropical humid climate of Kerala, India. *Clim Change* 44:495–514

- Schär C, Ban N, Fischer EM, et al (2016) Percentile indices for assessing changes in heavy precipitation events. *Clim Change* 137:201–216
- Schipper AM, Hilbers JP, Meijer JR, et al (2019) Projecting terrestrial biodiversity intactness with GLOBIO 4. *Global Chang Biol.* 26, no. 2 760-771.
- Seneviratne SI, Donat MG, Pitman AJ, et al (2016) Allowable CO₂ emissions based on regional and impact-related climate targets. *Nature* 529:477–483
- Seo SB, Kim Y-O, Kim Y, Eum H-I (2019) Selecting climate change scenarios for regional hydrologic impact studies based on climate extremes indices. *Clim Dyn* 52:1595–1611
- Sharma A, Goyal MK (2017) Assessment of ecosystem resilience to hydroclimatic disturbances in India. *Glob Chang Biol* 24:432–441
- Sheffield J, Wood EF, Roderick ML (2012) Little change in global drought over the past 60 years. *Nature* 491:435–438
- Shukla J, Mooley DA (1987) Empirical prediction of the summer monsoon rainfall over India. *Mon Weather Rev* 115:695–704
- Shukla RP, Huang B (2016) Interannual variability of the Indian summer monsoon associated with the air – sea feedback in the northern Indian Ocean. *Clim Dyn* 46:1977–1990
- Sillmann J, Croci-Maspoli M, Kallache M, Katz RW (2011) Extreme cold winter temperatures in Europe under the influence of North Atlantic atmospheric blocking. *J Clim* 24:5899–5913
- Sillmann J, Kharin V V., Zwiers FW, et al (2013a) Climate extremes indices in the CMIP5 multimodel ensemble: Part 2. Future climate projections. *J Geophys Res Atmos* 118:2473–2493
- Sillmann J, Kharin V V, Zhang X, et al (2013b) Climate extremes indices in the CMIP5 multimodel ensemble: Part 1. Model evaluation in the present climate. *J Geophys Res Atmos* 118:1716–1733

- Singh KS, Bonthu S, Purvaja R, et al (2018) Prediction of heavy rainfall over Chennai Metropolitan City, Tamil Nadu, India: Impact of microphysical parameterization schemes. *Atmos Res* 202:219–234
- Singh N, Ranade A (2010) The wet and dry spells across India during 1951-2007. *J Hydrometeorol* 11:26–45
- Singh RP, Rovshan S, Goroshi SK, et al (2011) Spatial and temporal variability of net primary productivity (NPP) over terrestrial biosphere of India using NOAA-AVHRR based GloPEM model. *J Indian Soc Remote Sens* 39:345
- Sinha J, Jha S, Goyal MK (2019) Influences of watershed characteristics on long-term annual and intra-annual water balances over India. *J Hydrol* 577:123970
- Sippel S, Reichstein M, Ma X, et al (2018) Drought, heat, and the carbon cycle: a review. *Curr Clim Chang Reports* 4:266–286
- Sisco MR, Bosetti V, Weber EU (2017) When do extreme weather events generate attention to climate change? *Clim Change* 143:227–241
- Sivakumar B (2017) *Chaos in Hydrology*. Springer, Dordrecht. pp. 111–145
- Sklar A (1959) Fonctions de répartition à n dimensions et leurs marges. *Publ Inst Stat Univ Paris* 8:229–231
- Sloan S, Campbell MJ, Alamgir M, et al (2019) Trans-national conservation and infrastructure development in the Heart of Borneo. *PLoS One* 14:
- Song Z, Xia J, She D, et al (2020) The development of a Nonstationary Standardized Precipitation Index using climate covariates: a case study in the middle and lower reaches of Yangtze River Basin, China. *J Hydrol* pp. 125115
- Sooraj KP, Terray P, Mujumdar M (2015) Global warming and the weakening of the Asian summer monsoon circulation: assessments from the CMIP5 models. *Clim Dyn* 45:233–252

- Srivastava AK, Rajeevan M, Kshirsagar SR (2009) Development of a high resolution daily gridded temperature data set (1969 – 2005) for the Indian region. 254:249–254.
- Stegen JC, Swenson NG, Enquist BJ, et al (2011) Variation in above-ground forest biomass across broad climatic gradients. *Glob Ecol Biogeogr* 20:744–754
- Stewart FEC, Darlington S, Volpe JP, et al (2019) Corridors best facilitate functional connectivity across a protected area network. *Sci Rep* 9:1–9
- Stokes EC, Seto KC (2019) Characterizing urban infrastructural transitions for the Sustainable Development Goals using multi-temporal land, population, and nighttime light data. *Remote Sens Environ* 234:111430
- Subash N, Ram Mohan HS, Sikka AK (2011) Decadal frequency and trends of extreme excess/deficit rainfall during the monsoon season over different meteorological sub-divisions of India. *Hydrol Sci J* 56:1090–1109
- Subash N, Sikka AK (2014) Trend analysis of rainfall and temperature and its relationship over India. *Theor Appl Climatol* 117:449–462
- Sudheer KP, Bhallamudi SM, Narasimhan B, et al (2019) Role of dams on the floods of August 2018 in Periyar River Basin, Kerala. *Curr Sci* 116:
- Sugahara S, Da Rocha RP, Silveira R (2009) Non-stationary frequency analysis of extreme daily rainfall in Sao Paulo, Brazil. *Int J Climatol A J R Meteorol Soc* 29:1339–1349
- Tan X, Gan TY (2015) Contribution of human and climate change impacts to changes in streamflow of Canada. *Sci Rep* 5:17767
- Tebaldi C, Wehner MF (2018) Benefits of mitigation for future heat extremes under RCP4. 5 compared to RCP8. 5. *Clim Change* 146:349–361

- Thasneem SA, Chithra NR, Thampi SG (2019) Analysis of extreme precipitation and its variability under climate change in a river basin. *Nat Hazards* 98:1169–1190
- Theiler J, Eubank S, Longtin A, et al (1992) Testing for nonlinearity in time series: the method of surrogate data. *Phys D* 58:77–94
- Tian H, Chen G, Liu M, et al (2010) Model estimates of net primary productivity, evapotranspiration, and water use efficiency in the terrestrial ecosystems of the southern United States during 1895–2007. *For Ecol Manage* 259:1311–1327
- Toreti A, Cronie O, Zampieri M (2019) Concurrent climate extremes in the key wheat producing regions of the world. *Sci Rep* 9:1–8
- Towler E, Rajagopalan B, Gilleland E, et al (2010) Modeling hydrologic and water quality extremes in a changing climate: A statistical approach based on extreme value theory. *Water Resour Res* 46:11
- Trenberth KE, Dai A, van der Schrier G, et al (2014) Global warming and changes in drought. *Nat Clim Chang* 4:17–22
- Tucker CJ (1989) Comparing SMMR and AVHRR data for drought monitoring. *Int J Remote Sens* 10:1663–1672
- Tucker CJ, Choudhury BJ (1987) Satellite remote sensing of drought conditions. *Remote Sens Environ* 23:243–251
- Twine TE, Kucharik CJ (2009) Climate impacts on net primary productivity trends in natural and managed ecosystems of the central and eastern United States. *Agric For Meteorol* 149:2143–2161
- Uddin MS, Haque CE, Walker D (2020) Community resilience to cyclone and storm surge disasters: evidence from coastal communities of Bangladesh. *J Environ Manage* 264:110457
- UN (2017) South Asia: Flooding - Humanitarian Snapshot. United Nations Office for the Coordination of Humanitarian Affairs. New York
- Vicente-Serrano SM, Beguería S, López-Moreno JI (2010) A multiscale drought index sensitive to global warming: The standardized precipitation evapotranspiration index. *J Clim* 23:1696–1718

- Vicente-Serrano SM, Gouveia C, Camarero JJ, et al (2013) Response of vegetation to drought time-scales across global land biomes. *Proc Natl Acad Sci* 110:52–57
- Vicente-Serrano SM, Gouveia C, Camarero JJ, et al (2012) Drought Impacts on Vegetation Activity, Growth and Primary Production in Humid and Arid Ecosystems. *Cambio climático Extrem e impactos Asoc Esp Climatol Ser A* 691–698
- Vittal H, Karmakar S, Ghosh S (2013) Diametric changes in trends and patterns of extreme rainfall over India from pre-1950 to post-1950. *Geophys Res Lett* 40:3253–3258
- Wan Z, Wang P, Li X (2010) Using MODIS Land Surface Temperature and Normalized Difference Vegetation Index products for monitoring drought in the southern Great Plains , USA. *Int J Remote Sens* 25:61–72
- Wang Y, Meng F, Liu H, et al (2019) Assessing catchment scale flood resilience of urban areas using a grid cell based metric. *Water Res* 163:114852
- Ward PJ, Eisner S, Flörke M, et al (2014) Annual flood sensitivities to El Niño–Southern Oscillation at the global scale. *Hydrol Earth Syst Sci* 18:47–66
- Westra S, Alexander L V., Zwiers FW (2013) Global increasing trends in annual maximum daily precipitation. *J Clim* 26:3904–3918
- Whan K, Sillmann J, Schaller N, Haarsma R (2020) Future changes in atmospheric rivers and extreme precipitation in Norway. *Clim Dyn* 54:2071–2084
- Wilcox R (2005) Kolmogorov–smirnov test. *Encycl Biostat* pp. 4
- Willett KM, Sherwood S (2012) Exceedance of heat index thresholds for 15 regions under a warming climate using the wet-bulb globe temperature. *Int J Climatol* 32:161–177
- Winkelmann R (2012) Copula bivariate probit models: with an application to medical expenditures. *Health Econ* 21:1444–1455

- Wu C, Chen JM (2013) Diverse responses of vegetation production to interannual summer drought in North America. *Int J Appl Earth Obs Geoinf* 21:1–6
- Wu J, Shao C, Wang Q, et al (2015) A new framework for evaluating the impacts of drought on net primary productivity of grassland. *Sci Total Environ* 536:161–172
- Xiao M, Zhang Q, Singh VP (2017) Spatiotemporal variations of extreme precipitation regimes during 1961–2010 and possible teleconnections with climate indices across China. *Int J Climatol* 37:468–479
- Xiong L, Yu K, Gottschalk L (2014) Estimation of the distribution of annual runoff from climatic variables using copulas. *Water Resour Res* 50:7134–7152
- Xu X, Niu S, Sherry RA, et al (2012) Interannual variability in responses of belowground net primary productivity (NPP) and NPP partitioning to long-term warming and clipping in a tallgrass prairie. *Glob Chang Biol* 18:1648–1656
- Yadav RK, Rupa Kumar K, Rajeevan M (2009) Increasing influence of ENSO and decreasing influence of AO/NAO in the recent decades over northwest India winter precipitation. *J Geophys Res Atmos* 114:12
- Yadav RR (2013) Relationship between winter precipitation over the western Himalaya and central northeast India summer monsoon rainfall: a long-term perspective. *Quat Int* 304:176–182
- Yang X, Qian J (2019) Joint occurrence probability analysis of typhoon-induced storm surges and rainstorms using trivariate Archimedean copulas. *Ocean Eng* 171:533–539
- Yilmaz AG, Imteaz MA, Perera BJC (2017) Investigation of non-stationarity of extreme rainfalls and spatial variability of rainfall intensity–frequency–duration relationships: a case study of Victoria, Australia. *Int J Climatol* 37:430–442

- Yilmaz AG, Perera BJC (2014) Extreme Rainfall Nonstationarity Investigation and Intensity – Frequency – Duration Relationship. *J Hydrol Eng* 19:1160–1172
- Yin J, Guo S, He S, et al (2018a) A copula-based analysis of projected climate changes to bivariate flood quantiles. *J Hydrol* 566:23–42
- Yin Y, Ma D, Wu S (2018b) Climate change risk to forests in China associated with warming. *Sci Rep* 8:493
- Yin Y, Pan X, Yang X, et al (2019) Spatiotemporal Changes and Frequency Analysis of Multiday Extreme Precipitation in the Huai River Basin during 1960 to 2014. *Adv Meteorol* 2019:
- Yue C, Ciais P, Cadule P, et al (2014) Modelling the role of fires in the terrestrial carbon balance by incorporating SPITFIRE into the global vegetation model ORCHIDEE - Part 1: Simulating historical global burned area and fire regimes. *Geosci Model Dev* 7:2747–2767
- Zamani S, Gobin A, Van de Vyver H, Gerlo J (2016) Atmospheric drought in Belgium—statistical analysis of precipitation deficit. *Int J Climatol* 36:3056–3071
- Zhang L (2005) Multivariate Hydrological Frequency Analysis and Risk Mapping. Louisiana State University and Agricultural & Mechanical College pp. 1613
- Zhang L, Singh VP (2007) Bivariate rainfall frequency distributions using Archimedean copulas. *J Hydrol* 332:93–109
- Zhang Q, Li J, Singh VP, Xu CY (2013) Copula-based spatio-temporal patterns of precipitation extremes in China. *Int J Climatol* 33:1140–1152
- Zhang Q, Singh VP, Li J, et al (2012) Spatio-temporal variations of precipitation extremes in Xinjiang, China. *J Hydrol* 434–435:7–18
- Zhang S, Hu Y, Bao H, Li X (2014) Parameters determination method of phase-space reconstruction based on differential entropy ratio and RBF neural network. *J Electron* 31:61–67

- Zhang X, Alexander L, Hegerl GC, et al (2011) Indices for monitoring changes in extremes based on daily temperature and precipitation data. *Wiley Interdiscip Rev Clim Chang* 2:851–870
- Zhang X, Obringer R, Wei C, et al (2017) Droughts in India from 1981 to 2013 and Implications to Wheat Production. *Sci Rep* 7:44552
- Zhang X, Zwiers FW (2013) Statistical Indices for the Diagnosing and Detecting Changes in Extremes. *Extremes in Changing Climate*, Springer, pp 1–14
- Zhang X, Zwiers FW, Hegerl GC, et al (2007) Detection of human influence on twentieth-century precipitation trends. *Nature* 448:461–465
- Zhao F, Wu Y, Qiu L, et al (2018a) Spatiotemporal features of the hydro-biogeochemical cycles in a typical loess gully watershed. *Ecol Indic* 91:542–554
- Zhao F, Wu Y, Sivakumar B, et al (2019) Climatic and hydrologic controls on net primary production in a semiarid loess watershed. *J Hydrol* 568:803–815
- Zhao X, Yu B, Liu Y, et al (2018b) NPP-VIIRS DNB daily data in natural disaster assessment: evidence from selected case studies. *Remote Sens* 10:1526
- Zorita E, González-Rouco F, Legutke S (2003) Testing the Approach to Paleoclimate Reconstructions in the Context of a 1000-Yr Control Simulation with the ECHO-G Coupled Climate Model. *J Clim* 16:1378–1390
- Zscheischler J, Reichstein M, Von Buttlar J, et al (2014) Carbon cycle extremes during the 21st century in CMIP5 models: Future evolution and attribution to climatic drivers. *Geophys Res Lett* 41:8853–8861